Maheswaran Rathinasamy
S. Chandramouli · K. B. V. N. Phanindra
Uma Mahesh *Editors*

Water Resources and Environmental Engineering II

Climate and Environment

Springer

Water Resources and Environmental Engineering II

Maheswaran Rathinasamy · S. Chandramouli
K. B. V. N. Phanindra · Uma Mahesh
Editors

Water Resources and Environmental Engineering II

Climate and Environment

12 3

Editors
Maheswaran Rathinasamy
Department of Civil Engineering
Maharaj Vijayaram Gajapathi Raj College
Vizianagaram, Andhra Pradesh, India

K. B. V. N. Phanindra
Department of Civil Engineering
Indian Institute of Technology Hyderabad
Hyderabad, Telangana, India

S. Chandramouli
Department of Civil Engineering
Maharaj Vijayaram Gajapathi Raj College
Vizianagaram, Andhra Pradesh, India

Uma Mahesh
Department of Civil Engineering
National Institute of Technology Warangal
Warangal, Telangana, India

ISBN 978-981-13-2037-8 ISBN 978-981-13-2038-5 (eBook)
https://doi.org/10.1007/978-981-13-2038-5

Library of Congress Control Number: 2018951405

This Springer imprint is published by the registered company Springer Nature Singapore Pte Ltd.
The registered company address is: 152 Beach Road, #21-01/04 Gateway East, Singapore 189721, Singapore

Foreword

Judicious management of water resources is fundamental for achieving sustainable management of natural resources and ensuring environmental integrity. Technologies, such as remote sensing, navigation, space communication, geospatial tools, and Internet of things, are extremely useful in developing newer applications and tools for scientific data management and decision-making.

The international conference organized by the Department of Civil Engineering, MVGR College of Engineering (A), Vizianagaram, from 30 March to 01 April 2017, provided a much-needed platform to discuss the emerging technologies and opportunities in water, environment and climate change facets.

The effort of the organizers in bringing out a scientific book on conference deliberations and a compendium of papers needs a special compliment.

I strongly believe that the technical insights presented in this book will enrich the scientific community, provide inspiration to readers and lead to newer technological applications that would support human society in coping up with the challenges posed by impending climate change.

I wish the organizing committee of the conference a grand success.

Hyderabad, India

Y. V. Krishna Murthy
Director
National Remote Sensing Centre

Preface

With an ever-increasing demand for the development, the stress on water resources and environment is increasing day by day. The changing climate is further amplifying the effect resulting in severe drought, flood and pollution problems. In order to provide a platform for eminent scientists, researchers and students to discuss the emerging technologies in mitigating the problems related to water and environment, the International Conference on Emerging Trends in Water Resources and Environmental Engineering (ETWREE-17) was conducted by MVGR College of Engineering, Vizianagaram, Andhra Pradesh, India, from March 2017 to April 2017. About 100 participants from three different countries attended ETWREE-17. ETWREE-17 was organized by the Department of Civil Engineering, MVGR College of Engineering, and was sponsored by the Science and Engineering Research Board (SERB) and the National Remote Sensing Centre (NRSC).

The proceedings of this conference contain 60 papers which are included as two volumes. The response to ETWREE-17 was overwhelming. It attracted quality work from different areas related to water resources, environmental engineering and climate. From a total of 120 abstracts, we selected around 80 papers for presentation through a rigorous peer review process with the help of our programme committee members and external reviewers.

Dr. Y. V. N. K. Murthy, Director, NRSC, Hyderabad, conducted a special session on “Application of Remote Sensing in Water Resources”. Professor Rakesh Khosa, IIT Delhi, conducted a special session on “Enigma of Climate”. Professor D. Nagesh Kumar, IISc Bangalore, delivered a lecture on “Remote Sensing, GIS and DEM for Water Resources Assessment of a River Basin”. Professor Uma Mahesh, NIT Warangal, gave a lecture on “Non-Stationarity in Rainfall Intensity”. Dr. Brijesh Kumar Yadav, IIT Roorkee, conducted a session on “Engineered Bioremediation”. Dr. K. B. V. N. Phanindra, IIT Hyderabad, delivered a keynote on “Modeling Soil–Water–Disease Interactions of Flood-Irrigated Mandarin Orange Trees”.

Dr. Shishir Gaur, IIT BHU, conducted a special session on “Application of Simulation Optimization Model for Management of Groundwater Resources”. Dr. L. Suri Naidu, NUS, Singapore, delivered a lecture on “Food, Water and

Energy Nexus". Professor G. V. R. Srinivas Rao, Andhra University, conducted a session on "Multivariate Statistical Analysis of River Water Quality". Professor T. V. Praveen, Andhra University, delivered a lecture on "Salinity Intrusion Modelling". Dr. Y. R. S. Rao, NIH Kakinada, provided a lecture on "River Bank Filtration".

These sessions were very informative and beneficial to the authors and delegates of the conference. We thank all the keynote speakers and the session chairs for their excellent support in making ETWREE-17 a grand success. The quality of a contributed volume is solely due to the reviewers' efforts and dedication. We thank all the members of the advisory board of the conference for their support and encouragement.

We are indebted to the programme committee members Mr. A. V. S. Kalyan, Mr. Varaprasad and Mr. Sridhara Naidu for extending their help in preparing the manuscript.

We express our heartfelt thanks to chief patrons, Sri Ashok Gajapathi Raju, Chairman, MANSAS, and patron and Prof. K. V. L. Raju, Principal, MVGR College of Engineering, for their continuous support and encouragement during the course of the convention. We also thank all the faculty and administrative staff for their efforts.

We would also like to thank the authors and participants, who have made it for the conference. Finally, we would like to thank all the student volunteers who spent assiduous efforts in meeting the deadlines and arranging every detail to make sure smooth running of the conference. All the efforts are worth if the readers of this contributed volumes find them inspiring and useful. We also sincerely thank the press, print and electronic media for their excellent coverage of this convention.

Vizianagaram, India — Dr. Maheswaran Rathinasamy
Vizianagaram, India — Dr. S. Chandramouli
Hyderabad, India — Dr. K. B. V. N. Phanindra
Warangal, India — Prof. Uma Mahesh
December 2017

About This Book

This book covers a variety of topics related to water, climate and environment. The topics mainly focus on but not limited to hydrological modelling, water resources management, water conservation practices, applications of recent techniques for solving water-related issues, land use impact on water resources, climate change impacts, wastewater treatment and recovery, advances in hydraulics in rivers and ocean. This book is a collection of the best papers submitted in the First International Conference on Emerging Trends in Water Resources and Environmental Engineering held from 28 March 2017 to 1 April 2017 at MVGR College of Engineering, Vizianagaram, Andhra Pradesh, India. It was hosted by the Department of Civil Engineering, MVGR College of Engineering, with the support of Science and Engineering Research Board, India.

Contents

About the Editors

Dr. Maheswaran Rathinasamy is currently Associate Professor in the Department of Civil Engineering, MVGR College of Engineering, Vizianagaram. He received his bachelor's and master's degrees from Anna University, Chennai, and BIT Mesra, respectively. He obtained his Ph.D. from IIT Delhi. He is a recipient of INSPIRE Fellowship from the Department of Science and Technology, India, and Humboldt Fellowship from Alexander Von Humboldt Foundation, Germany. He has postdoctoral experience in the University of Minnesota, USA, and Potsdam Institute of Climate Impact Research, Germany. He is the principal investigator of funded research projects of the order of 1.5 crore rupees. He has around 30 international journal publications and 25 international conference publications. His research interests include stochastic hydrology, hydrological modelling, hydro-meteorological forecasting.

Dr. S. Chandramouli currently serves as Professor and HOD in the Department of Civil Engineering, MVGR College of Engineering, Vizianagaram. He received his M. Tech. in water resources engineering as specialization from REC, Warangal, in 2002. He obtained his Ph.D. in civil engineering from Andhra University, Visakhapatnam, in 2013. He worked in several organizations such as CES(I) Pvt. Ltd., Hyderabad; GVP College of Engineering, Visakhapatnam; and GMRIT, Rajam, for a period of 10 years. Currently, he is working in MVGR College of Engineering since 2011. He published more than 50 technical papers in various reputed journals and conferences. He has attended more than 60 professional training programmes organized by the prestigious institutions in India. He is Life Member of ISTE and IEI. He has completed one DST project as a co-principal investigator. He has reviewed many journal papers published by prestigious journals and conferences. He has organized many faculty development programmes and student training programmes.

Dr. K. B. V. N. Phanindra currently serves as Assistant Professor in the Department of Civil Engineering, IIT Hyderabad, India. He received his master's degree in hydraulics and water resources engineering from IIT Kanpur and Ph.D. in

water resources engineering from New Mexico State University (NMSU). He also holds a graduate minor degree in GIS from NMSU. To his credit, he has nine journal publications of international repute, three technical reports, one monograph and one chapter. He has completed three research projects funded by various ministries from the Government of India to the tune of about 1.6 crore rupees. His research interests include hydrogeologic characterization, groundwater flow and transport modelling, soil–water–crop interactions, remote sensing and GIS applications in groundwater.

Prof. Uma Mahesh is currently serving as Professor in the Department of Civil Engineering, National Institute of Technology, Warangal, Telangana, India. He has earlier served as Head of the Department from July 2008 to June 2010, as Dean, Students' Welfare, from July 2012 to March 2013 and as Dean, Planning & Development, from April 2013 to June 2014. His area of specialization is water resources with a focus on water resources systems, hydrologic modelling, irrigation management, water quality modelling and management, applications of soft computing techniques and modelling impacts of climate change. He is a recipient of the Jalamitra Award by the Government of AP in 2003 for successful implementation of Watershed Development Project in Warangal District, G M Nawathe Award for the paper presented at Hydro 2004 (annual conference of the Indian Society for Hydraulics) and Central Board of Irrigation and Power (CBIP) Award. Eight Ph.D. students have been graduated with him as their advisor. He is currently advising six Ph.D. students at NIT Warangal. He has published more than 60 papers in various reputed journals and conferences.

A Detailed Statistical Analysis of Rainfall of Thoothukudi District in Tamil Nadu (India)

Sathyanathan Rangarajan, Deeptha Thattai, Abhishek Cherukuri, Tanmoy Akash Borah, Joel Kuncheria Joseph and Arun Subbiah

Abstract The adverse change in climate in recent years influences different meteorological variables like precipitation, temperature and evapotranspiration. Agriculture and other related sectors which depend on the monsoon and timed irrigation schedules are seriously affected due to the changing pattern of rainfall. Thoothukudi, one among the four mega cities of Tamil Nadu, is a major driver of industrialisation, and the impact due to industrialisation on meteorological variables is unknown. In the present study, statistical analysis is carried out to ascertain possible trend in monthly, seasonal and annual historical time series of rainfall of Thoothukudi district in Tamil Nadu between the years 1901 and 2002. A detailed statistical analysis is performed by adopting most commonly used methods like Mann–Kendall's test, Sen's slope, departure analysis, rainfall anomaly index and precipitation concentration index. The north-east and south-west monsoons contribute more than 73% to the annual rainfall. A significant decreasing trend was observed for January, and no significant trend was found for other months and seasons. About 72% of the years received normal amount of rainfall; with no scanty and no rain category observed for the past 102 years. Moderate concentration of annual rainfall is witnessed with the mean PCI value about 15.

Keywords Tuticorin · Percentage departure · RAI · Mann–Kendall test Sen's slope · Frequency analysis and probability distribution · PCI

1 Introduction

Rainfall, being a major component of the water cycle, is an important source of freshwater on the planet and contributes around 2,16,000 m^3 of freshwater. According to the scientific evidence collected globally over a period of 100 years, climate

S. Rangarajan (B) · D. Thattai · A. Cherukuri · T. A. Borah · J. K. Joseph · A. Subbiah
Department of Civil Engineering, SRM Institute of Science and Technology, Kattankulathur 603203, Tamil Nadu, India
e-mail: sathyanathan.r@ktr.srmuniv.ac.in

M. Rathinasamy et al. (eds.), *Water Resources and Environmental Engineering II*,
https://doi.org/10.1007/978-981-13-2038-5_1

and temperature have begun to change globally beyond normal averages, and as a result, change in trend of rainfall has been detected. Reports show that there is a probability of global climate change in this century itself [1]. Variations in the global hydrological cycle influence the development of organisms [2]. A proper knowledge and understanding of variability of rainfall that occurs over a wide range of temporal scales can help with better risk management practices. Various researches indicate that precipitation patterns have been altered leading to increase in extreme weather events as result of global warming [3–6]. The global monsoon precipitation had an increasing trend from 1901 to 1955 and a decreasing trend later in the twentieth century [7]. While analysing precipitation trend and change point detection, nonparametric methods are usually preferred [8–10].

In a mainly agricultural country like India, which is dependent on the monsoon, rainfall data is necessary to plan and design water resource projects. Guhathakurta and Rajeevan pointed out the importance of studying the trend in monsoon rainfall in India [11]. Joshi et al. [12] attempted to study annual rainfall series of subregions of India to identify the climate changes. Sarkar and Kafatos [13] analysed the Indian precipitation pattern and its relationship with ENSO. Parthasarathy and Dhar studied the annual rainfall from 1901 to 1960 and found an increasing trend in and around Central India and a decreasing trend in some regions of eastern India [14].

Pal and Al-Tabbaa [15] predicted a decrease in pre-monsoon extreme rainfall and increased frequency of no rain days for Kerala, which could lead to water scarcity. Thomas and Prasanna Kumar observed a decreasing trend in south-west monsoon season and an increasing trend for the other seasons in Kerala [16].

Tamil Nadu experiences four monsoon seasons in a year, viz. north-east (NEM), south-west (SWM), pre-monsoon (Pre-mon) and winter. The aim of the present study is to analyse precipitation trends if any by various statistical methods for a 102-year rainfall data (1901–2002) of Thoothukudi district, Tamil Nadu.

1.1 Study Area

Thoothukudi (also called Tuticorin) district is situated along the Coromandel Coast of the Bay of Bengal, centred at 8.906°N latitude and 78.019°E longitude (Fig. 1). The district is located about 590 km south of Chennai, the state capital. The bounding districts are Virudhunagar, Ramanathapuram (north) and Tirunelveli (south and west). The Gulf of Mannar borders on the east. Tuticorin port is one of the fastest growing ports in India. The 4621 km^2 district has a coastline of 121 km. As of 2011, the population was 1,750,176. The minimum and maximum ambient temperatures in the area as per IMD Tuticorin are 19.4 °C (January) and 38.3 °C (May), respectively. The relative humidity varies from 52 to 90%. The normal annual rainfall in the region is 625.8 mm. The site falls under seismic zone II.

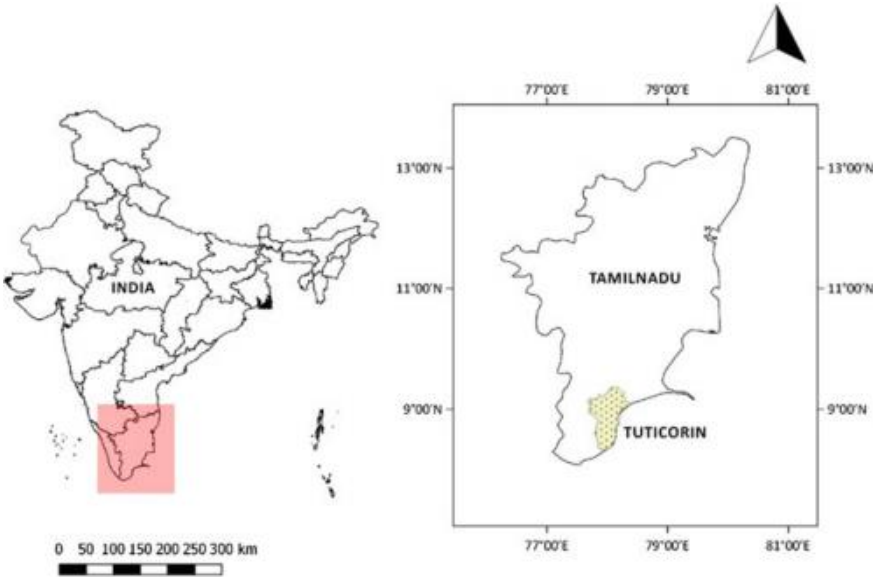

Fig. 1 Location map of Thoothukudi (Tuticorin) district

2 Methodology

2.1 Mann–Kendall Trend Test

Mann–Kendall's test is a rank-based nonparametric test to analyse time series data for consistently increasing or decreasing trends. In this test, the null hypothesis (H_o) is that there has been no trend in precipitation over time; the alternative hypothesis (H_a) is that there has been a trend (increasing or decreasing) over time [17, 18]. The test statistic S is defined as:

$$\sum_{i=1}^{n-1} \sum_{j=i+1}^{n} \text{sig}(X_j - X_i) \tag{1}$$

where n is the total length of data, X_i and X_j are two generic sequential data values, and function sign$(X_j - X_i)$ assumes the following values

$$\text{sign}(X_j - X_i) = \begin{cases} +1 & \text{if } (X_j - X_i) > 0 \\ 0 & \text{if } (X_j - X_i) = 0 \\ -1 & \text{if } (X_j - X_i) < 0. \end{cases} \tag{2}$$

2.2 Sen's Slope

The slope of n pairs of points is calculated by

$$Q_i = \frac{\left(X_j - X_k\right)}{(j-k)} \quad \text{for} \quad i = 1, 2, \ldots, N \tag{3}$$

where x_j and x_k are data values at times j and k ($j > k$), and the median of the value of Q_i is Sen's estimator slope.

$$\beta = \text{Sen's Estimator} = \begin{cases} Q_{n+1/2} & \text{if } N \text{ is odd} \\ \left(\frac{1}{2}\right)\left(Q_{\frac{n}{2}} + Q_{\frac{n+2}{2}}\right) & \text{if } N \text{ is even} \end{cases} \tag{4}$$

A positive value of β implies that there is an upward slope while a negative value of β indicates a downward slope [19, 20].

2.3 Frequency Analysis and Probability Distribution

From a frequency analysis, the rainfall or the return period for a design can be obtained. The first step in the frequency analysis is to sort the rainfall data in the descending order, and the serial rank number ranging from 1 to n is assigned. The Weibull distribution analysis [21] is performed to arrive at the probability of exceedance and return period.

$$\text{Weibull's estimate of probability of exceedance} = \frac{r}{n+1} \times 100 \tag{5}$$

where r = order of rank of the event and n = number of events.

2.4 Departure Analysis of Rainfall

The percentage departure (D%) of annual rainfall is calculated to understand the trend of drought years. Equation 6 computes the values as [16]

$$D\% = \frac{X_i - X_m}{X_i} \times 100 \tag{6}$$

where X_m = Mean annual rainfall and X_i = Annual rainfall of the given year.

The percentage departure of annual and monthly rainfall and the excess, normal, deficit, scanty and no rainfall years is derived from Table 1.

Table 1 Classification of regional rainfall distribution based on percentage departure (after Indian Meteorological Department)

Terminology	Definition
Excess	Percentage departure of realised rainfall from normal rainfall is +20% or more
Normal	Percentage departure of realised rainfall from normal rainfall is between −19 and 19%
Deficit	Percentage departure of realised rainfall from normal rainfall is between −20 and −59%
Scanty	Percentage departure of realised rainfall from normal rainfall is between −60 and −99%
No rain	Percentage departure of realised rainfall from normal rainfall is −100%

In India, "drought" as adopted by the Indian Meteorological Department (IMD) is a situation when the deficiency of rainfall in an area is 25% or more than the long-term average (LTA) in a given period. This term is further divided into "moderate" and "severe". The drought is considered as "moderate" if the deficiency of rainfall is between 26 and 50% and "severe" if it is more than 50% [22].

2.5 Rainfall Anomaly Index (RAI)

Van Rooy [23] designed the rainfall anomaly index (RAI) in the year 1965. The RAI considers the rank of the precipitation values and helps to determine the magnitude of positive and negative precipitation anomalies for the given period.

$$\text{RAI} = \pm 3 \frac{P - \bar{P}}{\bar{E} - \bar{P}} \tag{7}$$

where P = Measure of precipitation, $\bar{P}$ = Mean precipitation and $\bar{E}$ = Average of 10 extrema (min and max).

The range of RAI values is divided into nine categories: extremely wet, very wet, moderately wet, slightly wet, near normal, slightly dry, moderately dry, very dry and extremely dry as shown in Table 2.

2.6 Precipitation Concentration Index (PCI)

The precipitation concentration index (PCI) is estimated on seasonal and annual distributions, variations and trends [24]. The seasonal estimations were based on four seasons (i.e. NEM, SWM, Winter and Pre-mon). The PCI is analysed at different timescales to identify the rainfall patterns (Table 3).

Table 2 Classification of RAI values

Range of values	Classification
≥3.00	Extremely wet
2.00 to 2.99	Very wet
1.00 to 1.99	Moderately wet
0.50 to 0.99	Slightly wet
0.49 to −0.49	Near normal
−0.50 to −0.99	Slightly dry
−1.00 to −1.99	Moderately dry
−2.00 to −2.99	Very dry
≤−3.00	Extremely dry

Table 3 Classification of rainfall according to the PCI values

PCI value	Distribution of rainfall
PCI ≤ 10	Low precipitation distribution
11–15	Moderate precipitation concentration
16–20	Irregular distribution
PCI > 20	Strongly irregular distribution

The PCI is calculated by the following equation:

$$\mathrm{PCI}_{\mathrm{annual}} = \frac{\sum_{i=1}^{i=12} P_i^2}{\left(\sum_{i=1}^{i=12} P_i\right)^2} \times 100 \tag{8}$$

where P_{i} is the monthly rainfall for the *i*th month. In addition to this, PCI for the seasonal scales was also computed.

3 Results and Discussions

3.1 General Analysis

Various statistical analyses were conducted for the precipitation data for Tuticorin district for the years 1901–2002. The annual rainfall varied from 645.96 to 1388.94 mm, and the average normal rainfall was 981.78 mm. The standard deviations for the individual months varied between 28.10 and 80.46 mm. The coefficient of variation (CV) was calculated to determine the spatial pattern of interannual variability of monthly precipitation in the district. The CV varied from 42.28% in October to 124.37% in February. The CV of the annual precipitation over the study period was around 16.33%. However, the relatively low CV for annual rainfall (16.33%) shows the less interannual variability of annual rainfall in Tuticorin. For January–March, CV values

Table 4 Monthly and seasonal mean of rainfall, standard deviation, coefficient of variance and percentage distribution from 1901 to 2002

Month	Average	SD	% CV	% Contribution
Jan	24.98	28.1	112.51	2.54
Feb	33.59	41.78	124.37	3.42
Mar	29.35	33.18	113.06	2.99
Apr	85.5	55.77	65.23	8.71
May	86.1	58.3	67.71	8.77
Jun	111.76	79.15	70.82	11.38
Jul	63.15	52.45	83.06	6.43
Aug	56.75	36.8	64.85	5.78
Sep	63.36	36.81	58.1	6.45
Oct	190.3	80.46	42.28	19.38
Nov	166.66	75.05	45.03	16.98
Dec	70.27	56.44	80.32	7.16
Annual	81.81	13.36	16.33	100
NEM	427.23	124.78	29.21	43.63
SWM	295.02	112.88	38.26	29.89
Winter	58.57	48.89	83.46	6.06
Pre-mon	200.95	83.16	41.38	20.42

were >100%; whereas for October and November, CV values were lower (around 45%). This indicates lesser variability in winter and larger variability in summer. The NEM and SWM contribute the maximum to the annual rainfall (>73%). The NEM caters to around 43% of the annual precipitation, whereas the SWM contributes around 30%. The winter monsoon contributes the least to the annual rainfall, around 6% (Table 4).

3.2 Long-Term Patterns in Mean Annual and Seasonal Precipitation

The annual and seasonal precipitation data were used to study the variation in the time series. Figure 2 shows the time series of rainfall over Tuticorin for the entire period. Figure 3 shows the time series over the four seasons.

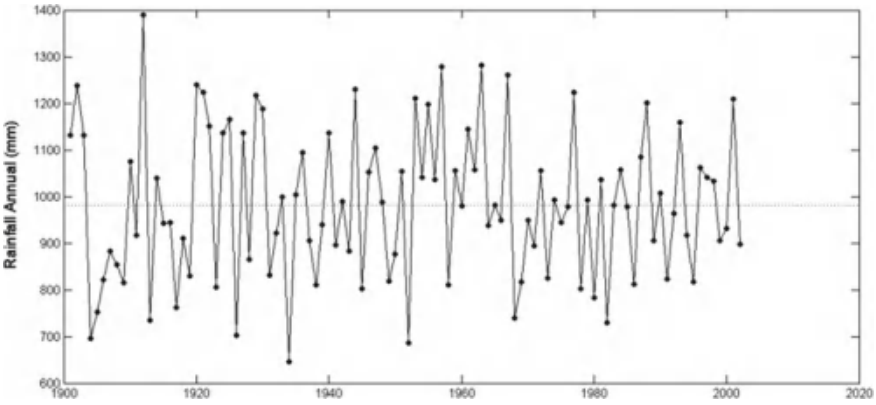

Fig. 2 Annual rainfall over Tuticorin (1901–2002). The dashed line is the average

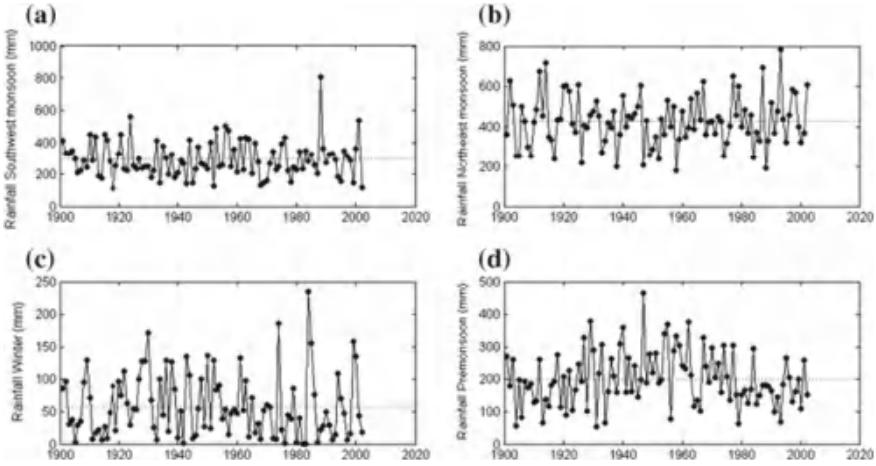

Fig. 3 Seasonal time series of rainfall **a** south-west monsoon, **b** north-east monsoon, **c** winter and **d** pre-monsoon. The dashed line is the average

3.3 Results of Mann–Kendall's and Sen's Slope Test

The results of the Mann–Kendall's and Sen's slope test are presented in Table 5. A positive value (β) indicates an increasing trend and negative value (β) indicates a decreasing trend in Sen's slope analysis. For Mann–Kendall's test statistic, $z > 1.96$ confirms a significant rising trend, while $z < -1.96$ confirms falling trend at 95% confidence level. A decreasing trend was observed only for January, and no significant trend was found for the other months and seasons. Sen's slope values also indicated no trend.

Table 5 Results of Mann–Kendall's test and Sen's slope values (1901–2002) for Tuticorin

Month	MK value (Z-value)	Sen's slope (β-value)
Jan	−2.559	−0.121
Feb	1.090	+0.070
Mar	−0.466	−0.016
Apr	−0.040	−0.007
May	−0.173	−0.033
Jun	−1.284	−0.308
Jul	1.498	+0.180
Aug	−0.827	−0.093
Sep	0.416	+0.041
Oct	−0.301	−0.073
Nov	0.364	+0.088
Dec	0.752	+0.115
Annual	0.237	+0.122
NEM	0.150	+0.046
SWM	−0.393	−0.144
Winter	−1.035	−0.126
Pre-mon	−0.294	−0.083

3.4 Results of Weibull's Frequency Distribution

Using the Weibull's frequency distribution method, the probabilities of exceedance of the ranked annual rainfall data at 50, 75 and 90% were calculated (Table 6).

3.5 Results of Departure Analysis

Table 7 depicts the departure analysis of rainfall. It shows the number of years with excess, normal, deficit, scanty or no amount of rainfall.

Tuticorin district of Tamil Nadu has had no "no rain" or scanty year in the study period (Fig. 4). This indicates that there was no severe drought for the past 102 years. According to the drought classification of IMD [25, 26], Tuticorin experienced 11 "deficit" years during the first 51 years (1901–1951) and nine during the last 51 years (1952–2002). Both the severity of drought and excess of rainfall have a decreasing trend. The data of the last two decades (1981–2002) shows only one "deficit" year and zero "excess" rainfall year. The decade-wise departure of annual rainfall indicates the first decade (1901–1910) as the driest decade, having a maximum of three "deficit" years and the last decade as the wettest (1991–2002) having only one "deficit" year. In the history of 102 years, it is found that Tuticorin has mostly experienced normal rainfall for 72 years, "deficit" for 20 years and "excess" rainfall for 9 years.

Table 6 Probabilities of exceedance of the ranked annual rainfall data estimated with Weibull's distribution

Month	50%	75%	90%
Jan	14.57	3.87	0.65
Feb	15.81	3.26	0.53
Mar	16.87	5.62	1.30
Apr	78.30	42.18	21.07
May	74.15	38.26	11.74
Jun	90.18	51.18	24.15
Jul	44.60	24.18	12.54
Aug	50.84	25.90	16.81
Sep	59.97	34.74	22.71
Oct	184.15	129.58	92.89
Nov	155.81	121.68	66.02
Dec	53.91	25.19	11.32
NEM	424.88	349.09	254.32
SWM	269.64	224.64	153.13
Winter	47.57	16.98	6.85
Pre-mon	189.59	137.55	99.02
Annual	979.79	832.04	783.24

Table 7 Departure analysis of annual precipitation

Terminology	Number of years (1901–2002)	Number of years (1901–1951)	Number of years (1952–2002)
Excess	9	5	4
Normal	73	35	38
Deficit	20	11	9
Scanty	0	0	0
No rain	0	0	0

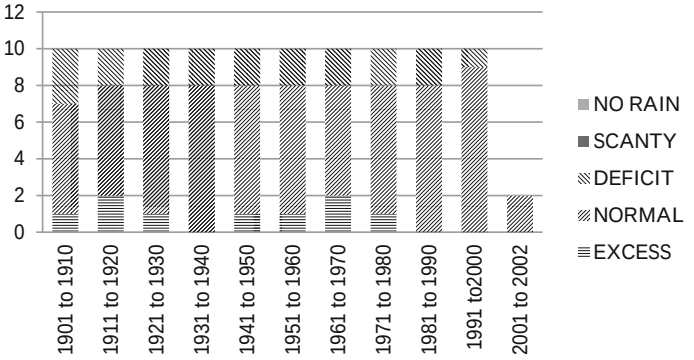

Fig. 4 Decade-wise distribution of annual rainfall

Table 8 Rainfall anomaly index

Range of values	Classification	Number of years (1901–2001)	Number of years (1901–1951)	Number of years (1952–2002)
≥3.00	Extremely wet	4	1	3
2.00 to 2.99	Very wet	12	7	5
1.00 to 1.99	Moderately wet	13	10	3
0.50 to 0.99	Slightly wet	13	1	10
0.49 to −0.49	Near normal	19	7	12
−0.50 to −0.99	Slightly dry	11	5	6
−1.00 to −1.99	Moderately dry	17	10	7
−2.00 to −2.99	Very dry	9	5	4
≤−3.00	Extremely dry	4	3	1

3.6 Results of Rainfall Anomaly Index (RAI)

The rainfall anomaly index from 1901 to 2002 (Table 8) shows the classification of different categories of rainfall anomalies and the number of years of occurrence.

Four extremely dry and extremely wet years were observed during the study period. Three out of four extremely dry years occurred during the first five decades, which indicates that 1901–1951 was drier than the next 51 years. The dry years (from extremely dry to slightly dry) follow a decreasing trend, and a reduction of 21.73% is seen over the period of 102 years. A total of 23 dry years were recorded for the first 51 years, while the number of dry years decreased to 18 years for the remaining period (Fig. 5). Tuticorin mostly enjoys a normal amount of rainfall ranging from −0.49 to 0.49. The number of wet years in the recent 51 years (1952–2002) also increased when compared to the initial years (1901–1951). Though the initial five decades have many dry events, they rarely extend beyond three consecutive years and a balance in number of wet and dry years is noticed in the last six decades till 2002.

3.7 Results of Precipitation Concentration Index (PCI)

The mean PCI for Tuticorin is 15, which shows that the annual rainfall is of moderate concentration (Fig. 6). Strong irregularity was observed only for three years. Since NEM is significant over Tuticorin, such irregularity can be associated with it. The PCI is between 16 and 20 for 31 years, indicating lesser contribution of NEM towards the annual precipitation (Fig. 7). The NEM contribution was still lower for the years which had PCI between 11 and 15. The rainfall concentration of pre-monsoon season showed higher variability, implying inconsistency in rainfall.

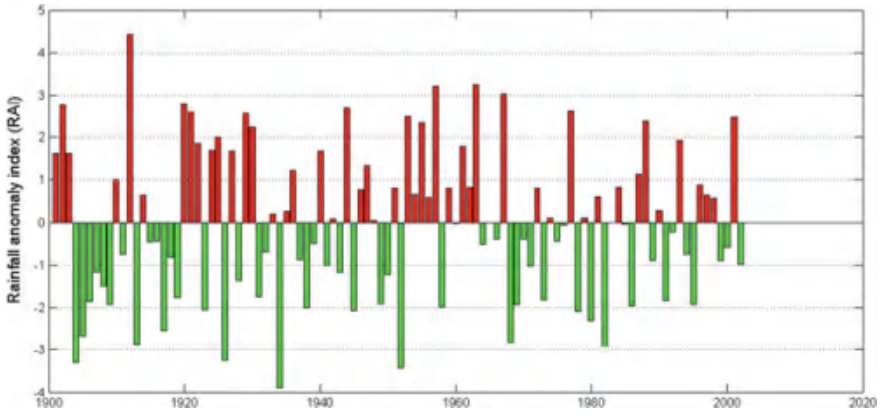

Fig. 5 Rainfall anomaly index for Tuticorin during 1901–2002

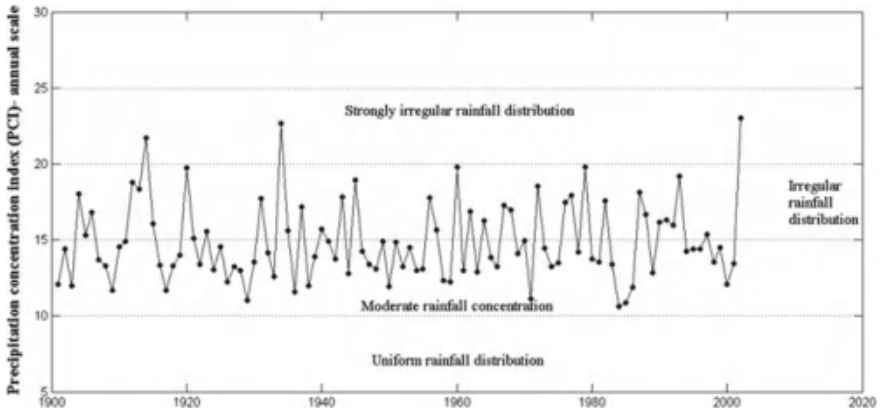

Fig. 6 Precipitation concentration index (PCI) of annual rainfall (1901–2002)

4 Conclusions

In this study, various statistical analyses were done to determine the rainfall trends and patterns in Tuticorin district, Tamil Nadu, for 102 years (1901–2002). The annual rainfall in this area varied from 646 to 1389 mm, with a normal annual rainfall of 982 mm. The north-east monsoon has a large contribution (43%), and the least contribution (6%) is realised during winter monsoon. Mann–Kendall's and Sen's slope tests showed no significant trend for all months except January. The precipitation concentration index indicates that the rainfall concentration in the Tuticorin district is moderately concentrated. Some significant irregularities in annual precipitation were observed for all the monsoon seasons. The departure analysis suggests a decreasing trend in extreme climate, and no severe drought was found over the past 102 years. The rainfall anomaly index shows that Tuticorin mostly enjoys a normal amount of

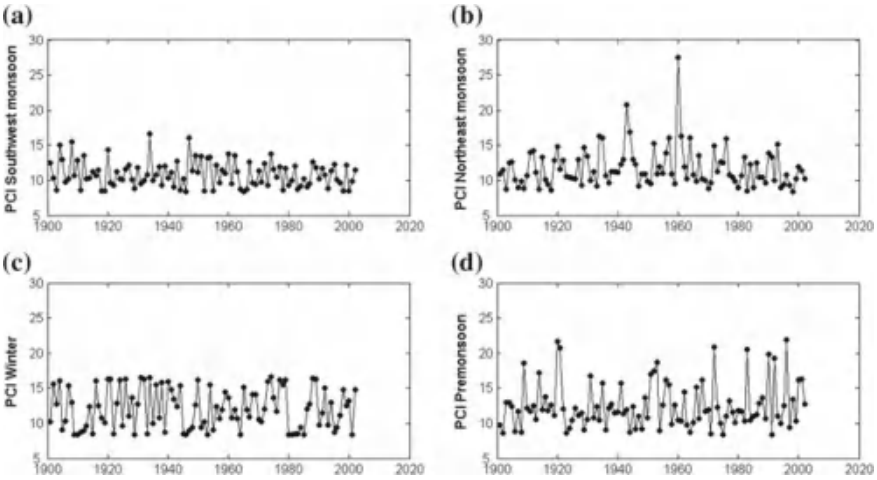

Fig. 7 Precipitation concentration index (PCI) of seasonal rainfall **a** SWM, **b** NEM, **c** Winter and **d** Pre-monsoon

rainfall ranging from −0.49 to 0.49. After analysing the trend of rainfall for the past 102 years, it can be predicted that this region will face no major change in trend in the near future.

References

1. IPCC.: The Physical Science Basis. Contribution of Working Group I to the Fourth Assessment Report of the Intergovernmental Panel on Climate Change. Cambridge University Press, Cambridge, United Kingdom and New York, NY, USA, p. 996 (2007)
2. Kishtawal, C.M., Krishnamurti, T.N.: Diurnal variation of summer rainfall over taiwan and its detection using TRMM observations. J. Appl. Meteorol. **40**(3) (2001)
3. Briffa, K.R., van der Schrier, G., Jones, P.D.: Wet and dry summers in Europe since 1750: evidence of increasing drought. Int. J. Climatol. **29**, 1894–1905 (2009)
4. Vasiliades, L., Loukas, A., Patsonas, G.: Evaluation of a statistical downscaling procedure for the estimation of climate change impacts on droughts. Nat. Hazards Earth Syst. Sci. **9** (2009)
5. Zhang, Q., Xu, C.Y., Gemmer, M., Chen, Y.D., Liu, C.: Changing properties of precipitation concentration in the pearl river Basin. China Stoch. Environ. Res. Risk Assess **23**(3), 377–385 (2009)
6. Ghahraman, B.: Time trend in the mean annual temperature of Iran. Turk. J. Agric. For. **30**, 439–448 (2006)
7. Zhang, L., Zhou, T.: An assessment of monsoon precipitation changes during 1901–2001. Clim. Dyn. **37**, 279–296 (2011)
8. Nasri, M., Modarres, R.: Dry spell trend analysis of Isfahan province. Iran. Int. J. Climatol. **29**, 1430–1438 (2009)
9. Sonali, P., Kumar, D.N.: Review of trend detection methods and their application to detect temperature changes in India. J. Hydrol. **476**, 212–227 (2013)
10. Wang, W., Bobojonov, I., Härdle, W.K., Odening, M.: Testing for increasing weather risk. Stoch. Environ. Res. Risk Assess. **27**, 1565–1574 (2013)

11. Guhathakurta, P., Rajeevan, M.: Trends in rainfall pattern over India. Int. J. Climatol. **28**, 1453–1469 (2008)
12. Joshi, M.K., Pandey, A.C.: Trend and spectral analysis of rainfall over india during 1901–2000. J. Geophys. Res.: Atmosph. **116**, D06104 (2011)
13. Sarkar, S., Kafatos, M.: Inter annual variability of vegetation over the indian sub-continent and its relation to the different meteorological parameters. Remote Sens. Environ. **90**, 26–280 (2004)
14. Parthasarathy, B., Dhar, O.N.: Secular variations of regional rainfall over India. Q. J. R. Meteorol. Soc. **100**, 245–257 (1974)
15. Pal, I., Al-Tabbaa, A.: Assessing seasonal precipitation trends in India using parametric and non-parametric statistical techniques. Theor. Appl. Climatol. (2010)
16. Thomas, J., Prasannakumar, V.: Temporal analysis of rainfall (1871–2012) and drought characteristics over a tropical monsoon-dominated state (Kerala) of India. J. Hydrol. (2016)
17. Mann, H.B.: Nonparametric tests against trend. Econometrica **13**(3), 245–259 (1945)
18. Kendall, M.G.: Rank correlation methods. Griffin, London (1975)
19. Theil, H.: A rank invariant method of linear and polynomial regression analysis, Part 3. Nederl. Akad. Wetensch. Proc. **53**, 1397–1412 (1950)
20. Sen, P.K.: Estimates of the regression coefficient based on Kendall's Tau. J. Am. Stat. Assoc. **63**, 1379–1389 (1968)
21. Raghunath, H.M.: Hydrology. New Age International Publishers, New Delhi, pp. 221–234 (2006)
22. Thomas, T., Nayak, P.C., Ghosh, N.C.: Spatiotemporal Analysis of drought characteristics in the bundelkhand region of central india using the standardized precipitation index. J. Hydrol. (2015)
23. Van Rooy, M.P.: A rainfall anomaly index (RAI) independent of time and space. Notos **14**, 43–48 (1965)
24. Oliver, J.E.: Monthly precipitation distribution: a comparative index. Prof. Geogr. **32**(3), 300–309 (1980)
25. Attri, S.D., Tyagi, A.: Climate profile of India. Contribution to the Indian Network of Climate Change Assessment (National Communication-II), Ministry of Environment and Forests, India Meteorological Department (2010)
26. Thomas, T., Jaiswal, R.K., Nayak, P.C., Ghosh, N.C.: Comprehensive evaluation of the changing drought characteristics in Bundelkhand region of Central India. Meteorol. Atmos. Phys. **127**(2), 163–182 (2015)

Rainfall Projection in Yamuna River Basin, India, Using Statistical Downscaling

Siddharth Chaudhary, A. Agarwal and Tai Nakamura

Abstract This paper exhibits a strategy to build up a downscaling model using the artificial neural network (ANN) to obtain a projection of monthly mean precipitation (MMP) at river basin scale. Moreover, we establish an association between local climate variables and large-scale variables known as atmospheric circulation variables using statistical downscaling. National Centers for Environmental Prediction (NCEP) reanalysis data was applied on the model for calibration and validation for the time frame of January 1971 to December 2005. Similarly, RCP 4.5 scenario of CanCM4 was used for future projection till December 2035. The model developed shows the value of the coefficient of determination as 0.988 for calibration and for validation 0.883. Therefore, we accept the model and it is used for projection and forecasting of precipitation till 2035 on the Yamuna river basin.

Keywords Statistical downscaling · Artificial neural network
Global circulation model · Climate change

1 Introduction

In recent past, many studies have been conducted on finding an appropriate downscaling technique for projection of monthly precipitation at river basin scale [1–3]. The projected rainfall at basin scale is used for many scientific purposes such as climate change impact assessment [4], drought analysis [3] and flood frequency analysis [5]. In the climate change studies, global circulation models (GCMs) is generally

S. Chaudhary (B) · T. Nakamura
Remote Sensing and GIS, Asian Institute of Technology, Klong Luang, Thailand
e-mail: chaudharysiddharth@outlook.com

A. Agarwal
Institute of Earth and Environmental Science, University of Potsdam, Potsdam, Germany

A. Agarwal
Research Domain Transdisciplinary Concepts & Methods, Potsdam Institute
for Climate Impact Research, Telegrafenberg, Potsdam, Germany

M. Rathinasamy et al. (eds.), *Water Resources and Environmental Engineering II*,
https://doi.org/10.1007/978-981-13-2038-5_2

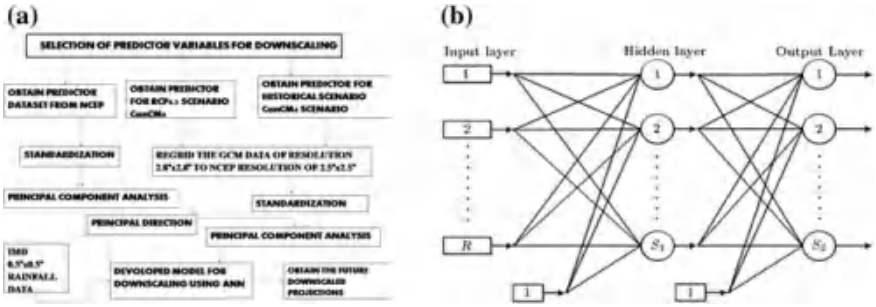

Fig. 1 **a** Methodology for ANN downscaling; **b** MLP model structure

used because it simulates past, present and future time series of all the climate variables across the globe. The results simulated by the GCM are generated, keeping all the atmospheric forcing both internal and external, various scenarios for greenhouse gases and also the social and economical changes. The resolution of GCM data is at a coarser resolution, and hence, we cannot use it for studying the climate change impact assessment on hydrological regime of a river basin. Downscaling, a statistical and dynamical approach, is used to draw high-resolution information from coarser resolution variables [6]. In dynamic downscaling, we are able to embed the regional climate model (RCM) into GCM. This technique makes use of the numerical meteorological model to show that how local weather conditions are affected due to change in global pattern. There are many advantages of dynamic downscaling but due to high computational time and its complexity, it is not a very popular method. Whereas statistical downscaling is a technique in which an empirical relationship is established between the predictors and predictands. Predictors are the atmospheric variables which are generated by the GCM, and predictands are regional climate data. Predictors like mean sea level pressure, specific humidity, geopotential height, air temperature are related to the point scale variables called predictands like rain gauge stations as shown in Fig. 1. The relationships established are finally used for forecasting the information regarding climate for the future period. Wilby et al. [7] give some implicit assumptions in statistical downscaling. These assumptions are listed below:

1. The predictors are variables of relevance and are realistically modelled by GCM.
2. The predictors employed fully represent the climate change signal.
3. The relationship is valid under altered conditions.

2 Methodology

The model used for projecting rainfall over the Yamuna river basin in this study is artificial neural network (ANN). The model used is a non-regression model, and it helps in establishing a relationship between the predictors and predictands. ANN model works similar to the biological neural network system.

ANN model can be trained using backpropagation method. It is generally used when we need to do supervised learning. This method is more efficient in finding the gradient of the error function. The methodology of downscaling using the ANN is shown in Fig. 1a.

2.1 Multilayer Perception Network

MLP is also known as a feedforward network. It is based on the mapping input pattern space to output space. In this method, the information is transferred with the help of the connections between the neurones in the forward direction only. This kind of network does not have any feedback or memory. Figure 1b shows three layer MLP.

2.2 Standardisation

Once the potential predictors are selected, they are needed to be standardised. The main purpose of standardisation is to reduce the systematic biases in the variance and mean of GCM outputs in correspondence to the observed or NCEP data. Standardisation is applied before statistical downscaling is applied. Standardisation is applied on predictor variable for the baseline period by subtracting each data by its mean and dividing it by standard deviation. This method has a major limitation due to its consideration of biases only in mean and variances and not in other statistical parameters.

2.3 Principal Component Analysis

For the development of the empirical or statistical relationship, we cannot use the data directly. There are mainly two reasons behind this: (i) multidimensionality and (ii) multicollinearity.

Computational time required for the analysis is increased due to multidimensionality. It is observed that there is an increase in the sparseness of the data and this affects the output. It is really important to know the internal data pattern and its variability. If the data is reduced without considering the above two, then the accuracy of the model will reduce. Multicollinearity shows a high correlation between various predictors and may lead to solving these problems before we establish any statistical relationship.

PCA is a very important tool used in statistical downscaling studies [8]. It is used to for reducing the dimensions and multicollinearity of the data. PCA generates principal components which have almost similar variability as compared to the original data by analysing and identifying the patterns in the data.

3 Study Area and Data Used

The study has been conducted for the Yamuna river basin which is a sub-basin of Ganga river basin and is located in north-western part of India as shown in Fig. 2a. Yamuna basin lies between 22.50°N to 32.00°N latitude and 73.20°E to 81.50°E longitude. The total area covered by the basin is 3,66,233 km^2 which is approximately 10.7% of Ganga basin. There is great variation in the elevation of land surface ranging from 62 to 6288 m above mean sea level. The main source of Yamuna river lies in the Yamunotri glacier (Mussorie range) in the Uttarakhand, India. The following states fall in the boundary of the Yamuna basin: Himachal, Haryana, Rajasthan, Madhya Pradesh, Uttar Pradesh and Uttarakhand. The percentage of the area covered by the states is shown in Fig. 2b, and the Yamuna basin is shown in Fig. 2c.

Annual rainfall in the Yamuna basin shows variations ranging from 400 to 1200 mm. Moreover, the basin is highly influenced by the event of south-west monsoon during months of June and September due to which the basin gets replenished. Winter rainfall in this region is very less. The rainfall distribution shows an increasing nature from north-west to south-east direction. The climatic condition of the basin can be broadly classified into three categories: (a) Humid: for upstream Himalayan catchment; (b) Semi-Arid: north-west to western catchment; and (c) Sub-Humid: south-west catchments. The mean maximum temperature of the basin is 24 to 42.4 °C and the mean minimum temperature is −1 to 11.0 °C.

4 Data Used

The global circulation model (GCM) used in the study is developed by Canadian centre for climate modelling and analysis (CanCM4) [9]. The spatial resolution of GCM used is 2.8125° × 2.8125°. Data for historical scenarios are extracted for the period of January 1971–December 2005, and for RCP 4.5, it is extracted for January 2016–December 2035. The GCM is represented in the form of 20 grid points and is shown in Fig. 3. The list of predictor variables used for downscaling precipitation data over Yamuna river basin is shown in Table 1. The data is available freely and can be downloaded from www.ccma.bc.ec.gc.ca.

Predictors used in the study were selected on the basis of the study conducted by Anandhi et al. [1]. A dataset of the predictors for the period of January 1971 to December 2004 over the area from 22.50°N to 32.00°N and from 73.20°E to 81.50°E is obtained from NCEP. The NCEP data is represented in the form of 12 grid points and is in monthly scale. The resolution of the NCEP data is 2.5° × 2.5°. The precipitation data is in gridded format with a resolution of 0.5° × 0.5° and it is taken from Indian Metrological Department (IMD). For the study purpose, we regrid the GCM data points to NCEP data points.

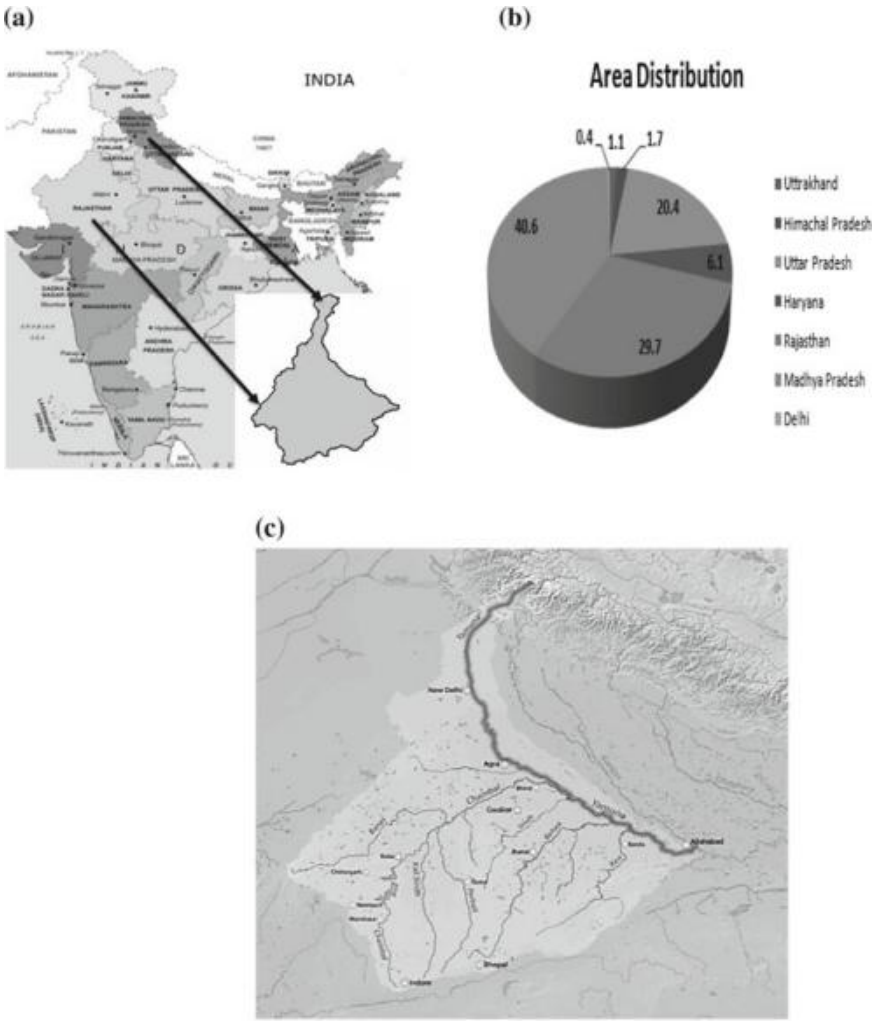

Fig. 2 **a** Represents the location of study area in the context of Indian topology; **b** represents the area distribution of Yamuna river Basin state-wise; **c** geographical location of Yamuna river basin

5 Results

5.1 Calibration and Validation

The ANN model was developed for the Yamuna river basin, and the model was calibrated for the time period (1971–1990), validated for 1991–2005. Maximising the efficiency of the model is the main objective of the method. The time series

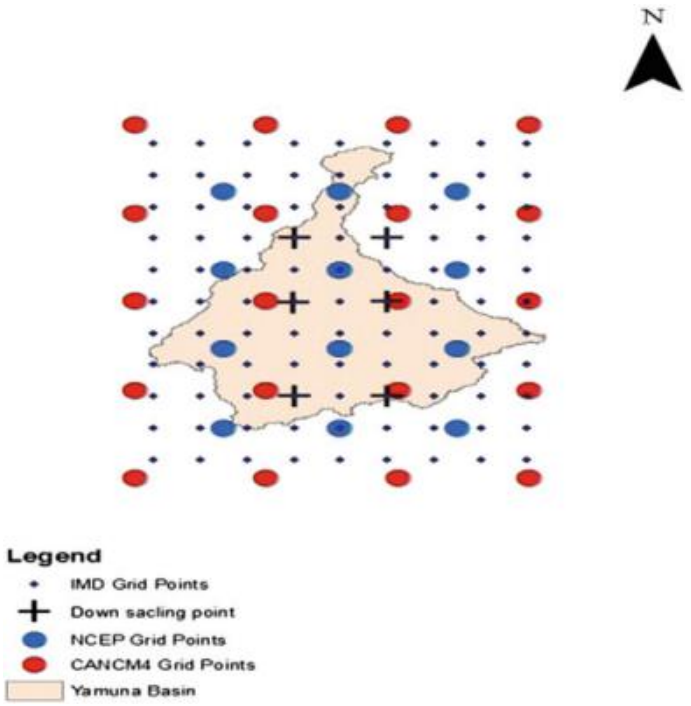

Fig. 3 Geographical position of NCEP grid points covering the Yamuna basin

Table 1 List of predictor variables

Predictor variable	Pressure level (mb)
Air temperature	1000,850,500,250
Eastward wind	1000,850,500,250
Northward wind	1000,850,500,250
Geopotential height	1000,850,500,250
Surface temperature	
Mean sea level pressure	

Team, E. W. (n.d.). Physical Sciences Division. Retrieved, from https://www.esrlnoaa.gov/psd/data/gridded/data.ncep.reanalysis.html

plot for observed and simulated rainfall for both calibration and validation period is shown in Fig. 4c, d.

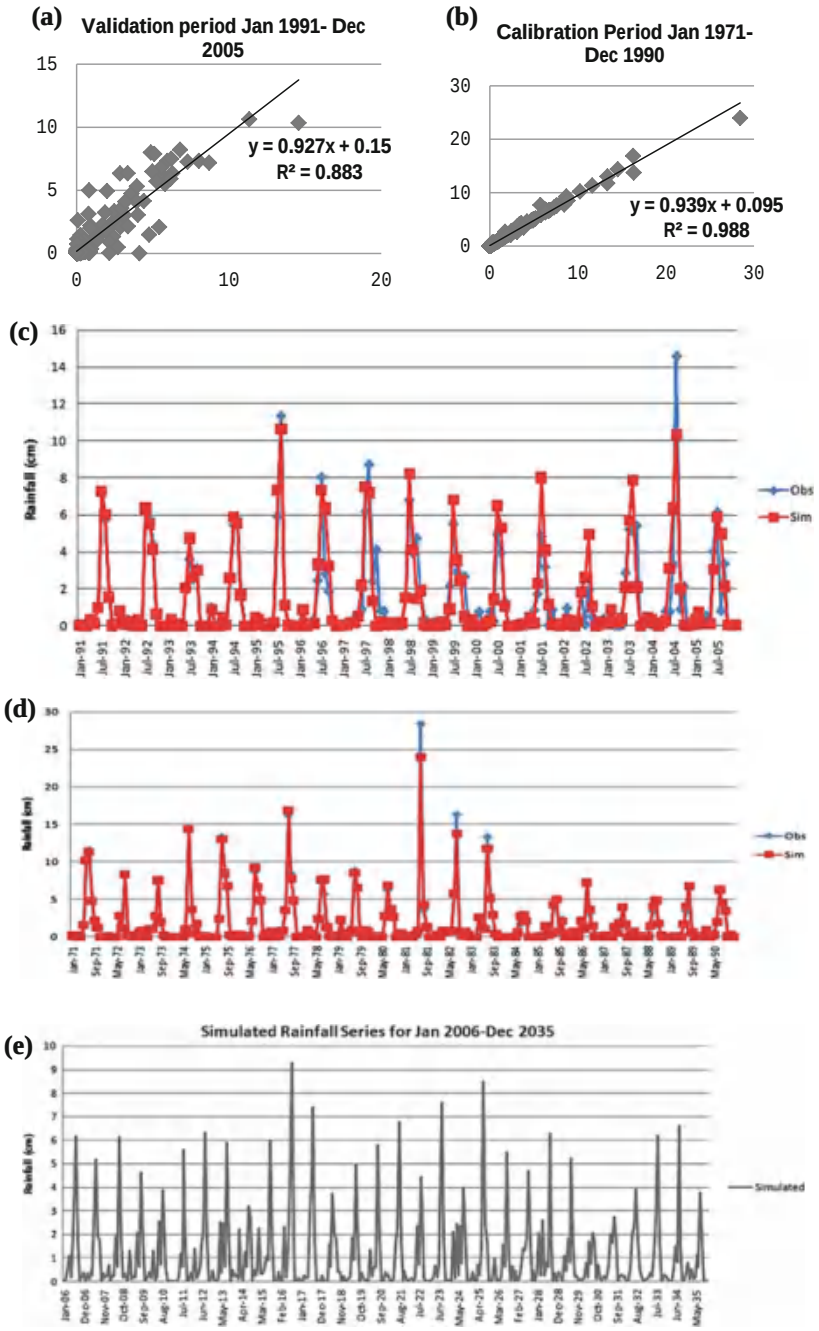

Fig. 4 **a** Scatter plot for calibration period, **b** scatter plot for validation period, **c** observed and simulated rainfall for 1971–1991, **d** observed and simulated rainfall for 1991–2005, **e** projected rainfall for 2006–2035

Monthly observed and simulated precipitation was compared at six different locations in the basin. Comparison for station "X" is shown in this paper. It is observed that observed and simulated results show a similar trend for both calibration and validation period. The developed model shows satisfactory results, and the statistical analysis for the calibration and validation period can be seen in the table. The coefficient of determination (R^2) is calculated, and the result obtained is within an acceptable range. Due to this, we accept the model and it is used for projection or forecasting of precipitation till 2035 on the river basin which is shown in Fig. 4e. Scatter plot for calibration and validation period is shown in Fig. 4a, b.

6 Conclusion

For the present study, we have downscaled GCM output to precipitation at a finer resolution of 0.5 × 0.5 over Yamuna river basin. This task is achieved by applying statistical downscaling using the artificial neural network. The results show that simulated rainfall using ANN for CanCM4 historical scenarios provides a good match with the observed data. For the future projection under RCP4.5 scenarios, it is observed that there will be a decrease in rainfall. The projected rainfall may create a hypothesis that wet area will get wetter and dry area will get drier. The projection shows a significant trend and shows that there will be a major change in the magnitude and pattern of rainfall. The model developed simulated satisfactory results but failed to capture extreme events. This method needs to be modified so that it will be able to capture extreme events. The reason for this failure might be due to the use of principal component analysis. PCA neglects few components which show a small percentage of original variability but these components might be important for explaining extreme events. The overall contribution of this study is a projection of rainfall at a finer resolution till the year 2035. Rainfall projection can be used by policymakers for calculating water availability at the regional level and for inter-basin water transfer. It can further be used for management of agricultural water, hydraulic structure design. It is advised to use different types of downscaling models, GCM and emission scenarios when we need to study climate change.

Acknowledgements This research was funded by Deutsche Forschungsgemeinschaft (DFG) (GRK 2043/1) within the graduate research training group Natural risk in a changing world (NatRiskChange) at the University of Potsdam (http://www.uni-potsdam.de/natriskchange).

References

1. Anandhi, A., Srinivas, V.V., Nagesh Kumara, D., Ravi, N.: Role of predictors in downscaling surface temperature to river basin in India for IPCC SRES scenarios using support vector machine. Int. J. Climatol. **29**, 583–603 (2009)
2. Lakhanpal, A.: Statistical downscaling of GCM outputs using wavelet based model. Doctoral dissertation, Indian Institute of Technology, Delhi (2015)
3. Sehgal, V., Sridhar, V., Tyagi, A.: Stratified drought analysis using a stochastic ensemble of simulated and in-situ soil moisture observations. J. Hydrol. **545**, 226–250 (2017)
4. Benestad, R.E., Hanssen-Bauer, I., Forland, E.J.: An evaluation os statistical models for downscaling precipitation and their ability to capture long-term trends. Int. J. Climatol. **2795**, 649–655 (2007)
5. Coulibaly, P., Dibike, Y.B.: Downscaling of global climate model outputs for flood frequency analysis in the Saguenay river system. Final Project Report prepared for the Canadian Climate Change Action Fund, Environment Canada, Hamilton, Ontario, Canada (2004)
6. Chu, J.T., Xia, J., Xu, C.Y., Singh, V.P.: Statistical downscaling of daily mean temperature, pan evaporation and precipitation for climate change scenarios in Haihe River, China. Theor. Appl. Climatol. **99(**1–2), 149–161 (2010)
7. Wilby, R.L., Wigley, T.M.L.: Downscaling general circulation model output: a review of methods and limitations. Prog. Phys. Geogr. **21**, 530–548 (1997)
8. Agarwal, A.: Hydrologic regionalization using wavelet based multiscale entropy technique. Doctoral dissertation, Indian Institute of Technology, Delhi (2015)
9. Lakhanpal, A., Sehgal, V., Maheswaran, R., Khosa, R., Sridhar, V.: A non-linear and non-stationary perspective for downscaling mean monthly temperature: a wavelet coupled second order Volterra model. Stoch. Env. Res. Risk Assess. **31**(9), 2159–2181 (2017). https://doi.org/10.1007/s00477-017-1444-6

Rainfall Trend Analysis Using Nonparametric Test: A Case Study of Malegaon City

Preeti Ramkar and S. M. Yadav

Abstract Rainfall is the important factor in hydrological cycle having spatial and temporal variability. The present study deals with the identification of nature of rainfall trend at Malegaon. The study area is categorized as semiarid region having an area of 1825.13 km^2. The average annual rainfall for Malegaon is 580.5 mm and prone to drought. In this study, daily rainfall data of Malegaon for period of 34 years were collected and analyzed. The total annual rainfall series was checked for normality and serial correlations before applying trend tests. The trend of rainfall time series of total monthly rainfall is obtained by applying Mann–Kendall test and Sen's slope test. The investigation is based on the results of the monthly rainfall data using non parametric test. The nature of rainfall trends for long period of Malegaon shows decreasing trend. Further, the overall variability in the total annual rainfall has been quantified by computing rainfall variability index which shows most of the years of the study area as dry period.

Keywords Rainfall trend analysis · Malegaon · Rainfall variability
Mann–Kendall · Sen's slope

1 Introduction

The rainfall is a major part of hydrologic cycle, and its variability on temporal and spatial scales is of prime importance considering both scientific and socioeconomic perspectives. There is huge variation in rainfall pattern across the country, with annual rainfall ranging from 12,000 mm in eastern side to less than 100 mm in the western side of India. Due to such vast variability observed in the precipitation pattern across the country, the assessment of spatial and temporal variations in rainfall on

P. Ramkar (B) · S. M. Yadav
Civil Engineering Department, SVNIT, Surat, India
e-mail: preeti.ramkar@gmail.com

S. M. Yadav
e-mail: shivnam27@gmail.com

M. Rathinasamy et al. (eds.), *Water Resources and Environmental Engineering II*,
https://doi.org/10.1007/978-981-13-2038-5_3

basin scale is of vital importance for effective management of water resources in the region. The variability and trends in precipitation pattern were studied by various researchers across the globe [1–4]. In this study, they have analyses rainfall series for the period of 1871–2000 for the statistical characteristics and long term changes over Indian monsoon. Guhathakurta et al. [5] performed linear trend detection tests for 36 meteorological subdivisions of India for a period, of 102 years from 1901 to 2003, and reported significant decreasing trend for Jharkhand and other two subdivisions, while significant rising trend for Gangetic West Bengal, West, and other subdivisions during the southwest monsoon. Machiwal and Jha [6] comprehensively presented different statistical tests for finding data time series properties of maximum daily and annual rainfall at Kharagpur, West Bengal state of India. Kumar and Jain [3] from their study on precipitation trends across major Indian River basins reported that out of 22 basins, 6 basins showed increasing trends, while 15 basins depicted decreasing trend in annual rainfall. A decrease of about 2.59% was observed in the annual precipitation over entire Madhya Pradesh, India, from 1901 to 2002 [7], while no significant change was reported in the hilly state of Assam, India, of the same period [8]. Thomas et al. [9] from their study shows that variability of rainfall for centrally located Narmada basin has positive trend at 95% significance level having Z value 3.66 over entire the basin. Meshram et al. [2] examined rainfall variability spatially and temporally using monthly rainfall data for 102 years (1901–2002) for sixteen stations in the state of Chhattisgarh, India. In the present study, the total monthly rainfall was analyzed to determine the variations and trend in occurrence of rainfall for Malegaon city. The identification of nature of trend in total monthly rainfall is done by using Mann–Kendall and Sen's slope estimator nonparametric test. Along with this, the variability index over the study area is also found out.

2 Study Area

Malegaon is the crowded city and a municipal corporation of Nashik district of Maharashtra, India. The map of the study area is shown in Fig. 1. The study area is the second largest city of Nashik district having population of 4.71 lakhs. It is placed 108.63 km away to the northeast of Nasik. The study area is 1825.13 km^2 and surrounded by Chalisgaon to eastern side and Satana and Kalvan to the western side. It includes 155 big villages and 76 small villages. It is on the Mumbai-Agra National Highway (NH-3) at the junction of the Mausam and Girna rivers, at an elevation of 438 m (1437 feet) having latitude 18.42N and longitude 77.53E. It is based at around 280 km northeast of the Maharashtra state capital Mumbai. Malegaon has good network with nearer cities like Nashik, Manmad, Mumbai, and Dhule. Due to the growing population, the city has all district administration offices. It has an average literacy rate of more than 70% that is higher than national rate of literacy. The annual average rainfall of it is 580.5 mm. There are two major projects such as Chankapur and Punad and three minor projects namely Haranbari, Kelzar, and

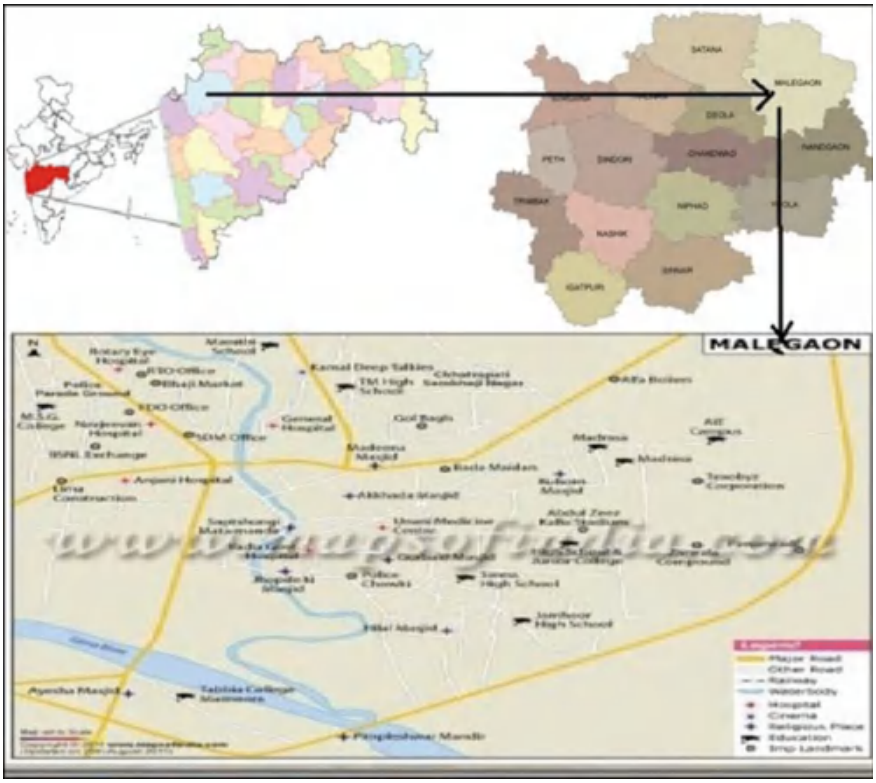

Fig. 1 Study area Malegaon (*Source* Maps of India)

Nagasakya to the upstream of Girna dam. The main drinking water demand of the study are is fullfilled by Chankapur dam and remaining by lift scheme from Girna dam.

3 Materials and Methodology

The main aim of this study is to identify nature of trend by the use of statistical nonparametric tests, i.e., Mann–Kendall test and Sen's slope test, and variability of rainfall based on monthly rainfall data of Malegaon for 34 years.

3.1 Mann–Kendall Test

Mann–Kendall test is most predominantly used test for trend analysis of any hydroclimatic series for checking spatial variation and temporal deviation. The Mann–Kendall test is a nonparametric test for defining a trend in a time series without indicating the type of trend, i.e., linear or nonlinear. The null hypothesis proposed is that the time series has *no trend*. The alternative hypothesis is that the time series has either an upward or downward trend. Consider the annual time series X_t, $t=1, 2,\ldots, n$. Each value of the series X_t is compared with all subsequent values X_{t+1}, and a new series is generated and S is calculated as follows:

$$s = \sum_{k=1}^{n-1} \sum_{j=k+1}^{n} \operatorname{sgn}\left(x_j - x_k\right) \tag{1}$$

$$\operatorname{sgn} = \begin{cases} +1 & \text{if}\left(x_j - x_k\right) > 0 \\ 0 & \text{if}\left(x_j - x_k\right) = 0 \\ -1 & \text{if}\left(x_j - x_k\right) < 0 \end{cases}$$

The statistic of test, Z, is calculated as follows:

$$z = \begin{cases} \frac{s-1}{\sqrt{\text{Var}(S)}} & \text{if } s > 0 \\ 0 & \text{if } s = 0 \\ \frac{s+1}{\sqrt{\text{Var}(s)}} & \text{if } s < 0 \end{cases} \tag{2}$$

The Mann–Kendall test is a two-tailed statistical test, where the test should be correlated by a critical value of standard normal deviate, $Z_{\alpha/2}$. In case $Z_{\alpha/2} \leq Z \leq Z_{1-\alpha/2}$, the null hypothesis H_0 is approved by the use of percent error. If the null hypothesis is rejected, the time series X_t will have increasing or decreasing trend when S is positive or negative respectively.

3.2 Sen's Slope Estimator

The nonparametric robust estimate for quantifying monotonic trend in hydrologic time series given by Hirsch et al. [10] is given by

$$\beta = \text{Median}\left(\frac{X_j - X_i}{j - i}\right) \quad \forall i < j \tag{3}$$

where

β	slope between data points,
X_i and X_j, X_i	data measurement at time i,
X_j	data measurement at time j, and
j	time after time i. A positive value of β shows an increasing trend, and a negative value depicts a decreasing trend [11].

3.3 Variability Index

The variability index of rainfall is calculated by the use of standardized precipitation departure. This index helps to segregate the available rainfall time series into different climatic conditions such as 'very dry climatic year,' 'normal climatic year,' 'wet climatic year,' and 'very wet climatic year' [12]. The rainfall variability index (D) was calculated as follows:

$$D_i = \frac{(P_i - \mu)}{\sigma} \tag{4}$$

where

D_i	rainfall variability index for the year,
P_i	annual rainfall for a year i,
μ	mean, and
σ	standard deviation of annual precipitation series.

The vaule of D which ranges in between +0.5 to –0.5 is characterized as a normal year, where as the values of D between +0.5 to +1 and more than +1 indicate the wet year and very wet year respectively. Similarly, the values of D between -0.5 to -1 and less than -1 indicate the 'dry year' and 'very dry year,' respectively [12].

4 Results and Discussion

The significant falling trend of precipitation is observed for the months of January, May, June, October, and November, whereas in the months of July, August, and September, remarkable increasing trend is seen for monthly rainfall for 1981–2014. Figure 2 shows monthly rainfall for different months for entire period of the study area. The preliminary statistical analysis were done using mean, standard deviation, coefficient of variation, skewness, and kurtosis which is given as Table 1. The trend analysis results of both Mann–Kendall test and Sen's slope test are given in Table 2. The results obtained from Mann–Kendall and Sen's slope estimator test show negative value for June and October months, thereby representing a downward trend. The July, August, and September months show rising trends. The rainfall trend using

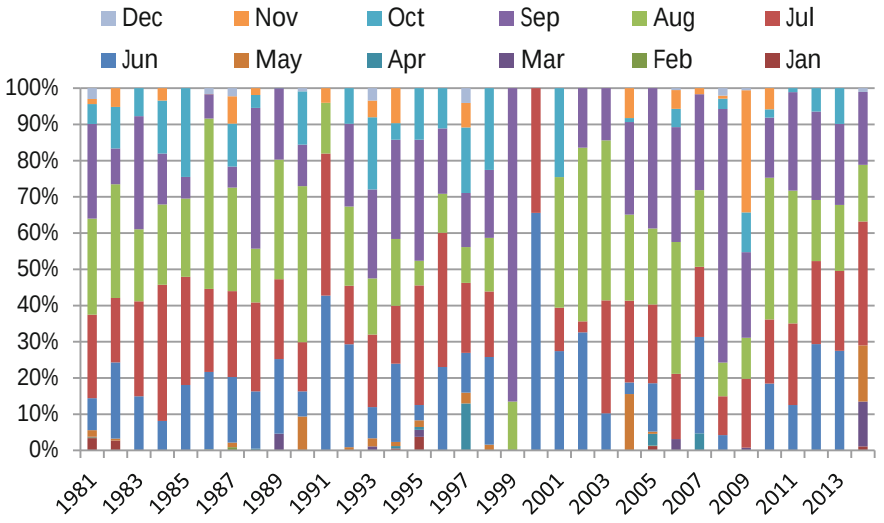

Fig. 2 Monthly rainfall for different months for period 1981–2014

Table 1 Statistical properties of monthly rainfall at Malegaon for 1981–2014

Month	Mean (mm)	Standard deviation	CV (%)	Skewness	Kurtosis
January	3.585	7.083	197.560	1.731	1.441
February	3.382	8.562	253.123	3.454	11.614
March	5.032	14.426	286.675	3.402	11.673
April	0.944	1.891	200.310	2.227	4.458
May	6.482	15.977	246.474	3.954	17.238
June	109.806	64.091	58.367	0.901	0.939
July	174.762	65.116	37.260	0.900	2.073
August	183.891	98.736	53.693	0.285	−0.650
September	137.944	85.174	61.746	1.106	1.585
October	52.224	44.885	85.948	0.663	−0.470
November	19.915	41.139	206.577	2.503	5.346
December	5.359	12.452	232.371	3.122	10.951

Sen's slope is shown in Fig. 3. January, February, March, April, May, November, and December months show no trend according to Sen's slope test. Minimum monthly average rainfall for 34 years was noted in February (0.91 mm), while maximum rainfall occurs in the month of August (183.89 mm).

Table 2 Trend analysis of total monthly rainfall series of Malegaon

Month	Mann–Kendall Z statistic	P value	Sen's slope value (β)	Nature of trend (β)
January	−0.060	0.664	0	No trend
February	0.142	0.146	0	No trend
March	0.147	0.146	0	No trend
April	0.133	0.168	0	No trend
May	−0.027	0.576	0	No trend
June	−0.152	0.898	−1.33	Decreasing
July	0.230	**0.029**	1.964	Increasing
August	**0.059**	0.319	1.154	Increasing
September	0.198	**0.052**	2.535	Increasing
October	−0.071	0.718	−0.54	Decreasing
November	−0.054	0.658	0	No trend
December	**0.043**	0.384	0	No trend

Bold values indicate that trends are statistically significant at 5% significance level

Fig. 3 Sen's slope trend for different months for period 1981–2014

The rainfall variability index has been computed, and on the basis of it, the periods are classified as normal, dry, wet, very dry, and very wet years of rainfall. The variability in rainfall pattern for the study area by applying rainfall variability index is shown in Fig. 4. It is observed that the study area receives below normal rain, while 24% of time it experienced very dry periods and has resulted in water scarcity conditions. Overall, the rainfall variability in the basin over the period of 33 years (1981–2014) was found to be skewed toward dry condition.

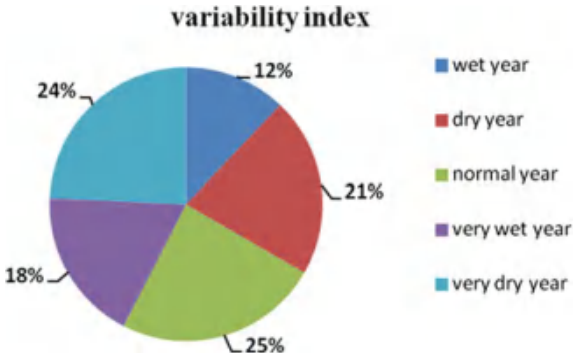

Fig. 4 Distribution of variability index for Malegaon

5 Conclusion

The Mann–Kendall test shows increasing trend in total monthly rainfall for July, August, and September, while decreasing trend is observed for January, May, June, October, and November. Further, four months namely July, August, September, and December show statistically significant trend at 5% significance level. Sen's slope estimator test results show downward trend for the January, March, April, and May months, whereas the July, August, and September months show increasing trend. The months of January, February, March, April, May, November, and December show no trend. The rainfall variability index across the study area is leaning toward normal to dry condition. From results, it is clear that 45% of time dry to very dry condition has been received in the study area, while 25% of time receives normal rainfall. Furthermore, over 70% rainfall occurs in June to September, and remaining months are showing a remarkable decreasing trend. However, the study area reveals other perspectives of drought which will be helpful in management and mitigation of drought condition in this particular area.

References

1. Partal, T., Kahya, E.: Trend analysis in Turkish precipitation data. Hydrol. Process. **20**, 2011–2026 (2006)
2. Meshram, S.G., Singh, V.P., Meshram, C.: Long-term trend and variability of precipitation in Chhattisgarh State, India. Theor. Appl. Climatol. (2016)
3. Kumar, V., Jain, S.K., Singh, Y.: Analysis of long-term rainfall trends in India. Hydrol. Sci. J. **55**, 484–496 (2010)
4. Krishnakumar, K.N., Prasada Rao, G.S.L.H.V., Gopakumar, C.S.: Rainfall trends in twentieth century over Kerala, India. Atmos. Environ. **43**, 1940–1944 (2009)
5. Guhathakurta, P., Rajeevan, M.: Trends in the rainfall pattern over India. Int. J. Climatol. **28**, 1453–1469 (2008)
6. Machiwal, D., Jha, M.K.: Comparative evaluation of statistical tests for time series analysis: application to hydrological time series. Hydrol. Sci. **53**, 353–366 (2008)

7. Duhan, D., Pandey, A.: Statistical analysis of long term spatial and temporal trends of precipitation during 1901–2002 at Madhya Pradesh, India. Atmos. Res. **122**, 136–149 (2013)
8. Goyal, M.K.: Statistical analysis of long term trends of rainfall during 1901–2002 at Assam, India. Water Resour. Manag. **28**, 1501–1515 (2014)
9. Thomas, T., Gunthe, S.S., Sudheer, K.P., Ghosh, N.C.: Analysis of monsoon rainfall variability over Narmada basin in central India: Implication of climate change. J. Water Clim. Chang. **6**, 615–627 (2015)
10. Hirsch, R.M., Slack, J.R., Smith, R.A.: Techniques of trend analysis for monthly water-quality data. Water Resour. Res. **18**, 107–121 (1982)
11. Xu, Z.X., Li, J.Y., Liu, C.M.: Long-term trend analysis for major climate variables in the Yellow River basin*. Hydrol. Process. **21**, 1935–1948 (2007)
12. L'Hôte, Y., Mahé, G., Somé, B., Triboulet, J.P.: Analysis of a Sahelian annual rainfall index from 1896 to 2000; the drought continues. Hydrol. Sci. J. **47**, 563–572 (2002)

Statistical Analysis of Long-Term Temporal Trends of Temperature During 1901–2002 at Kancheepuram in Tamil Nadu (India)

Sathyanathan Rangarajan, Deeptha Thattai, Utkarsh Jaiswal and Nikhil Chaurasia

Abstract In recent years, climate change has impacted globally in the form of increased precipitation, rising temperature and sea level, and withdrawal of glaciers, among others. Kancheepuram district falls under the northeastern agroecological zones of Tamil Nadu. Agriculture is the main occupation and is mainly dependent on the monsoon. Since the potential agricultural yields are predicted to decrease for the projected increase in temperature, the aim of the present study is to investigate potential trends in 102 years of temperature. The statistical analyses have been carried out to detect change point if any and the possible trend in monthly, seasonal, and annual historical series of minimum and maximum temperatures between the years 1901 and 2002. The most commonly used Mann–Kendall test and Sen's slope estimator test are used to detect the trend in the time series. Pettitt's test, standard normal homogeneity test are applied to detect possible change points.

Keywords Kancheepuram · Mann–Kendall test · Sen's slope estimator test Pettitt's test · Standard normal homogeneity test

1 Introduction

Analysis of meteorological conditions is essential to any agricultural work and in particular for livestock industry. Meteorological factors, namely rainfall, temperature, wind speed, relative humidity, affect livestock and agriculture [1–3]. The trend detection in meteorological variables is an important research area, as trends impact the distribution of water across the globe [3, 4]. Though the weather is subject to natural variability, the recent climate change effects add to the unpredictability such as increased frequency of extreme weather events [5, 6]. The rise in temperatures affects the availability of water, ecosystem functions, and global feedbacks [7]. Besides, it

S. Rangarajan (B) · D. Thattai · U. Jaiswal · N. Chaurasia
Department of Civil Engineering, SRM Institute of Science and Technology, Kattankulathur 603203, Tamil Nadu, India
e-mail: sathyanathan.r@ktr.srmuniv.ac.in

M. Rathinasamy et al. (eds.), *Water Resources and Environmental Engineering II*,
https://doi.org/10.1007/978-981-13-2038-5_4

also reduces the frost days in the mid-latitudes with an increase in extreme warm days. Moreover, increase in temperature leads to reduction in precipitation which is disastrous for the tropical regions [8].

2 Study Area

Kancheepuram is a district in the Indian state of Tamil Nadu, with the headquarters situated 72 km (45 miles) southwest of Chennai (Fig. 1) and bounded by Bay of Bengal (east), Vellore and Tiruvannamalai districts (west), Thiruvallur and Chennai districts (north), and Viluppuram district (south). The area of the district is 4,432 km^2. The maximum and minimum temperatures range from 28 to 45 °C and 14 to 24 °C, respectively.

The district is mainly dependent on monsoon rainfall, and the major contribution is from northeast (54%) and southwest (36%) monsoon. The average annual rainfall for the district is 1200 mm [5].

Box plot showing the characteristics of minimum and maximum temperatures is presented in Figs. 2 and 3.

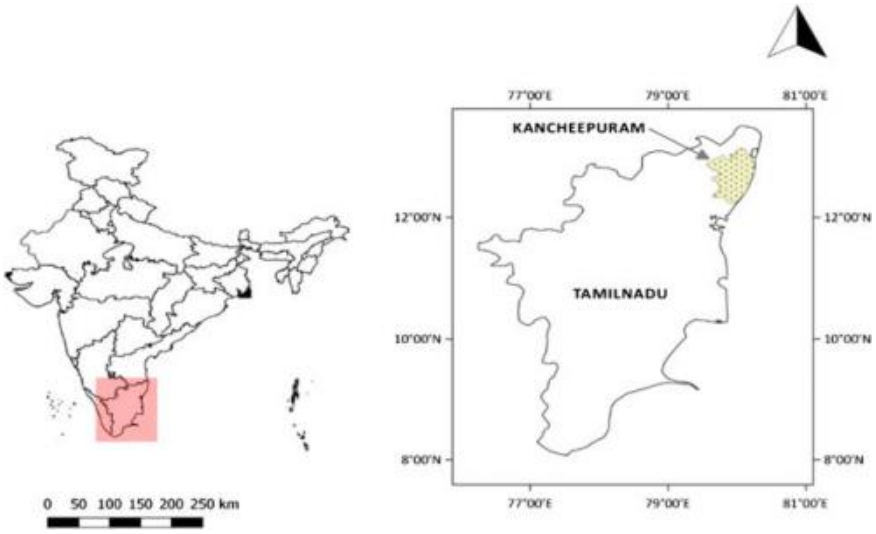

Fig. 1 Location map of Kancheepuram district

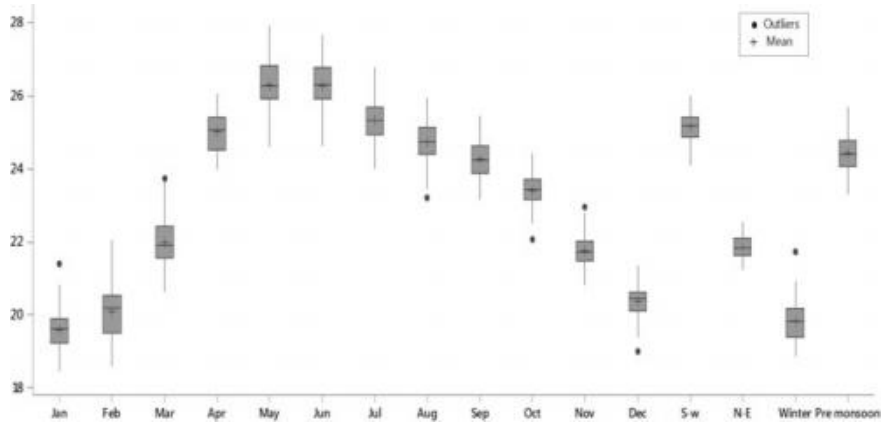

Fig. 2 Box plot of monthly minimum temperatures averaged over years

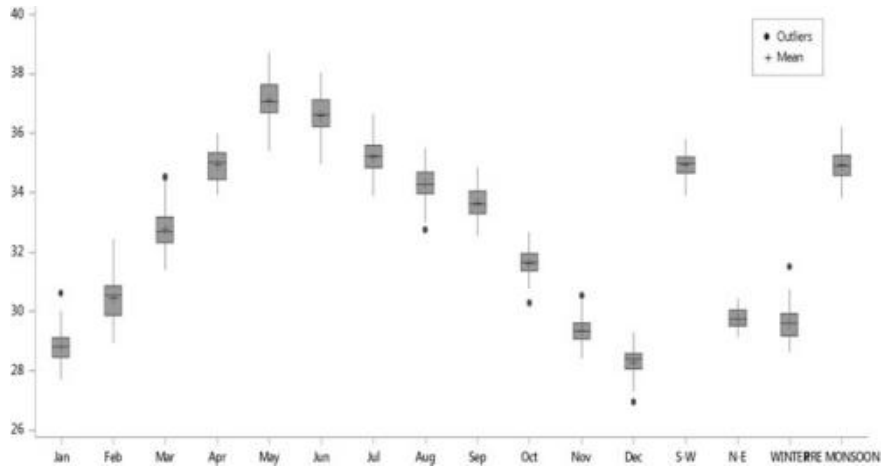

Fig. 3 Box plot of monthly maximum temperatures averaged over years

3 Methodology

3.1 Mann–Kendall's Test

The Mann–Kendall test is employed to detect trends in time series. The null hypothesis, H_0, is that there is no trend in the data. The alternative hypothesis, H_A, is that the data follow an increasing or decreasing trend [9–11]. The Mann–Kendall test statistic is calculated according to:

$$S = \sum_{i=1}^{n} \sum_{j=i}^{i-1} \text{sign}(x_i - x_j). \tag{1}$$

where n is the total length of data, x_i and x_j are two generic sequential data values, and function $\text{sign}(x_i - x_j)$ assumes the following values

$$\text{sign}(x_i - x_j) = \begin{cases} 1, & \text{if } (x_i - x_j) > 0. \\ 0, & \text{if } (x_i - x_j) = 0. \\ -1, & \text{if } (x_i - x_j) < 0. \end{cases} \tag{2}$$

3.2 Pettitt's Test

Pettitt's test is applied to detect a single change point in a meteorological time series with continuous data. It tests the H_0: The T variables follow one or more distributions that have the same location parameter (no change), against the alternative: A change point exists [11, 12]. The nonparametric statistic is defined as:

$$K_T = \max|U_t| \tag{3}$$

where

$$U_t = \sum_{i=1}^{t} \sum_{j=t+1}^{n} \text{sign}(x_t - x_j). \tag{4}$$

$$\text{sign}(x_t - x_j) = \begin{cases} 1, & \text{if } (x_i - x_j) > 0. \\ 0, & \text{if } (x_i - x_j) = 0. \\ -1, & \text{if } (x_i - x_j) < 0. \end{cases} \tag{5}$$

3.3 Sen's Slope Test

This test computes both the slope (i.e., linear rate of change) and intercept according to Sen's method. First, a set of linear slopes is calculated as follows:

$$T_i = \frac{x_j - x_k}{j - k} \quad \text{where } i = 1, 2, 3, \ldots, N \quad \text{and } j > k \tag{6}$$

where x_1, x_2, x_3, …, x_j, x_k, …, x_n are the data values, and the median of N values of T_i series can be obtained as Sen's estimator of slope [11, 13].

4 Analysis of Result

4.1 Result of Change Point Analysis

For the determination of change point in different monthly and seasonal minimum and maximum temperatures, Pettitt's test has been applied. The results are presented in Table 1. It is observed that the minimum temperature series of January, September, October, November, December, and NE monsoon depicted a change point mainly in 1975 and 1977. The change point for a monthly series of minimum and maximum temperature series has been presented in Figs. 4 and 5. The change points occurred in the year 1975 for November and December series, 1977 for January and October series, and 1975 for NE monsoon season. From the analysis, it may be concluded that most of the change points occurred between 1975 and 1980.

Table 1 Results of change point analysis

Period	Minimum temperature			Maximum temperature		
	Pettitt's statistic	Shift	Year of shift	Pettitt's statistic	Shift	Year of shift
January	1,156	Yes	1977	1,170	Yes	1977
February	1,479	Yes	1957	1,475	Yes	1957
March	1,941	Yes	1950	1,947	Yes	1950
April	1,914	Yes	1968	1,917	Yes	1968
May	1,097	Yes	1963	1,070	Yes	1963
June	628	No	–	630	No	–
July	706	No	–	711	No	–
August	655	No	–	666	No	–
September	928	Yes	1985	989	Yes	1985
October	1,127	Yes	1977	1,134	Yes	1977
November	1,249	Yes	1975	1,249	Yes	1975
December	1,494	Yes	1975	1,494	Yes	1975
SW	699	No	–	703	No	–
NE	1,609	Yes	1975	1,597	Yes	1975
Winter	1,355	Yes	1957	1,372	Yes	1957
Pre-monsoon	1,967	Yes	1963	1,971	Yes	1963

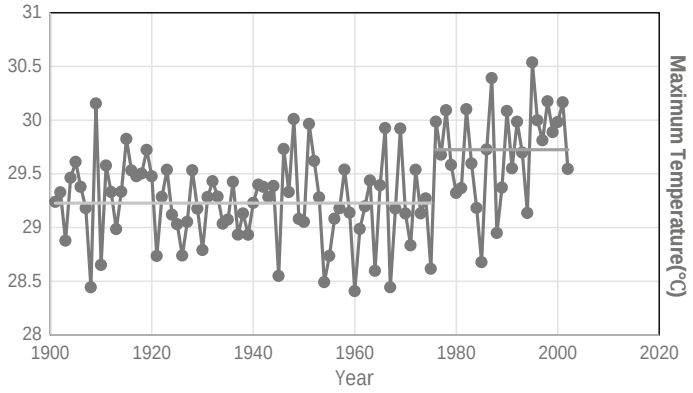

Fig. 4 Change points in maximum temperature series for the month of November

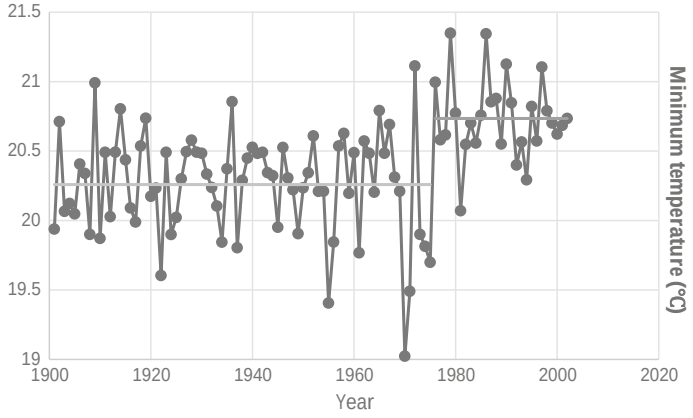

Fig. 5 Change points in minimum temperature series for the month of December

4.2 Trend Detection Analysis

The trend analysis of minimum and maximum temperatures was carried out for three different periods, namely P-1 (1901–1975), P-2 (1955–2002), and P-3 (whole series). For the determination of trend, Mann–Kendall's test has been applied on monthly and seasonal series of minimum and maximum temperatures and compared with the standard value of normal cumulative distribution at 95% confidence level, which is ± 1.96. A test statistic having value more than 1.96 confirms a significant rising trend, while -1.96 confirmed falling trend at 5% significance or 95% confidence level. The test statistics and possible trend in different series of maximum and minimum temperature are presented in Tables 2 and 3.

The minimum temperatures for the period 1901–1975 (P-1) showed a significant falling trend from June to August and SW monsoon series at 5% significance level.

Table 2 Mann–Kendall's test statistics and trend in different periods of minimum temperature series

Period	1901–1975 (P-1)		1955–2002 (P-2)		1901–2002 (P-3)	
	Test statistics	Trend	Test statistics	Trend	Test statistics	Trend
January	−0.40	Rising	3.45	Rising	3.00	Rising
February	1.94	Rising	3.25	Rising	4.91	Rising
March	3.88	Rising	3.63	Rising	7.10	Rising
April	2.72	Rising	4.03	Rising	6.59	Rising
May	0.37	–	3.18	Rising	3.04	Rising
June	−2.08	Falling	2.55	Rising	−1.06	–
July	−2.33	Falling	3.35	Rising	−0.37	–
August	−2.25	Falling	3.58	Rising	0.16	–
September	−1.27	–	3.89	Rising	2.03	Rising
October	−0.47	–	3.08	Rising	2.82	Rising
November	−1.25	–	4.08	Rising	2.96	Rising
December	−0.55	–	3.14	Rising	3.93	Rising
S–W	−2.60	Falling	4.32	Rising	0.81	–
N–E	−0.97	–	4.45	Rising	4.12	Rising
Winter	1.28	–	3.90	Rising	4.76	Rising
Pre-monsoon	2.89	Rising	4.71	Rising	7.10	Rising

The trend analysis confirmed a significant rising trend in all monthly and seasonal series during the period 1955–2002 (P-2). Further, a significant rise was detected in minimum temperature in almost every monthly series (except June, July, and August) and seasonal series (except SW monsoon). The maximum temperature for period 1901–1975 (P-1) showed a significant falling trend in June, July, and SW monsoon series. The trend analysis confirmed a significant rising trend in all monthly and seasonal series during the period 1955–2002 (P-2). Further, a significant rise was detected in maximum temperature in almost every monthly series (except May, June, July, and August) and seasonal series (except SW monsoon).

The monthly and seasonal series of minimum and maximum temperatures when plotted and fitted linearly showed that both series exhibited strong rising trend during periods P-2 and P-3, while insignificant trend was detected in P-1 (Fig. 6).

4.3 Sen's Slope Estimator Test

Sen's slope was computed to know the prevailing trend in monthly and seasonal series of minimum and maximum temperatures. Sen's slope parameters for minimum and

Table 3 Mann–Kendall's test statistics and trend in different periods of maximum temperature series

Period	1901–1975 (P-1)		1955–2002 (P-2)		1901–2002 (P-3)	
	Test statistics	Trend	Test statistics	Trend	Test statistics	Trend
January	−0.34	–	3.45	Rising	3.07	Rising
February	1.92	Rising	3.17	Rising	4.88	Rising
March	3.76	Rising	3.61	Rising	7.03	Rising
April	2.73	Rising	4.05	Rising	6.60	Rising
May	0.40	–	3.23	Rising	3.05	–
June	−2.08	Falling	2.55	Rising	−1.07	–
July	−2.36	Falling	3.33	Rising	−0.39	–
August	−2.27	–	3.64	Rising	0.18	–
September	−1.28	–	3.88	Rising	2.02	Rising
October	−0.44	–	3.11	Rising	2.86	Rising
November	−1.24	–	4.07	Rising	2.96	Rising
December	−0.39	–	3.07	Rising	4.00	Rising
S–W	−2.63	Falling	4.38	Rising	0.17	–
N–E	−0.98	–	4.36	Rising	4.04	Rising
Winter	1.26	–	3.91	Rising	4.79	Rising
Pre-monsoon	2.91	–	4.76	Rising	7.12	Rising

maximum temperature series are presented in Table 4. The analysis of Sen's slope estimator clearly indicated a positive trend in P-2 (1955–2002) and P-3 (1901–2002) periods for both maximum and minimum temperature series, while the same was mostly negative in P-1 (1901–1975).

5 Conclusion

Water resource sector is the most affected sector due to possible climate change as the availability of water is directly influenced by different climatological variables. A warmer climate can also disrupt the ongoing cropping pattern of this area. It may a cause serious threat to the stability of agriculture ecosystem, especially due to increased temperature. In the present study, change point detection using Pettitt's test followed by trend analysis with the help of Mann–Kendall's test has been applied to monthly and seasonal long-term series of minimum and maximum temperatures of Kancheepuram, a district in Tamil Nadu state of India. From the change point analysis, it may be concluded that the minimum and maximum temperatures are

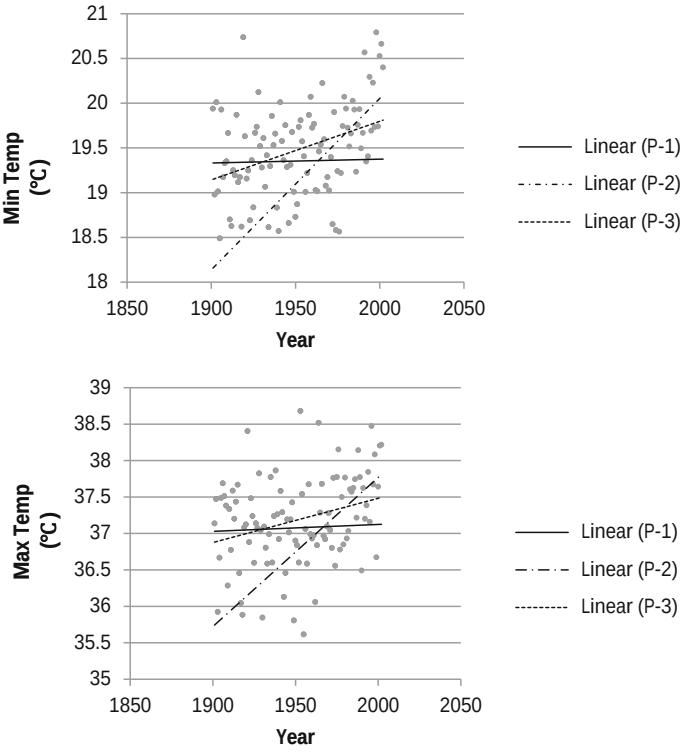

Fig. 6 Fitting of linear trends in minimum and maximum temperature series

equally vulnerable from climate change as monthly (except June, July and August) and southwest monsoon series indicated a change point at 5% significant level.

The result of trend analysis of minimum temperatures concluded that a falling trend was found in few monthly southwest monsoon series in the period 1901–1975 (P-1) that reversed for every monthly and seasonal series with rising trend for the period 1955–2002 (P-2) at 5% significance level. Sen's slope analysis for both minimum and maximum temperatures shows negative slope for monthly and seasonal series in the period 1901–1975 (P-1), which reversed to positive slope for the period 1955–2002 (P-2). From the statistical analysis of change point and trend, it may be concluded the changes in climate would have a direct effect on the crop production. The productivity of the crops may also be hit due to the unusual warming. A warmer climate would also have major adverse effects on water use and availability in these areas.

Table 4 Sen's slope for minimum and maximum temperatures

Period	Minimum temperature			Maximum temperature		
	1901–1975 (P-1)	1955–2002 (P-2)	1901–2002 (P-3)	1901–1975 (P-1)	1955–2002 (P-2)	1901–2002 (P-3)
January	−0.00100	+0.019489	+0.00543	−0.00084	+0.01996	+0.00563
February	+0.00700	+0.020911	+0.01208	+0.00696	+0.02093	+0.01207
March	+0.01154	+0.023999	+0.01573	+0.01115	+0.02432	+0.01576
April	+0.00714	+0.016354	+0.01146	+0.00714	+0.01627	+0.01147
May	+0.00101	+0.025741	+0.00752	+0.00125	+0.02548	+0.00750
June	−0.00713	+0.018968	−0.00200	−0.00710	+0.01894	−0.00204
July	−0.00742	+0.024671	−0.00069	−0.00757	+0.02543	−0.00067
August	−0.00823	+0.026193	+0.00028	−0.00821	+0.02636	+0.00036
September	−0.00373	+0.022540	+0.00397	−0.00374	+0.02247	+0.00396
October	−0.00095	+0.012342	+0.00355	−0.00092	+0.01222	+0.00360
November	−0.00300	+0.021667	+0.00470	−0.00294	+0.02171	+0.00472
December	−0.00071	+0.012157	+0.00495	−0.02639	+0.11476	+0.00500
SW	−0.02639	+0.089366	+0.00120	−0.02639	+0.08936	+0.00030
NE	−0.00470	+0.046253	+0.01400	−0.00477	+0.04617	+0.00460
Winter	+0.00736	+0.040783	+0.01816	+0.00730	+0.04097	+0.00915
Pre-monsoon	+0.02000	+0.068241	+0.03439	+0.01996	+0.06852	+0.01142

References

1. Buhairi Al, M.H.: Analysis of monthly, seasonal and annual air temperature variability and trends in Taiz city—Republic of Yemen. J. Environ. Prot. **1**, 401–409 (2010)
2. Smadi, M.M.: Observed abrupt changes in minimum and maximum temperatures in Jordan in the 20th century. Am. J. Environ. Sci. **2**(3), 114–120 (2006)
3. Sivakumar, T., Thennarasu, A., Rajkumar, J.S.I.: Trend analysis of the climatic parameters (2001–2007) for the Northeastern Zone of Tamil Nadu. Int. J. Environ. Sci. Technol. **2**(3), 83–86 (2012)
4. Smadi, M.M., Zghoul, A.: A sudden change in rainfall characteristics in Amman, Jordan during the mid 1950's. Am. J. Environ. Sci. **2**(3), 84–91 (2006)
5. De, U.S., Dube, R.K., Prakasa Rao, G.S.: Extreme weather events over India in the last 100 years. J. Ind. Geophys. Union **9**(3), 173–187 (2005a)
6. Gallagher, C., Lund, R., Robbins, M.: Change point detection in climate time series with long-term trends. J. Clim. **26**, 4994–5006 (2012). https://doi.org/10.1175/JCLI-D-12-00704.1
7. Hipel, K.W., McLoed, A.I.: Time series modelling of water resources and environmental systems. Elsevier, Amsterdam (1994)
8. Mondal, A., Khare, D., Kundu, S.: Spatial and temporal analysis of rainfall and temperature trend of India. Theor. Appl. Climatol. **122**, 143–158 (2015)
9. Karmeshu, N.: Trend detection in annual temperature and precipitation using the Mann Kendall Test—a case study to assess climate change on select states in the Northeastern United States. Master of Environment Studies Capstone project, University of Pennsylvania USA (2012) http://repository.upenn.edu/mes_capstones/47

10. Libiseller, C., Grimvall, A.: Performance of partial Mann-Kendall Tests for trend detection in the presence of covariates. Environmetrics **13**, 71–84 (2002). https://doi.org/10.1002/env.507
11. Menne, J.M., Williams, C.N.J.: Detection of undocumented change points using multiple test statistics and composite reference series. J. Clim. **18**, 4271–4286 (2005)
12. Pettitt, A.N.: A non-parametric approach to the change-point problem. Appl. Stat. **28**, 126–135 (1979)
13. Yue, S., Pilon, P.: A comparison of the power of the t test, Mann-Kendall and Bootstrap Tests for trend detection. Hydrol. Sci. J. **49**(1), 21–37 (2004)

Evaluation of Different Solar Radiation Estimation Methods for Indian Locations

Sirisha Adamala and Y. V. Krishna Reddy

Abstract This study aims to determine or estimate solar radiation (R_s) for 20 meteorological stations in India and to compare R_s using six equations (Hargreaves, Allen, Hunt, Annandale, Li and sunshine hours based). The required data for the R_s estimation was extracted from CLIMWAT 2.0 software. The data contains a long-term monthly average of maximum air temperature (°C) and minimum air temperature (°C), relative humidity (%), sunshine hours (h/day), wind speed (km/day), effective rainfall (mm/month) and solar radiation (MJ m^{-2} d^{-1}). The estimated values were compared with measured values using two performance indicators, viz. root-mean-squared error (RMSE) and modelling efficiency (ME). The result showed that the sunshine hour-based method performed best among the all R_s estimation methods at almost all stations (except Bangalore, Ludhiana and Silchar). Therefore, R_s estimation method is recommended for Indian locations. However, both the Annandale and Hargreaves methods are performed better than other methods.

Keywords Solar radiation · Sunshine hours · Air temperature
Performance indicator · India

1 Introduction

Solar radiation (R_s) is the primary energy source, which governs many biological and physical processes. Its measurement or estimation is needed in many simulation studies: hydrology, climatology, ecology, agriculture and environment. However, its

S. Adamala
ICAR-National Academy of Agricultural Research Management (NAARM), Rajendranagar, Hyderabad 500030, Telangana, India
e-mail: sirisha.adamala@icar.gov.in

Y. V. Krishna Reddy (B)
Agricultural Engineering Department, Aditya Engineering College, Surampalem, East Godavari, India
e-mail: krishnareddy029@gmail.com

M. Rathinasamy et al. (eds.), *Water Resources and Environmental Engineering II*,
https://doi.org/10.1007/978-981-13-2038-5_5

direct measurement is limited over worldwide meteorological stations due to many factors such as cost, maintenance, labour requirement, tedious, accuracy, calibration requirements and errors [1, 2]. Therefore, a number of methods have been developed in the past for indirect estimation of R_s using variables such as sunshine hours, air temperature, precipitation, relative humidity and cloudiness [3–7].

Hargreaves [13, 14] proposed a procedure to estimate R_s from mean temperature difference (TD in °C) as $\left(R_s = 0.16 \times R_a \times \mathrm{TD}^{0.5}\right)$. Chegaar [11] modified an empirical model (originally formulated to compute the monthly global irradiation) to develop a global R_s estimation model using sunshine hour data for some Algerian and Spanish sites. Chen [12] calibrated three air temperature-based and two sunshine-based global radiation models at 48 climatic locations using daily data all over China. Bandyopadhyay [10] studied on the estimation of R_s from routinely measured air temperature extremes for 29 Indian stations. Liu [9, 17] found out suitable method among seven models to estimate R_s on the Tibetan Plateau based on the validation of developed models using measured pyranometer data. Li [16] developed a generalized model to estimate R_s with a daily measured climatic data of maximum air temperature (T_{max}, °C) and minimum air temperature (T_{min}, °C) and location data of longitude, latitude and altitude for China (Guizhou and Sichuan basins).

Among the all meteorological variables, air temperature data is mostly used and is readily available at all the weather stations. Therefore, the air temperature can be used in R_s estimation at all the weather stations. Further, several studies have reported different methods to estimate R_s indirectly using air temperature data. However, their potentiality and applicability are needed to be tested for accurate estimation of R_s for different climatic locations. The main purpose of the present work is to compare R_s estimation performance of different methods under different climate conditions of India.

2 Methods

2.1 Study Area Description

For R_s estimation, a total of 20 stations spread all over India were selected as study area. Table 1 shows the characteristics of chosen stations along with the locally calibrated Angstrom coefficients. Figure 1 shows the locations of chosen study sites in India. The CLIMWAT 2.0 software (http://www.fao.org/land-water/databases-and-software/climwat-for-cropwat/en/) provides a long-term (at least 15 years) mean monthly observed agro-climatic data of 5000 stations over worldwide. Therefore, the required data for the R_s estimation was extracted from CLIMWAT 2.0 software. The data contains a long-term monthly average of T_{max} and T_{min} (°C), sunshine hours (h/day), average relative humidity (%), mean wind speed (km/day), effective rainfall (mm/month) and solar radiation (MJ m^{-2} d^{-1}).

Table 1 Characteristics of chosen stations for R_s estimation

Station	Lat (°N)	Long (°E)	Altitude (m)	Agro-ecological zones	Angstrom coefficients	
					a	*b*
Akola	20.70	77.03	282	Hot semi-arid	0.25	0.49
Amritsar	31.63	74.86	234	Hot semi-arid	0.21	0.49
Aurangabad	19.88	75.33	581	Hot semi-arid	0.25	0.50
Bangalore	12.96	77.58	921	Hot semi-arid	0.28	0.52
Chitradurga	14.23	76.43	733	Hot semi-arid	0.27	0.51
Cuttack	20.46	85.93	27	Hot sub-humid	0.25	0.48
Darjeeling	27.05	88.26	2128	Warm per humid	0.23	0.58
Dehra-Dun	30.31	78.03	682	Warm sub-humid	0.22	0.51
Indore	22.71	75.80	567	Hot semi-arid	0.24	0.50
Jabalpur	23.20	79.95	393	Hot sub-humid	0.24	0.50
Jaipur	26.85	75.81	435	Hot semi-arid	0.23	0.50
Jammu	32.66	74.83	367	Warm sub-humid	0.21	0.50
Ludhiana	30.86	75.93	255	Hot sub-humid	0.21	0.49
Midnapore	22.41	87.31	45	Hot sub-humid	0.24	0.48
Pune	18.53	73.85	559	Hot semi-arid	0.26	0.50
Raipur	21.23	81.65	298	Hot sub-humid	0.25	0.49
Rajkot	22.30	70.78	138	Hot semi-arid	0.24	0.48
Ranchi	23.43	85.40	647	Hot sub-humid	0.24	0.51
Silchar	24.75	92.80	29	Hot sub-humid	0.24	0.48
Tiruchirappalli	10.76	78.71	88	Hot semi-arid	0.29	0.47

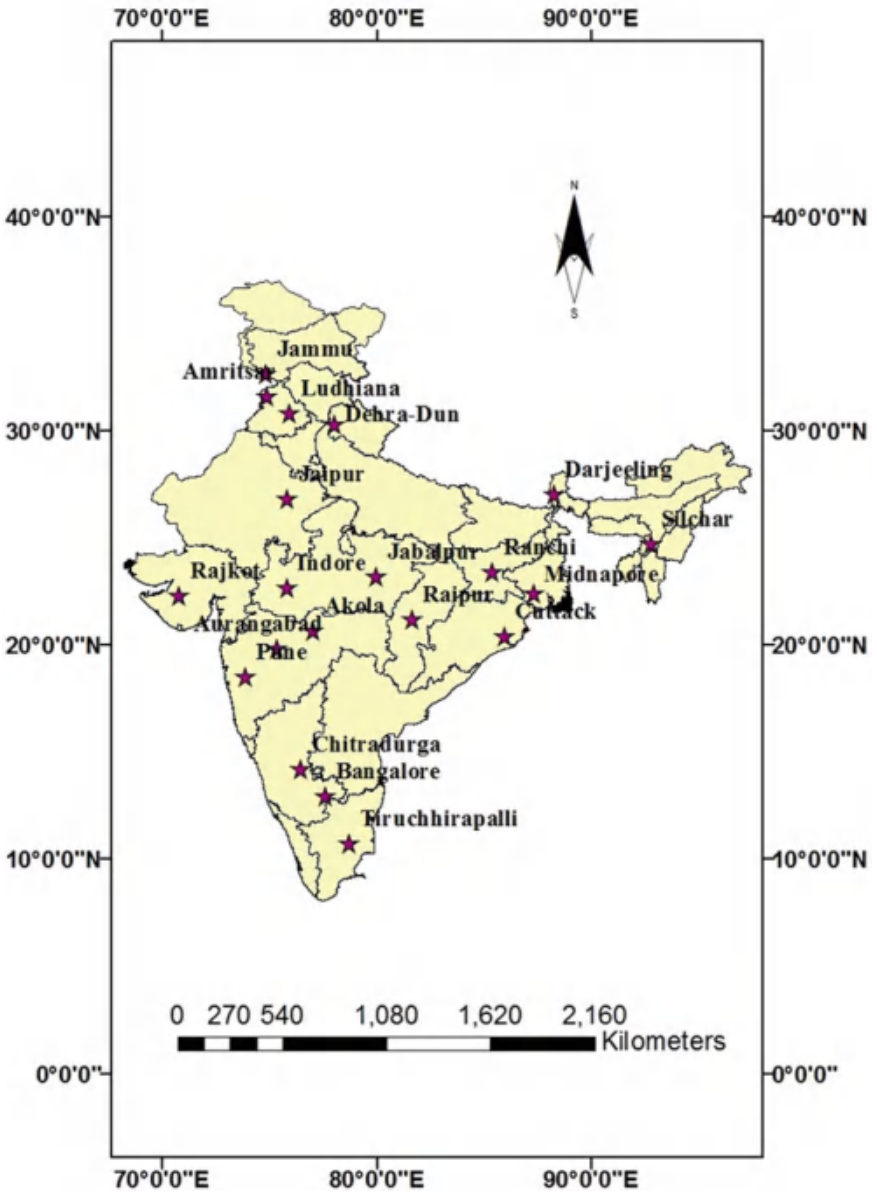

Fig. 1 Study area locations in India

2.2 Earlier Studies of Solar Radiation Estimation

Hargreaves equation to estimate solar radiation (R_s, MJ m^{-2} d^{-1}) is based on the data of T_{max} and T_{min} [14]:

$$R_s = K_r\left(T_{max} - T_{min}\right)^{0.5} R_a \tag{1}$$

R_a = extraterrestrial radiation (MJ m^{-2} d^{-1}), and K_r = an empirical coefficient (unitless). The value of K_r is 0.16 for interior regions and 0.19 for coastal regions [5].

According to Annandale [9], the corrected K_r (K_r') can be calculated based on the elevation (Z, m) as:

$$K_r' = \left(1 + 2.7 \times 10^{-5} Z\right) K_r \tag{2}$$

The estimation of K_r as a function of atmospheric pressure is as [13]:

$$K_r = K_{ra}\left(\frac{P}{P_o}\right)^{0.5} \tag{3}$$

where K_{ra} = empirical coefficient, which is = 0.17 for interior region and = 0.20 for coastal region, P_o = mean atmospheric pressure at sea level (kPa), and P = mean atmospheric pressure at the site (kPa) which can be estimated as:

$$P = P_o\left(\frac{293 - 0.0065Z}{293}\right)^{5.26} \tag{4}$$

R_s can also be calculated using extraterrestrial radiation (R_a) and relative sunshine duration as:

$$R_s = \left(a + b\frac{n}{N}\right) R_a \tag{5}$$

where 'a' and 'b' = Angstrom coefficients, n = actual duration of sunshine (h), and N = maximum possible duration of sunshine or daylight hours (h).

The estimation of R_s based on T_{max} and T_{min} [14]:

$$R_s = a_2(T_{max} - T_{min})^{0.5} R_a + b_2 \tag{6}$$

where a_2 and b_2 = regression coefficients.

Li [16] suggested an empirical relationship between R_s and air temperature as:

$$R_s = \left(a_1 T_{max} + b_1 T_{min} + c_1\right) R_a \tag{7}$$

where a_1, b_1 and c_1 are empirical constants and their values are 0.043, −0.04 and −0.072, respectively.

2.3 Characteristics for Comparison Between Different Methods

The estimated R_s model can be evaluated based on different performance indices, namely root-mean-squared error (RMSE) and model efficiency (ME).

$$\text{ME} = \frac{\sum_{i=1}^{n}(X_{o,i} - \bar{X}_o)^2 - \sum_{i=1}^{n}(X_{p,i} - X_{o,i})^2)}{\sum_{i=1}^{n}(X_{o,i} - \bar{X}_o)^2} \tag{8}$$

$$\text{RMSE}(\%) = \frac{\left(\sum_{i=1}^{n}(X_{p,i} - X_{o,i})^2/n\right)^{0.5}}{\bar{X}_o} \times 100 \tag{9}$$

where n = number of observation points, $X_{p,i}$ = estimated R_s, $X_{o,i}$ = observed R_s, and $\bar{X}_o$ = average of observed R_s.

It is stated that for a perfect model where observed R_s values are exactly matching with the estimated R_s values, the value of ME is 1.0. If ME value resulted near to zero, it indicates poor performed model, where there is a large difference in estimated and observed R_s values [15]. Similarly, lower values of RMSE indicate better performance and vice versa [16, 17].

3 Results and Discussion

Generally, the Angstrom coefficients (a, b) depend on latitude and month. In this study, the Angstrom coefficients 'a' and 'b' are strongly correlated with the latitude (L, °N) and elevation (Z, m) of the locations, respectively, during regression analysis.

$$a = -3.517 \times 10^{-3}\text{L} - 1.492 \times 10^{-6}\text{Z} + 0.3263 \tag{10}$$

$$b = 5.042 \times 10^{-4}\text{L} - 4.845 \times 10^{-5}\text{Z} + 0.4644 \tag{11}$$

The locally calibrated Angstrom coefficients 'a' and 'b' values are shown in Table 1, which are used for estimating R_s from measured sunshine hours (Eq. 5) and gave minimum RMSE values between measured R_s and estimated R_s at all stations. The results found that the values of Angstrom coefficients $a = 0.25$ and $b = 0.50$ in India are closely matching with the recommended values for an average climate.

Table 2 displays the performance of different R_s estimation methods considered in this study with respect to measured R_s at 20 stations. It was observed that the Li [16] method (Eq. 7) performed very poorly for all stations with negative ME and very high RMSE values as compared to the other methods. The original Hargreaves [13] method failed to show good results for low latitude stations such as Bangalore and Tiruchirappalli, which resulted in negative ME values (Table 2). Annandale [9] method for altitude correction, which is a modification to original Hargreaves [13] method, showed similar poor performance for almost all stations except Aurangabad,

Jaipur, Pune and Raipur, where the performance was improved. At all these stations, latitude is strongly correlated to the elevation and the value of Angstrom coefficient '*b*' is almost equal to the recommended value (i.e. 0.5).

The other modification of Hargreaves [13] for altitude correction proposed by Allen [8] showed better results for lower altitude stations (Cuttack, Midnapore and Silchar). Using calculated Angstrom coefficient (Eqs. 10–11), R_s estimated from measured sunshine data (Eq. 5) provides better results (ME almost equal to 1.00 and lowest RMSE) among all methods applied in this study at all stations. Hunt [15] method performed very well with less RMSE values at all stations as compared to Hargreaves [13].

Table 3 showed the ranking of different R_s estimation methods based on RMSE values for each location considered in this study. Among all methods, sunshine hour-based method gave lowest RMSE values than other methods at all stations (except Bangalore, Ludhiana and Silchar). Li [16] method was found to be the poorest based on high RMSE values at all stations. It is found that both the R_s estimation methods, i.e. Hargreaves [14] and Annandale [9] methods, were performed superior as compared to other methods (except sunshine hour-based method) for few stations. It is also found that the Hargreaves [14] method was better than that given in Annandale [9] at low elevation stations (Akola and Amritsar). The other modifications of Hargreaves [13] method for altitude correction, i.e. Allen [8] and Hunt [15], ranked good for few climatic locations. However, these methods found to be unsuitable for estimating monthly R_s. Therefore, care should be taken while using these methods for Indian climate. In this study, though the location-wise individual ranking was different from the R_s ranking (Table 3) for a few climatic locations, the overall average ranking was found to be similar.

4 Summary and Conclusions

As an energy factor, solar radiation (R_s) is one of the most critical and important meteorological variables to be measured from the existing instruments or to be estimated from the developed empirical models based on some input data. Its measurement or estimation is necessary for carrying out basic research related to agriculture and water resources. However, its measurement is very limited at a number of meteorological stations over worldwide. There exist different methods to estimate R_s based on air temperature data. The measured/observed R_s values were extracted from CLIMWAT 2.0 software for 20 Indian stations. The estimated R_s values form six different models were compared with the measured R_s, to evaluate the suitability of these methods for different Indian climates. The comparison was made with two indices, namely root-mean-squared error (RMSE) and model efficiency (ME). The comparison results suggested that the performance of each method varies with the location/station. The sunshine hour-based method performed best at all stations (except Bangalore, Ludhiana and Silchar). Therefore, this method is recommended for most Indian climatic locations. Further, after the sunshine hour-based method, the Hargreaves [14] and

Table 2 R_s estimation performance of different methods

Sl. No.	Stations	Hargreaves [14]		Allen [8]		Hunt [15]		Annandale [9]		Li [16]		Sunshine hours based	
		RMSE (%)	ME	RMSE (%)	ME	RMSE (%)	ME	RMSE (%)	ME	RMSE (%)	ME	RMSE (%)	ME
1	Akola	7.54	0.75	10.39	0.52	10.88	0.48	7.85	0.73	10.66	0.50	1.63	0.99
2	Amritsar	12.14	0.72	16.89	0.45	18.98	0.31	12.69	0.69	20.33	0.21	8.98	0.84
3	Aurangabad	6.31	0.82	6.09	0.83	5.90	0.84	6.05	0.84	11.75	0.38	0.58	1.00
4	Bangalore	18.05	−0.68	17.59	−0.60	6.66	0.77	16.23	−0.36	29.78	−3.57	7.04	0.74
5	Chitradurga	8.31	0.56	7.67	0.62	6.28	0.75	7.67	0.62	19.42	−1.42	4.50	0.87
6	Cuttack	9.21	0.35	7.72	0.54	5.13	0.80	9.21	0.35	22.40	−2.86	2.66	0.95
7	Darjeeling	15.26	0.20	16.62	0.05	7.03	0.83	16.14	0.10	45.63	−6.17	3.29	0.96
8	Dehra-Dun	8.18	0.86	9.28	0.82	7.83	0.87	9.28	0.82	13.64	0.61	5.33	0.94
9	Indore	5.97	0.88	8.09	0.78	11.20	0.58	6.98	0.84	14.31	0.31	2.25	0.98
10	Jabalpur	5.84	0.88	8.69	0.74	8.94	0.73	6.67	0.85	16.33	0.09	2.31	0.98
11	Jaipur	11.60	0.57	8.72	0.76	12.17	0.52	10.61	0.64	14.90	0.29	3.46	0.96
12	Jammu	11.34	0.81	13.79	0.72	9.01	0.88	12.06	0.79	13.70	0.72	8.65	0.89
13	Ludhiana	6.82	0.92	5.72	0.94	12.00	0.74	6.50	0.92	16.88	0.49	6.95	0.91
14	Midnapore	8.54	0.51	6.28	0.74	6.41	0.73	8.54	0.51	22.86	−2.49	4.48	0.87
15	Poona	10.25	0.65	7.84	0.79	9.82	0.68	9.26	0.71	20.86	−0.46	1.32	0.99
16	Raipur	7.63	0.73	7.01	0.78	10.35	0.51	7.39	0.75	18.47	−0.55	1.62	0.99
17	Rajkot	7.24	0.78	12.95	0.28	8.32	0.70	7.84	0.74	15.16	0.02	4.48	0.91
18	Ranchi	12.99	0.57	13.91	0.50	7.12	0.87	13.64	0.52	14.87	0.43	1.49	0.99
19	Silchar	6.75	0.61	3.72	0.88	11.94	−0.22	6.75	0.61	22.58	−3.35	4.51	0.83
20	Tiruchirappalli	12.01	−0.40	8.40	0.31	6.60	0.58	12.01	−0.40	25.44	−5.29	3.73	0.86

Table 3 Ranking of different R_s estimation methods based on RMSE values

Sl. No.	Stations	Hargreaves [14]	Allen [8]	Hunt [15]	Annandale [9]	Li [16]	Sunshine hours based
1	Akola	2	4	6	3	5	1
2	Amritsar	2	4	5	3	6	1
3	Aurangabad	5	4	2	3	6	1
4	Bangalore	5	4	1	3	6	2
5	Chitradurga	5	3	2	3	6	1
6	Cuttack	4	3	2	4	6	1
7	Darjeeling	3	5	2	4	6	1
8	Dehra-Dun	3	4	2	4	6	1
9	Indore	2	4	5	3	6	1
10	Jabalpur	2	4	5	3	6	1
11	Jaipur	3	2	5	4	6	1
12	Jammu	3	7	2	4	6	1
13	Ludhiana	3	1	5	2	6	4
14	Midnapore	4	2	3	4	6	1
15	Poona	5	2	4	3	6	1
16	Raipur	4	2	5	3	6	1
17	Rajkot	2	5	4	3	6	1
18	Ranchi	3	5	2	4	6	1
19	Silchar	3	1	5	3	6	2
20	Tiruchirappalli	4	3	2	4	6	1

Annandale [9] methods performed well with low RMSE values and good ranking for most of the locations. The Allen [8] and Hunt [15] methods performed well for a few stations, but were found to be unsuitable for monthly Rs estimates as a whole and the Li [16] method was found to be the poorest method for all locations except for Akola as compared to all methods monthly applications, and it is unsuitable for Indian climate.

References

1. Adamala, S., Raghuwanshi, N.S., Mishra, A., Tiwari, M.K.: Evapotranspiration modeling using second-order neural networks. J. Hydrol. Eng. **19**(6), 1131–1140 (2014a)
2. Adamala, S., Raghuwanshi, N.S., Mishra, A., Tiwari M.K.: Development of generalized higher-order synaptic neural-based ET_o models for different agroecological regions in India. J. Irrig. Drain. Eng. **140**(12) (2014b) https://doi.org/10.1061/(asce)ir.1943-4774.0000784
3. Adamala, S., Raghuwanshi, N.S., Mishra, A.: Generalized quadratic synaptic neural networks for ET_o modeling. Environ. Process. **2**(2), 309–329 (2015a)

4. Adamala, S., Raghuwanshi, N.S., Mishra, A., Tiwari, M.K.: Closure to evapotranspiration modeling using second-order neural networks. J. Hydrol. Eng. **20**(9), 07015015 (2015b)
5. Adamala, S.: Evapotranspiration and evaporation modeling using higher-order neural networks. PhD Dissertation, Indian Institute of Technology, Kharagpur, West Bengal, India (2015c)
6. Adamala, S., Raghuwanshi, N.S., Mishra, A., Singh, R.: Generalized wavelet-neural networks for evapotranspiration modeling in India. ISH J. Hydraul. Eng. 1–13 (2017a) https://doi.org/10.1080/09715010.2017.1327825
7. Adamala, S.: Temperature based generalized wavelet-neural network models to estimate evapotranspiration in India. Inf. Process. Agric. **5**(1), 149–155 (2017b) https://doi.org/10.1016/j.inpa.2017.09.004
8. Allen, R.G.: Evaluation of procedures for estimating mean monthly solar radiation from air temperature. Food and Agriculture Organization of the United Nations (FAO), Rome, Italy (1995)
9. Annandale, J. G., Jovanovic, N. Z., Benade, N. and Allen, R. G.: Software for missing data error analysis of Penman–Monteith reference evapotranspiration. Irrig. Sci. **21**, 57–67 (2002)
10. Bandyopadhyay, A., Bhadra, A., Raghuwanshi, N. S. and Singh, R.: Estimation of monthly solar radiation from measured air temperature extremes. Agri. For. Meteor. **148**(11), 1707–1718 (2008)
11. Chegaar, M., Lamri, A. and Chibani, A.: Estimating global solar radiation using sunshine hours. Rev. Energ. Ren.: Physique Energetique 7–11 (1998)
12. Chen, R., Ersi, K., Yang, J., Lu, S. and Zhao, W.: Validation of five global radiation models with measured daily data in China. Energy Conv. Manage. **45**, 1759–1769 (2004)
13. Hargreaves, G. H. and Samani, Z. A.: Estimating potential evapotranspiration. J. Irrig. Drain. Eng. Div. **108**(3), 225–230 (1982)
14. Hargreaves, G.H.: Simplified coefficients for estimating monthly solar radiation in North America and Europe. Dept. Biology Irrig. Eng., Utah State University, Logan, Utah (1994)
15. Hunt, L.A., Kuchar, L., Swanton, C.J.: Estimation of solar radiation for use in crop modelling. Agric. Forest Meteorol. **91**, 293–300 (1998)
16. Li, M-F., Liu, H-B., Guo, P-T. and Wu, W.: Estimation of daily solar radiation from routinely observed meteorological data in Chongqing, China. Energy Conv. Manage. **51**(12), 2575–2579 (2010)
17. Liu, J., Liu, J., Linderhilm, H. W., Chen, D., Yu, Q., Wu, D. and Haginoya, S.: Observation and calculation of the solar radiation on the Tibetan Plateau. Energy Conv. Manag.**57**, 23–32 (2012)

Assessment of Changes in Wetland Storage in Gurupura River Basin of Karnataka, India, Using Remote Sensing and GIS Techniques

Subrahmanya Kundapura, Renuka Kommoju and Irshan Verma

Abstract In view of the significant importance of wetlands in the ecosystem and regional economy, an attempt has been made to analyze the impact of land use/land cover dynamics and other contributing factors on spatial status of Gurupura river basin wetland ecosystem located in Karnataka region. The impact assessment has been carried out by analyzing the multi-temporal changes in the storage capacities of wetlands in the watershed, by using remote sensing data of LISS-III. The multi-temporal land use/land cover statistics will reveal the significant changes that have taken place over time in the watershed. The runoff generated can be easily calculated from this information which gives an idea of the total input into the system. In response to these upstream watershed changes, wetland has exhibited changes in spatial extension, structure, and hydrological characteristics. As a consequence of continuously changing land use/land cover characteristics and unpredictability of the monsoon, the wet land ecosystems have exhibited considerable changes in spatial extent and their storage capacities. Overall, there has been degradation in the storage capacities of the wetland ecosystems of the region causing a multitude of adverse effects such as increase in floods and submergence of mainland.

Keywords Remote sensing · Wetland ecosystems · Land use/land cover

1 Introduction

Wetlands hold a vital role in the hydrological dynamic of a watershed. They are widely regarded as the 'kidneys' of the hydrological system, fittingly so, as wetlands play a major role in the ecosystem by providing an efficient way for sediment and toxic removal. By retaining the surface runoff and slowly discharging it back to the hydrological cycle, wetlands not only filter the sediment and toxic wastes but also

S. Kundapura (B) · R. Kommoju · I. Verma
Department of Applied Mechanics and Hydraulics, National Institute of Technology Karnataka, Surathkal, India
e-mail: subrahmanyakundapura@gmail.com

M. Rathinasamy et al. (eds.), *Water Resources and Environmental Engineering II*,
https://doi.org/10.1007/978-981-13-2038-5_6

provide opportunities for ground-water recharge and discharge, flood mitigation, and flow regulation. The filtering process reduces many problems of the likes of saltwater intrusion and increasing sediment deposits. Wetland systems also aid the process of nutrient cycling in the region. This is of prime importance for the vegetation growth in the region, and this vegetation further curbs the erosion process. Wetlands are also notorious for shoreline protection and acting as wind breaks to prevent erosion by wind [1, 2]. One of the most important aspects of wetlands is the amazing streak of wildlife finding habitat in these systems. Wetland systems are home to many species of migrating birds and other flora and fauna. Therefore, for the conservation of these flora and fauna, the conservation of wetlands becomes imperative [3].

In hydrology, a water balance equation can be used to describe the flow of water in and out of a system. A system can be one of several hydrological domains, such as a column of soil or a drainage basin or a wetland [4–6]. A general water balance equation is:

$$P = Q + E + \Delta S \tag{1}$$

where

P Precipitation
Q Runoff
E Evapotranspiration
ΔS Change in the storage

The basic hydrology of a wetland system can be related to any system with defined inputs and outputs. The inputs to a wetland system are the precipitation, the surface-water inflow, and the ground-water inflow. Evapotranspiration, surface-water outflow, ground-water outflow are the outputs from the system. The water balance equation for a wetland can be written as follows

$$P + \mathrm{SWI} + \mathrm{GWI} = \mathrm{ET} + \mathrm{SWO} + \mathrm{GWO} + \Delta S \tag{2}$$

where P is precipitation, SWI is surface-water inflow, SWO is surface-water outflow, GWI is ground-water inflow, GWO is ground-water outflow, ET is evapotranspiration, and ΔS is change in storage [7–10].

To make an assessment in the changes in storage capacities, an effort has been made in this study to incorporate the input factor of surface-water inflow to give an idea of the changing situation. The surface-water inflow can be easily calculated by using remotely sensed data and the Soil conservation Services Curve Number (SCS-CN) method [11–13]. The SCS-CN is a simple, widely used, and efficient method for determining the approximate amount of runoff from a rainfall even in a particular area. Although the method is designed for a single storm event, it can be scaled to find average annual runoff values [14–16]. The stat requirements for this method are very low rainfall amount and curve number. The curve number is based on the area's hydrological soil group, land use, treatment, and hydrological condition [17, 18]. The former being of greatest importance.

2 Study Area

The Gurupura River or Phalguni River or sometimes Kulur River has its origins in the Western Ghats, which drains itself in the Arabian Sea at Mangalore. The New Mangalore Port (NMPT) and Mangalore Chemicals and Fertilizers are situated at the northern banks of Phalguni River. Once upon a time, it formed northern boundary of Mangalore city along with Netravati River as southern boundary. The study area chosen for this study is the entire Gurpur river basin. The complete area of the river basin is about 874.68 km^2 with the drainage length of the river being 52.31 km approximately. The complete basin lies between 12° 50′ 24″N and 13° 11′ 24″N latitude and 74° 45′ 0″E and 75° 21′ 0″E longitude as is shown in the figure. The basin area lies in the Survey of India (SOI) toposheet No. 48L/13/NW, 48L/13/NE, 48L/13/SE, 48L/13/SW.

3 Data Used

3.1 Rainfall

The rainfall data used for this study was obtained from Indian Meteorological Department (IMD). The dataset obtained was a 0.5° × 0.5° daily rainfall dataset. The rainfall maps were prepared from this dataset under GIS environment by plotting the gridded rainfall data with the coordinate grid around the study area. Spatially interpolated maps of rainfall were prepared from the grid points containing rainfall information by applying Universal Kriging technique [19–21]. Maximum rainfall intensity is found in the study area in the month of July, in fact 30–35% of the total rainfall occurs in the month of July. Also there is an increase in rainfall in 2010 than 2003.

3.2 Soil Data

Soil maps in GIS compatible shapefile format were obtained from National Bureau of Soil Survey and Land Use Planning (NBSS&LUP) and Food and Agricultural Organization-UNESCO (FAO-UNESCO). By cross-referencing both the datasets, the derived product obtained was the hydrological soil group classification of the study area in the following four classes

- Group A: Soils in this group have low runoff potential when thoroughly wet. Water is transmitted freely through the soil. Group A soils typically have less than 10% clay and more than 90% sand or gravel and have gravel or sand textures.

- Group B: Soils in this group have moderately low runoff potential when thoroughly wet. Water transmission through the soil is unimpeded. Group B soils typically have between 10 and 20% clay and 50–90% sand and have loamy sand or sandy loam textures.
- Group C: Soils in this group have moderately high runoff potential when thoroughly wet. Water transmission through the soil is somewhat restricted. Group C soils typically have between 20 and 40% clay and less than 50% sand and have loam, silt loam, sandy clay loam, clay loam, and silty clay loam textures.
- Group D: Soils in this group have high runoff potential when thoroughly wet. Water movement through the soil is restricted or very restricted. Group D soils typically have greater than 40% percent clay, less than 50% sand, and have clayey textures.

3.3 Land Use/Land Cover Maps

The land use/land cover maps of the study area were prepared using the satellite data of LISS-III sensor mounted on IRS-P6. The satellite data has a resolution of 23.5 m and is capable of recording in four different bands in the spectral range of 0.52–1.70 μm. This range corresponds to the visible as well as the near-infrared portions of the spectrum. LISS-III images for 2003 and 2010 were obtained from National Remote Sensing Center (NRSC). The data was subjected to supervised maximum likelihood classification, and the results obtained are shown in Figs. 1 and 2 with area-wise details in Tables 1 and 2.

Table 1 Area-wise breakup of different land use/land cover classes for 2003

Land cover class	Area (km^2)	Percentage area
Built up	22	2.61
Water bodies	12	1.43
Dense vegetation	428	50.83
Cultivated without conservation	258	30.64
Barren land	122	14.4

Table 2 Area-wise breakup of different land use/land cover classes for 2010

Land cover class	Area (km^2)	Percentage area
Built up	47	5.58
Water bodies	5	0.59
Dense vegetation	303	35.99
Cultivated without conservation	391	46.43
Barren land	96	11.41

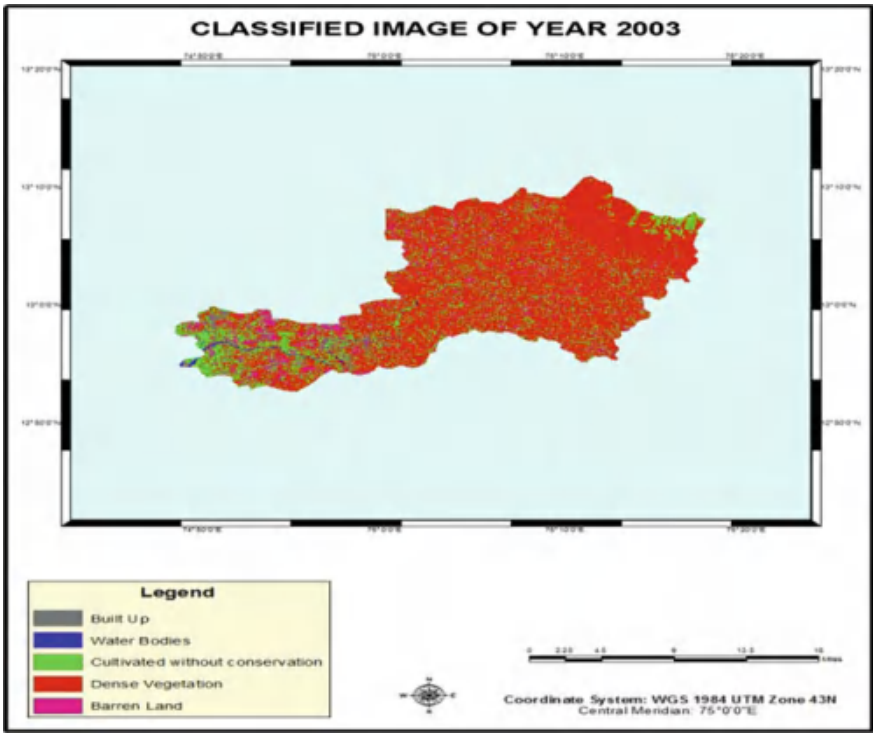

Fig. 1 Classified image for 2003

An increase is seen in the land class of built-up area and cultivated land, whereas dense vegetation, barren lands, and water bodies have suffered decreases in their extents from 2003 to 2010.

The watershed was obtained by techniques of Automated Watershed Delineation. Due to more accuracy and dedicated scripts attributing to easy delineation, the method used in this study is the watershed delineation tool developed independently by GIS student Dwain Caldwell of GeoTREE University of Geography. The purpose of the script is to allow manual delineation of watershed boundaries. The tool requires a Digital Elevation Model and a pour point (i.e., outlet points for the watersheds you would like to delineate) raster dataset.

The Digital Elevation Model for the study area was downloaded from Bhuvan portal. The pour point used was Adoor gauging station. The results of the script include the basin, watershed, stream network, stream order network, filled DEMs, flow accumulation rasters, and flow direction rasters.

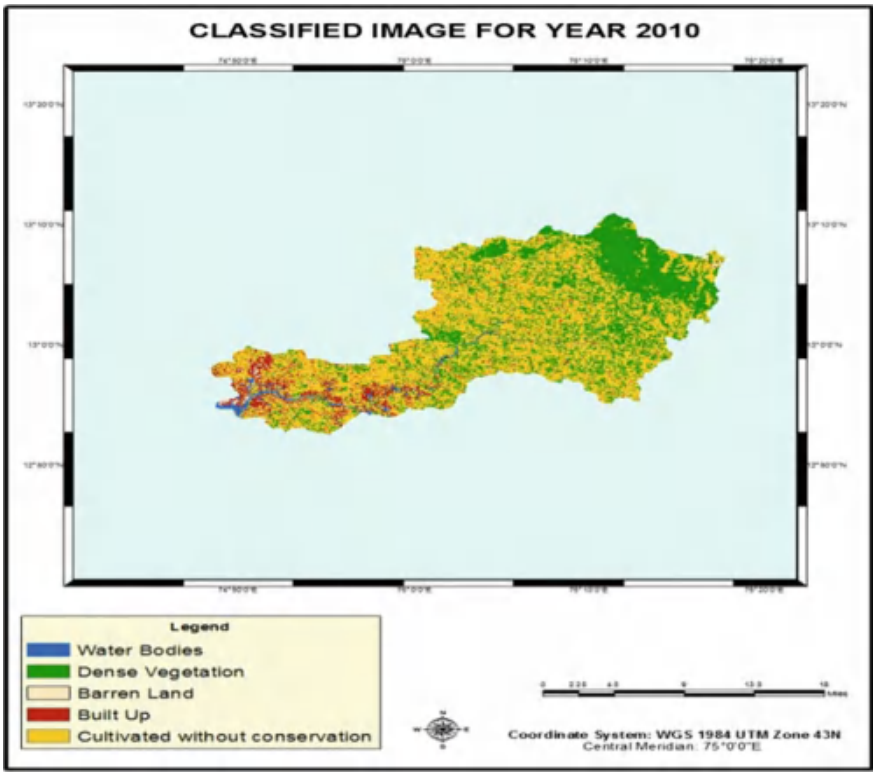

Fig. 2 Classified image for 2010

4 Results and Discussions

4.1 Runoff Estimation

Further, the classified images were intersected with the hydrological soil group map in order to determine the curve numbers for each class. The result produced was the curve number map of the entire area. The curve numbers are calculated by assuming the average Indian wetness conditions of AMC II.

Since curve number for each land use/land cover class has different value under different situations, area weighted curve number is calculated for each class. Following equation can be used to calculate weighted curve number [16, 22].

$$\text{Weighted Curve Number} = \frac{\sum_{i=1}^{n}(\text{CN}_i \times A_i)}{A} \tag{3}$$

Table 3 Area and hydrological soil group-wise breakdown of the different land use/land cover classes for 2003

Land cover class	Total area (km^2)	Hydrological soil group B		Hydrological soil group C		Hydrological soil group D	
		Area (km^2)	CN	Area (km^2)	CN	Area (km^2)	CN
Built up	22	5.7	98	5	98	11.3	98
Dense vegetation	428	22	57	340	71	66	78
Water bodies	12	8	100	3.3	100	0.7	100
Cultivated without conservation	258	57	71	158	78	43	81
Barren	122	9	61	97.5	74	15.5	80
						Weighted CN = 68.97	

Table 4 Area and hydrological soil group-wise breakdown of the different land use/land cover classes for 2010

Land cover class	Total area (km^2)	Hydrological soil group B		Hydrological soil group C		Hydrological soil group D	
		Area (km^2)	CN	Area (km^2)	CN	Area (km^2)	CN
Built Up	47	10.1	98	15.2	98	21.7	98
Dense vegetation	303	11	57	264	71	28	78
Water bodies	5	0.9	100	2.2	100	1.9	100
Cultivated without conservation	391	40	71	299	78	52	81
Barren	96	31	61	37	74	31	80
						Weighted CN = 74.53	

where

CN_i Curve number from 1 to any number n
A_i Area corresponding to CN_i
A Total area of the watershed

The results obtained are shown in Tables 3 and 4.

It is interesting to note the increase in the curve number from 68.97 in 2003 to 74.53 in 2010. The same can be attributed to the increase in the impermeable surfaces

in the form of built-up land and cultivated land. Both built-up land and cultivated land have increased by 53 and 34%, respectively, causing an uprise in the curve number.

After calculating the curve numbers, the runoff calculations can be done by employing SCS-CN method.

The general equation for the SCS curve number method is as follows:

$$Q = \frac{(P - \text{Ia})^2}{(P - \text{Ia}) + s} \tag{4}$$

where

Q Runoff (mm)
P Rainfall (mm)
Ia Initial abstraction
S Maximum potential retention after runoff begins

$$\text{Ia} = 0.3S \tag{5}$$

Therefore,

$$Q = \frac{(P - 0.3S)^2}{(P + 0.7S)} \tag{6}$$

$$S = \frac{25{,}400}{254 + \text{CN}} \tag{7}$$

The initial Eq. (4) is based on trends observed in data from collected sites; therefore, it is an empirical equation instead of a physically based equation. After further empirical evaluation of the trends in the database, the initial abstractions, Ia, could be defined as a percentage of S (5). With this assumption, the Eq. (6) could be written in a more simplified form with only three variables. The parameter CN is a transformation of S, and it is used to make interpolating, averaging, and weighting operations more linear (7).

The obtained results are in the form of runoff maps for the study area. The results indicate an increased runoff in 2010 as compared to 2003. Another interesting feature is the increased runoff in the month of November in 2010 as compared to the month of November in 2003. The predicted runoff values can be compared to the available stream gauging data of Adoor station obtained from India Water Resources Information System (IWRIS) portal version 4.0. The stream gauging data is first converted from total runoff to surface runoff by performing base flow separation by using Web-Based Hydrograph Analysis Tool (WHAT) available at https://engineering.purdue.edu/~what/.

The obtained results are shown in Table 5 and Figs. 3, 4.

Table 5 Comparison of available observed data of surface runoff and the predicted values

Month	2003		2010	
	Observed discharge (m^3/s)	Predicted discharge (m^3/s)	Observed discharge (m^3/s)	Predicted discharge (m^3/s)
August	147	125.6	154.94	130
September	34.73	23.7	63.78	51.2
October	33.57	26.9	33.56	26.6
November	5.915	0	30.7	20.82

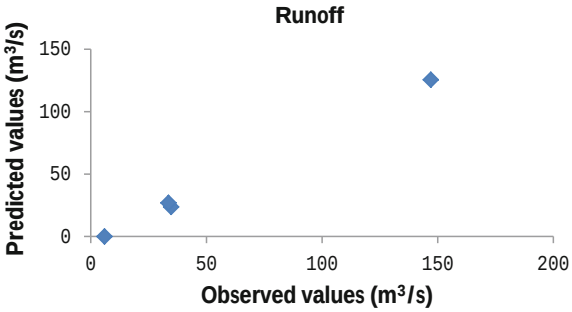

Fig. 3 Plot of observed runoff versus predicted runoff for 2003

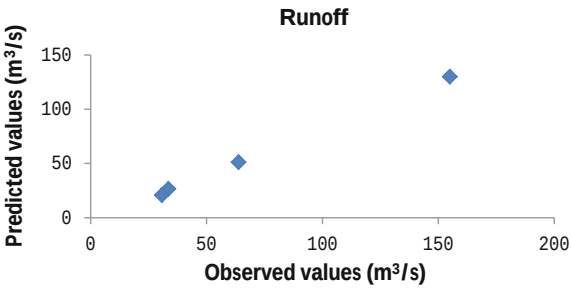

Fig. 4 Plot of observed runoff versus predicted runoff for 2010

4.2 Calculating the Surface-Water Storage

Considerable surface water bodies were extracted from the classification images of the respected years. These polygons provided the spatial location and the area of the water bodies. The depth required for volume calculation was actuated by the 3-D profile of the study area, which was generated earlier, as shown in Figures 6.7 and 6.8. The polygon features were overlayed on the TIN of the study area, and the volume was found out by "Calculate Polygon" tool available in 3-D analyst toolset in ARC GIS 10.1. From these polygons, volume was calculated as shown in Tables 6, 7 and Fig. 5.

Also the total amount of incoming runoff is available for this storage volume. Now for the water balance equation, the two parameters, i.e., the runoff input and

Table 6 Calculated volume and surface area of the visible water bodies

Year	Calculated volume (m^3)	Surface area (m^2)
2003	23552.2896	3,100,515
2010	1366.032806	849,756

Table 7 Total runoff generated and the total storage volume available for years 2003 and 2010

Year	Calculated volume (m^3)	Total runoff (m^3/s)
2003	3794.535572	16622.12
2010	1366.032806	30929.94

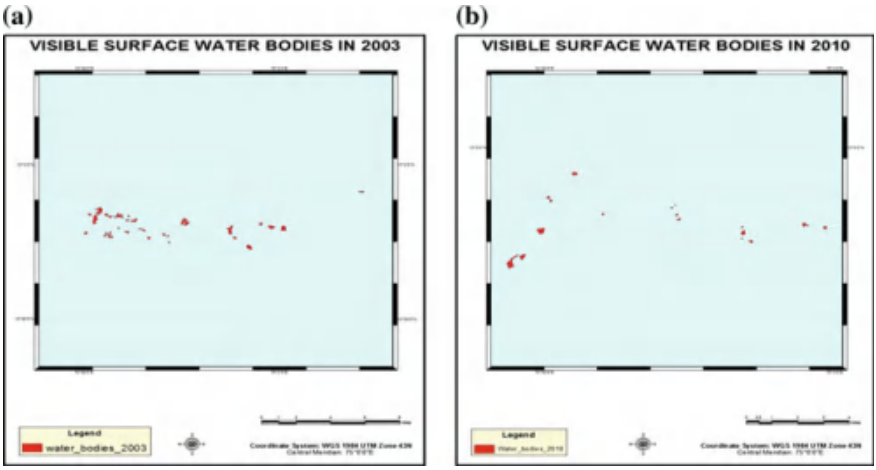

Fig. 5 Visible water bodies. **a** In 2003 and **b** in 2010

the storage volume, are known. The total runoff in 2003 and 2010 along with their storage volumes is represented in the following table.

It is observed that despite an increase in the total runoff in the 2010, there is steep decrease in the storage volume available for that runoff. The storage volume has decreased by 36%.

5 Conclusions

An attempt was made to assess the changes in the wetland storage by taking into account the two important aspects of the water balance equation, i.e., the surface-water inflow and the changes in storage. The surface-water inflow was estimated using SCS-CN method using moderate resolution LISS-III data. The resolution of the satellite data hampers the accuracy of the classification of the image into various land use/land cover classes. The classified images of the study years, i.e., 2003 and 2010, demonstrate the effect of increasing anthropogenic activities in the study area.

It can be duly noted by the fact that the built-up area has increased by 53% over the course of 7 years of the study. In the same time frame, the cultivated land including pastures and groves has seen an increase of 37%. It is also noted that the volume to the surface storage in the study area has decreased by 36% over the time frame of 7 years, whereas over the same time frame the runoff generated has increased. A major of portion these mentioned surface water bodies are the wetlands in the study area. Wetlands are well known to absorb the effects of excess runoff and help in preventing floods. But the current situation certainly points to a grave condition where the storage available for the absorption of runoff may not be enough to wary the effects of incoming runoff. This may lead to the constant flooding of low-lying areas and urban settlements. Therefore, an immediate need stems from the situation to protect and promote wetlands in the region.

References

1. Dhawale, A.W.: Runoff estimation for Darewadi Watershed using RS and GIS. Int. J. Recent Technol. Eng. **1**, 6 (2013)
2. Pandey, A., Dabral, P.P.: Estimation of runoff for hilly catchment using satellite data. J. Indian Soc. Remote Sens. **32**, 2 (2004)
3. Black, P.E.: Watershed Hydrology, vol. 2, pp. 231–236. Ann Arbor Press Inc., Chelsea (1996)
4. Brodie, R.S., Hostetler, S.: A review of techniques for analysing base flow from stream hydrographs. J. Am. Water Resour. Assoc. **53**(8), 579–663 (2010)
5. Prakasa Rao, B.S., Pernaidu, P., Amminedu, E., Rao, T.V., Sathi Devi, K., Jagadeeswara Rao, P., Srinivas, N., Bhaskara Rao, N.: Run-off and flood estimation in Krishna River delta using remote sensing and GIS. J. Indian Geophys. Union **15**(2), 101–112 (2011)
6. Chapman, T.G., Maxwell, A.I.: Baseflow separation—comparison of numerical methods with tracer experiments. Hydrological and Water Resources Symposium, Institution of Engineers Australia, Hobart, pp. 539–545
7. Ramakrishnan, D., Bandyopdhyay, A., Kusuma, K.N.: SCS-CN and GIS based approach for identifying potential water harvesting sites in the Kali Watershed, Mahi River Basin, India. J. Earth Syst. Sci. **118**(4), 355–368 (2009)
8. Furey, P., Gupta, V.K.: A physically based filter for separating base flow from streamflow time series. Water Resour. Res. **37**, 2709–2722 (2001)
9. Gonzales, A.L., Nonner, J., Heijkers, J., Uhlenbrook, S.: Comparison of different base flow separation methods in a lowland catchment. Hydrol. Earth Syst. Sci. **13**, 2055–2068 (2009)
10. Rouhania, H., Malekianb, A.: Automated methods for estimating base flow from stream flow records in a semi arid watershed. DESERT **17**, 203–209 (2012)
11. Adornado, H.A., Yoshida, M.: GIS-based watershed analysis and surface run-off estimation using curve number (CN) value. J. Environ. Hydrol. **18**, 1–10 (2010)
12. Arnold, J.G., Allen, P.M.: Automated methods for estimating base flow and ground water recharge from stream flow records. J. Am. Water Resour. Assoc. **35**(2), 411–424 (1999)
13. Arnold, J.G., Allen, P.M., Muttiah, R., Bernhardt, G.: Automated base flow separation and recession analysis techniques. Ground Water **33**(6), 1010–1018 (1995)
14. Mishra, S.K., Jain, M.K., Bhunya, P.K., Singh, V.P.: Field applicability of the SCS-CN-based Mishra-Singh general model and its variants. J. Water Resour. Manag. **19**, 37–62 (2006)
15. Sundar Kumar, P.: Estimation of rainfall-runoff of the Vijayawada City by SCSCN method using remote sensing and GIS. **1**(11), 1–4 (2012)
16. Nayak, T., Verma, M.K., Hema Bindu, S.: SCS curve number method in Narmada Basin. Int. J. Geomat. Geosci. **3**(1) (2012)

17. Eckhardt, K.: Analytical sensitivity analysis of a two parameter recursive digital base flow separation filter. Hydrol. Earth Syst. Sci. **16**, 451–455 (2012)
18. Latha, M., Rajendran, M., Murugappan, A.: Comparison of GIS based SCS-CN and strange table method of rainfall-runoff models for Veeranam Tank, Tamil Nadu, India. Int. J. Sci. Eng. Res. **3**(10) (2012)
19. Lim, K.J., Engel, B.A., Tang, Z., Choi, J., Kim, K.-S., Muthukrishnan, S., Tripathy, D.: Automated web GIS based hydrograph analysis tool. WHAT. J. Am. Water Resour. Assoc. **41**(6), 1407–1416 (2005)
20. National Engineering Handbook: United States Department of Agriculture, Part 630 Hydrology (2007)
21. Gupta, P.K., Panigrahy, S.: Predicting the spatio-temporal run-off generation in India using remotely sensed input and soil conservation service curve number method. Curr. Sci. **95**(11), 1580–1588 (2008)
22. Chow, V.T., Maidment, D.R., Mays, L.W.: Applied Hydrology. Tata McGraw-Hill Publications. New York (2010)
23. Zhan, X., Huang, M.-L.: ArcCN-Runoff: an ArcGIS tool for generating curve number and runoff maps. Environ. Model. Softw. **19**, 875–887 (2004)

Multivariate Statistical Analysis of River Water Quality—A Study on River Godavari in Andhra Pradesh

G. V. R. Srinivasa Rao, M. Rajesh Kumar, T. P. Sreejani and P. V. R. Sravya

Abstract A study on the seasonal fluctuations in the quality of water in river Godavari at Rajahmundry, Dowleswaram, and Polavaram is aimed at in this work. Water quality indices (WQI) are computed in two methods, viz. NSFWQI and WAI-WQI methods. The water quality data pertaining to the period 2002–2016 is analyzed for its seasonal variation using multivariate statistical methods like CA, PCA, FA and taking into consideration the physico-chemical, biological, and irrigation parameters. The study based on WQI indicated that the quality of water in river Godavari at Polavaram is medium and at Rajahmundry and Dowleswaram is poor for domestic purposes. Similarly, for irrigation purposes, the WQI study indicated that the quality of water is nearer to good at Polavaram and Medium at Rajahmundry and Dowleswaram. The multivariate statistical analysis of the data and the studies based on WQI are found to be in good correlation.

Keywords Rajahmundry · Dowleswaram · Polavaram · WQI
Multivariate statistical methods

1 Introduction

Water is one of the basic requirements for the sustenance of life on the earth. The health of human beings and the quality of water is closely related. Therefore, the quality of water is now being recognized as a major concern as it is getting deteriorated by human activities, day by day. However, the availability of pure water became a matter of concern in the present day world due to population explosion and indiscriminate exploitation of the water resources.

G. V. R. Srinivasa Rao (B) · M. Rajesh Kumar · T. P. Sreejani
Department of Civil Engineering, A U Engineering College (A), Andhra University, Visakhapatnam, India
e-mail: gvrsrao@gmail.com

P. V. R. Sravya
Department of Civil Engineering, ANITS, Thagarapuvalasa, Visakhapatanam, India

M. Rathinasamy et al. (eds.), *Water Resources and Environmental Engineering II*,
https://doi.org/10.1007/978-981-13-2038-5_7

With the increasing pressure of human population, there developed severe stress on water resources. At the same time, the quality of surface water resources are being deteriorated due to the ill effects of urbanization, industrialization, and modern agricultural activities. Moreover, the surface water sources are more vulnerable to pollution due to the easy accessibility for the disposal of wastewaters into them. In these conditions, statistical modelling will enable researchers and governments to understand the variations of river water quality at specified locations.

The multivariate statistical analysis is a powerful tool for the analysis of large data sets of water quality parameters and to determine the parametric variations affecting the overall quality of water and a mechanism to justify these variations [1]. The seasonal variations of Cauvery river water quality studied using multivariate statistical analysis has shown that all the parameters contributed equally and significantly [2]. Similar methods are used by González et al. [3] for the assessment of water quality and its variations in the river Potrero de los Funes, Argentina. Mandal et al. [4] assessed the seasonal variation of physicochemical characteristics of the water quality in Torsha river.

Thareja et al. [5] analyzed 14 physico-chemical parameters from Jal Sansthan, Benajhabar, Kanpur, sampling station in PCA which produced two significant components explaining more than 99.31% of the variance with anthropogenic and industrial effects representing 64.47 and 34.84%, respectively. The FA and PCA of the study on the Sakarya river in Turkey has shown that the pollution levels in the river varied with that of agricultural and domestic pollutants joining the river [6]. The multivariate statistical methods are successfully used to obtain the pollution factor caused due to the different sources of pollution, such as domestic sewage, industrial wastes, stormwater drains, by Gupta et al. [7] while assessing the marine water quality in Maharashtra, west coast of India. Similarly, these methods are effectively used to assess the quality of water in the catchment of TPU, Kuala Lumpur, Malaysia, by Ajorlo et al. [8].

2 Study Area

The sampling stations at Polavaram, Rajahmundry, and Dowleswaram located on the banks of river Godavari in Andhra Pradesh are considered for the study. Polavaram, Rajahmundry, and Dowleswaram are located on 17.2479°N and 81.6432°E, 17.0005°N and 81.8040°E, and 16.9507°N and 81.7820°E, respectively. At Polavaram, a multipurpose hydro-electric project is under construction and at Dowleswaram, a barrage exists which supplies water for irrigation purposes.

3 Methodology

(a) **Data**:

The data is collected from Irrigation & CAD Department, Hydrology Project Circle, Hyderabad, Government of Andhra Pradesh, for Rajahmundry and Dowleswaram points and from Central Water Commission, Hyderabad, for Polavaram point for the period 2002–2016. The seasons considered for the study are from March to June (pre-monsoon), July to October (monsoon), and November to February (post-monsoon). The data include the physico-chemical parameters, biological parameters, and irrigation parameters: pH, Electrical conductivity, total dissolved solids, Ca, hardness, chlorides, total alkalinity, bicarbonates, carbonates, sodium, potassium, calcium, magnesium, fluorides, nitrite-nitrogen, nitrate-nitrogen, phosphates, BOD, COD, DO, DO_Sat.%, percent sodium, residual sodium carbonate, sodium absorption ratio.

(b) **WQI**:

Water quality indices (WQI) are calculated in both WAIWQI and NSFWQI methods.

(i) **WAIWQI** which ranges from 0 to 100 and above representing excellent to unsuitable for the usage is calculated using the following equations.

$$\mathrm{WQI} = \sum Q_i W_i / \sum W_i \tag{1}$$

$$Q_i = 100 * \{(V_i - V_o)/(S_i - V_o)\} \tag{2}$$

$$W_i = K/S_i \tag{3}$$

$$K = 1/\sum (1/S_i) \tag{4}$$

where

- Q_i Quality rating scale of each parameter
- V_i Estimated concentration of ith parameter in the analyzed water
- V_o The ideal value of pure water
- S_i Standard value of ith parameter
- W_i The unit weight for each water quality parameter
- K Proportionality constant.

(ii) **NSFWQI** which ranges from 0 to 100 representing poor to excellent quality is calculated as given below.

$$\mathrm{WQI} = \sum \mathrm{SI}_i \tag{5}$$

$$\mathrm{SI}_i = w_i \times q_i \tag{6}$$

$$w_i = 1/s_i \tag{7}$$

where

SI_i subindex of ith parameter
w_i relative weight and is calculated as
s_i standard values of parameters
q_i quality rating of ith parameter
c_i experimental value

(c) **Multivariate Statistical Analysis**:

SPSS 20.0 is used to conduct FA, CA, and PCA in the present study. The analysis is conducted as given below.

(i) **Missing Value Incorporation and Validation of Data**:

Missing data reduce the representativeness of the sample and of any statistical analysis. It occurs when no value is stored in the data sets of the observed variables. Initially, the parametric variables are classified into categorical and quantitative variables. From this, the missing value patterns are analyzed. Then the statistical tests are conducted before obtaining the final data set output.

Validation of data aims at identification of suspicious and invalid cases and data variables in a data set and produces the descriptive summaries of analysis of variables while ignoring the weight variable specifications. Data obtained from the missing value analysis is given as input for data validation. Duplicate cases are identified in the process and descriptive statistics are analyzed to conduct few statistical tests to validate the data.

(ii) **Factor Analysis**:

In factor analysis, the values of observed data are expressed as functions of a number of possible factors in order to reduce the correlational data to a smaller number of dimensions or factors. A rectangular array of the correlation coefficients popularly known as correlation matrix is generated for all the variables. Based on the correlation coefficients of the variables, the factors are extracted from correlation matrix. The factors are then rotated to maximize the relationship between the variables and other factors.

(iii) **Cluster Analysis**:

This is a statistical technique used to divide the data into group cases and further into homogenous subgroups based on responses to variables. Hierarchical clustering is adopted in the present study since it is the most commonly used method and computes the proximity matrix of the difference or similarity of every case with every other case.

(iv) **Principal Component Analysis**:

PCA is eigen vector-based multivariate analysis. In PCA, the data gets transformed in a way that the largest parametric variance of the data occupies the first component and the second largest variance lies on the second component and so on.

4 Results and Discussion

(a) **Water Quality Indices**:

The water quality indices obtained for river Godavari at three study locations are given in Tables 1 and 2.

(b) **Multivariate Statistical Analysis**:

The analysis of physicochemical parameters at Polavaram by using FA indicated that four significant factor loadings with 50.73% of the variance in data sets are observed, and the factors are alk-total, Ca, HCO_3, alk-phenol, CO_3, $NO_2 + NO_3$, NO_3–N. The high factor loadings indicate that these parameters are in high concentrations and cause variation in WQI. It is observed that DO and DO_Sat.% played a vital role in polluting the water body w.r.t biological parameters. It is further observed that the EC is the main factor with 23.42% of the variance affecting the quality of water for the irrigation purposes.

Three significant factor loadings with 99.44% of the variance in data sets are obtained in FA, and the factors are EC, F, NO_2–N, $NO_2 + NO_3$ w.r.t physicochemical parameters at Rajahmundry. Two significant factor loadings with 65.60% of the variance in data sets are obtained in FA w.r.t biological parameters at Rajahmundry. DO, DO_Sat.%, BOD are found to cause variation in WQI. Regarding irrigation parameters, three significant factor loadings with 30.42% of the variance in data sets comprising of EC_FLD, TDS, Total Hardness, Na%, SAR, RSC are observed.

Three significant factor loadings with 99.44% of the variance in data sets are obtained in FA w.r.t physicochemical parameters at Dowleswaram. EC, alk-total, alk-phen, EC_FLD, HCO_3 are the high factor loadings obtained causing variation in WQI. Two significant factor loadings with 63.01% of the variance in data sets are obtained in FA for biological parameters at Dowleswaram. DO, DO_Sat.%, BOD had the highest loading factors. Three Significant factor loadings with 57.26% of the variance in data sets are obtained in FA for irrigation parameters at Dowleswaram, and EC_FLD, SAR, RSC are found to have the highest loading factors.

Six principal components are generated in PCA w.r.t physicochemical parameters at Polavaram explaining 69.20% of the total variance. The principal components having high factor loadings are EC, alk-total, HCO_3, alk-phenol, CO_3, $NO_2 + NO_3$, NO_3–N, NO_2–N. Three principal components are generated in PCA for biological parameters at Polavaram explaining 81.44% of the total variance. The principal components having high factor loadings are DO (mg/L) and DO_Sat.%, BOD_3. Four principal components are generated in PCA for irrigation parameters at Polavaram explaining 70.41% of the total variance with high factor loadings, and they are HAR_Ca, HAR_total, EC_GEN, SAR, Na%, RSC, and NH_3–N.

One principal component is generated in PCA of biological parameters at Rajahmundry explaining 79.20% of the total variance. DO_Sat.% is found to be the highest loading factor. Three principal components are generated PCA of biological parameters at Rajahmundry explaining 39.67% of the total variance. EC_FLD, HAR_total, RSC are found to have the highest loading factors.

Table 1 Seasonal averages of NSFWQI

Study area	Rajahmundry			Dowleswaram			Polavaram		
Seasonal variations	Parameters								
	Physicochemical	Biological	Irrigation	Physicochemical	Biological	Irrigation	Physicochemical	Biological	Irrigation
Pre-monsoon	48.55	66.51	34.13	46.60	69.14	34.94	53.47	61.62	55.12
Quality rating	Fair	Med.	Fair	Fair	Med.	Fair	Med.	Med.	Med.
Monsoon	51.05	66.61	25.54	53.50	71.86	24.13	55.07	52.16	48.24
Quality rating	Med.	Med.	Fair	Med.	Good	Poor	Med.	Med.	Fair
Post-monsoon	52.15	70.76	28.24	67.24	69.19	32.36	58.47	58.97	53.50
Quality rating	Med.	Good	Fair	Med.	Med.	Fair	Med.	Med.	Med.

Table 2 Seasonal averages of WAIWQI

Study area	Rajahmundry			Dowleswaram			Polavaram		
Seasonal variations	Parameters								
	Physicochemical	Biological	Irrigation	Physicochemical	Biological	Irrigation	Physicochemical	Biological	Irrigation
Pre-monsoon	42.70	68.32	39.70	40.54	65.34	44.26	54.04	29.61	24.53
Quality rating	Good	Poor	Good	Good	Poor	Good	Poor	Good	Exlnt
Monsoon	47.77	68.10	34.81	47.42	70.37	27.52	51.29	23.94	20.21
Quality rating	Good	Poor	Good	Good	Poor	Good	Poor	Exlnt	Exlnt
Post-monsoon	49.63	72.30	37.83	62.76	68.58	47.45	60.68	28.33	25.60
Quality rating	Good	Poor	Good	Poor	Poor	Good	Poor	Good	Good

One principal component is generated in PCA of physicochemical parameters at Dowleswaram explaining 99.20% of the total variance. Fe is found to have the highest loading factor. One principal component is generated in the principal component analysis of biological parameters at Dowleswaram explaining 64.90% of the total variance in the data sets. DO_Sat.% is found to have the highest loading factor. Two principal components are generated in principal component analysis of irrigation parameters at Dowleswaram explaining 58.62% of the total variance in the data sets. EC_FLD and SAR had the highest loading factors.

From the cluster analysis conducted for both physicochemical and biological parameters at Rajahmundry and Dowleswaram, it is observed that the monsoon season bears the higher pollution loadings with DO_Sat.% affecting the degree of pollution. CA conducted for irrigation parameters shows that EC_FLD and TDS affect the degree of pollution at both Rajahmundry and Dowleswaram. From the comparative study of CA with WQI, it is observed that the clusters obtained vis-à-vis WQI are in good correlation.

5 Conclusions

Study based on WQI indicated that the quality of water in river Godavari at Polavaram is medium and at Rajahmundry and Dowleswaram is poor for domestic purposes. However, for irrigation purposes, the study indicated that the quality of water is nearer to good at Polavaram and medium at Rajahmundry and Dowleswaram. From the multivariate statistical analysis conducted, it is observed that the clusters formed vis-à-vis WQI are in good correlation.

References

1. Kennel, P.R.: Chemometrics in assessment of seasonal variation of water quality in fresh water systems. Environ. Monit. Assess. **174**, 529–545 (2011). https://doi.org/10.1007/s10661-010-1476-6
2. Venkatesharaju, K., Somasekhar, R.K., Prakash, K.L.: Determination of water quality index and sustainability of an urban water body in Shimoga Town, Karnaka. KMITL Sci. Technol. J. **12**(1) (2012)
3. González, S.O., Almeida, C.A., Quintar, S., Mallea, M.A., González, P.S.: Application of multivariate statistical techniques to evaluate organic pollution on a river in Argentina. Interdiscip. J. Appl. Sci. **6**, 27–42 (2011)
4. Mandal, H.S., Das, A.: Assessment of seasonal variation in physico-chemical characteristics and quality of Torsha River water for irrigation used in Cooch Behar and Jalpaiguri districts of Wast Bengal, India. J. Chem. Pharm. Res. **3**(6), 265–270 (2011)
5. Thareja, S., Choudhury, S., Trivedi, P.: Assessment of water quality of Ganga River in Kanpur by using principal component analysis. Adv. Appl. Sci. Res. **2**(5), 84–91 (2011)

6. Yerel, S., Ankara, H.: Application of multivariate statistical techniques in the assessment of water quality in Sakarya River, Turkey. J. Geol. Soc. India **79**, 89–93 (2012)
7. Gupta, I.: Chemometric data analysis of marine water quality in Maharashtra, West coast of India. Indian J. Geo-Mar. Sci. **42**(1), 97–105 (2013)
8. Ajorlo, M., Abdullah, R.B., Yusoff, M.K., Halim, R.A., Hanif, A.H.M., Willms, W.D., Ebrahimian, M.: Multivariate statistical techniques for the assessment of seasonal variations in surface water quality of pasture ecosystems. Environ. Monit. Assess. **185**, 8649–8658 (2013). https://doi.org/10.1007/s10661-013-3201-8

A Study on Seasonal Variation of the Groundwater Chemistry in Andhra University Campus, Visakhapatnam

G. V. R. Srinivasa Rao, Y. Abbulu, T. P. Sreejani and S. Priyanka

Abstract An attempt has been made in this work to evaluate the quality of groundwater at Andhra University campus, Visakhapatnam, Andhra Pradesh, India, and its suitability for domestic purpose. Groundwater samples are collected from the twenty-five bore wells located in the campus during the post-monsoon (November 2015–February 2016), Pre-monsoon (March 2016–June 2016) and Monsoon (July 2016–October 2016) periods at regular intervals of time and are analysed for various physico-chemical parameters using standard laboratory procedures. Data analysis is done by using Aquachem 2014.2 software. Piper tri-linear diagrams and Durov diagrams are drawn using the concentrations of various cations and anions. The dominance of major cations and anions is observed as $Mg^{2+} > Ca^{2+} > Na^{+} > K^{+}$ and $Cl^{-} > HCO_3^{-} > SO_4^{2-} > CO_3^{-}$, respectively. From Piper plots, it is observed that majority of groundwater samples exhibited that $Ca^{2+} + Mg^{2+}$ significantly exceeded $Na^{+} + K^{+}$ and $Cl^{-} + SO_4^{2-}$ exceeded $HCO_3^{-} + CO_3^{2-}$ in Post-Monsoon, Pre-Monsoon and Monsoon periods. The pH and TDS parts of the Durov plot reveal that the quality of groundwater is in the range of drinking water standards during all the seasons.

Keywords Piper tri-linear diagram · Durov diagram
Physico-chemical parameters · Aquachem 2014.2

1 Introduction

Water is a valuable and crucial resource for the sustenance of life and for any developmental activity. Most of the times groundwater forms a potential source of water supply all over the world. However, in the recent past groundwater quality is getting deteriorated due to various reasons and making it unsuitable for drinking purposes.

G. V. R. Srinivasa Rao (B) · Y. Abbulu · T. P. Sreejani · S. Priyanka
Department of Civil Engineering, A U Engineering College (A), Andhra University, Visakhapatnam, India
e-mail: gvrsrao@gmail.com

M. Rathinasamy et al. (eds.), *Water Resources and Environmental Engineering II*,
https://doi.org/10.1007/978-981-13-2038-5_8

Hence, it became necessary to assess the groundwater quality spatially over sufficient periods of time to arrive at its suitability for various purposes.

Groundwater, in general, is less susceptible to bacterial pollution when compared with the surface water. But it contains several chemical elements like Ca^{+2}, Mg^{+2}, Na^{+}, K^{+}, HCO_3^{-}, Cl^{-} and SO_4^{2-} which play an important role in the classification and assessment of quality of groundwater. The groundwater quality data can be interpreted through Piper tri-linear plots and Durov diagrams. The present study involves the assessment of the groundwater quality at Andhra University campus, Visakhapatnam, in terms of Piper tri-linear plots, Durov diagrams by analysing groundwater samples over a period of one year during different seasons.

Earlier studies w.r.t. groundwater chemistry indicate that studies on hydrogeochemistry enable the researchers to evaluate the elevated concentrations of certain ions and their interrelationships which in turn will be helpful to assess the reasons behind like anthropogenic processes. In a study conducted by Seyflaye et al. [1], the high-level concentrations of nitrates are related to the processes like leaching of fertilizers and pesticides into the ground, return flow of irrigation water, etc. The hydro-chemical studies enable to know how the chemical composition of groundwater varies w.r.t. to types of water. Hydro-geochemical parameters of groundwater are largely controlled by the flow patterns of groundwater that follow the topographical features of the study area. In a study conducted by Hamzaoui-Azaza et al. [2], it is observed that the mineralization of the groundwater increased significantly following the direction of flow of groundwater.

The Piper diagrams as well as Durov diagrams drawn for the working of hydrogeochemical facies indicate the variability of water quality parameters falling within acceptable range or not. Ghoraba and Khan [3]. In a study conducted by Ramkumar et al. [4] near a coastal zone, higher concentrations of ions were observed during the post-monsoon indicating the intrusion of saline water into the coastal area. However, in the pre-monsoon season the ionic concentrations indicated the return flow into the coastal aquifer. In a study on groundwater quality in the coastal aquifers at south Chennai, India, Kumar et al. [5] observed that most of the sampling points cluster on Na^{+} and Cl^{-} and the mixed facies of Ca^{+}–Mg^{+}–Cl^{-} of the tri-linear diagram indicated that the dominant ions of groundwater are derived from sea water intrusion.

The hydrogeological facies using Piper and Durov diagrams drawn in a study conducted by Khan et al. [6] in the Indus basin of Pakistan have shown that groundwater mixing creating environmental issues like lowering of water table and saltwater intrusion. In a study conducted in southern Gaza strip, Jabel et al. [7] observed that the groundwater is alkaline in nature with the ionic abundance of the cations following the order $Na^{+} > Mg^{2+} > Ca^{2+} > K^{+}$ and anions $Cl > HCO^{3} > SO_4^{2-} > NO^{3-}$ and F. The Gibb's diagram indicated that the groundwater chemistry is controlled by ion exchange, evaporation and the anthropogenic activities. The isotopic and geochemical modelling techniques enable understanding of shallow water systems and the underlying causes of salination by Abu-Jaber [8].

2 Study Area

Andhra University campus located in Visakhapatnam, Andhra Pradesh, lying between latitude 17º 43′ 5.38″N and longitude 83º 19′ 17.61″E with an area of 422 acres and a varying elevation from 10 MSL to 62.5 MSL is considered as a study area for this research work. The average annual rainfall is 955 mm and the mean annual temperature and humidity are 23.7 °C and 67–78%, respectively. The study area is divided into two campuses, viz. South campus and North campus.

3 Methodology

3.1 Analysis of Groundwater Quality

Groundwater samples collected from the existing 25 bore wells in the campus during the periods November 2015–February 2016 (post-monsoon season), March 2016–June 2016 (pre-monsoon season) and July 2016–October 2016 (monsoon season) were analysed for their physico-chemical parameters. These parameters include pH, electrical conductivity, alkalinity, hardness, total dissolved solids, sulphates, chlorides, bicarbonates, iron, magnesium, calcium, sodium, potassium and fluorides in standard procedures.

3.2 Piper Tri-linear Diagrams

Piper tri-linear plots are plotted using Aquachem 2014.2 for post-monsoon, pre-monsoon and monsoon periods. On the left triangle, the cations are plotted, whereas the anions are plotted on the right triangle. The concentrations of cations and anions are expressed as percentages in meq/l. Each point is then projected into the upper field along a line parallel to the upper margin of the field. The point at which the extension intersects shows the characteristics of water representing the relationship among $Na^+ + K^+$, $Cl^- + SO_4^{-2}$, $HCO_3^- + CO_3^-$ and $Ca^{+2} + Mg^{+2}$.

3.3 Durov Diagrams

The Durov diagrams are plotted using Aquachem 2014.2. Using these diagrams, the groundwater quality and its evolution can be understood and the geochemical processes can be displayed. In Durov diagram, it is possible to depict pH and TDS in addition to cations and anions.

4 Results and Discussions

The results of the study in terms of the maximum and minimum values of different water quality parameters during the post-monsoon (November 2015–February 2016), pre-monsoon (March 2016–June 2016) and monsoon (July 2016–October 2016) seasons are presented in Table 1.

4.1 Piper Tri-linear Plots

It is observed from the Piper plots that 95% of the samples fall under Ca^{2+}–Mg^{2+}–HCO_3^- facies (Type-1 water), 5% of the samples fall under Ca^{2+}–Mg^{2+}–Cl^-–SO_4^{2-} facies (Type IV water), and also majority of groundwater samples exhibit that the combination of Ca^{2+} + Mg^{2+} exceeded the combination

Table 1 Average parametric values (November 2015–October 2016)

S. No.	Parameter	Post-monsoon (November 2015–February 2016)	Pre-monsoon (March 2016–June 2016)	Monsoon (July 2016–October 2016)
1	pH	6.01–7.99	6.01–8.62	6.00–8.62
2	Electrical conductivity (µs/cm)	0.01–20.22	0.10–874.80	0.10–2.90
3	Calcium (mg/l)	78–226	62–380	66–190
4	Magnesium (mg/l)	18–238	10–308	12–358
5	Sodium (mg/l)	10.5–97.2	6.8–99	1.2–98.1
6	Potassium (mg/l)	4.3–30	4.2–28.3	5.7–29.9
7	Bicarbonate (mg/l)	170–690	5–690	5–515
8	Carbonate (mg/l)	20–170	30–240	10–210
9	Chlorides (mg/l)	91.97–219.93	79.97–337.4	37.99–213.93
10	Sulphates (mg/l)	9.8–92.91	6.8–89.95	1.5–92.92
11	Iron (mg/l)	0.01–0.05	0.02–0.5	0.01–0.1
12	Fluoride (mg/l)	0.08–0.50	0.03–0.29	0.04–0.48
13	Total dissolved solids (mg/l)	300–1860	240–1940	200–1860
14	Total alkalinity (mg/l)	225–680	15–740	125–555
15	Total hardness (mg/l)	126–344	110–448	116–450

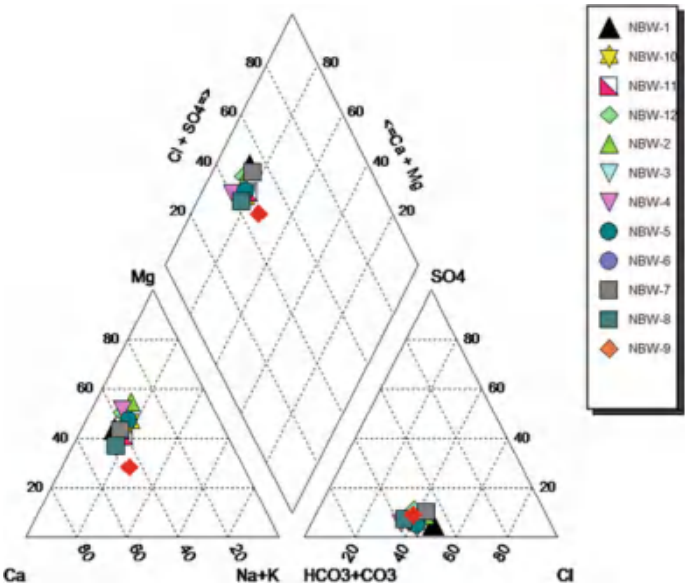

Fig. 1 Piper tri-linear plot for North campus, AU, post-monsoon (November 2015–February 2016)

of $Na^+ + K^+$. Similarly, the $Cl^- + SO_4^{2-}$ combination exceeded the $HCO_3^- + CO_3^{2-}$ combination in post-monsoon period.

It is observed that during the pre-monsoon period, 33% of the samples fall under Ca^{2+}–Mg^{2+}–HCO_3^- facies (Type-1 water), 67% of the samples fall under Ca^{2+}–Mg^{2+}–Cl^-–SO_4^{2-} facies (Type-IV water), and also majority of groundwater samples exhibit that the combination of $Ca^{2+} + Mg^{2+}$ exceeded the combination of $Na^+ + K^+$. Similarly, the $Cl^- + SO_4^{2-}$ combination exceeded the $HCO_3^- + CO_3^{2-}$ combination in pre-monsoon period.

Further, it is observed that during the monsoon period that 50% of the samples fall under Ca^{2+}–Mg^{2+}–HCO_3^- facies (Type-1 water), 50% of the samples fall under Ca^{2+}–Mg^{2+}–Cl^-–SO_4^{2-} facies (Type-IV water), and also majority of groundwater samples exhibited that the combination of $Ca^{2+} + Mg^{2+}$ exceeded the combination of $Na^+ + K^+$. Similarly, the $Cl^- + SO_4^{2-}$ combination exceeded the $HCO_3^- + CO_3^{2-}$ combination in monsoon period.

The ionic dominance exhibited the following pattern: $Mg^{2+} > Ca^{2+} > Na^+ > K^+$ and $Cl^- > HCO_3^- > SO_4^{2-} > CO_3^-$. Majority of groundwater samples exhibited that $Ca^{2+} + Mg^{2+}$ significantly exceeded $Na^+ + K^+$ and $Cl^- + SO_4^{2-}$ exceeded $HCO_3^- + CO_3^{2-}$ in all the three seasons (Figs. 1, 2, 3, 4, 5 and 6).

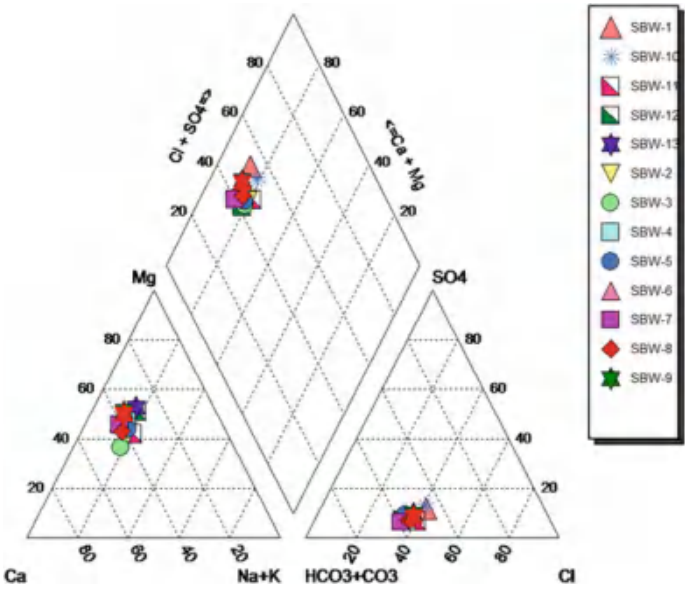

Fig. 2 Piper tri-linear plot for South campus, AU, post-monsoon (November 2015–February 2016)

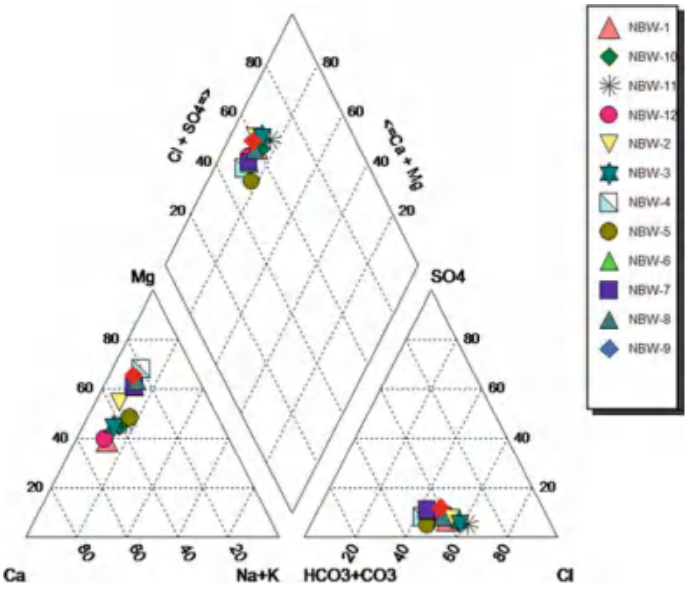

Fig. 3 Piper tri-linear plot for North campus, AU, pre-monsoon (March 2016–June 2016)

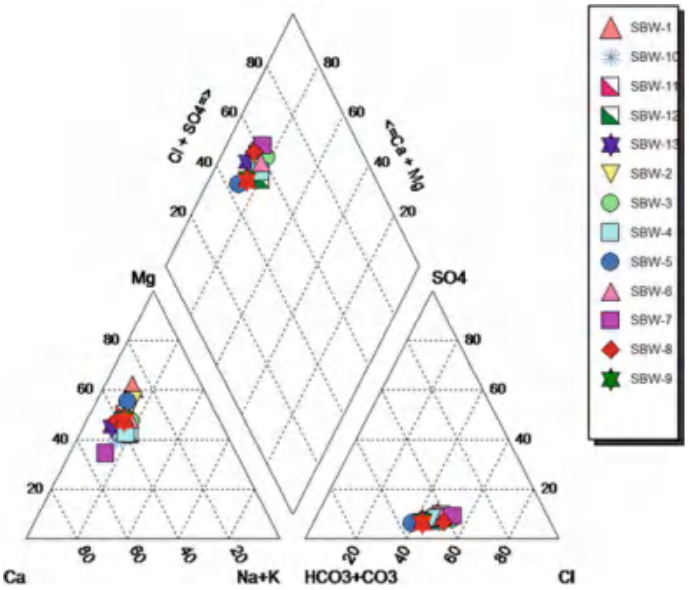

Fig. 4 Piper tri-linear plot for South campus, AU, pre-monsoon (March 2016–June 2016)

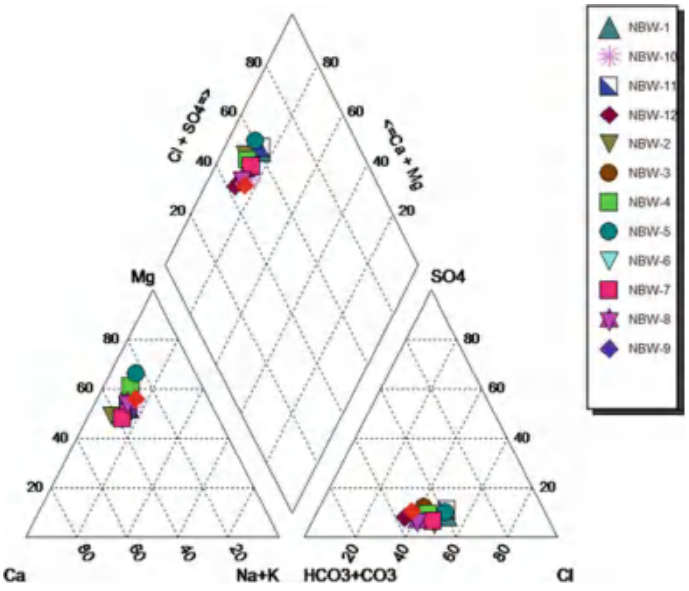

Fig. 5 Piper tri-linear plot for North campus, AU, monsoon (July 2016–October 2016)

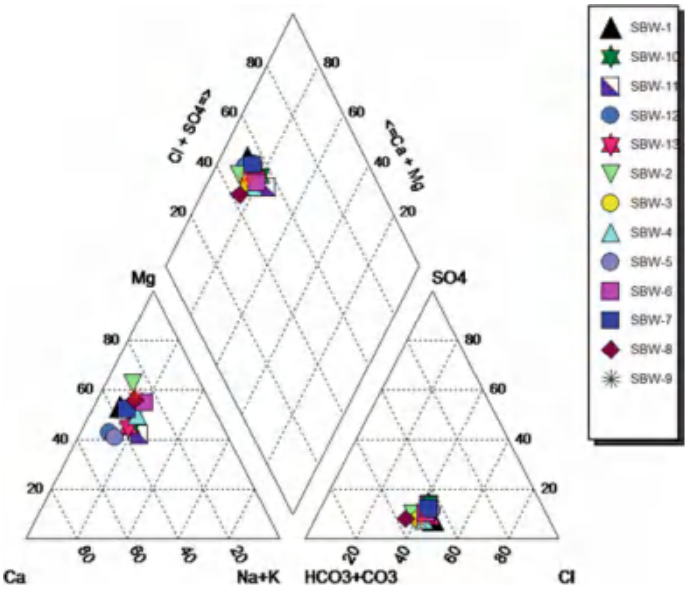

Fig. 6 Piper tri-linear plot for South campus, AU, post-monsoon (July 2016–October 2016)

4.2 Durov Diagrams

From the Durov plots, it is observed that the majority of groundwater samples are in the phase of dissolution in all the three seasons. The pH and TDS values from plots lie in the range of drinking water standards (Figs. 7, 8, 9, 10, 11 and 12).

5 Conclusions

1. The hydro-geochemical studies on groundwater quality in Andhra university using Piper tri-linear diagrams and Durov plots have shown that the $Ca^{2+} + Mg^{2+}$ significantly exceeded $Na^{+} + K^{+}$ and $Cl^{-} + SO_4{}^{2-}$ exceeded $HCO_3{}^{-} + CO_3{}^{2-}$ in post-monsoon, pre-monsoon and monsoon periods.
2. The groundwater in the major portion of the study area falls under type I water in which the dominating ions are Ca^{2+}–Mg^{2+}–$HCO_3{}^{-}$.
3. The groundwater in few pockets of the study area falls under the type IV water in which the dominating ions are Ca^{2+}–Mg^{2+}–Cl^{-}–$SO_4{}^{2-}$.
4. The presence of hardness in groundwater in the study area is established with the Piper and Durov diagrams.

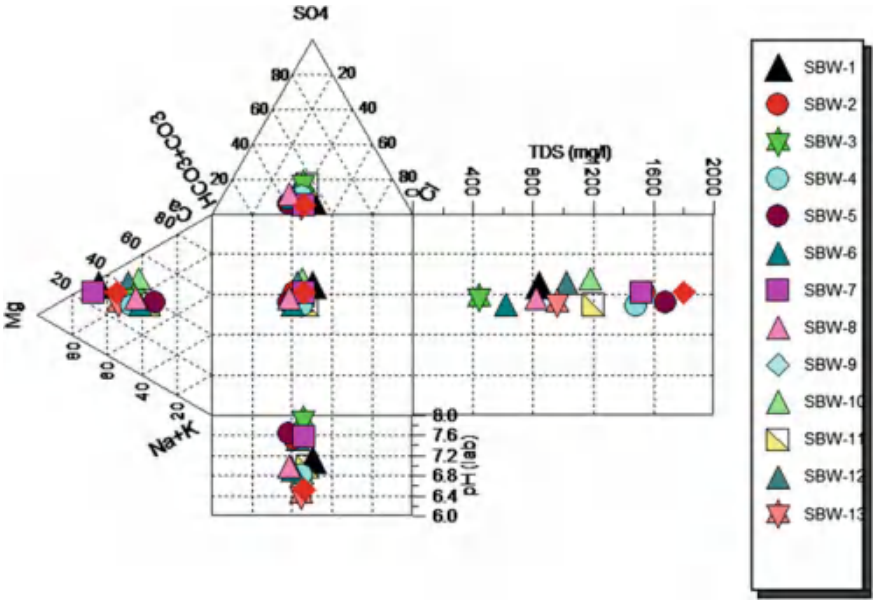

Fig. 7 Durov plot in North campus, AU, post-monsoon (November 2015–February 2016)

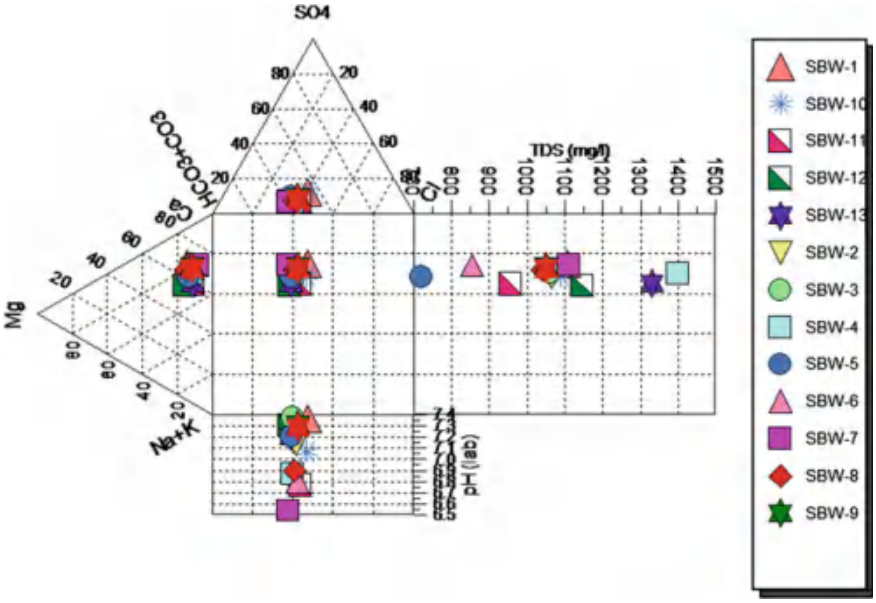

Fig. 8 Durov plot in South campus, AU, post-monsoon (November 2015–February 2016)

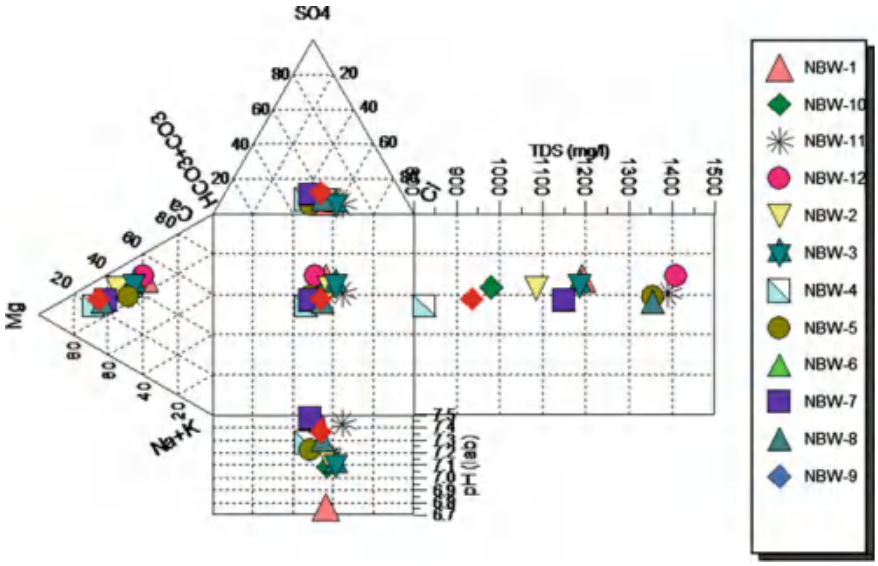

Fig. 9 Durov plot in North campus, AU, pre-monsoon (March 2016–June 2016)

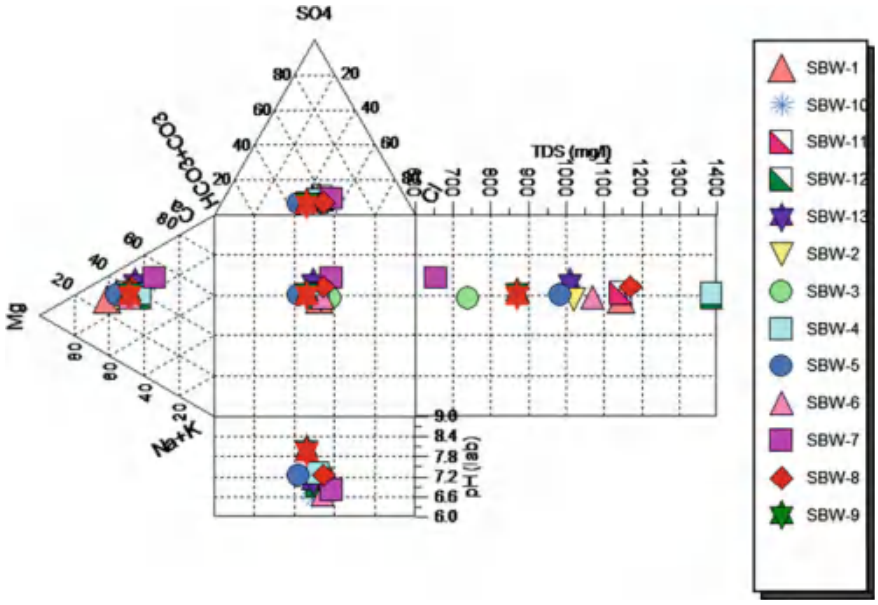

Fig. 10 Durov plot in South campus, AU, pre-monsoon (March 2016–June 2016)

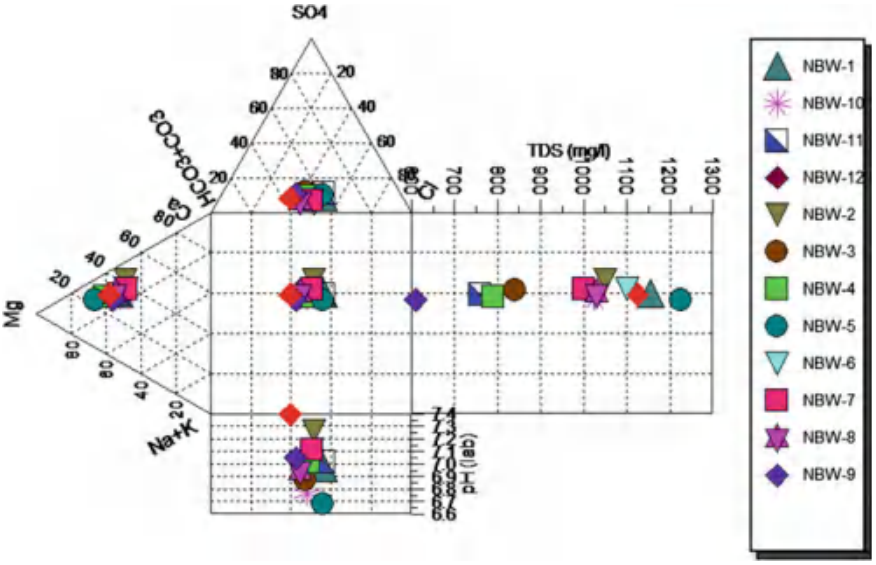

Fig. 11 Durov plot in North campus, AU, monsoon (July 2016–October 2016)

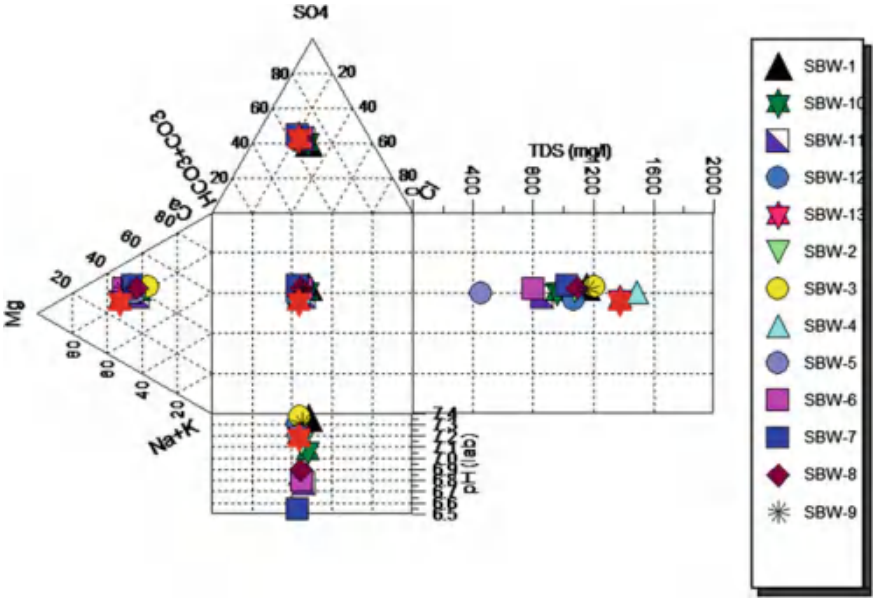

Fig. 12 Durov plot in South campus, AU, monsoon (July 2016–October 2016)

Acknowledgements The authors acknowledge Department of Science and Technology (DST), New Delhi, and Andhra University, Visakhapatnam, for sponsoring a research project under which the present work is carried out.

References

1. Seyf-laye, A.-S.M., Liu, M., Djaneye-Boundjou, G., Liu, F., Kamaletdinova, M.L., Bawa, M., Chen, H.: Hydrochemical investigation of groundwater contamination in an urban area of Beijing aquifer: impact of irrigation with industrial waste water. Afr. J. Agric. Res. **6**(31), 6555–6562 (2011)
2. Hamzaoui-Azaza, F., Ketata, M., Bouhlila, R., Gueddari, M., Riberio, L.: Hydrogeochemical characteristics and assessment of drinking water quality in Zeuss–Koutine aquifer, southeastern Tunisia. Environ. Monit. Assess **174**, 283–298 (2011). https://doi.org/10.1007/s10661-010-1457-9
3. Ghoraba, S.M., Khan, A.D.: Hydrochemistry and groundwater quality assessment in Balochistan Province, Pakistan. IJRRAS **17**(2) (2013)
4. Ramkumar, T., Venkataramanan, S., Anithamary, I., Ibrahim, S.M.S.: Evaluation of hydrogeochemical parameters and quality assessment of the groundwater in Kottur blocks, Tiruvarur district, Tamilnadu, India. Arab. J. Geosci. **6**, 101–108 (2013)
5. Kumar, S.K., Bharani, R., Magesh, N.S., Godson, P.S., Chandra Sekhar, N.: Hydrogeochemistry and groundwater quality appraisal of part of South Chennai coastal aquifers, Tamil Nadu, India using WQI and Fuzzy logic method. Appl. Water Sci. **4**, 341–350 (2014)
6. Khan, D., Mona, A.H., Iqbal, N.: Groundwater quality evaluation in Thal Doab of Indus basin of Pakistan. J. Mod. Eng. Res. **4**(1), 2249–6645 (2014)
7. Jabal, M.S.A., Abustan, I., Rozaimy, M.R., El Najar, H.: Groundwater beneath the urban area of Khan Younis City, southern Gaza Strip (Palestine): hydrochemistry and water quality. Arab. J. Geosci. **8**, 2203–2215 (2015)
8. Abu-Jaber, N., Ismail, M.: Hydrogeochemical modelling of the shallow groundwater in the northern Jordan Valley. Environ. Geol. **44**, 391–399 (2003). https://doi.org/10.1007/s00254-003-0770-9

Evaluation of Biogas Production Potential by Anaerobic Co-digestion with Substrate Mixture of Fruit Waste, Lawn Grass, and Manures

Atul Navnath Muske and P. Venkateswara Rao

Abstract The main benefits of co-digestion lies in balancing several parameters like carbon-to-nitrogen ratio (C/N), pH with bacterial diversity. The present research work was carried out by using the mixture of wastes comprising citrus pulp (CP), lawn grass (LG), and chicken manure (CM). From the study, it was found that biogas produced from the co-digestion of three component substrates is higher than that of mono- and binary digestion. In this co-digestion, higher biogas production was found out at reducing the concentration of CP and as the C/N ratio increased, biogas potential initially increased and then declined. Maximum biogas potential achieved with CP/CM of 25:75 and C/N ratio of 25:1 was 454.15 ml/g VS added. The result suggested that the biogas generation can be maximized by identifying the suitable proportion of organic waste mixture composition.

Keywords Anaerobic co-digestion · Central composite design · Biogas yield

1 Introduction

Anaerobic digestion (AD) is a biological process used to convert organic wastes into a stable product for application to land without causing adverse environmental effects. AD is a widely used technology for organic wastes treatment and energy recovery. Because of energy shortages and environmental problems in the past decade, this technology has received great attention. In this process, proper environmental conditions should be maintained, for example, number of substrates, temperature, and ammonium content. Single substrates for AD have drawbacks, including non-

A. N. Muske (B)
National Institute of Technology, Warangal, India
e-mail: muskeatual@gmail.com

P. Venkateswara Rao (B)
Civil Engineering Department, Water & Environment Division, National Institute of Technology, Warangal, India
e-mail: pvenku@gmail.com

M. Rathinasamy et al. (eds.), *Water Resources and Environmental Engineering II*,
https://doi.org/10.1007/978-981-13-2038-5_9

optimum carbon/nitrogen (C/N) ratios, low pH of the substrate itself, poor buffering capacity, and high concentration of ammonia [1]. For solving problems due to mono-digestion, it will be better to use more than one substrate. Previous studies have shown that co-digestion of mixture of substrates may result in better digestion performance. Co-digestion of dairy manure, chicken manure, and wheat straw performed better than individual digestion because of balanced C/N ratio [1]. This occurs through use of feed substrates with balanced nutrient composition, which stimulate the synergistic effects of microorganisms, an associated increase in buffering capacity, and a reduced effect of toxic compounds on the digestion process [2].

Ammonium nitrogen is a very important in all bioprocess, particularly in AD for bacterial growth; however, the high concentration of ammonium nitrogen especially free ammonium (NH_3) is toxic for anaerobic microorganism. Mesophilic reactor has a higher tolerance on total ammonium nitrogen (TAN) than thermophilic reactor [3]. From the literature, it is concluded that chicken manure (CM) has higher nitrogen content (low C/N ratio) due to uric acid and undigested protein, and after decomposition it will be contained in the form of TAN and NH_3.

Substrate concentration is another important operational factor for the stability of reactor and biogas production. As increasing the substrate concentration would bring fast bacterial growth and reaction rate but also develop inhibition from the soluble compound like TAN produced from the degradation [4]. Because of accumulation of TAN in digester alkalinity will be increased, and as a consequence, the pH of reactor will be above 8.5 which is inhibitory to the methanogens.

The most recalcitrant part of the substrate like grass is the presence of lignin content, due to its hydrophobic nature [5]. One of the main obstacles in utilizing grass biomass as feedstock for biogas production is its complex cell wall structure [6]. Enhanced biodegradation and solubility of crystalline cellulose and hemicellulose could lead to more efficient hydrolysis of grass. The dairy and poultry manure co-digested with switch grass resulted in accumulation of volatile fatty acid (VFA) [7]. The accumulation of VFA resulted in irreversible digester acidification, as accumulation of VFA increased leads to reducing the pH of digester.

Fruits have high moisture and organic content and are readily biodegradable; therefore, AD is considered as suitable method for fruit waste management. But methane production from the fruits can be affected by the chemical composition and presence of flavor compounds [8]. In this study, peel waste from citrus waste is not included because of limonene content, which is inhibitory to microorganism.

The purpose of this study was to investigate the feasible mixture combination and optimizing the feeding of waste combination for AD. For central composite design (CCD) [9], the CP, CM, and LG were used as factor or independent variables.

2 Materials and Methods

2.1 Substrates

Fresh CP, CM, and LG were used as substrates for AD. CP, CM, and LG residues were collected from fruit juice shop in Warangal, livestock farm located in Madikonda, Kazipet and NIT Warangal campus, India, respectively. Before being put into the reactor, the LG was air-dried and ground into 2–3 mm size. The dairy manure is used as inoculums which were collected from dairy industry located near Kazipet, India. After collecting from dairy, manure has been cleaned from large inert and animal food particle. The chemical characterization of each waste and inoculum was tested in this study as given in Table 1. The sampling was carried out in triplicates.

2.2 Experimental Design

AD was carried out in batch operations under mesophilic condition (35 °C). The present study was performed using CCD with three factors of the CP, LG, and CM in (TS %). The compositions in different setups were as fallows. In setup 1, different ranges for various substrates were selected in between 4 and 8 total solids (TS %). Each bottle contained 35 ml of inoculum having 2.304 g VS (volatile solids) and 35 ml of corresponding substrate mixture combination shown in Table 4. The inoculum to substrate (I/S) maintained to be 1 (on volume basis). All the reactors were carried out in duplicate, except center point which was repeated six times to reduce errors. The blank contains 35 ml of inoculum and 35 ml of distilled water. Bottles were incubated in a laboratory oven at 35 °C for 60 days, and biogas generation was measured on daily basis.

In setup 2, batch experiments were carried out based on CCD with two factors of the CP/CM and C/N ratios. Each bottle contained 30 ml of inoculum having 1.3 g VS (volatile solids), and remaining 30 ml is corresponding substrate mixture combination. The inoculum to substrate (I/S) maintained to be 1. All the reactors were carried out in duplicate, except center point which was repeated six times. The blank

Table 1 Properties and characterization of substrate and inoculums

Characteristics	Citrus pulp (CP)	Lawn grass (LG)	Chicken manure (CM)	Dairy manure
TS (%)	11.2	40.3	42.5	8
VS (% of TS)	91.2	90	60	96
C/N*	24	50	6	20
pH	5	8	5	6

*Represent values are taken from literature (CP, LG, and CM are from 10, 9, and 8, respectively)

Table 2 Real and coded values of factor

Factor	Variable	Coded levels of variables				
		$\alpha = -1.633$	-1	0	1	1.633
CP	Citrus pulp (TS %)	2.734	4	6	8	9.266
LG	Lawn grass (TS %)	2.734	4	6	8	9.266
CM	Chicken manure (TS %)	2.734	4	6	8	9.266

contains 30 ml of inoculum, and 30 ml of distilled water was also run to determine the endogenous biogas production and minimize the background error. Bottles were incubated in a laboratory oven at 35 °C for 90 days, and biogas generation was measured on daily basis by using water displacement method.

2.2.1 Analysis

Central composite design is a second-order factorial design employed when the number of runs for a full factorial design is too large to be practical. This type of factorial design usually consists of a $2k$ factorial nucleus, six replications of the central point, and $2 * k$ axial points, where k is the number of factors evaluated. More specifically, in the present study the three factors were CM, CP, and LG are in TS %. Factorial design levels are coded from -1 to +1. Central point is replicated six times in order to estimate experimental error. Axial points ensure design rotatability, and their distance to the central point (α) is calculated according to Eq. (1) given below.

$$\alpha = 2^{k/4} \tag{1}$$

The variables, X_i, were coded as x_i according to Eq. (2) given below, such that X_0 corresponded to the central value:

$$x_i = \left(X_i - X_i^*\right)/\Delta X_i; \quad \text{where } i = 1, 2, 3, \ldots, k; \tag{2}$$

where

x_i is the dimensionless coded value of an independent variable,
X_i is the actual value of an independent variable for the ith test,
X_i^* is the actual value of an independent variable at the center point and
ΔX_i is the step change.

All the evaluated levels were combined in twenty different combinations. Coded and real values for each factor are presented in Table 2 for setup 1. For setup, two the different levels in the experiment are shown in Table 3, and all levels were combined in nine different combinations.

Table 3 Coded and real levels of factor

Factor	Variable	Coded levels of variables				
		$\alpha = -1.4$	-1	0	1	1.4
CP/CM*	Citrus pulp/chicken manure ratio	14.64	25	50	75	85.3
C/N	Carbon/nitrogen ratio	17.92	20	25	30	32.1

*Represent as the percentage of CP in mixture of CP and CM

2.3 Analytical Techniques

TS, VS, and pH analysis were performed in accordance with APHA. The volume of biogas was measured by water displacement method. Methane content in the produced biogas was analyzed by using gas chromatograph (model YL6500, Env.lab, NIT Warangal).

3 Result and Discussion

3.1 Characteristics of Substrate

From the present study, it is observed that there is high VS/TS ratio in all substrates presented in Table 1. High VS/TS ratio is favorable for biogas production. In some of the substrate having high VS/TS ratio like LG, these wastes are difficult to degrade. The reports were found that in [6, 7] where they concluded that lingo-cellulose compounds are not easily degradable because of complex cell wall structure, which contains large amount of fiber that will reduce biogas production.

Several reports suggested that optimum C/N ratios in anaerobic digesters are to be maintained in the range of 20–30. Except for CP, C/N ratios in LG and CM were both outside the range as presented in Table 1. A lower C/N ratio causes ammonia accumulation and pH values exceeding 8.5, which is toxic to methanogenic bacteria, C/N ratio of chicken manure was lower, which may cause more ammonium nitrogen release. High C/N ratio is an indication of rapid consumption of nitrogen by methanogens and accumulation of volatile fatty acid which will cause lower pH (<6.5) and result in lower biogas production. From Table 1, it can be conclude that because of LG in mixture the availability of food is more because of high carbon content, which is beneficial to methanogens production and as increasing concentration of CM in mixture having more nitrogen content which is inhibitory activity after some limit to methanogens production.

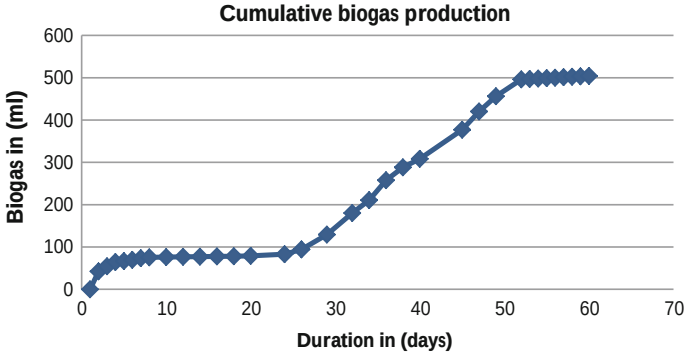

Fig. 1 Cumulative biogas production for reactor R6 (setup 1)

3.2 Biogas Production

3.2.1 Effect of Feeding Composition on Co-digestion Process (Setup 1)

Cumulative biogas production in anaerobic co-digestion of reactor R6 is shown in Fig. 1. The daily biogas production of all reactors during AD has been measured, and it can be seen that biogas production nearly in all reactor started quickly after beginning but there is lag period of 1–2 week in digestion process. This lag period is because of slow hydrolysis reaction. Biogas production curve obtained is having similar results as explained by Wang et al. [1], for C/N ratio 25.

Co-digestion of animal manure with a low C/N ratio with feedstock containing low level of nitrogen (high C/N ratio) gave more stable operational performance because of high buffering capacity of manure instead of digesting single substrate only. The biogas yield will be higher in a co-digestion process due to synergetic effects within the system.

The cumulative biogas production and biogas yield for all reactors are presented in Table 4. It can be concluded that from the present study, the production of biogas from R6 reactor having low solid content (4.91%) result was different as explained by Ahn et al. [7] with production of biogas from poultry manure co-digested with switch grass of high solid content (15%). Maximum biogas production observed in run order R6 was 527.5 ml.

3.2.2 Effect of C/N Ratio on Biogas Potential (Setup 2)

The experimental design combinations of C/N ratio, CP/CM ratio, and responses from experiment are presented in Table 5. As compared to setup 1, in this setup it can be seen that biogas production nearly in all reactor started quickly after beginning, as shown in Fig. 2 but stopped after three to four weeks. From the obtained result of

Table 4 Cumulative biogas production and biogas potential (setup 1)

Run order	CP (TS %)	LG (TS %)	CM (TS %)	Biogas (ml)	Biogas (ml/g VS)
R1	6	6	2.7	80.4	51.54
R2	6	9.2	6	111.4	49.95
R3	9.2	6	6	121	54.26
R4	6	6	9.2	126.6	57.8
R5	6	2.7	6	99.8	66.09
R6	2.7	6	6	527.5	349.33
R7	4	8	8	106.5	51.69
R8	4	4	4	100	79.82
R9	8	8	4	99.6	46.98
R10	8	4	8	120.7	58.31
R11	8	4	4	95.7	56.96
R12	4	4	8	95.6	58.65
R13	8	8	8	120.4	48.16
R14	4	8	4	94	55.95
R15	6	6	6	111.27	39.02
R16	6	6	6	111.27	39.02
Dairy manure (TS = 8%)				320.8	140.53

Table 5 Anaerobic co-digestion of CP, LG, and CM at different CP/CM ratios (setup 2)

Reactors	Factors		Volatile solid (VS) %			Biogas in (ml)	Biogas potential (ml/g VS)
	CP/CM	C/N	CP	CM	LG		
T1	75	30	49.18	16.39	34.42	128.6	98.92
T2	25	20	18.98	56.96	24.05	128	98.46
T3	75	20	73.77	24.59	1.639	115.4	88.76
T4	25	30	12.65	37.97	49.36	961.6	739.69
T5	85.3	25	74.52	12.78	12.69	97.2	74.76
T6	50	32.1	25.57	25.57	48.85	103.2	79.38
T7	50	17.9	45.81	45.81	8.371	94	72.3
T8	14.6	25	8.84	51.58	39.56	1001.4	770.3
T9	50	25	35.71	35.71	28.57	110.6	85.07
Blank	VS = 1.3 g					411.0	316.15

setup 2, it can be concluded that as increasing C/N ratio, biogas production increased and further increase in C/N ratio it is declining. From the above statement, it says that AD will work efficiently at C/N ratio in between 25 and 30.

From the presented study obtained responses were same as Sanjaya [8] explained biogas production of CP in mono-digestion at 0.15 g of VS is 491.24 ml/g VS added.

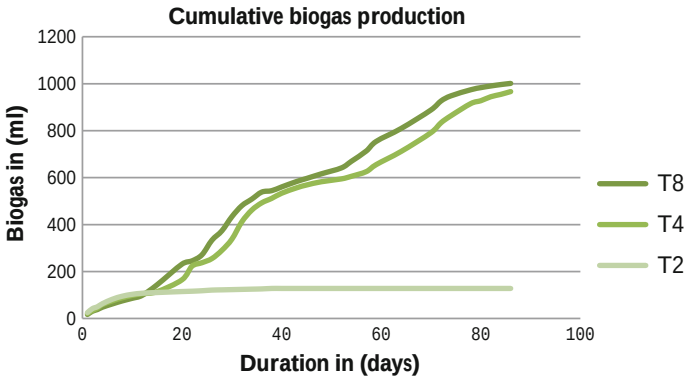

Fig. 2 Cumulative biogas production for reactor T8 (setup 2)

However, results obtained in this study were 1.48 times more than result as mentioned by Kun et al. [4] for mono-digestion of CM at 6% of TS. Maximum biogas potential observed at CP/CM ratio of 14.6:85.3 and a C/N ratio of 25:1 was 454.15 ml/g VS added.

4 Conclusion

The present study was performed to find out biogas production potential of manures using anaerobic co-digestion. From the results, it observed that the co-digestion of manure with grass and citrus pulp resulted in significant production of biogas when compared to the mono-digestion of the waste substrates. It also concluded that the increase in biogas generation may be because of synergetic effect and balanced C/N ratio. C/N ratios of 25:1 had better digestion performance because of stable pH. Maximum biogas potential was achieved in co-digestion with a CP, CM, and LG (TS %) of 2.7:6:6 mixture combinations and at CP/CM ratio 14.6:85.3 and C/N ratio of 25:1. Further study on these waste combinations is required and will be fruitful.

Acknowledgements The authors wish to thank Department of Biotechnology—Government of India, for funding this work (Sanction order No: BT/PR6328/GBD/27/387/2012) and Department of Civil Engineering, National Institute of Technology, Warangal, for providing support to carry out present work.

References

1. Wang, X.J., Yang, G.H., Feng, Y.Z., Ren, G.X., Han, X.H.: Optimizing feeding composition and carbon–nitrogen ratios for improved methane yield during anaerobic co-digestion of dairy, chicken manure and wheat straw. J. Bioresour. Technol. **120**, 78–83 (2012)
2. Abouelenien, F., Namba, Y., Kosseva, M.R., Nishio, N., Yutaka, N.: Enhancement of methane production from co-digestion of chicken manure with agricultural wastes. J. Bioresour. Technol. **159**, 80–87 (2014)
3. Niu, Q., Takemura, Y., Kubota, K., Li, Y.-Y.: Comparing mesophilic and thermophilic anaerobic digestion of chicken manure: microbial community dynamics and process resilience. J. Waste Manag. **43**, 114–122 (2015)
4. Li, K., Liu, R., Sun, C.: Comparison of anaerobic digestion characteristics and kinetics of four livestock manures with different substrate concentrations. J. Bioresour. Technol. **198**, 133–140 (2015)
5. Nizami, A.-S., Korres, N.E., Murphy, J.D.: Review of the integrated process for the production of grass biomethane. J. Environ. Sci. Technol. **43**, 8496–8508 (2009)
6. Yu, L., Bule, M., Ma, J., Zhao, Q., Frear, C., Chen, S.: Enhancing volatile fatty acid (VFA) and bio-methane production from lawn grass with pretreatment. J. Bioresour. Technol. **162**, 243–249 (2014)
7. Ahn, H.K., Smith, M.C., Kondrad, S.L., White, J.W.: Evaluation of biogas production potential by dry anaerobic digestion of switch grass-animal manure mixture. J. Biochem. Biotechnol. **160**, 965–975 (2010)
8. Sanjaya, A.P., Cahyanto, M.N., Millati, R.: Mesophilic batch anaerobic digestion from fruit fragments. J. Renew. Energ. **98**, 135–141 (2016)
9. Wang, X., Yang, G., Li, F., Feng, Y., Ren, G., Han, X.: Evaluation of two statistical methods for optimizing the feeding composition in anaerobic co-digestion: mixture design and central composite design. J. Bioresour. Technol. **131**, 172–178 (2013)

Ceramic Membrane: Synthesis and Application for Wastewater Treatment—A Review

D. Vasanth and A. D. Prasad

Abstract In recent years, ceramic membranes have gained significant attention due to their excellent thermal, mechanical, and chemical tolerance. Alumina, zirconia, and clays are the primary raw materials used to fabricate the ceramic membranes. So far, ceramic membranes have been found to be suitable for various separation applications such as desalination, industrial effluent treatment, food processing, and drinking water production. For ceramic membranes, microfiltration process targeting wastewater treatment is promising. Among various wastewater treatment processes, ceramic membranes have the edge to treat oily wastewater and separate chromium from waste streams. This article presents the review of ceramic membrane for the treatment of oily and chromium wastewater.

Keywords Clay · Wastewater · Mechanical stability · Corrosion resistance

1 Introduction

Over the past few decades, membrane-based separation technology established in various industrial process include air separation, desalination of sea and brackish water, hydrogen recovery from refinery gas streams, and wastewater treatment. From a material's perspective, membrane technology market is dominated by the application of inexpensive polymer membranes. Polymeric membranes possess lower combinations of chemical, mechanical, and thermal stability. Due to these reasons, the feedstock needs to be preprocessed to undergo treating with polymeric membrane technology. For example, to minimize membrane fouling, feedstock pH needs to be

D. Vasanth (B)
Department of Biotechnology, National Institute of Technology Raipur, Raipur 492010, Chhatisgarh, India
e-mail: dvasanth.bt@nitrr.ac.in

A. D. Prasad
Department of Civil Engineering, National Institute of Technology Raipur, Raipur 492010, Chhatisgarh, India

M. Rathinasamy et al. (eds.), *Water Resources and Environmental Engineering II*,
https://doi.org/10.1007/978-981-13-2038-5_10

altered. Similarly, hot streams are cooled to 25–50 °C to safeguard the shelf life of polymeric membranes.

Compare to polymeric membranes, ceramic membranes provide higher combinations of chemical, mechanical, and thermal stability [1]. This is due to the fact that ceramic membranes are fabricated at high sintering temperatures, which are well above the temperatures that exist for various intermediate streams in the process industries. Further, ceramic membranes can be subjected to rigorous cleaning schemes due to their higher corrosion resistance. In addition, the mechanical strength of a ceramic matrix is bound to be higher than that of the polymeric film due to the inherent properties of the materials. Various primary inorganic materials that can be used to fabricate inorganic membranes include alumina-, zirconia-, glass-, and clay-based materials.

To date, ceramic membranes have been successfully used for different applications namely desalination, industrial effluent treatment, food processing, and drinking water production. However, ceramic membranes have been found to be more suitable for wastewater treatment applications. Among various wastewater treatment processes, ceramic membranes have the edge to treat oil–water emulsions, separate of chromium from synthetic solutions. Below a review of ceramic membrane is presented in these two fields of wastewater treatment.

2 Oily Wastewater Treatment

Oily wastewaters are largely released from different process industries include transportation, petrochemical, metallurgical, and petroleum refineries. Concentrations of oil in these waste streams vary between 50 and 1000 mg/L [2–4]. In order to prevent environmental issues, these streams need to be treated before they are discharged. Further, pollution control board has set norms for the discharge of oily wastewater at an allowable grease and oil concentration of 10–15 mg/L [5]. Ceramic membranes are very attractive due to their promising advantages namely tolerance to thermal, biological, and chemical effects. Ceramic membranes are less susceptible to fouling and much more sensitive to control with respect to the operating conditions. The efficiency of ceramic membranes for the separation of oil–water emulsions was reported extensively by various researchers worldwide.

The performance of $ZrO_2/\alpha\text{-}Al_2O_3$ membrane was tested for the purification of oil–water emulsion and obtained 99.8% of oil removal with 93 L/m^{2}h of permeate flux at a feed concentration of 5000 mg/L [6]. Zhong et al. [7] investigated a new scheme combining flocculation and microfiltration for purification of oil–water emulsions. The authors reported an oil separation of 99.8% and permeate flux of 170 L/m^{2}h at a pressure and feed concentration of 0.1 MPa and 6000 mg/L, respectively. Using kaolin, the ceramic membrane (pore size of 10 μm) was fabricated for purification of oily wastewater. The influence of process conditions namely transmembrane pressure, feed concentration, and cross-flow velocity upon membrane efficiency was studied [4]. Cui et al. [8] investigated the performance of two

different ceramic membranes (pore sizes of 1.2 and 0.4 μm) showed an oil separation of 99% and permeate flux of 36 L/m^{2}h at a pressure and feed concentration of 50 kPa and 100 mg/L, respectively. Ebrahimi et al. [9] have used different microfiltration/ultrafiltration/nanofiltration ceramic membranes (average pore sizes between 0.2 μm and 750 Da) for the treatment of water produced in crude oil fields. Their studies indicated that the rejection and flux varied from 58 to 82% and 200 to 55 L/m^{2}h, respectively, for a feed concentration of 149–113 mg/L at an applied pressure of 1 bar. The low-cost ceramic membranes were prepared and used for the purification of oily wastewater by Nandi et al. Further, the effect of feed concentration and operating pressure on the separation efficiency of membrane was investigated. The authors achieved an oil separation and permeate flux of 98.8% and 5.36×10^{-6} m^3/m^{2}s, respectively, at a pressure of 69 kPa and feed concentration of 250 mg/L [10]. At a pressure of 0.16 MPa, Zhou et al. [11] observed that ZrO_2/Al_2O_3 composite membranes show high separation and flux of 97.8% and 441 L/m^{2}h, respectively, during the oily wastewater treatment at a feed concentration of 1000 mg/L.

The performance of tubular ceramic membranes for microfiltration oily wastewater was evaluated. The influence of process conditions such as pressure, cross-flow velocity, and temperature on the membrane flux, total organic carbon removal, and fouling resistance was tested. The oil rejection of 85% and permeate flux of 250 L/m^{2}h were achieved at a pressure and feed concentration of 1.25 bar and 26 mg/L, respectively [12]. Pan et al. [13] prepared titanium dioxide dynamic membranes for the cross-flow microfiltration of oily wastewater. The authors reported that the rejection of 99% and permeate flux of 858 L/m^{2}h at a pressure and feed concentration of 0.125 MPa and 500 mg/L, respectively. Kaolin-based ceramic membranes were synthesized using dry compaction method for purification of oil–water emulsions. The membrane provides good rejection performance (80–90%) and flux (24×10^{-6} m^3/m^2 s) for the separation of oil–water emulsions [14]. The tubular membrane was elaborated for the treatment of oily wastewater and offers the excellent rejection of oil (99.98%) and flux of 3.16×10^{-5} m/s [15]. Alumina–diatomite composite membranes were synthesized using pressing and dip-coating method. The membranes provide an extremely high oil removal (99.9%) at a feed concentration of 600 mg/L [16]. Recently, other kaolin-based ceramic membranes were prepared for the purification of oily wastewater. The authors reported that the fabricated membranes provided excellent removal of oil which is due to its excellent hydrophilicity characteristic [17].

From the material perspectives, the preparation and application of ceramic membranes for the purification of oily wastewater are attractive owing to their salient features. Table 1 summarizes data obtained for the ceramic membrane-based treatment of oil–water emulsions.

Table 1 A summary of the literature reported membrane performance characteristics for the treatment of oily wastewater

Membrane	Feed concentration (mg/L)	Rejection (%)	Flux (L/m^2h)	Pressure (bar)	Reference
ZrO_2/Al_2O_3	1000	97.8	441	1.6	[11]
γ-Al_2O_3/α-Al_2O_3	5000	99.8	18	1	[6]
α-Al_2O_3/α-Al_2O_3	5000	99.9	22	1	[6]
α-Al_2O_3/α-Al_2O_3	5000	94.3	27	1	[6]
ZrO_2/α-Al_2O_3	5000	99.8	93	1	[6]
ZrO_2	6000	99.8	170	1	[7]
Kaolin	3000	–	–	2	[4]
NaA/α-Al_2O_3	100	98.8	36	0.5	[8]
NaA/α-Al_2O_3	500	99.5	31	0.5	[8]
Al_2O_3	179	59	200	1	[9]
Al_2O_3	149	58	200	1	[9]
Mixed clay ceramic membrane	250	98.8	19.3	0.69	[10]
α-Al_2O_3	26	85	250	1.25	[12]
Carbon/titania	500	99	858	1.25	[13]
Kaolin	–	90	86.4	–	[14]
Mixed clays	–	99.98	114.48	69	[15]
Diatomite–alumina	600	99.99		101	[16]

3 Removal of Chromium

The chromium-containing wastewater is hazardous to the human health and environment. Leather tanning, pigment, and metallurgical industries are the large producer of wastewater containing chromium that needs to be treated before discharge. The maximum concentration of total chromium in drinking water should not exceed 0.05 mg/L (World Health Organization). Further, USEPA has set the discharge limit of Cr (VI) to natural water streams below 0.05 mg/L.

During the past decade, the application of membrane filtration for chromium removal has been constantly increasing due to its inherent separation capabilities. Membrane processes such as ultrafiltration and nanofiltration have been extensively studied for the separation of chromium metal. Pagana et al. [18] introduced combined adsorption–ultrafiltration technique for the separation of chromium from wastewater using Fe_2O_3 adsorbent and γ-Al_2O_3 ultrafiltration membranes (pore size of ~3–4 nm) and achieved 99.9% removal for a feed concentration of 0.5 mg/L. Korus and Loska [19] used a polyelectrolyte-assisted ultrafiltration process to examine the rejection of chromium from synthetic solution and inferred very high chromium (100%) removal at a pH of 6 for feed concentrations of 5 and 50 mg/L, respectively. In another work, the authors Pagana et al. [20] studied an adsorption–membrane process for

Table 2 Performance characteristics of membrane for chromium removal from aqueous solutions

Membrane	Method of filtration	Feed concentration (mg/L)	Rejection (%)	Reference
γ-Al_2O_3	Combined adsorption–permeation process	0.5	99.9	[18]
α-Al_2O_3/γ-Al_2O_3	Combined adsorption–permeation process	0.5	90	[20]
Clay/MCM-48	Microfiltration	1000	81	[21]

the separation of chromium and obtained 90% rejection at a feed concentration of 0.5 mg/L. Recently, Basumatary et al. [21] developed a MCM-48 composite membrane for the separation of hexavalent chromium. The maximum removal of 81% was achieved at a feed concentration and pressure of 1000 ppm and 207 kPa, respectively (Table 2).

4 Perspectives

This article presents a review on ceramic membranes for wastewater treatment, particularly, treatment of oily wastewater and removal of chromium from aqueous solution. The critical insight into various literatures indicates that the ceramic membranes are potential to treat the oily wastewater as well as chromium separation. Further, it is noted that alumina, zirconia, kaolin, and mixed clays were primarily used for the production of ceramic membrane. The maximum oil concentration of 6000 ppm was investigated for the purification of oily wastewater. Also, the literatures indicate that combined process such as adsorption–ultrafiltration (AUF) and polyelectrolyte-assisted UF was mainly used for the removal of chromium ions.

References

1. Monash, P., Pugazhenthi, G.: Addition of TiO_2 on the properties of ceramic membrane supports and its influence on the separation of oil and BSA protein from its solution. Desalination **279**, 104–114 (2011)
2. Arnot, T.C., Field, R.W., Koltuniewicz, A.B.: Cross-flow and dead-end microfiltration of oily-water emulsions. Part II. Mechanisms and modelling of flux decline. J. Membr. Sci. **169**, 1–15 (2000)
3. Cumming, I.W., Holdich, R.G., Smith, I.D.: The rejection of oil by microfiltration of a stabilized kerosene/water emulsion. J. Membr. Sci. **169**, 147–155 (2000)

4. Mohammadi, T., Pak, A., Karbassian, M., Golshan, M.: Effect of operating conditions on microfiltration of an oil–water emulsion by a kaolin membrane. Desalination **168**, 201–205 (2004)
5. Hua, F.L., Tsang, Y.F., Wang, Y.J., Chan, S.Y., Chuand, H., Sin, H.N.: Performance study of ceramic microfiltration membrane for oily wastewater treatment. Chem. Eng. J. **128**, 169–175 (2007)
6. Yang, C., Zhang, G., Xu, N., Shi, J.: Preparation and application in oil-water separation of ZrO_2/α-Al_2O_3 MF membrane. J. Membr. Sci. **142**, 235–243 (1998)
7. Zhong, J., Sun, X., Wang, C.: Treatment of oily wastewater produced from refinery processes using flocculation and ceramic membrane filtration. Sep. Purif. Technol. **32**, 93–98 (2003)
8. Cui, J., Zhang, X., Liu, H., Liu, S., Yeung, K.L.: Preparation and application of zeolite/ceramic microfiltration membranes for treatment of oil contaminated water. J. Membr. Sci. **325**, 420–426 (2008)
9. Ebrahimi, M., Shams Ashaghi, K., Engel, L., Willershausen, D., Mund, P., Bolduan, P., Czermak, P.: Characterization and application of different ceramic membranes for the oil-field produced water treatment. Desalination **245**, 533–540 (2009)
10. Nandi, B.K., Moparthi, A., Uppaluri, R., Purkait, M.K.: Treatment of oily wastewater using low cost ceramic membrane: comparative assessment of pore blocking and artificial neural network models. Chem. Eng. Res. Des. **88**, 881–892 (2010)
11. Zhou, J., Chang, Q., Wang, Y., Wang, J., Meng, G.: Separation of stable oil-water emulsion by the hydrophilic nano-sized ZrO_2 modified Al_2O_3 microfiltration membrane. Sep. Purif. Technol. **75**, 243–248 (2010)
12. Abadi, S.R.H., Sebzari, M.R., Hemati, M., Rekabdar, F., Mohammadi, T.: Ceramic membrane performance in microfiltration of oily wastewater. Desalination **265**, 222–228 (2011)
13. Pan, Y., Wang, T., Sun, H., Wang, W.: Preparation and application of titanium dioxide dynamic membranes in microfiltration of oil-in-water emulsions. Sep. Purif. Technol. **89**, 78–83 (2012)
14. Emani, S., Uppaluri, R., Purkait, M.K.: Microfiltration of oil–water emulsions using low-cost ceramic membranes prepared with the uniaxial dry compaction method. Ceram. Int. **40**, 1155–1164 (2014)
15. Kumar, R.V., Ghoshal, A.K., Pugazhenthi, G.: Elaboration of novel tubular ceramic membrane from inexpensive raw materials by extrusion method and its performance in microfiltration of synthetic oily wastewater treatment. J. Membr. Sci. **490**, 92–102 (2015)
16. Yeom, H.-J., Kim, S.C., Kim, Y.-W., Song, I.-H.: Processing of alumina-coated clay–diatomite composite membranes for oily wastewater treatment. Ceram. Int. **42**, 5024–5035 (2016)
17. Hubadillah, S.K., Othman, M.H.D., Harun, Z., Ismail, A.F., Rahman, M.A., Jaafar, J., Jamil, S.M., Mohtor, N.H.: Superhydrophilic, low cost kaolin-based hollow fibre membranes for efficient oily-wastewater separation. Mater. Lett. **191**, 119–122 (2017)
18. Pagana, A.E., Sklari, S.D., Kikkinides, E.S., Zaspalis, V.T.: Microporous ceramic membrane technology for the removal of arsenic and chromium ions from contaminated water. Microporous Mesoporous Mater. **110**, 150–156 (2008)
19. Korus, I., Loska, K.: Removal of Cr(III) and Cr(VI) ions from aqueous solutions by means of polyelectrolyte-enhanced ultrafiltration. Desalination **247**, 390–395 (2009)
20. Pagana, A.E., Sklari, S.D., Kikkinides, E.S., Zaspalis, V.T.: Combined adsorption-permeation membrane process for the removal of Chromium(III) ions from contaminated water. J. Membr. Sci. **367**, 319–324 (2011)
21. Basumatary, A.K., Vikram Singh, P., Vinoth Kumar, R., Ghoshal, A.K., Pugazhenthi, G.: Development and characterization of a MCM-48 ceramic composite membrane for the removal of Cr(VI) from an aqueous solution. ASCE J. Environ. Eng. http://dx.doi.org/10.1061/(ASCE)EE.1943-7870.0000993

A Brief Study of the January 28, 2017, Chennai Oil Spill

Deeptha Thattai, Sathyanathan Rangarajan and Abhishek Senthil

Abstract At least 20 metric tons of petroleum oil lubricant was spilled 2 nautical miles off the Kamarajar Port, Chennai, at 04:00 h on January 28, 2017, when two ships collided with each other. The coast of north Chennai was engulfed with the oil and hundreds of volunteers spent days trying to remove it from the beaches. Reports suggest that some of the oil has traveled south as far as Mahabalipuram, 75 km from the spill point, after two weeks. In this study, we use the GNOME model to recreate the spill as it happened and analyze the extent of dispersion of the spill for two weeks after the incident. The spread of the oil and what could have been done to prevent it are discussed.

Keywords Chennai oil spill · GNOME · Marine pollution

1 Introduction

When oil spills occur in coastal waters, they cause enormous damage to the native flora and fauna and to the people living along that coast. Even if the spill occurs at some distance from the coast, the prevailing winds and currents may move the spill toward the coast. It is well known that coasts are important regions for transport, fishing, and tourism. All these activities will come to a halt in the event of a spill. The impact of a spill is dependent on many factors such as type of oil, quantity, prevailing wind and current conditions, physical parameters of the water, and bathymetry and geometry of the affected area [1]. Lighter oils, while more toxic, evaporate fast but heavy oils stick to the sands and rocks and stay for a long time [1]. The heavy oil thus continues to impact a few generations of the habitats.

Oil spill affects on a larger scale the animals and plants living along the coastal areas [2]. Another major effect of the oil spills is economic, which results when

D. Thattai (B) · S. Rangarajan · A. Senthil
Department of Civil Engineering, SRM Institute of Science and Technology, Kattankulathur 603203, Tamil Nadu, India
e-mail: deepthathattai.v@ktr.srmuniv.ac.in

M. Rathinasamy et al. (eds.), *Water Resources and Environmental Engineering II*,
https://doi.org/10.1007/978-981-13-2038-5_11

nautical transport in the spill area is affected. Moreover, cleaning and removing the spills from the coastal area are quite cumbersome and expensive.

It is important to have operational forecast models and pollutant transport models for a sustainable spill management system [3]. Implementing a transport model immediately after a spill with the existing wind and current patterns will give a fast response to the potential movement of the spill. This will help in planning for the immediate curtailing of the spread and disposing the oil effectively. It is a must for coastal regions, especially ports and biologically sensitive areas, to have a model set up and ready to run.

2 Study Area

Chennai is located at 13.04°N latitude and 80.17°E longitude on the southeast coast of India and in the northeast corner of Tamil Nadu (Fig. 1). It is located on a flat coastal plain known as the Eastern Coastal Plains [4]. Chennai is the fourth prosperous city in the country, the capital of Tamil Nadu, and an important port city. Its main attraction is the coastline stretching along the Bay of Bengal. This coastline covers a few beaches, each having its own significance. One of these beaches, the Marina beach, is the second largest beach in the world [4] and is the source of fisheries for fishermen living in the coastal area. Other coastal activities include occasional boating and carnivals, which create a pleasant environment for the people who are working professionally in the city. The Besant Nagar beach and the coast stretching south of it till Neelankarai is a well-known turtle nesting area [4]. Olive Ridley turtles migrate here in January–March to lay eggs on the beaches. The Adyar creek empties into the Bay of Bengal near Besant Nagar and there are a few extant mangroves here, though most have been decimated by urbanization.

2.1 Effect of Oil Spill in Chennai

At 4 am on January 28, 2017, the ship BW Maple, an LPG tanker, collided with the petroleum tanker Dawn Kanchipuram just two nautical miles off the Kamarajar Port [5]. As a result, the fuel pipeline of Dawn Kanchipuram was snapped and heavy oil started to leak into the ocean, damaging the nearby aquatic flora and fauna. Though initially the spill itself, and later the extent of spill, was denied and fudged by the concerned agencies, the large patches of oil on the water and blobs of oil depositing on the coasts were all too visible, and media coverage in print, online, and TV was extensive. People along the coasts noticed that the spill was affecting the fishes. Dead fish and turtles were found on the beaches. As the prescribed devices and oil cleaning agents were not enough to contain the spread, thousands of volunteers were roped in to manually clean the stretch. Due to the initial delays, the oil spread fast along the coast till south Chennai and a few patches reached even further. The extent of

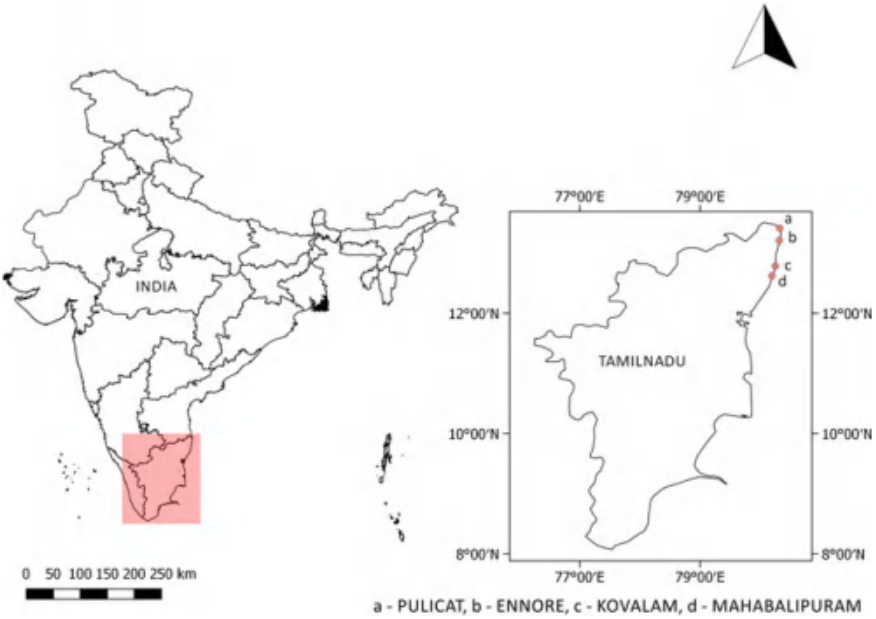

Fig. 1 Location map of Chennai coast with the spill-affected areas highlighted (**a**, **b**, **c**, and **d**)

damage due to the heavy oil, which would have sunk to the bed, was not known immediately; this was the turtle nesting season and the turtles would also have been impacted.

3 GNOME Model

The General NOAA Operational Modeling Environment (GNOME) model is an interactive simulation model of pollutant trajectories in the ocean [6]. Inputs to GNOME are location maps, bathymetry of the study area, data from circulation models, location and properties of the pollutant, existing wind and currents, and other environmental data if needed. Outputs are in the form of graphs, movies, and data files. GNOME is a 2D Eulerian/Lagrangian model. It is run in two modes—standard, where all files are already set up and the users can just download and run; and diagnostic, where the users have flexibility in choosing their files and parameters.

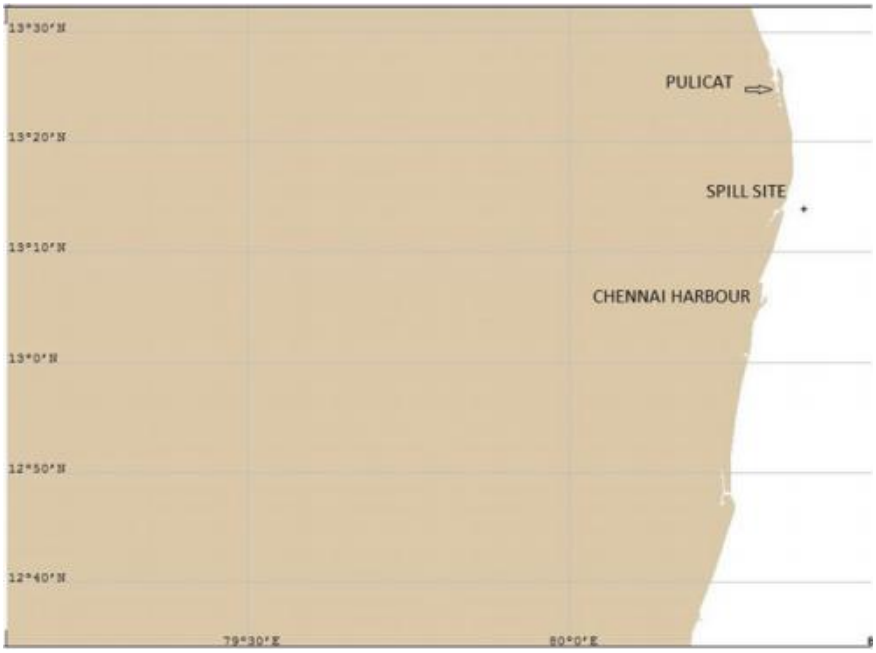

Fig. 2 Location of the spill site (+ symbol in map) with respect to Chennai harbor. Pulicat lagoon is also shown on the map

3.1 Model Setup

The GNOME model was set up for the Chennai region manually in the diagnostic mode. The shoreline was generated from the Global Custom Map Generator of NOAA's GOODS page (http://gnome.orr.noaa.gov/goods) by providing the boundary latitudes and longitudes. The map was created from Pulicat in the north to Mahabalipuram in the south, a straight-line distance of 88 km along the coast (Fig. 2).

The surface currents were input from the Hybrid Coordinate Ocean Model (HYCOM) in the GOODS page. These are estimates from the global HYCOM model for the time span under study. The wind data were taken from the NCEP Global Forecast System. A spill of 20 metric tons of fuel oil #6 was stipulated for the simulation. The spill location and time were provided at the exact point of the actual spill and the time of occurrence (04:00 h on January 28, 2017, at 13° 13.74N and 80° 21.83E). The model was run for 14 days at 0.25 h interval.

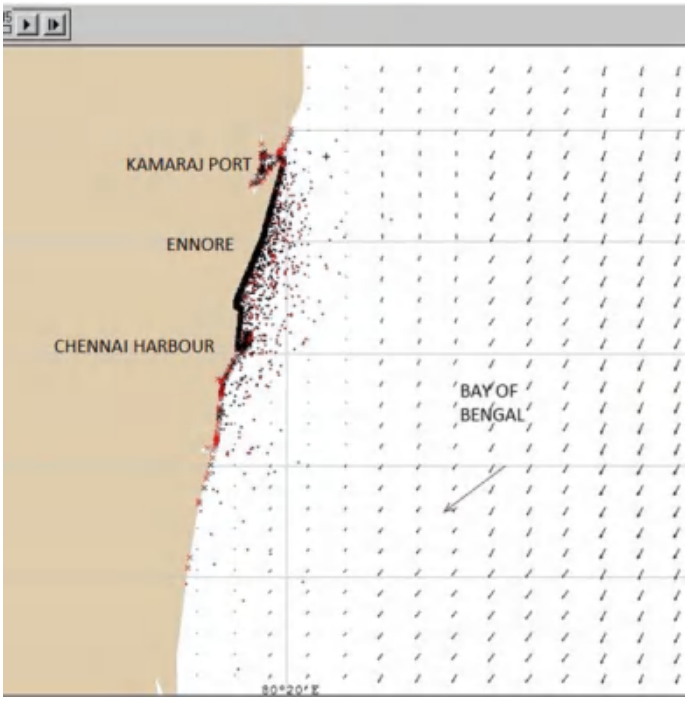

Fig. 3 Movement of the spill on Day 2 after the incident. The oil has already crossed Chennai harbor. The long arrow is the wind vector and the smaller arrows are the ocean currents

4 Results and Discussion

Figure 3 shows the spread of oil along the Chennai coast on Day 2. It is clear that the entire beach was filled with the oil. The oil that was released was a petroleum oil lubricant, dark, waxy, bunker oil [7]. Both the current and wind directions were toward the southwest direction, a worst-case scenario for the Chennai coast and city. Hence, the oil covered the coast instead of moving out to sea. The time of spill was also unfortunately the nesting season for turtles along Besant Nagar to Neelankarai, areas which lie immediately south of the spill. By Day 5, the oil spill had reached Besant Nagar in the simulation (Fig. 4). Even by not accounting for the minimum regret solution in GNOME, which shows the probable area of impact, the spread had impacted Besant Nagar. The oil spread reached Mahabalipuram by Day 14 (Fig. 5).

Reports by the National Remote Sensing Centre (NRSC) indicated that the oil spread reduced significantly by February 8. The satellite images displayed in the NRSC Web site showed an area only till the north half of Chennai [8]. However, the model suggests that the spread was much farther than that till Mahabalipuram. Media reports also confirmed the presence of oil in Mahabalipuram, even after accounting for the removal of oil by thousands of volunteers [9]. The model results are consistent

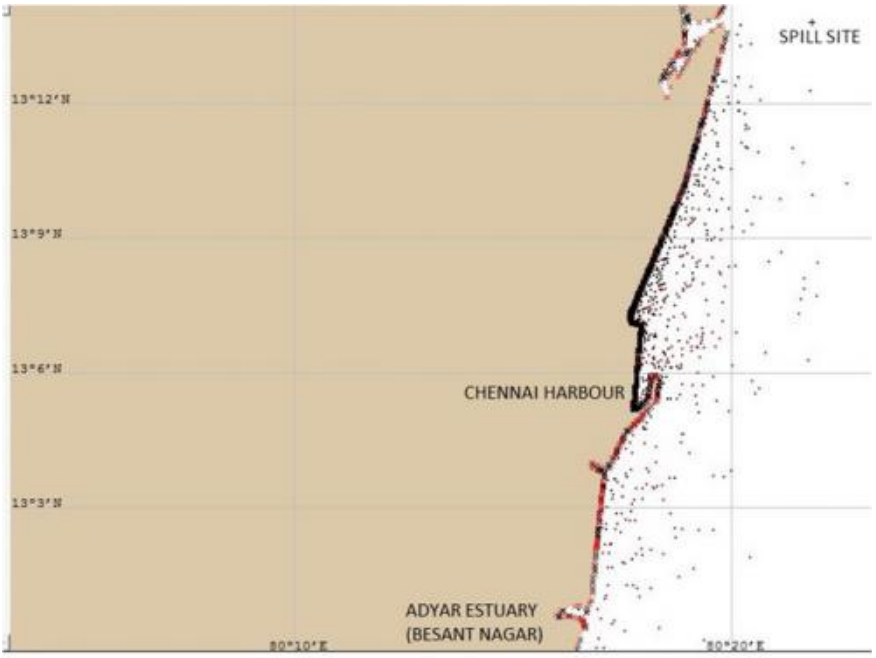

Fig. 4 Movement of the spill on Day 5 after the incident with minimum regret solution. The oil spread has reached Besant Nagar in south Chennai

with the report; they were also corroborated by a report from INCOIS, who ran the model with real-time data and came to the same conclusion [10]. The INCOIS model was run by scientists after a request was made by the Coast Guard [10]. The spread of oil in the model study also moved northward reaching the tip of Pulicat Lake, as the winds and currents shifted (Fig. 6). This was also corroborated by media reports [11].

A very simple model was attempted in this study, with existing data. A local hydrodynamic model was not used due to lack of time, which could have given a better picture of the coastal circulation; instead, data from global models were used. Still, the results obtained are not far off the mark compared to reports. If it is not a difficult task to work on such a model and have plans for mitigation in advance, the question is why it has not been done for such an important area. Kankara et al. [12] have already shown the importance of such a planning in their paper. They used stationary winds in different seasons and did an elaborate study using satellite imagery and hydrodynamic models to prepare a coastal resource map for Chennai. When the spill happened on January 28, none of the agencies were prepared. The state government initially denied the event and then played down the quantity and extent of spill. The Coast Guard, which is equipped to deal with spills, was not informed in time. Experts were not immediately brought in for consultation. As a

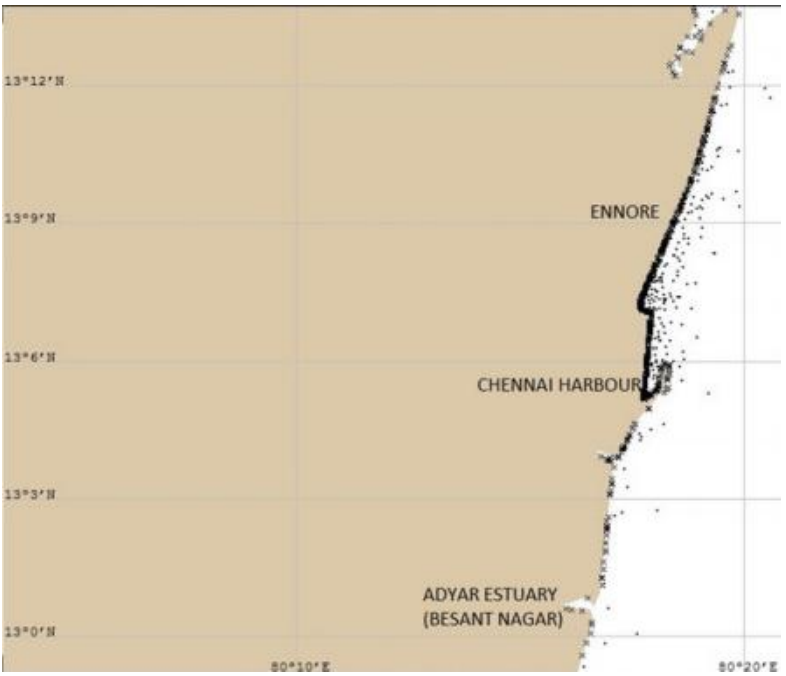

Fig. 5 Movement of the spill on Day 5 after the incident without minimum regret solution. The oil spread has reached Besant Nagar in south Chennai

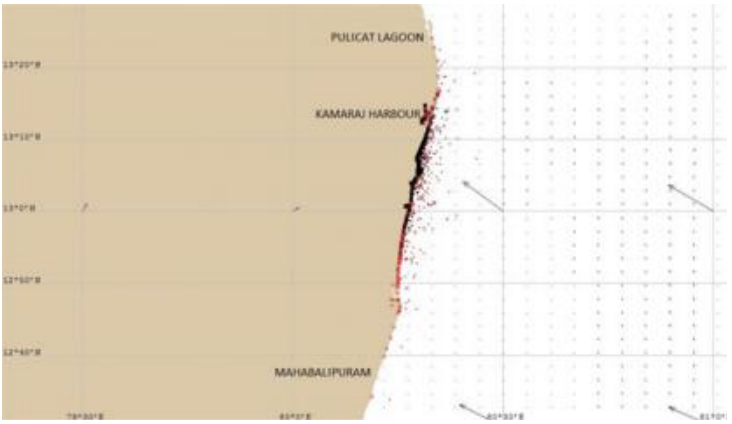

Fig. 6 Movement of the spill on Day 14 after the incident. The probability of oil spread reached Mahabalipuram, around 82 km from Ennore. There is also some spread toward Pulicat in the north. The wind and current are directed toward the northwest

result, there was total mismanagement and safety was thrown to the winds, with untrained citizen volunteers brought in to clean a hazardous material. The political

crisis in the state government added to the chaos and indecisive state. This shows that experts must handle incidents of this nature independent of political interference and control measures must not be delayed. Act first and answer later should be the motto.

5 Conclusions

A simple oil spill model was recreated in GNOME to study the Chennai oil spill that happened on January 28, 2017, off Kamarajar harbor. Even without real-time data, the model was able to predict the movement of oil in concurrence with media reports and an INCOIS model. If a better model had been set up by the concerned agencies earlier and used with real-time data immediately after the spill, the oil movement could have been predicted and prevented to some extent on the same day. Instead, around 80 km of the coast suffered from major and minor effects of the oil spill and the long-term effects will be appearing still. This is clearly a management failure and one that should not be allowed to be repeated.

Acknowledgements The authors thank the management of SRM Institute of Science and Technology and the HOD, Civil Engineering, for support and guidance.

References

1. http://www.itopf.com/knowledge-resources/documents-guides/document/tip-13-effects-of-oil-pollution-on-the-marine-environment/. Accessed 19 Aug 2017
2. Conserve Energy Future. www.conserve-energy-future.com/effects-of-oil-spills.php
3. Marta-Almeida, M., et al.: Efficient tools for marine operational forecast and oil spill tracking. Mar. Poll. Bull. **71**(1–2), 139–151 (2013)
4. Wikipedia. https://en.wikipedia.org/wiki/Chennai#Geography. Accessed 20 Mar 2017
5. Times of India. 28 Jan. http://timesofindia.indiatimes.com/india/chennai-oil-spill-as-it-happened/articleshow/56939334.cms. Accessed 20 Mar 2017
6. Zelenke, B., O'Connor, C., Barker, C., Beegle-Krause, C.J., Eclipse, L. (eds.).: General NOAA Operational Modeling Environment (GNOME) Technical Documentation. U.S. Dept. of Commerce, NOAA Technical Memorandum NOS OR&R 40. Emergency Response Division, NOAA, Seattle, WA, p. 105 http://response.restoration.noaa.gov/gnome_manual (2012)
7. http://www.hindustantimes.com/interactives/chennai-oil-spill-collision-cover-up/. Accessed 20 Mar 2017
8. National Remote Sensing Centre. https://nrsc.gov.in/Oil_Spill_Study. Accessed 20 Mar 2017
9. http://www.thehindu.com/news/cities/chennai/As-clean-up-continues-oil-spill-reaches-Mamallapuram/article17295236.ece. Accessed 20 March 2017
10. http://www.thehindu.com/news/cities/chennai/52-km-coastline-affected-due-to-oil-spill-INCOIS/article17264951.ece. Accessed 20 March 2017
11. http://www.newindianexpress.com/cities/chennai/2017/feb/03/sand-properties-of-chennais-beach-change-after-oil-spill-1566498.html. Accessed 20 March 2017
12. Kankara, R.S., Arockiaraj, S., Prabhu, K.: Environmental sensitivity mapping and risk assessment for oil spill along the Chennai Coast in India. Mar. Poll. Bull. **106**(1–2), 95–103 (2016)

Multivariate Statistical Analysis of Water Quality of Godavari River at Polavaram for Irrigation Purposes

M. Rajesh Kumar, R. Vijay Kumar, T. P. Sreejani, P. V. R. Sravya and G. V. R. Srinivasa Rao

Abstract A study on the seasonal variation of quality of River Godavari waters at Polavaram in Andhra Pradesh is made using different multivariate statistical methods. The water quality indices (WQIs) are computed using WAIWQI and NSFWQI methods. The data obtained from the Central Water Commission, Hyderabad, Andhra Pradesh, for a period of decade, i.e. 2002–2012, is taken into consideration for conducting the study. Twelve parameters are being considered for analysis related to water suitability for irrigation purposes. Using this analysis, the principal parameters affecting the quality of water during the study period are obtained. The cluster analysis (CA) conducted on temporal basis displayed clusters of the years based on their similarity. When this cluster analysis is compared with the water quality indices determined using WAIWQI and NSFWQI methods, it is found that the clusters vis-à-vis the WQIs are in good correlation. From the results obtained, it is concluded that the quality of water in River Godavari at Polavaram is found to be suitable for irrigation purposes.

Keywords Multivariate statistical analysis · Cluster analysis (CA) · WQI NSFWQI · Godavari · Polavaram

1 Introduction

Understanding the factors and processes which affect the river water quality is of concern in river water quality studies. Water quality is affected by both natural processes and anthropogenic activities. Hence, monitoring of river water quality became one of the highest priorities in environmental legislations [1]. The issue related to

M. Rajesh Kumar · R. Vijay Kumar · T. P. Sreejani · G. V. R. Srinivasa Rao (B)
Department of Civil Engineering, A U Engineering College (A), Andhra University, Visakhapatnam, India
e-mail: gvrsrao@gmail.com

P. V. R. Sravya
Department of Civil Engineering, ANITS, Thagarapuvalasa, Visakhapatnam, India

M. Rathinasamy et al. (eds.), *Water Resources and Environmental Engineering II*,
https://doi.org/10.1007/978-981-13-2038-5_12

water quality studies is the complexity involved in the analysis of the large number of variables. The classification and the interpretation of the data and the subsequent modelling are the most important steps in the water quality-related studies [2]. The status of river water quality can be evaluated using water quality indices (WQIs), which are numbers formulated mathematically using large amounts of water quality data [3]. Water quality index (WQI) can be defined as the rating reflecting the composite influence of a number of water quality factors on the overall quality of water, represented as a single numerical value. This is the most effective way of communicating the information on water quality trends to policy makers, to formulate public policy for the implementation of the water quality improvement programmes effectively [4]. Certain activities like disposal of treated and untreated industrial effluents along with agricultural wastes may also result in degradation of river water quality [5]. Multivariate statistical analysis is capable and is an useful tool for finding the similarity among the complicated factors in a system so that the complex phenomena can be made simple for extracting the important and relevant information for the analysis and discrimination of test results to formulate effective and responsive management policies [6]. The cluster analysis (CA) and factor analysis (FA) can be used effectively for the interpretation of complex data matrices to understand the water quality systems, and to identify the factors which influence water systems for finding a reliable solutions to problems associated with water pollution [7].

2 Study Area

In all the peninsular rivers of India, Godavari is the largest one with a drainage area of 312,812 km^2. Pranhita, Indravati, and Sabari are its principal tributaries contributing 80% flow. 110 BCM of water flows in River Godavari per year at an average. The study area, i.e. Polavaram mandal, lies on the banks of River Godavari comprising of 23 villages (Fig. 1).

3 Methodology

As shown in the flow chart, the methodology involves data collection, data segregation, missing value analysis, validation of data, WQI analysis, multivariate statistical analysis, and result analysis (Fig. 2).

4 Results

The WQIs w.r.t. the three seasons, viz. pre-monsoon, monsoon, and post-monsoons, are evaluated, and the results are given in Table 1.

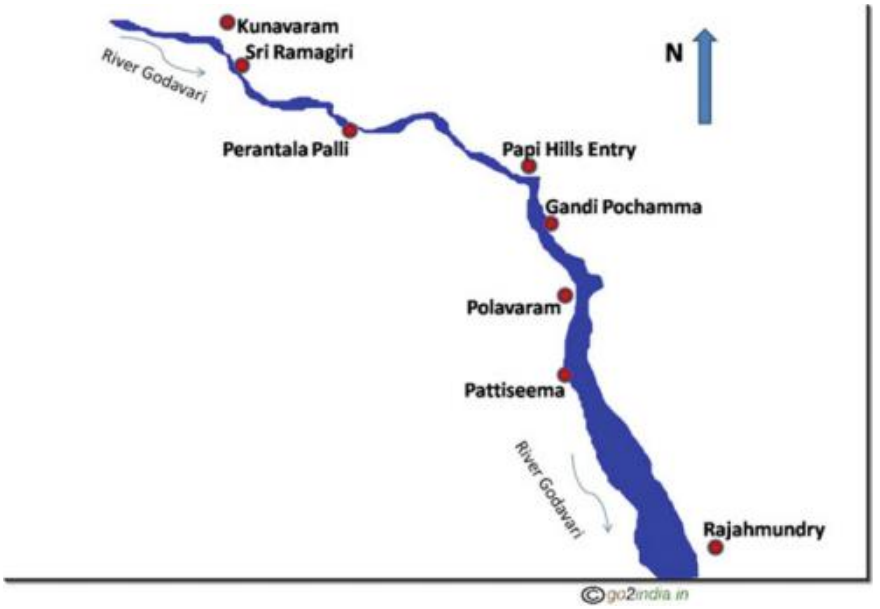

Fig. 1 Study area (Polavaram)

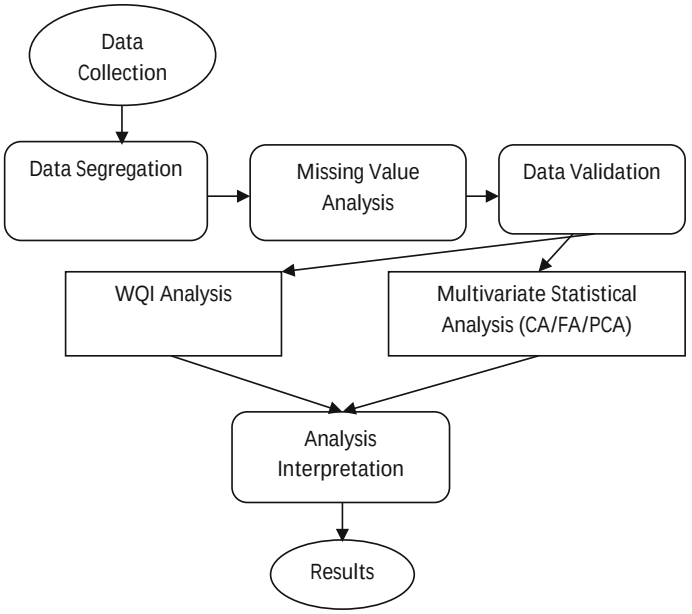

Fig. 2 Flow chart: methodology

Table 1 Seasonal variations of WQI

WQI seasons	NSFWQI	Quality rating	WAIWQI	Quality rating
Pre-monsoon	55.12	Medium	28.53	Good
Monsoon	52.25	Medium	26.21	Good
Post-monsoon	53.50	Medium	25.60	Good

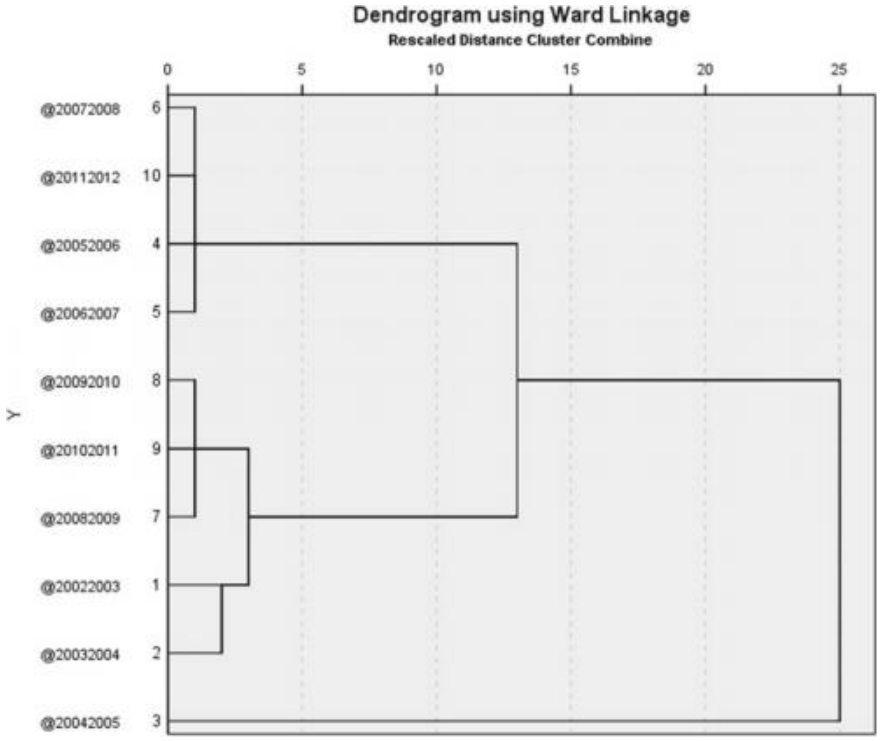

Fig. 3 Dendrogram for the study period (2002–2012)

The cluster analysis is conducted taking the 12 irrigational parameters into consideration. The dendrograms for the irrigational parameters for the seasonal variations are shown in Figs. 3, 4, 5, and 6.

The dendrograms are constructed using ward linkage method and are drawn for rescaled distance cluster combines. The water quality parameters for a particular year are considered as one case, and in total, ten cases are used representing ten years of study period, for constructing dendrograms.

PCA is conducted taking into consideration 12 irrigational parameters, and the results are shown as scree plot in Fig. 7 and given in Table 2.

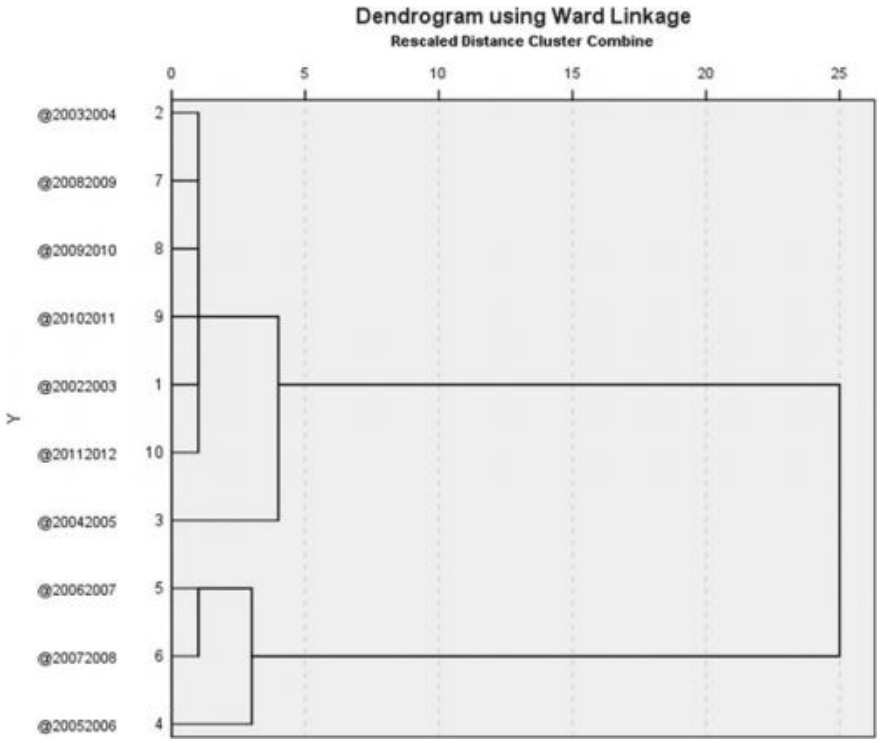

Fig. 4 Dendrogram (pre-monsoon seasons) (2002–2012)

Principal component analysis of the above-cited data shows that four principal components are generated explaining the 70.41% variance. The principal components having high factor loadings are PC1: HAR_Ca, HAR_total, EC_GEN, PC2: SAR, Na%, PC3: RSC, PC4: NH_3–N. These parameters have high factor loadings which indicate that these parameters are in high concentrations and are the more effective among other parameters in affecting the quality of water.

FA is conducted taking into consideration 12 irrigational parameters, and the results are shown as scree plots in Fig. 8 and given in Table 3.

One factor explaining 23.42% of the variance is generated in FA. Following parameters had high factor loadings Factor 1: EC_Gen. EC_Gen indicates that these are the most influential parameters affecting water quality in the study area.

Table 2 Rotated component matrix (2002–2012)

Parameters	Component			
	PC1	PC2	PC3	PC4
HAR_Ca ($mgCaCO_3$/l)	0.785	−0.033	0.142	−0.301
HAR_Total ($mgCaCO_3$/l)	0.911	−0.040	−0.183	0.103
RSC (–)	0.195	0.297	0.852	0.077
SAR (–)	0.077	0.952	0.134	0.067
EC_GEN (µmho/cm)	0.866	0.275	−0.025	0.167
pH_GEN (pH units)	0.654	−0.093	0.038	0.062
B (mg/l)	0.090	0.029	−0.084	0.580
Cl (mg/l)	0.373	0.692	−0.281	0.035
SO_4 (mg/l)	0.338	0.373	−0.660	0.254
Na% (%)	−0.192	0.905	0.215	0.041
NH_3–N (mg/l)	−0.094	−0.015	0.038	0.804
NO_3–N (mg/l)	−0.149	0.485	−0.120	−0.352
Eigen values	2.996	2.755	1.382	1.317
% of variance	24.968	22.957	11.517	10.971
Cumulative %	24.968	47.925	59.442	70.413

Table 3 Factor matrix (2002–2012)

Parameters	Factor
	FA1
HAR_Ca ($mgCaCO_3$/L)	0.518
HAR_Total ($mgCaCO_3$/L)	0.754
RSC (–)	0.187
SAR (–)	0.431
EC_GEN (µmho/cm)	0.956
pH_GEN (pH units)	0.427
B (mg/l)	0.130
Cl (mg/l	0.605
SO_4 (mg/l)	0.481
Na% (%)	0.199
NH_3–N (mg/l)	0.004
NO_3–N (mg/l)	0.058
Eigen values	2.811
% of variance	23.427
Cumulative %	23.427

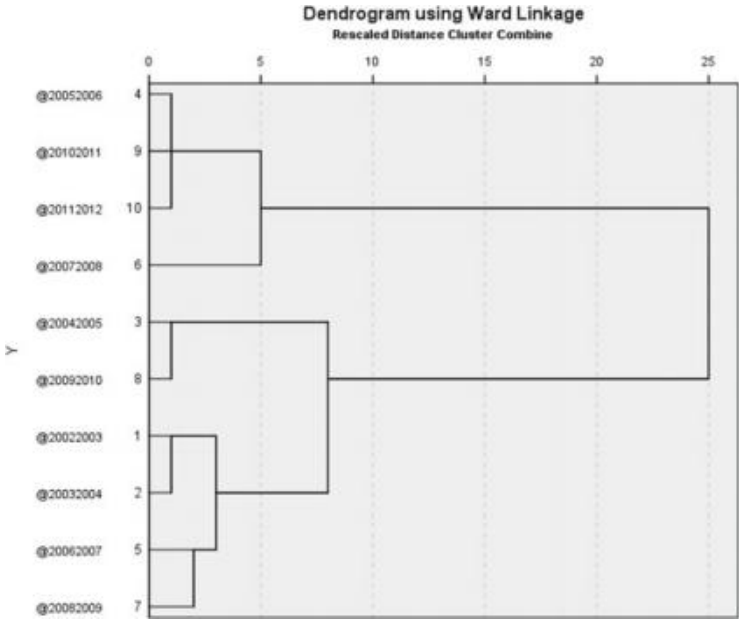

Fig. 5 Dendrogram (monsoon seasons) (2002–2012)

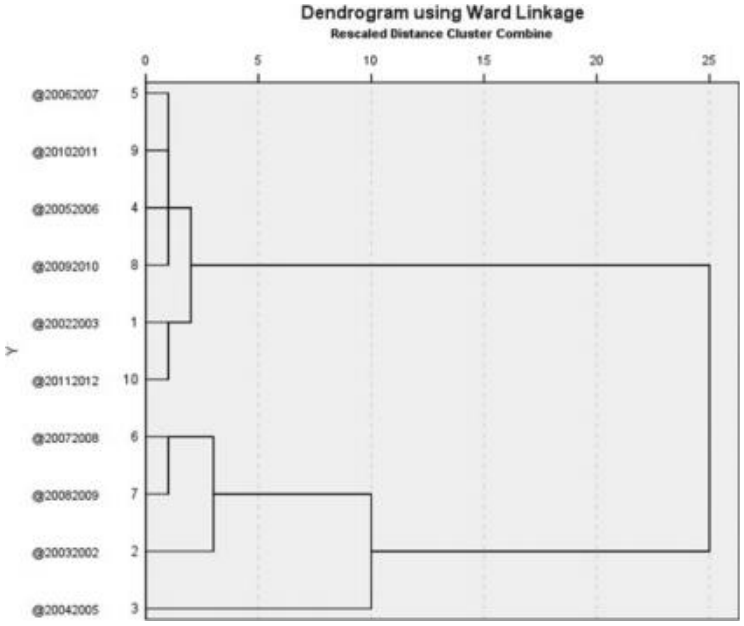

Fig. 6 Dendrogram (post-monsoon seasons) (2002–2012)

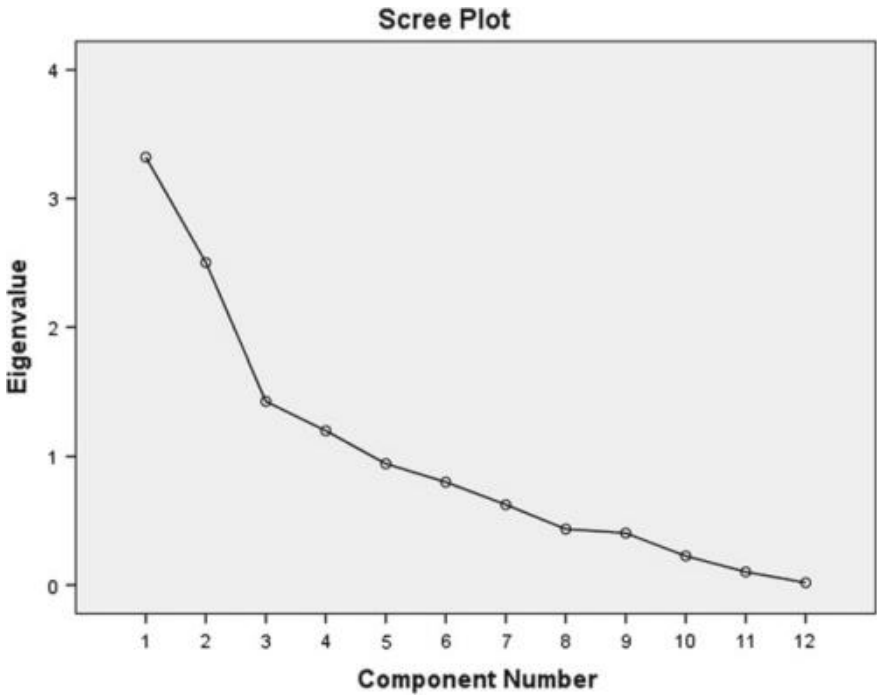

Fig. 7 Scree plot: principal component analysis (PCA) (2002–2012)

Principal components and factors obtained from both analyses, i.e. PCA and FA, brought out the same parameters which are marked as influential parameters. The strong factor loadings identified are Har_Tot, EC_Gen, SAR, Na%. These parameters are found to affect the quality of water that may result in the following effects when the water is utilized for irrigation water purpose without proper treatment.

5 Conclusions

1. From FA and PCA, it is observed that the hardness, sodium absorption ratio, electrical conductivity, residual sodium chloride, and ammoniacal nitrogen are the principal parameters affecting the quality of water during the study period.
2. The cluster analysis (CA) conducted on temporal basis w.r.t. parameters related to the irrigation purposes displayed two clusters in Fig. 2. When this cluster analysis is compared with the water quality indices determined using WAIWQI and NSFWQI methods, it is found that the clusters vis-à-vis the WQIs are in good correlation.

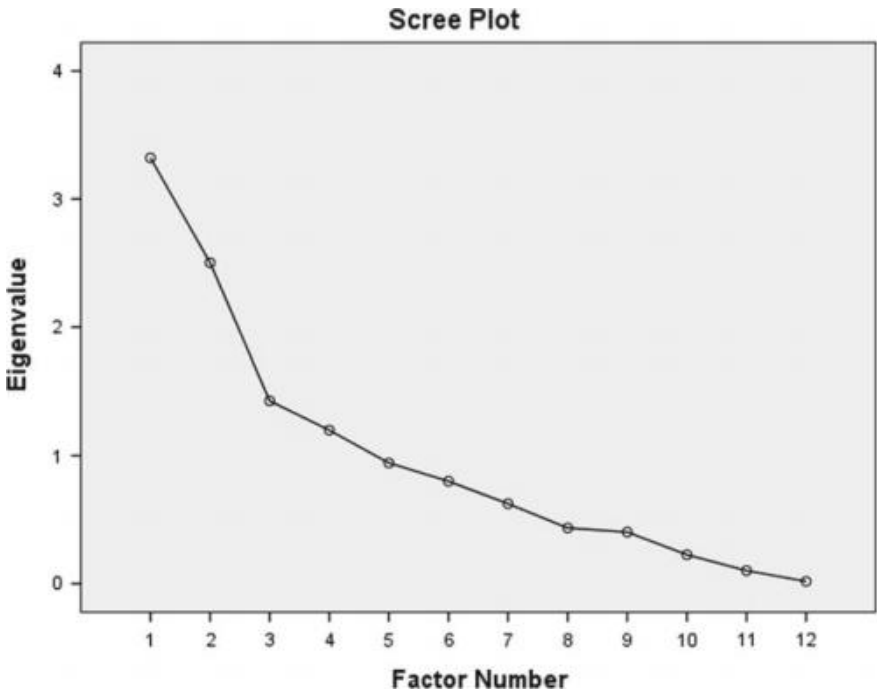

Fig. 8 Scree plot: factor analysis (FA) (2002–2012)

3. A good correlation is found between the clusters obtained in the cluster analysis done w.r.t different seasons of the study period and the water quality indices determined in both WAIWQI and NSFWQI methods.
4. From the water quality indices obtained in both WAIWQI and NSFWQI methods w.r.t. the parameters related to irrigation purposes, it is observed that quality of water ranged from medium to good in all the three seasons.

References

1. Yerel, S., Ozbay, N., Ankara, H.: Application of factor analysis in the assessment of water quality in Sakarya River (Turkey). In: 1st International Symposium on Sustainable Development, Sarajevo (2009)
2. Thareja, S., Choudhury, S., Trivedi, P.: Assessment of water quality of Ganga River in Kanpur by using principal components analysis. Adv. Appl. Sci. Res. **2**(5), 84–91 (2011)
3. Mohamed, I., Othman, F., Ibrahim, A.I.N., Alaa-Eldin, M.E., Yunus, R.M.: Assessment of water quality parameters using multivariate analysis for Klang River basin, Malaysia. Environ. Monit. Assess **187**, 4182 (2015)
4. Kalavathy, S., Sharma, T.R., Sureshkumar, P.: Water quality index of river Cauvery in Tiruchirappalli district, Tamilnadu. Arch. Environ. Sci. **5**, 55–61 (2011)

5. Kundu, S.: Assessment of surface water quality for drinking and irrigation purposes: a case study of Ghaggar River system surface waters. Bull. Environ. Pharmacol. Life Sci. **1**(2), 01–06 (2012)
6. Wu, E.M.Y., Kuo, S.L.: Applying a multivariate statistical analysis model to evaluate the water quality of a watershed. Water Environ. Res. **84** (2012)
7. Ismail, A.H., Abed, B.S., Abdul-Qader, S.: Application of multivariate statistical techniques in the surface water quality assessment of Tigris River at Baghdad stretch, Iraq. J. Babylon Univ. Eng. Sci. **22**(2) (2014)

Vermicomposting of Primary Clarified Tannery Sludge Employing *Eisenia fetida*

Rohan Kumar Choudhary, Ankita Swati and Subrata Hait

Abstract Leather tanneries sludge is categorized under hazardous waste owing to its properties comprising of organic content, chloride, heavy metals, and pathogenic occurrence. The main objective of the present study was to assess the sustainable vermiconversion of tannery sludge in its raw state employing *Eisenia fetida* over eight-week trial. No mortality with positive growth of 10–30% was attained in all the reactors. Total carbon, pH, and C:N ratio decreased from initial in the range of 12–23.5, 3–17, and 31–55%, respectively, in the final products. Electrical conductivity, salinity, and total nitrogen showed a substantial increase from initial in all trials. A significant decrease of 75–99.5% was attained in the pathogenic load of both total and fecal coliforms from initial in all the reactors. The vermicomposting process has the potential to stabilize and convert hazardous industrial tannery sludge into quality organic manure of agronomic importance without any adverse effect on the earthworms.

Keywords Tannery sludge · *Eisenia fetida* · Cow dung · Stabilization · Pathogens Vermicomposting

1 Introduction

The leather processing industries or tanning industries are among the top ten foreign exchange earners of the country [1]. Nevertheless, tanning industry is one of the most polluting industries operating mostly in low- and middle-income countries creating heavily polluted industrial zones. India, a developing country, is the second largest producer of heavy leather in the world with production of 700,000 tons of wet salted hides and skin [2]. There are about 42,000 units consisting of around 75% small-sized, 20% medium-sized, and 5% large-sized units clustered mostly (88%) in states

R. K. Choudhary · A. Swati · S. Hait (B)
Department of Civil and Environmental Engineering,
Indian Institute of Technology Patna, Bihta 801103, Bihar, India
e-mail: shait@iitp.ac.in

M. Rathinasamy et al. (eds.), *Water Resources and Environmental Engineering II*,
https://doi.org/10.1007/978-981-13-2038-5_13

like Uttar Pradesh (UP), West Bengal (WB), and Tamil Nadu (TN) [3]. Moreover, the predominant tanning method followed worldwide involves the use of chromium salts (Cr III) as a tanning agent. Unfortunately, only a fraction (30–50%) of chromium salts is utilized in the tanning process and the rest is discharged along with the wastewater [4, 5]. Additionally, tanneries generate a huge amount of wastewater in the tune of 1200–1300 m^3/day as well as about 500 kg/tonne raw hide of tannery sludge produced during tannery wastewater treatment in common effluent treatment plants (CETPs) [4, 6]. Tannery wastes, both wastewater and sludge, produced are categorized as hazardous waste owing to their characteristics especially high organic and heavy metals (Cr III) content [5, 7, 8]. Further, these wastes are discharged and/or dumped untreated or partially treated into flowing surface water or on lands causing irreparable damage to ecosystems with increased health risks. The tannery sludge exhibits variation in constituents present but normally possesses high water content, oil, grease, lime, chromium (Cr), residuary sulfide, chloride, organic and inorganic contaminants as well as pathogens mostly of fecal origin [6, 7, 9–11].

Numerous potential solutions of tannery sludge treatment, viz. pyrolysis, solidification, incineration, anaerobic digestion, or use as inert material in bricks, have been adopted [4, 5, 7, 12]. However, gaseous emissions, operational difficulties, toxic residue releases, high use of chemicals, and high operation costs limit their application. Consequently, scientific interest has been drawn on the environmentally safe treatment of the tannery sludge such as composting and vermicomposting processes. Composting is the thermophilic biological decomposition process where microorganisms act on the organic matter in aerobic conditions to convert it into simpler forms [8, 9], while vermicomposting is a mesophilic waste bio-oxidation and stabilization process where earthworms and microorganisms jointly process wastes under aerobic condition to produce chemically stable and nutrient-rich biofertilizer (vermicompost) [6]. However, vermicomposting is a better option as it results in a homogeneous product (vermicompost) with better quality in terms of desirable aesthetics, reduced levels of pathogenic microorganisms, and more available plant nutrients [6, 8, 9]. Moreover, the time required for complete stabilization and sanitization of waste is less. The aim of the present study is to evaluate the possibility and feasibility of employing vermicomposting technique for treatment and management of tannery sludge for its end use for agronomic purposes. In this context, the primary clarified tannery sludge obtained from CETP is mixed with partially dried cow dung in varying proportion, viz. 0:100, 10:90, 25:75, 40:60, and 50:50, on wet weight basis in order to make it palatable to earthworm *Eisenia fetida*. Also, various physicochemical and microbiological parameters and biomass gain were taken as indicators of the suitability of the feed mixtures for earthworms. The main objective of the present study was to assess the sustainable vermiconversion of primary clarified tannery sludge and the role of *E. fetida* in pathogen reduction over eight-week trial.

2 Materials and Methods

2.1 Tannery Sludge

Primary clarified tannery sludge (PCTS) was obtained as and when required from a CETP based on activated sludge process (ASP) at Banthar, Kanpur, Uttar Pradesh, India. Prior to experimentation, PCTS was characterized for various physicochemical and microbiological parameters.

2.2 Bulking Agent

In the present study, cow dung (CD) was used as a bulking agent to take care of high water content in tannery sludge before vermiconversion. Raw CD was necessitated to partially air-dry in sun for one week for expunging obnoxious gases and heat to prevent earthworm mortality. Prior to use as a bulking material, the partially dried CD was also characterized for various physicochemical and microbiological parameters.

2.3 Eisenia fetida *(Earthworms)*

Epigeic earthworm species *E*. *fetida* was used in the present study. The earthworm culture was procured from Regional Agricultural University (RAU), Pusa, Bihar, India. The earthworms were cultured and developed in small-scale plastic reactors in the laboratory feeding on the partially dried CD. Mature (clitellated) earthworms from the laboratory stock culture were subsequently used for the purpose of this study.

2.4 Experimental Methodology

2.4.1 Physicochemical and Microbiological Analysis of Tannery Sludge, Bulking Agent, and Vermicompost

The PCTS partially dried CD as bulking agent and vermicompost were characterized for various physicochemical and microbiological parameters according to the procedures mentioned in the Standard Methods for Examination of Water and Wastewater and Test Methods for the Examination of Composting and Compost [13, 14]. The samples were analyzed for various physicochemical parameters like pH, electrical conductivity (EC), salinity (SAL), moisture content (MC), total solids (TS), volatile solids (VS), fixed solids (FS), total carbon (C) and total nitrogen (N)

and microbiological parameters like total coliforms (TC) and fecal coliforms (FC). The pH, EC, and SAL were determined by preparing a suspension of the sample using distilled water in the ratio of 1:10 (w/v) and then stirred at 230 rpm for 30 min. The MC and TS contents were determined by drying the samples at 70 ± 2 °C for 24–72 h using hot air oven. The VS and FS content were determined by muffling the known weight of samples in a muffle furnace at 550 ± 5 °C for 2 h. Further, the samples were dried in oven at 60 ± 2 °C for 24–72 h and then ground using mortar and pestle for homogeneity and sieved through 0.2 mm sieve prior to estimation of C and N using elemental CHNS Analyzer. The microbiological parameters like TC and FC were performed by the most probable number (MPN) test mentioned in the USDA and USCC [13], and APHA et al., [14]. Most of the analyses were performed immediately after collection and/or preparation of the samples. The values reported for the parameters are the mean of the triplicate on dry weight basis.

2.4.2 Experimental Design for Vermicomposting of Tannery Sludge

Vermicomposting of tannery sludge was performed in PVC-made reactors under controlled environmental conditions. The circular reactors (diameter: 180 mm and depth: 100 mm), with 0.025 m^2 of exposed top surface area, were covered using perforated lids to provide proper air ventilation and restrict the movement of earthworms out of the reactors. The reactors were filled with a mixture of tannery sludge and cow dung in varying proportion, viz. 0:100 (T_0), 10:90 (T_1), 25:75 (T_3), 40:60 (T_4), and 50:50 (T_5) on wet weight basis in triplicates along with control. The total weight of each reactor was 1 kg, and the reactors were kept inside the wooden vermichamber. Before the introduction of earthworms, aerobic preprocessing of the reaction mixture was performed for 13 days [15]. Earthworm (*E. fetida*) was introduced into each of the reactors at a stocking density of 1.5 kg/m^2. All replicates were fed in a single batch with enough feeding material for the entire eight-week duration of vermicomposting. The moisture level was maintained throughout the study at 60–70% by periodic sprinkling of tap water. All the reactors were manually examined for survival and growth of earthworms at the end of the vermicomposting process. The gain in biomass of earthworms was estimated on the basis of total weight gain and the number of earthworms present in the reactor. The values were determined as the live weight of earthworms upon hand sorting from the reactors. The vermicompost was analyzed for various physicochemical and microbiological parameters.

3 Results and Discussion

3.1 Physicochemical and Microbiological Characterization of Tannery Sludge and Cow Dung

The properties of tannery sludge usually show a wide variation owing to the type of the raw material processed, i.e., hides/skins sourced from various animals and the type of the target finished leather product. In addition to these two major factors, other secondary factors, viz. type of tanning process, tanning agent, process water requirement, and type of the tanning unit whether small-, medium-, or large-sized unit, affect the properties of tannery sludge. Depending on these factors, each tanning unit utilizes a wide range of raw materials including active tanning agent, salts, and other chemicals affecting the properties of tannery sludge. In the present study, the PCTS as collected from the CETPs was observed to be dark gray in color and alkaline in nature with more than 90% water content and significant presence of both total and fecal coliforms. The physicochemical and microbiological characteristics of the PCTS are reported in Table 1.

3.2 Physicochemical and Microbiological Changes During Vermicomposting of Tannery Sludge

During vermicomposting of tannery sludge mixed in varying proportion with cow dung, significant changes in physicochemical and microbiological parameters of the

Table 1 Physicochemical and microbiological parameters of tannery sludge and cow dung

Parameters	PCTS	CD
pH	8.30 ± 0.02	9.08 ± 0.72
EC (mS/cm)	2.33 ± 0.01	6.06 ± 0.03
Salinity (PPT)	1.21 ± 0.01	0.48 ± 0.02
Moisture content (%)	90.70 ± 1.56	42.13 ± 0.61
Total solid (%)	9.36 ± 0.84	57.87 ± 0.44
Volatile solid (%)	3.49 ± 1.10	37.62 ± 0.89
Fixed solid (%)	5.87 ± 2.08	20.25 ± 2.13
Total carbon (%)	8.24 ± 0.42	27.22 ± 4.86
Total nitrogen (%)	4.30 ± 1.28	3.17 ± 1.74
Total coliforms (MPN/100 mL)	5.4 E05	7.8 E05
Fecal coliforms (MPN/100 mL)	2.7 E04	2.0 E05

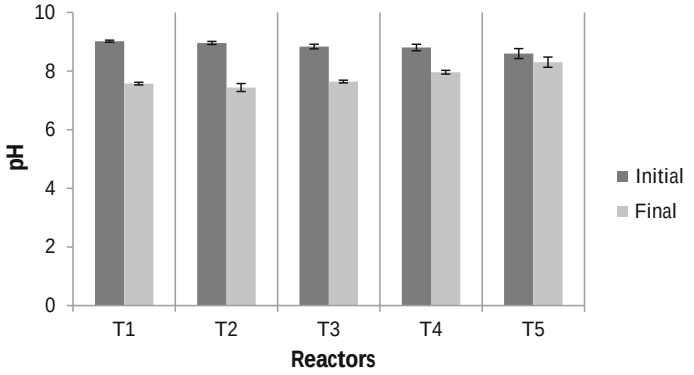

Fig. 1 Changes in pH during vermicomposting

vermicomposted material were observed. It is evident from the present study that tannery sludge in its raw state is harmful to *E*. *fetida* earthworms. However, treatment (T_5) containing 50% of the tannery sludge on wet weight basis is acceptable to earthworms and the vermicompost produced showed a significant difference for all physicochemical and microbiological parameters. The changes in different physicochemical and microbiological parameters during vermicomposting employing *E*. *fetida* have been discussed in detail in the subsequent sections.

3.2.1 pH

A slight decrease in pH of vermicomposted material relative to the initial substrate mixture is attained in all treatments. The maximum reduction of around 17% was in reactors T_1, while reactors T_5 showed the lowest reduction in pH of about 3%. The decrease in pH (3–17%) is positively correlated with the increasing concentration of tannery sludge (0–50%) as shown in Fig. 1. The decreasing trend in pH during vermicomposting is similar to the findings of other researchers [16–18]. The percentage decrease in pH of the final vermicompost is in the order of $T_2 > T_1 > T_3 > T_4 > T_5$. The formation of organic acids and ultimately CO_2 by microbial action due to the decomposition and mineralization of organic matter content (fulvic and humic acids) is responsible for the decrease in pH.

3.2.2 Electrical Conductivity (EC) and Salinity (SAL)

Similar to several other studies on the vermicomposting process, a significant increase in EC of the vermicompost was observed in all treatments as compared to the initial substrate [1, 6, 16–18]. The initial characteristics of the substrate showed highest EC in T_5 (1.682 mS/cm), and it decreased with a decrease in tannery sludge content

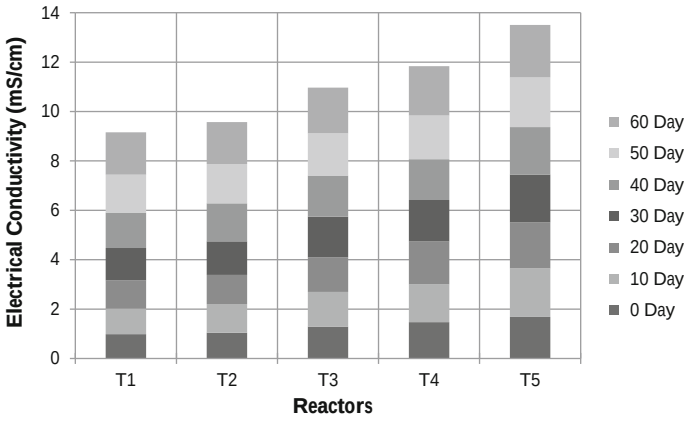

Fig. 2 Changes in electrical conductivity during vermicomposting

in the order of $T_5 > T_4 > T_3 > T_2 > T_1$. However, the increase in EC from initial was in the range of 21–42% for vermicompost in all the treatments. The EC of the vermicompost from different reactors is analyzed after every 10 days as depicted in Fig. 2. The increase is related to the release of different ions or mineral salts in available forms like ammonium, phosphate, and potassium during organic matter stabilization [16–18]. The maximum percentage increase was in treatment T_1 (42%), and it decreased with increasing sludge content, suggesting that EC is negatively correlated to the sludge content.

The EC also reflects the salinity of the vermicompost material, and similar trend of salinity with respect to EC is observed in all treatments. A marked increase in the range of 15–44% from initial values was observed in all treatments. Salinity is directly related to the content of total dissolved solids in the substrate, and it increases with the decomposition and release of mineral ions from the substrate, while EC considers only the conductive entities. The increase in salinity with respect to all the treatments during 60 days vermicomposting trials is shown in Fig. 3.

3.2.3 Volatile Solids (VS) and Fixed Solids (FS)

A significant decrease in the VS content and a proportional increase in the FS content indicate decomposition and mineralization of substrate material. The percentage loss in the VS content of the vermicompost was in the range of 19.5–25%. The maximum loss was observed in T_5 treatment in the order of $T_5 > T_2 > T_4 > T_3 > T_1$. Further, the proportional percentage increase in the content of FS was attained in the range of 21–37% in all trials.

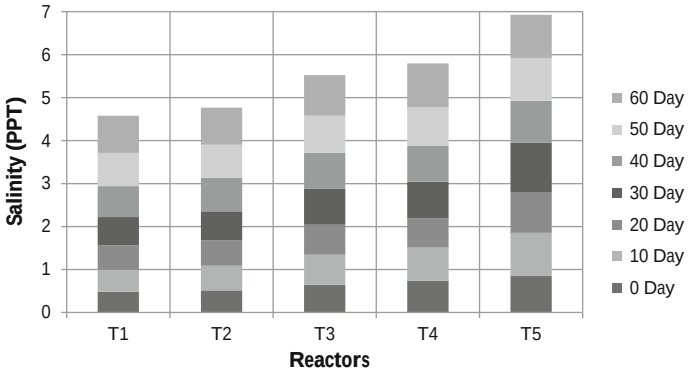

Fig. 3 Variation in salinity of the substrates during vermicomposting

3.2.4 Total Carbon (C) and Total Nitrogen (N) Content

Significant reduction in C of vermicompost in all treatments was obtained in comparison with the initial substrate content (Fig. 4). The loss in C content during vermicomposting was in the range of 12–23.5%. The maximum loss was observed in treatment T_2, and it followed in a particular order of $T_2 > T_1 > T_3 > T_4 > T_5$. Further, a proportional increase in N content was observed in all the reactors from the initial values (Fig. 4). The increase in N was in the range of 16–42% in the order of $T_2 > T_3 > T_4 > T_5 > T_1$. The observed results in the present study are supported by other researchers focusing on the vermicomposting of municipal and industrial wastes [1, 6, 16–18]. The decrease in C content and a proportional increase in N content are due to microbial metabolism involved in decomposition and mineralization of organic matter content, leading to the formation of CO_2 and ammonium, nitrate and nitrites as well as earthworm N excrements [16].

The decrease in C with a simultaneous increase in N content leads to an overall decrease in C:N ratio of the vermicomposted material. The percentage decrease in C:N ratio of the vermicompost obtained from all the reactors was in the range of 31–55% and in the order of $T_2 > T_3 > T_4 > T_5 > T_1$. The decreasing trend of C:N ratio during vermicomposting is in agreement with the studies of other researchers [1, 6, 16–18]. Further, the C:N ratio below 25 shows an advanced degree of stabilization and acceptable maturity [16]. Moreover, the C:N ratio in the final vermicompost is in the range of 17.4–22.6 in the order of $T_1 < T_2 < T_3 < T_4 < T_5$.

3.2.5 Microbiological Parameters

The microbiological parameters in terms of total and fecal coliforms content in the vermicompost are assessed in order to determine the role of earthworms in pathogen reduction during vermicomposting. It is evident from the present study that ver-

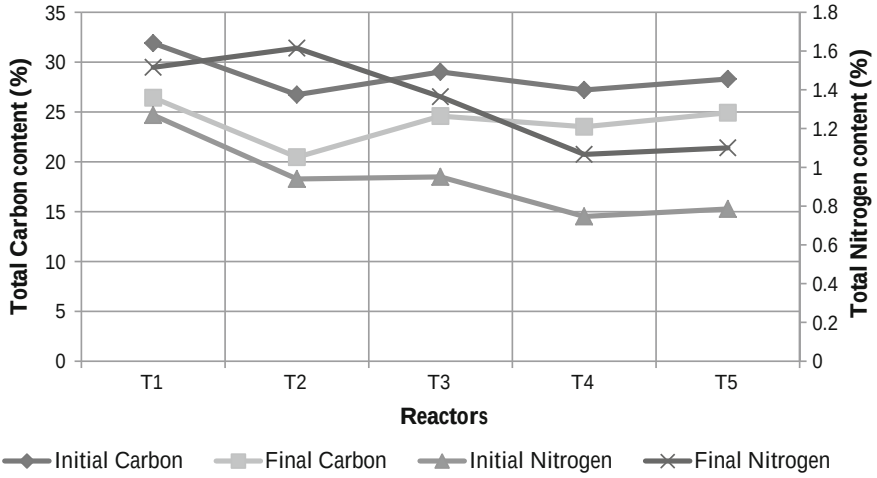

Fig. 4 Variation in total carbon (C) and nitrogen (N) content during vermicomposting

micomposting caused a significant reduction in the pathogenic load of the initial substrate. Significant reduction of around 75–99.5% in the pathogenic content of both total and fecal coliforms was obtained in all trials. The reduction of pathogens during vermicomposting can be attributed to various earthworm actions like intestinal enzymatic action, secretion of coelomic fluids having antimicrobial properties, and grazing actions [16].

3.3 Growth and Fecundity of Earthworm E. fetid *During Vermicomposting of Tannery Sludge*

No mortality was observed in any reactor during the entire 60-day vermicomposting of tannery sludge as aerobic preprocessing of 13 days was done prior to vermicomposting. Contrary to the findings of Vig et al. [6], the final biomass gain in earthworms was found to increase by around 10–30% as compared to the initial biomass in all trials. Further, the biomass gain was proportional to the increasing sludge concentration but up to a certain limit of 25% tannery sludge, beyond which the percentage increase was lesser as shown in Fig. 5.

4 Conclusions

It is evident from the present study that tannery sludge (100%) is toxic to earthworms and therefore it is mixed with other organic waste, i.e., cow dung, to enhance

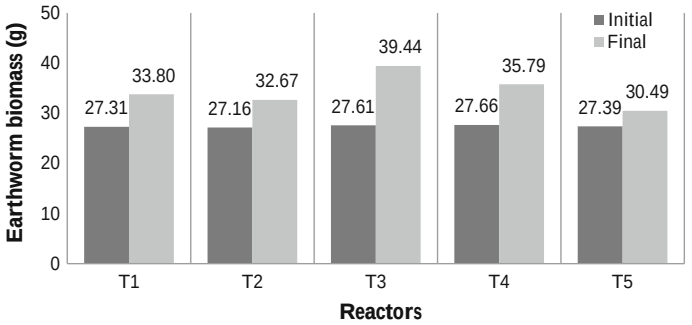

Fig. 5 Earthworm biomass gain in different reactors during vermicomposting

the nutrient contents. The obtained results showed that vermicompost produced by *E. fetida* possesses higher electrical conductivity and nitrogen content with lower C:N ratio. Also, there was a significant reduction in carbon content, suggesting that vermicomposting is effective in the transformation of the organic content of toxic tannery sludge. The decrease in pH with a simultaneous increase in electrical conductivity and salinity contribute to the point that decomposition and mineralization have occurred during 60 days vermicomposting of primary clarified tannery sludge in its crude form employing *E. fetida*. Further, an effective reduction in the pathogenic content of both total and fecal coliforms was obtained during 8-week vermicomposting process in all trials. Therefore, it is successfully shown in the present study that vermicomposting process is effective in both transformation and pathogen reduction, thereby converting a toxic hazardous industrial sludge into a valuable product of agronomic importance.

References

1. Nunes, R.R., Bontempi, R.M., Mendonça, G., Galetti, G., Rezende, M.O.: Vermicomposting as an advanced biological treatment for industrial waste from the leather industry. J. Environ. Sci. Health, Part B **51**(5), 271–277 (2016)
2. Gupta, A.K., Sinha, S.: Phytoextraction capacity of the *Chenopodiumalbum* L: grown on soil amended with tannery sludge. Biores. Technol. **98**, 442–446 (2007)
3. Gupta, S., Sharma, M., Singh, U.N.: Tannery clusters in India and waste management practices in tannery intensive states–inventory and status. J. Environ. Sci. Toxicol. Food Technol **8**, 2319–2399 (2014)
4. Montañés, M.T., Sánchez-Tovar, R., Roux, M.S.: The effectiveness of the stabilization/solidification process on the leachability and toxicity of the tannery sludge chromium. J. Environ. Manage. **143**, 71–79 (2014)
5. Kavouras, P., Pantazopoulou, E., Varitis, S., Vourlias, G., Chrissafis, K., Dimitrakopulos, G.P., Mitrakas, M., Zouboulis, A.I., Karakostas, Th, Xenidis, A.: Incineration of tannery sludge under oxic and anoxic conditions: study of chromium speciation. J. Haz. Mater. **283**, 672–679 (2015)

6. Vig, A.P., Singh, J., Wani, S.H., Singh, D.S.: Vermicomposting of tannery sludge mixed with cattle dung into valuable manure using earthworm *Eisenia fetida* (Savigny). Biores. Technol. **102**(17), 7941–7945 (2011)
7. Basegio, T., Berutti, F., Bernardes, A., Bergmann, C.P.: Environmental and technical aspects of the utilization of tannery sludge as a raw material for clay products. J. Eur. Ceram. Soc. **22**, 2251–2259 (2002)
8. Haroun, M., Idris, A., Omar, S.R.S.: Physico-chemical characterization of compost of the industrial tannery sludge. J. Eng. Sci. Technol. **2**(1), 81–94 (2007)
9. Haroun, M., Idris, A., Omar, S.: Analysis of heavy metals during composting of the tannery sludge using physicochemical and spectroscopic techniques. J. Hazard. Mater. **165**(1–3), 111–119 (2009)
10. Contreras-Ramos, S.M., Alvarez-Bernal, D., Trujillo-Tapia, N., Dendooven, L.: Composting of tannery effluent with cow manure and wheat straw. Biores. Technol. **94**(2), 223–228 (2004)
11. Kilic, E., Font, J., Puig, R., Çolak, S., Çelik, D.: Chromium recovery from tannery sludge with saponin and oxidative remediation. J. Hazard. Mater. **185**, 456–462 (2011)
12. Yılmaz, O., Kantarli, I.C., Yuksel, M., Saglam, M., Yanik, J.: Conversion of leather wastes to useful products. Resour. Conserv. Recycl. **49**, 436–448 (2007)
13. U.S.D.A., U.S.C.C.: Test Methods for the Examination of Composting and Compost. United States Department of Agriculture, United States Composting Council, Washington, DC (2002)
14. A.P.H.A., A.W.W.A., W.E.F.: Standard Methods for the Examination of Water and Wastewater, vol. 22 (2012)
15. Swati, A., Hait, S.: Four-pronged pre-processing approaches for maximum utilization of raw tannery sludge by earthworms. In: International Conference on Water, Environment, Energy and Society (ICWEES-2016) (2016)
16. Hait, S., Tare, V.: Optimizing vermistabilization of waste activated sludge using vermicompost as bulking material. Waste Manag. **31**(3), 502–511 (2011)
17. Hait, S., Tare, V.: Vermistabilization of primary sewage sludge. Biores. Technol. **102**(3), 2812–2820 (2011)
18. Hait, S., Tare, V.: Transformation and availability of nutrients and heavy metals during integrated composting-vermicomposting of sewage sludges. Ecotox. Environ. Saf. **79**, 214–224 (2012)

Temperature-Phased Anaerobic Co-digestion of Food Waste and Rice Husk Using Response Surface Methodology

Smruti Ranjan Sahoo and P. Venkateswara Rao

Abstract High biodegradability of food waste (FW) is a major problem in anaerobic digestion (AD) as it inhibits the process due to rapid acidification leading to very low pH levels. In order to overcome the problem, substrates possessing high C/N ratio can be used as co-substrate to offset the rapid acidification. In this study, rice husk (RH) has been used as co-substrate along with FW at two temperature regions, thermophilic and mesophilic, respectively. Various waste mixture combinations were formed based on total solid (TS%) content and FW percentage using Box-Behnken model. From the study, it was found that biogas produced from the co-digestion and temperature-phased reaction is higher than that of mono digestion and single temperature reaction. In this co-digestion, higher biogas production was found out by increasing the percentage of food waste in the mixture. Maximum biogas potential (729 mL) was achieved with mixture combination of FW (15% TS), RH (15% TS) and percentage of FW (50%). The experimental data were analysed using the chosen model had given the maximum biogas yield of 736 mL, which is very close to the result obtained from the experiments.

Keywords Temperature-phased anaerobic co-digestion · Box-Behnken
Biogas potential

1 Introduction

The growth of societies, rapid urbanisation resulting in producing higher amount of municipal solid waste (MSW). FW is the major portion of MSW consisting of about 40% in India. India is basically an agricultural country, so concerns over managing FW and agricultural waste (AW) are increasing day by day. Among various

S. R. Sahoo (B)
National Institute of Technology, Warangal, India
e-mail: smruti.ranjan863@gmail.com

P. Venkateswara Rao
Civil Engineering Department, National Institute of Technology, Warangal, India

M. Rathinasamy et al. (eds.), *Water Resources and Environmental Engineering II*,
https://doi.org/10.1007/978-981-13-2038-5_14

alternatives used for stabilising and disposing of AW and FW, AD is most economical and viable. AD is beneficial in ecological point of view as it produces energy and decreases greenhouse gas emission. Significant removal of organic matter is digested in AD and the nutrients present in the digestate can make the process to be more attractive.

The anaerobic microorganisms are classified based on their growth temperature region: psychrophilic (T < 20 °C), mesophilic (20 °C < T < 45 °C), thermophilic (45 °C < T < 60 °C) and hyperthermophilic (T > 60 °C). Thermophilic and mesophilic temperature regions are most widely used in treating organic wastes. Every temperature region has its own advantages and disadvantages as in thermophilic region the metabolic activity of microorganisms increased resulting in higher reaction rates and at the same time it also possess the higher rate of inactivating the pathogens [1]. Similarly in mesophilic reactions, it is stable, requires lesser energy and has lesser probability of inhibition of long-chain fatty acids [2].

Temperature-phased anaerobic co-digestion (TPAD) combines two temperature regions and tries to get the advantages of both the regions and minimising the limitations. Use of TPAD can improve the hydrolysis phase of low biodegradable substances like agricultural wastes possessing high C/N ratio and high lignin content by operating the hydrolytic phase at thermophilic temperature region, which is the limiting step of AD.

India is an agrarian country where the majority of the population depends on agriculture for their livelihood. Every year a huge amount of agricultural waste is produced which are not easily biodegradable due to their higher C/N ratio and higher lignin content. Monodigestion of agricultural wastes is not viable because of its composition. Similarly, FW is highly biodegradable which causes accumulation of volatile fatty acids resulting acidification of reactors leading to sickness. Co-digestion of FW along with agricultural wastes can be a probable solution in order to overcome above problems. RH possesses higher C/N ratio compared to FW, which enables its co-digestion potential as the favourable C/N ratio can be achieved by mixing these two.

There are several factors which influence the AD of organic wastes and their range for optimum conditions is known for the selected mixture combinations. Design of experiments and statistical approaches will conserve the time and resources to obtain valid combinations in spite of practicing several trials routinely. Classical approaches like keeping one factor constant and varying others were also time consuming and unable to find true optimum because of the interactions between independent factors [3]. In order to overcome the above problem, response surface methodology (RSM) can be used where the factors are governed by a model and responses can be analysed with respect to the factors. This study was carried out to investigate the effects of factors (FW TS%, RH TS% and FW%) on temperature-phased anaerobic co-digestion of FW and RH. RSM by the Box-Behnken model was used to find optimum combination of factors to get maximum biogas production.

2 Materials and Methods

2.1 Substrates and Inoculum

The substrates used in this study are FW and RH. FW was collected from the institutional food court (IFC) of National Institute of Technology, Warangal. Polythene bags were used to collect the FW from the IFC continuously for a week as the menu of IFC was getting repeated in every week. After collecting, the inorganic materials like polythenes, bones and lemon residues were sorted out and removed manually. The FW was pulverised using a mixer grinder to make it homogenous. The mixed FW was stored in the refrigerator below 4 °C till its use. Rice husk was collected from a local plant, Omkara Rice Mills, Warangal. The collected RH was ground properly in order to use as substrate. Fresh cow dung was collected and acclimatised with the selected substrates for 15 days in order to be used as mesophilic inoculum.

2.2 Experimental Setup

Box-Behnken model was used for setting up the reactors by taking three independent variables. The variables for the experimental work are total solid (TS) percentage of both FW and RH (5–15%), and the third variable was the percentage of FW in the mixture of FW and RH (25–75%). After using these variables with the model, 30 combinations were formed out including duplicates except the centre point which was repeated six times. The experiment was carried out in 120-ml glass bottles as batch mode. 20 ml each of FW and RH was taken as per the TS% and inoculum was added as per I/S ratio (VS basis) as 1. Then, bottles were kept in the temperature-controlled environment in two phases, first phase at thermophilic region (50 °C) for 4 days [1], and in second phase bottles were shifted to mesophilic region (35 °C) by adding mesophilic inoculum.

2.3 Statistical Analysis

The percentage of TS of FW and RH and the percentage of FW in the mixture were set as independent variables (factors). The influence of these factors on the biogas production (response) was analysed using Box-Behnken design. All the factors were checked at a higher level, central level and lower level in order to check the variability of the response. Duplicate of all the combinations and a blank solution without any substrate was made (Fig. 1 and Table 1).

Minitab 2017 software was used to conduct analyses of the variance (ANOVA) and mathematical regression models and to plot response surfaces. Functional relationships between responses (Y) and the set of factors (X_1, X_2, and X_3) were explained by

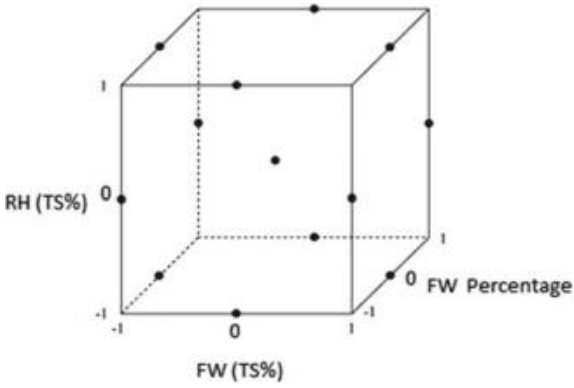

Fig. 1 Schematic diagram of Box-Behnken model for the experiment

Table 1 Levels of factors selected for the design

Variables	Factors	Levels of factors		
		−1	0	1
Food waste	FW TS%	5	10	15
Rice husk	RH TS%	5	10	15
FW percentage	FW percentage	25	50	75

estimating coefficients of the following first-order polynomial model (1) or second-order polynomial model (2) based on experimental data.

$$Y = \beta_0 + \beta_1 X_1 + \beta_2 X_2 + \beta_3 X_3 \tag{1}$$

$$Y = \beta_0 + \beta_1 X_1 + \beta_2 X_2 + \beta_3 X_3 + \beta_{12} X_1 * X_2 + \beta_{23} X_2 * X_3 + \beta_{13} X_1 * X_3 + \beta_{11} X_1^2 + \beta_{22} X_2^2 + \beta_{33} X_3^2 \tag{2}$$

From the equations, Y is the response, i.e., biogas production, X_1 is the TS percentage of FW, X_2 is the TS percentage of RH, and X_3 is the percentage of FW in the substrate mixture; β_0 is a constant, β_1, β_2 and β_3 are linear coefficients (main effects); $+\beta_{12}$, β_{13} and β_{23} are cross-product coefficients (binary interactions); and β_{11}, β_{22} and β_{33} are quadratic coefficients.

Analytical Techniques TS, VS and pH analyses were performed in accordance with APHA. The volume of biogas was measured by water displacement method. Methane content in the produced gas was analysed by using gas chromatograph (model YL6500, Environmental lab, NIT Warangal) (Table 2).

Table 2 Properties and characterisation of substrate and inoculum

Characteristics	FW	RH	Inoculum
TS (%)	26.2	91.3	16.21
VS (% of TS)	92.02	84.42	92.02
pH	4.2	5.8	7.5
C/N ratio [4]	16.89	38.2	19

3 Results and Discussion

3.1 Substrate Characteristics

In this study, the VS, TS and p^H were found out for the substrates. It was found that TS of RH was very high and VS was almost 85% of the TS which can be digested to produce biogas. All the substrates were having high VS/TS ratio which is suitable for biogas production. Lower C/N ratio promotes ammonia accumulation and enhancement in p^H which is toxic to methanogens. Higher C/N ratio indicates consumption of nitrogen by methanogens and accumulation volatile fatty acids (VFA). It is suggested by many authors that the optimum C/N ratio for AD lies between 20 and 30 and for p^H it is 6.5–8. In this study, these limits were maintained without addition of any external substances. So co-digestion was found useful as we don't need to add any buffering reagent to maintain p^H and C/N ratio was also maintained. From the analysis, Box-Behnken design gave that the reactions are controlled by second-order polynomial equation as described in Eq. 2. The results found from experimental data were fed to the model and predicted values for all the combinations were found out. Table 3 gives the detail explanations of the results. It has been found clearly that co-digestion enhanced the biogas production in comparison to mono digestion. The results obtained were compared with the only mesophilic digestion which was 584 ml [4]. Although the amount of energy consumption was found higher it gave more biogas comparable to single temperature digestion.

3.2 Biogas Production

Cumulative biogas production of run order 14 is shown in Fig. 2. Daily biogas production of all the reactors was taken by water displacement method, it was found that the biogas production was started quickly in all reactors, and as temperature-phased method was used, the hydrolysis process was started quickly and the digestion went on. Run order 14 gave 729 ml of biogas from the graph we can see that it went on increasing up to 34 days and afterwards it decreased and the cumulative gas production was found almost constant.

Table 3 Actual and predicted values of biogas (in ml) of the experiment

Run order	FW (TS%)	RH (TS%)	FW%	Response (biogas volume in ml)	Predicted (biogas volume in ml)
1	5	15	50	393.2	350.91
4	10	15	25	414.8	416.71
6	10	5	25	379.8	319.13
7	10	5	75	398.8	355.79
10	5	10	75	359.1	309.97
11	10	15	75	441.4	493.76
12	10	10	50	669.8	663.53
14	15	15	50	729	688.31
15	15	10	75	661.6	638.61
19	15	10	25	434.4	443.47
22	5	10	25	386.4	391.38
27	5	5	50	349.6	380.18
28	15	5	50	402	423.49

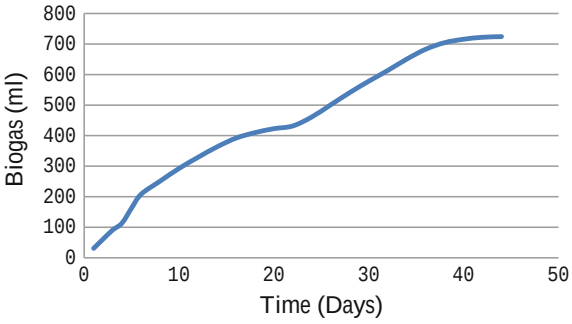

Fig. 2 Cumulative biogas production of run order 14

3.3 Statistical Analysis of Response with respect to Factors

The three-dimensional response surface of biogas production was plotted based on Eq. 3 to investigate the effects of factors on it. To evaluate the variability in biogas production, adjusted R^2 statistic was used instead of R^2 statistic to reduce insignificant terms in the model. Although R^2 always increases as terms are added to the model even if they are not significant, adjusted R^2 actually decrease if non-significant terms are added to a model. The R^2 and adjusted R^2 were calculated and are found to be 94.63 and 92.21%, respectively. The '*P*' values for all were found to <0.05 Based on experimental data, the model gave the following equation.

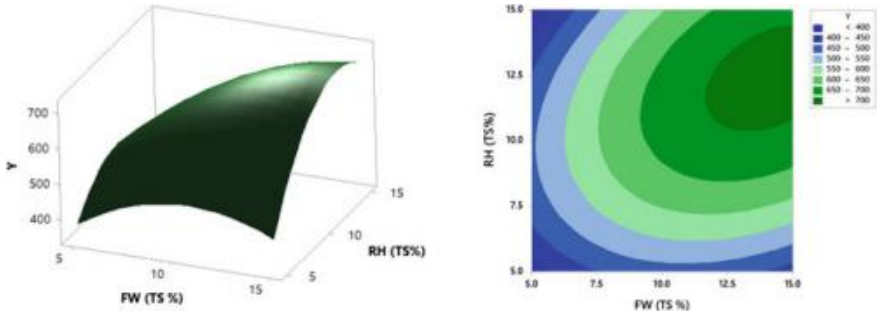

Fig. 3 Response surface (left) and contour (right) of biogas production depending on variation of FW (TS%) and RH (TS%)

$$\begin{aligned} Y = {} & -466 + 23.3\,\mathrm{FW(TS\%)} + 79.3\,\mathrm{RH(TS\%)} + 17.36\mathrm{FW\%} \\ & - 3.066\,\mathrm{FW(TS\%)} * \mathrm{FW(TS\%)} - 5.046\,\mathrm{RH(TS\%)} * \mathrm{RH(TS\%)} \\ & - 0.22556\,\mathrm{FW\%} * \mathrm{FW\%} + 2.941\,\mathrm{FW(TS\%)} * \mathrm{RH(TS\%)} \\ & + 0.553\,\mathrm{FW(TS\%)} * \mathrm{FW\%} + 0.081\,\mathrm{RH(TS\%} * \mathrm{FW\%)} \end{aligned} \quad (3)$$

The model predicted the result using this equation, and the biogas production was found to be 736 ml and also proposed the desired combination which was FW (TS%), RH (TS%), FW% 15%, 12.68% and 59.34%, respectively.

3.3.1 Effects of FW (TS%) and RH (TS%) on Response

The effects of FW (TS%) and RH (TS%) are shown in Fig. 3. As the solid contents of FW and RH goes on increasing, the biogas production also increased. The ridge shows the maximum biogas production at a TS of 15% which was found to be 729 ml. The contour plot provides a two-dimensional view of the surface where points that have the same response are connected to produce contour lines of constant responses. The contour shows the number of reactors within that particular region. Here, we can see that both the contour and surface plots are showing the similar trends. The ridge for the surface plot and the maximum value of the contour are occurring at same location that is at the topmost right corner indicating higher TS of FW and RH.

3.3.2 Effects of FW% and RH (TS%) on Response

The effects of FW% and RH (TS%) are shown in Fig. 4. As the FW% and RH (TS%) was increased, the biogas production was also enhanced but it has been found that after a certain limit, if the FW% was increased the biogas production was decreased. This may happen due to accumulation VFAs as FW is easily biodegradable. From the results, it is observed that the optimum FW% was found somewhere between

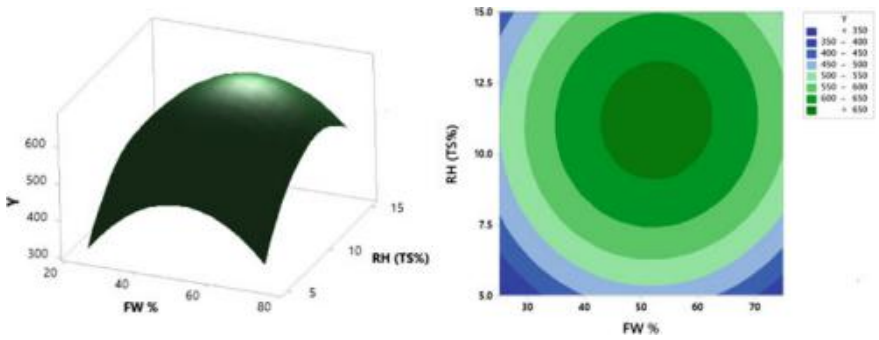

Fig. 4 Response surface (left) and contour (right) of biogas production depending on variation of FW% and RH (TS%)

50 and 60%. It was visualised that both the contour and surface plots are showing same trends. The ridge for the surface plot and the maximum value of the contour are occurring at same location that is at the mid of the plots indicating intermediate TS of RH and FW%.

3.3.3 Effects of FW% and FW (TS%) on Response

The effects of FW% and RH (TS%) are shown in Fig. 4. As the FW% and FW (TS%) was increased, the biogas production was also enhanced. Here also it was found that the FW% can be increased only up to a certain limit after which if it is increased it will impose inhibitory effects resulting in decrease in biogas production. It is seen that both the contour and surface plots are showing same trends. The ridge for the surface plot and the maximum value of the contour are occurring at same location that is at the top middle region indicating higher TS of FW and intermediate FW% (Fig. 5).

3.3.4 Optimisation Plot

All the experimental values were fed to the Box-Behnken model and were optimised to get the combination of factors for the best response. The optimisation plot found is shown in Fig. 6. From the plot it was found that the optimum condition was FW (TS%) is 15, RH (TS%) is 12.67 and FW% is 59.34 and the biogas production is 735.58 ml., which is nearly equal to the experimental work which was found to be 729 ml by combining FW (TS%), RH (TS%), FW% at 15%, 15% and 50%, respectively. The combination given by the model was also examined and found true.

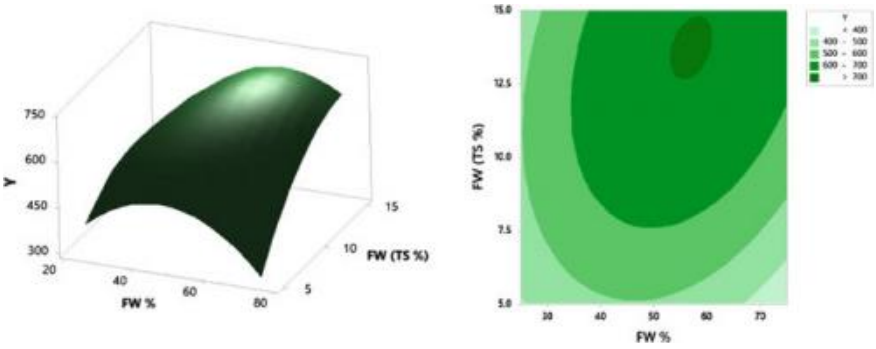

Fig. 5 Response surface (left) and contour (right) of biogas production depending on variation of FW% and FW (TS%)

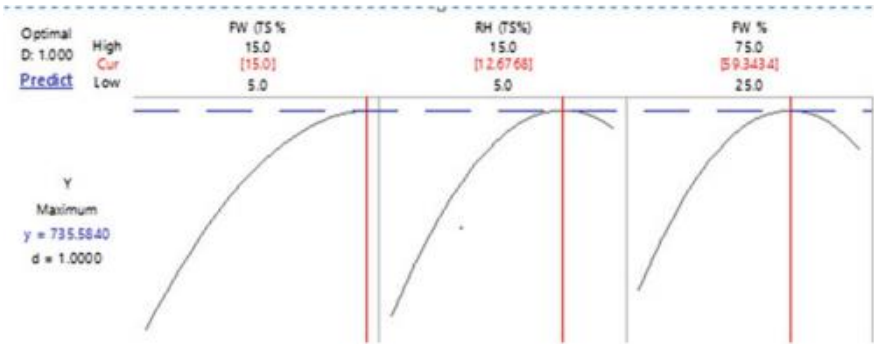

Fig. 6 Optimisation plot

4 Conclusion

The above study investigated the effects of FW (TS%), RH (TS%) and FW% on the biogas production. It also focused on the temperature-phased reaction and co-digestion. Box-Behnken design was used to find the optimum combination of the factors mentioned. The results revealed that at higher solids concentration and FW% higher than 50% had given higher biogas yield. As FW is highly biodegradable, RH can be used in order to avoid the accumulation of VFA and subsequent failure of the reactor. By using temperature-phased reaction, hydrolysis process was catalysed for the RH and produced higher biogas yield as the effect of co-digestion with FW. The maximum biogas was produced at a combination of FW (TS%), RH (TS%) and FW% of 15%, 15% and 50%, respectively, and was found to be 729 ml. The model developed based on the experimental values also found to be in agreement and the residual was found to be 6 ml. From the model, it is observed that TS% RH, TS% FW are found to be the significant variables, respectively. However, the %FW found to be not so significant when compared to the other input variables.

Acknowledgements The authors wish to thank Department of Biotechnology, Government of India, for funding this work (Sanction order No: BT/PR6328/GBD/27/387/2012) and Department of Civil Engineering, National Institute of Technology, Warangal, for providing support to carry out present work.

References

1. Fernández-Rodríguez, J., Pérez, M., Romero, L.I.: Temperature-phased anaerobic digestion of industrial organic fraction of municipal solid waste: a batch study. Chem. Eng. J. **270**, 597–604 (2015)
2. Fernández-Rodríguez, J., Pérez, M., Romero, L.I.: Semicontinuous temperature-phased anaerobic digestion (TPAD) of organic fraction of municipal solid waste (OFMSW). Comparison with single-stage processes. Chem. Eng. J. **285**, 409–416 (2016)
3. Kim, H.-W., Shin, H.-S., Han, S.-K., Oh, S.-E.: Response surface optimization of substrates for thermophilic anaerobic codigestion of sewage sludge and food waste. J. Air Waste Manag. Assoc. **57**, 309–318 (2012)
4. Haider, M.R., Zeshan, Yousaf, S., Malik, R.N., Visvanathan, C.: Effect of mixing ratio of food waste and rice husk co-digestion and substrate to inoculum ratio on biogas production. Biores. Technol. **190**, 451–457 (2015)
5. Wu, L.J., Kobayashi, T., Li, Y.Y., Xu, K.Q.: Comparison of single-stage and temperature-phased two-stage anaerobic digestion of oily food waste. Energy Convers. Manage. **106**, 1174–1182 (2015)
6. Kim, H.W., Shin, H.S., Han, S.K., Oh, S.E..: Response surface optimization of substrates for thermophilic anaerobic codigestion of sewage sludge and food waste. J. Air Waste Manage. Assoc. **57**, 309–318 (2012)
7. Wang, X., Yang, G., Feng, Y., Ren, G., Han, X.: Optimizing feeding composition and carbon-ntrogen ratios for improved methane yield during anaerobic co-digestion of dairy ,chicken manure and wheat straw. Bioresour. Technol. **120**, 75–83 (2012)

A Study on Effect of Water Temperature on the Seepage Pressure Under Subsurface Floor of a Barrage: A Case Study of Taraka Rama Tirtha Sagar Barrage, Vizianagaram

S. Chandramouli

Abstract An attempt is made to study the effect of water temperature on the seepage gradients below the subsurface floor of a Taraka Rama Tirtha Sagar (TRTS) barrage constructed across Champavati River. During 60% of the year, a constant temperature of 28 °C is maintained and varies during the remaining period. The kinematic viscosities of water are varying in the range of 0.008275–0.009038 cm^2/sin a year. The seepage velocities are found to vary in proportion to water temperature. The average seepage rate below the structure is estimated to be of 15 m^3/s. The pressure gradients obtained are within the permissible range. As the temperature increases, the residual head at the downstream of the structure decreases. High temperatures result in excessive gradients, and low temperatures lead to high residual pressures. It is concluded that the high and low temperatures affect the safety of the structure, and hence, proper protective measures are to be adopted.

Keywords Barrage · Water temperature · Kinematic viscosity · Seepage pressure Seepage velocity

1 Introduction

There is an ever-increasing demand on the water supply in today's society, and water resources conservation is mandatory to effectively utilize the available freshwater resources.

Hydraulic structures such as dams, weirs, barrages play a vital role in the conservation of water resources. The engineers must carefully design and construct these structures so that they perform efficiently. The most important element of any structure is its foundation. Many failures had been reported in the recent past either due to foundation failure or due to overall stability of the structure [1].

S. Chandramouli (B)
Department of Civil Engineering, MVGR College of Engineering, Vizianagaram, Andhra Pradesh, India
e-mail: chandramoulis@mvgrce.edu.in

M. Rathinasamy et al. (eds.), *Water Resources and Environmental Engineering II*,
https://doi.org/10.1007/978-981-13-2038-5_15

The most critical aspect that a designer should take into account is the failure due to seepage pressure and/or piping phenomenon at the toe of the structure. The estimation of flow of water through the subsoil below weirs or barrages is highly important for designing the subsurface floor. The principle of flow of water through soil medium was first investigated by Darcy in 1856 which is now referred as Darcy's law and states that the velocity of flow varies directly with the head and inversely with the length of the flow path. The amount of seepage flow of water through the subsoil depends on several factors. The viscosity of flowing water is one of them. As the viscosity of water changes with water temperature, the quantum of flow will vary.

The viscosity of a fluid greatly influences its motion. It is defined as the resistance offered by the fluid against deformation under the influence of a shear force regardless of its magnitude. It is known as dynamic viscosity or absolute viscosity or coefficient of viscosity or simply viscosity. The viscosity of a liquid depends upon two factors, namely intermolecular structure (cohesion) and molecular momentum transfer. In liquids, the cohesion is predominant and the molecular momentum transfer is very less. Thus, the viscosity of liquids depends mainly on cohesion. As the temperature increases, the cohesive force decreases rapidly resulting in decrease in the fluid viscosity. Poiseuille developed an expression for determining the kinematic viscosity (ν) of water at any temperature θ,

$$\nu = (0.0179)/\left(1 + 0.0337\,\theta + 0.000221\,\theta^2\right) \tag{1}$$

where ν is in cm^2/s and θ is in °C.

The effect of temperature on the flow of water was first investigated by Allen Hazen in 1892, and the following expression was found for the velocity of flow through sands,

$$V = 3.28\,c\,d^2(h/l)((t + 10)/60) \tag{2}$$

where V = Velocity of flow in ft/d of column of water of the same area as that of the sand; d = effective size of sand in mm; c = a coefficient which is usually taken as 1000; h/l = hydraulic gradient; t = temperature of the water in °F.

Thus, in the present study, an attempt has been made to study the effect of water temperature on the seepage pressure gradient under the subsurface floor of the Taraka Rama Tirtha Sagar barrage located at Kotagandredu Village of Gurlamandal, Vizianagaram (District), Andhra Pradesh, India.

2 Description of Study Area

The Taraka Rama Tirtha Sagar barrage has been proposed across Champavathi River to irrigate an extent of 24,710 acres of ayacut including stabilization of 8,172 acres of existing wet ayacut under Kumili channel system. Besides this, the scheme provides

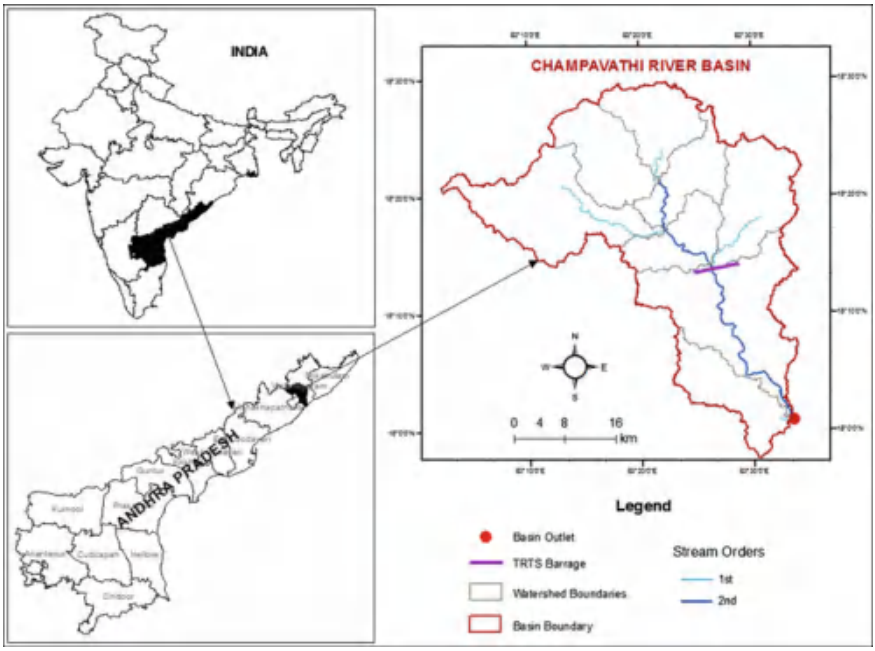

Fig. 1 Location map of Taraka Rama Tirtha Sagar Barrage in Champavathi River Basin

drinking water facility to the Vizianagaram municipality with 0.48 TMC of water. The salient features of the barrage are given below and location map of barrage shown in Fig. 1.

Barrage

Location: Kotagandredu Village of Gurlamandal, Vizianagaram (District), Andhra Pradesh (State), India

Longitude: 83° 26′ 32″ East	Latitude: 18° 13′ 44″ North
Catchment Area: 1,028.23 km^2	Maximum flood discharge (observed): 1,982 m^3/s
Full reservoir level: +42.50 m	Maximum water level: +43.50 m
Crest Level: +39.50 m	Length: 184 m
Number of Vents: 12	Number of Scour Vents: 1

Head Regulator

Discharge: 34.12 m^3/s	Number of Vents: 2
Sill Level: +39.80 m	Angle with Barrage: 900

Afflux Bunds

Top level of dam: +45.50 m	Length Left: 0.56 km Right: 1.10 km

Diversion Canal

Length: 13.428 km Full supply level: +39.98 m	Top level of dam: +41.18 m
Bed Width: 18.40 m	Surface Fall: 1 in 10,000 Side Slopes: 1.5:1
Full supply discharge: 2.4 m^3/s	Discharge: 1205 m^3/s

3 Review of Literature

Literature pertaining to the effect of water temperature on the seepage analysis is very limited. The expression based on the tests for the permeability of sands by considering the effect of water temperature and other parameters were proposed by Mavis and Wisley [2]. A detailed description of the design of subsurface floor under a weir or a barrage including seasonal variations based on model studies was provided by Khosla et al. [3]. In association with head data, the temperature data were also used in the formal solutions of the inverse problem to estimate groundwater flow and hydraulic conductivity by Anderson [4]. The author concluded that the temperature data in addition to head data are more useful for the calibration of groundwater flow models. Huang and Rudnicki [5] studied the migration of deeply buried groundwater by using a numerical simulation based on laboratory test results. They expressed that the pressure and temperature variation of seepage parameters in terms of the corresponding variation of the solid skeleton's permeability, porosity, compressibility coefficient, seepage fluid's viscosity and then through mathematical transformation and linearization methods. The mathematical model with pressure- and temperature-dependent coefficients was reduced to the same form as that of the standard form for seepage flow. Fard and Dezfouli [6] showed the vital importance of the precision tools in identifying the effects of components such as variations in temperature and seepage rate in the sustainability of the hydraulic structures on one hand and their operational efficiency aimed at optimum utilization of the renewable water resources on the other are to be studied. This paper investigates the effect of temperature on seepage analysis of hydraulic structures.

4 Data Collection

The basic data required for the present study are average monthly temperatures, subsurface soil characteristics and geometric and flow characteristics of the structure. The description of the data is presented below.

Table 1 Monthly water temperatures in the study area

Month	Average water temperature	
	°C	°F
January	25	77
February	27	80.6
March	27	80.6
April	28	82.4
May	29	84.2
June	28	82.4
July	28	82.4
August	28	82.4
September	28	82.4
October	28	82.4
November	28	82.4
December	26	78.8

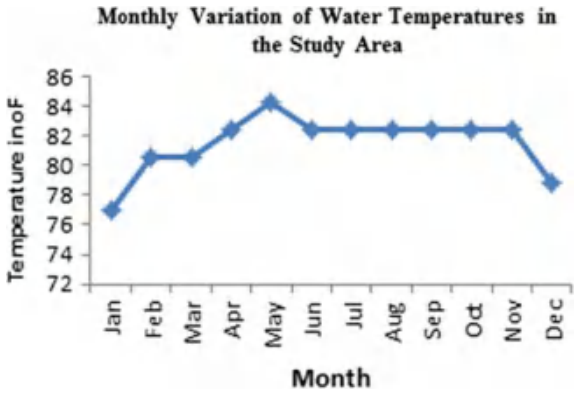

Fig. 2 Monthly average water temperature in the study area

Water Temperature

The monthly average water temperature in the study area is presented in Table 1, and the same has been shown in Fig. 2.

Subsoil Characteristics

The type of subsoil existing in this study area is sandy soil. The hydraulic conductivity of the sandy soil is taken as 0.04 m/s [7]. The effective size of the sand is 1.49 mm.

Geometric and Flow Characteristics of the Structure

Head causing flow (h) = 5.2 m

Length of the column of the sand (l) = 27.5 m

Depth of the column of the sand = 11 m

Width of the column of the sand = 184 m

Cross-sectional area of the sand column through which the seepage takes place = 2,024 m^2

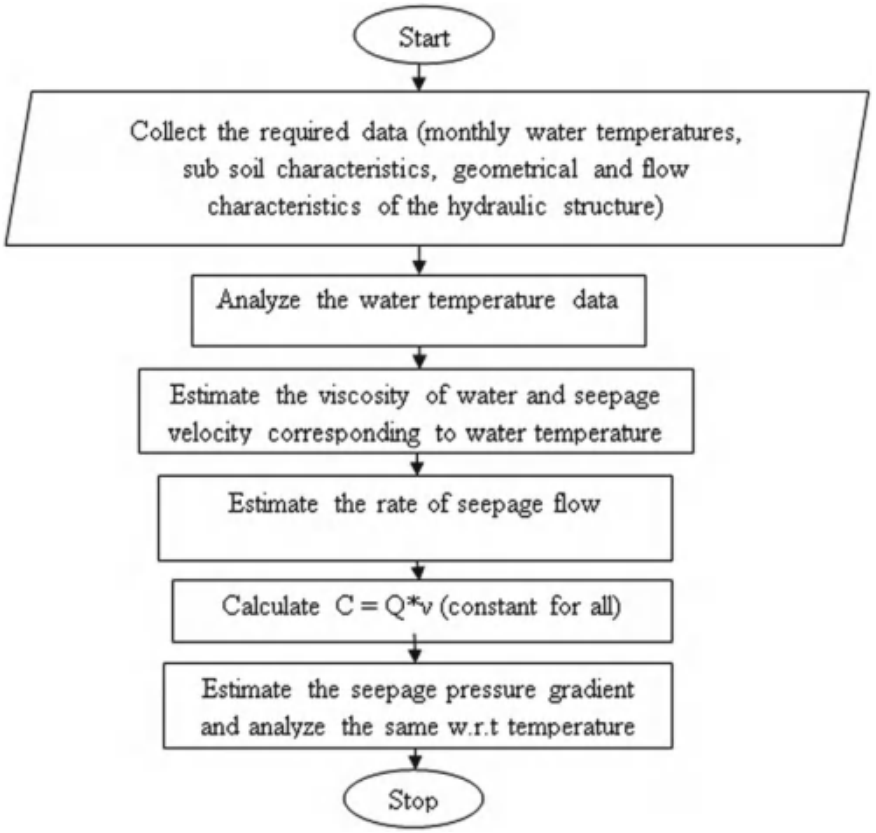

Fig. 3 Conceptual framework of methodology for study area

5 Methodology

The methodology followed in the present study is explained with the help of the following flowchart and shown in Fig. 3.

The kinematic viscosity of water and seepage velocity corresponding to water temperature was estimated using the Poiseuille's equation and Allen Hazen's equation, respectively. The rate of seepage is calculated using the continuity equation, i.e., $Q = AV$. The pressure gradient is determined with the formula developed by Khosla et al. [3] which are given below.

$$\mathrm{d}p/\mathrm{d}s = (C/K)(l/a)(l/v) \tag{3}$$

where v = kinematic viscosity of water; a = effective area of section of flow; V = velocity of seepage water; p = pressure in m of water; s = length along streamline; and K = hydraulic conductivity of the soil and $C = Q * v$ = constant.

Table 2 Monthly water temperatures and their kinematic viscosities

Month	Average water temperature in °C	Kinematic viscosity of water (ν) in cm^2/s
January	25	0.009037
February	27	0.008643
March	27	0.008643
April	28	0.008455
May	29	0.008274
June	28	0.008455
July	28	0.008455
August	28	0.008455
September	28	0.008455
October	28	0.008455
November	28	0.008455
December	26	0.008836

6 Results and Discussions

The various results obtained are presented in this section. It is observed from Fig. 1 that the water temperature in the study area is varying between 250 and 290 °C. For 58.33% duration of the year, a constant temperature of 280 °C is maintained and for the remaining period, it varies between 250 and 290 °C. So this variation in water temperature leads to changes in the viscosity of the flowing water. Hence, the present study is carried out to study the effect of temperatures on the pressure gradient below the subsurface floor of the proposed barrage. The kinematic viscosities corresponding to water temperatures are computed using the Poiseuille's equation and are presented in Table 2.

The monthly seepage velocities were computed using Allen Hazen' formula and Darcy's law using data provided in Table 3. Figure 4 shows the graphical representation of the same.

The effective size of the sand (d) = 1.49 mm. Head causing flow (h) = 5.2 m*

$$\begin{aligned}\text{Length of the column of the sand } (l) &= 27.5\,\text{m}\ h/l \\ &= \text{hydraulic gradient} \\ &= 0.189091.\end{aligned}$$

(*The head causing flow generally changes from year to year depending upon the inflow into the barrage but it has been assumed to be constant for all the months in this study.)

Table 3 Monthly water temperatures and the corresponding seepage velocities

Month	Water temperature in °F	Seepage velocity of flow	
		ft/day	m/s
January	77	1996.573	0.007043
February	80.6	2079.190	0.007334
March	80.6	2079.190	0.007334
April	82.4	2120.498	0.007480
May	84.2	2161.806	0.007626
June	82.4	2120.498	0.007480
July	82.4	2120.498	0.007480
August	82.4	2120.498	0.007480
September	82.4	2120.498	0.007480
October	82.4	2120.498	0.007480
November	82.4	2120.498	0.007480
December	78.8	2037.881	0.007189

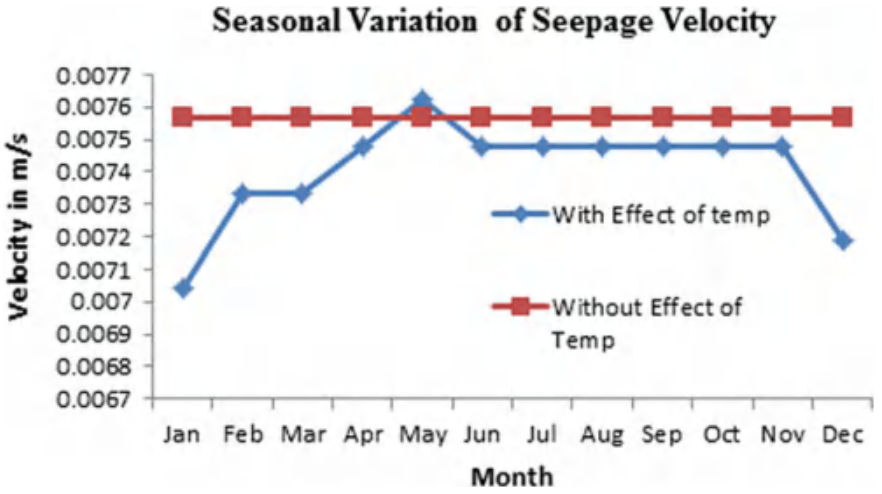

Fig. 4 Monthly water temperatures and the corresponding seepage velocities

It is observed from Table 3 and Fig. 3 that the seepage velocity of flow has the same trend as that of the temperature. So they are proportional to each other indicating that higher temperatures would lead to higher velocities of flow. The seepage velocity of flow without considering the effect of temperature was found using Darcy's law, and it is observed that it has a constant magnitude of 0.007564 m/s and almost all the seepage velocities based on temperature are observed to be less than this value. The seepage rates are computed based on continuity equation and are presented in Table 4. Also, the constant $C = Q * \nu$ is determined and presented in Table 4.

Table 4 Seepage rates and *C* values

Month	Q (m^3/s)	ν (m^2/s)	C
January	14.25597647	9.03755E−07	1.28839E−05
February	14.84587894	8.64313E−07	1.28315E−05
March	14.84587894	8.64313E−07	1.28315E−05
April	15.14083018	8.45590E−07	1.28029E−05
May	15.43578141	8.27493E−07	1.27730E−05
June	15.14083018	8.45590E−07	1.28029E−05
July	15.14083018	8.45590E−07	1.28029E−05
August	15.14083018	8.45590E−07	1.28029E−05
September	15.14083018	8.45590E−07	1.28029E−05
October	15.14083018	8.45590E−07	1.28029E−05
November	15.14083018	8.45590E−07	1.28029E−05
December	14.55092770	8.83691E−07	1.28585E−05
Average *C*			1.28166E−05

Table 5 Seasonal pressure gradients and head loss at d/s

Month	d*p*/ds	Head loss at the d/s in m	Residual head at the d/s in m
January	0.175166703	4.82	0.38
February	0.183160275	5.04	0.16
March	0.183160275	5.04	0.16
April	0.187215696	5.15	0.05
May	0.191310208	5.20	0.00
June	0.187215696	5.15	0.05
July	0.187215696	5.15	0.05
August	0.187215696	5.15	0.05
September	0.187215696	5.15	0.05
October	0.187215696	5.15	0.05
November	0.187215696	5.15	0.05
December	0.179143944	4.93	0.27

The seepage rate and *C* value based on Darcy's law are obtained as 15.3095 m^3/s and 1.26685E−07, respectively. In order to compute *C* value, the viscosity of water at 290 °C is considered.

From Table 4, it is observed that the seepage rates are almost equal but the amount of water lost through seepage is very high. So for effective water management, focus on the seepage reduction methods is recommended. The pressure gradients were calculated using the expression developed by Khosla et al. [3], and the same has been presented in Table 5 and Fig. 5.

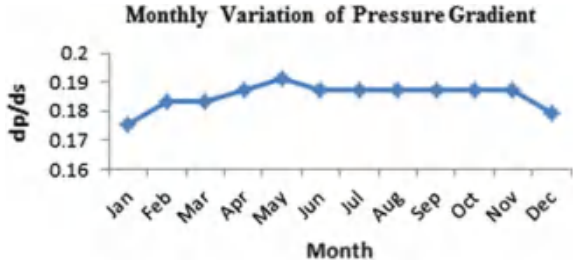

Fig. 5 Monthly variation of pressure gradient

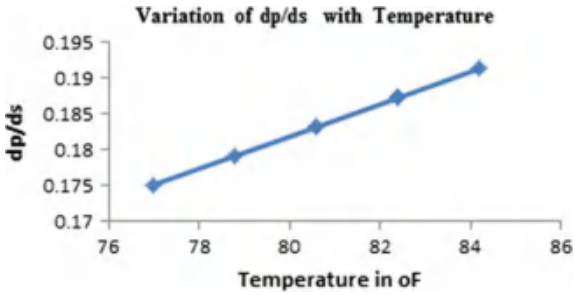

Fig. 6 Variation of d*p*/d*s* with temperature

Based on Darcy's law, the pressure gradient obtained is 0.190659339, the head loss and the residual head on the downstream obtained are 5.2 and 0 m, respectively. As per Khosla's theory, the safe exit gradient for sandy soils varies between 0.14 and 0.20. The pressure gradients obtained in the present study based on both the aspects are within the permissible range, so the structure is safe against piping. The variation of pressure gradient with respect to temperature is represented in Fig. 6.

It is observed that the pressure gradients also show the same trend as that of water temperatures. From the graph, it is observed that with an increase in temperature, the pressure gradient increases. This represents that the steepness of the gradient is high with higher temperatures. Higher values of gradient lead to failure of the structure. So while arriving at the pressure gradient, the effect of water temperature on the stability of the structure has to be considered. The variation of residual pressure heads with water temperature is shown in Fig. 7.

From Fig. 7, it is observed that as the water temperature increases, the residual head decreases. This represents that low water temperatures have more residual heads causing piping or undermining problem to the subsurface floor of the structure.

7 Conclusion

The aim of the present study is to investigate the effect of average monthly water temperature on the seepage pressure gradients below the subsurface floor of a barrage.

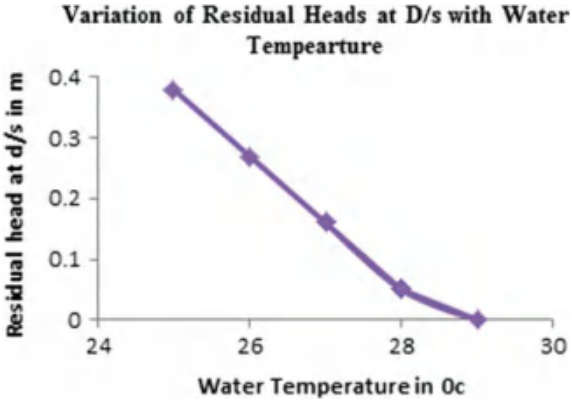

Fig. 7 Variation of residual heads at d/s with water temperature

A case study on the proposed barrage of Taraka Rama Tirtha Sagar at Kotagandredu Village of Gurlamandal in Vizianagaram District of Andhra Pradesh is presented. The following are the conclusions drawn from the present study.

- The monthly average water temperature data of the study area were analyzed and concluded that it is varying in between 250 and 290 °C and for 58.33% duration of the year, a constant temperature of 280 °C is maintained and for the remaining period of time, the temperature varies. So this variation in water temperature leads to change in the viscosity of the flowing water which tends to change the seepage velocity of flow below the structure.
- The kinematic viscosities corresponding to water temperatures are computed using the Poiseuille's equation are found to vary between 0.00827493 and 0.00903755 cm^2/s corresponding to the water temperatures in the range of 290 and 250 °C.
- The monthly seepage velocities are computed using Allen Hazen' formula and Darcy's law. It is observed that the seepage velocity of flow has the same trend as that of temperature. So it is concluded that they are proportional to each other indicating that a higher temperature leads to higher velocities of flow. The seepage velocity of flow without considering the effect of temperature is found using Darcy's law and has a magnitude of 0.007564 m/s, which is higher than that obtained by Allen's formula.
- The seepage rates were computed based on continuity equation and the constant $C = Q * \nu$ proposed by Khosla et al. [3] is determined. It is observed that C value obtained is almost constant in all seasons as proposed by Khosla's theory.
- The average amount of rate of seepage below the structure is estimated to be of 15 m^3/s which seems to be very high. So for effective water management, seepage reduction methods are recommended. However, the present study is not focused on this aspect.

- The pressure gradients are calculated using the formula developed by Khosla et al. [3]. The pressure gradients obtained in the present study are within the permissible range. So the structure is safe against piping.
- It is observed that the pressure gradients show the same trend as that of water temperatures representing that the steepness of the gradient is significant with higher temperatures. Higher values of gradient lead to failure of the structure. So while arriving at the pressure gradient, the effect of water temperature needs to be considered.
- The residual heads are calculated at the downstream of the structure. With increment in water temperature, the residual head is decreasing representing that low water temperatures have more residual heads causing piping or undermining problem to the subsurface floor of the structure.
- Finally, it can be concluded that both high and low temperatures are risky for the safety of the structure. So, proper protective measures are to be adopted under extreme temperatures.

References

1. Karim, R.A.: Variation of uplift pressure and exit gradient downstream of hydraulic structures. Report of Department of Irrigation and Drainage, University of Baghdad, pp. 1–34 (1988)
2. Mavis, F.T., Wisley, E.F.: A study of the permeability of sand. Bulletin 7, University of IOWA Studies in Engineering, IOWA (1936)
3. Khosla, A.N., Bose, N.K., Taylor, E.: Design of weirs on permeable foundations. Central Board of Irrigation and Power, India (1981)
4. Anderson, M.P.: Heat as a ground water tracer. Gr. Water **43**, 951–968 (2005)
5. Huang, T., Rudnicki, J.W.: A mathematical model for seepage of deeply buried groundwater under higher pressure and temperature. J. Hydrol. **327**, 42–54 (2005)
6. Fard, A.S., Dezfouli, A.B.Z.: Temperature distribution analysis in double-arced concrete dams under environmental reactions—a case study of the Dez Hydro-Electrical Dam in Northern Dezful. J. Acad. Appl. Stud. **3**(7), 71–78 (2013)
7. Garg, S.K.: A text book on irrigation engineering and hydraulic structures. Khanna Publishers, Delhi (2009)

Review of Application of Systems Engineering Approaches in Development of Integrated Solid Waste Management for a Smart City

V. R. Sankar Cheela and Brajesh Dubey

Abstract In the development of waste management systems in a smart city, systems planning and decision-making should include economic, environmental, and social sustainability indicators. Integrated solid waste management (ISWM) involves multiple operations by interconnecting a wide range of stakeholders. The constraints in decision-making process are posing a challenging task for the urban local bodies. Integration of the modern technologies and systems engineering approach provides a scope for synergizing the constraints, experts, and stakeholders. The output generated from this approach will provide better solutions for effective decision-making in an implementation of the solid waste systems for the development of smart sustainable cities. In this paper, three systems engineering approaches geographic information system (GIS), multi-criteria decision-making (MCDM), and life-cycle analysis (LCA) applications in solid waste management systems were reviewed. The holistic approach and framework for integrating these systems engineering approaches and technologies in development of ISWM for a smart city were presented.

Keywords Integrated solid waste management · Multi-criteria decision-making
Geographic information system · Life-cycle analysis
Spatial decision support systems

1 Introduction

The development activities in India are increasing to create solutions for better living. The economic, social, industrial, and environmental factors govern the progress of any development activity. Population densities, resource consumption, and economic activities increase in the cities due to urbanization and demographic transfers [1]. The initiatives of the Indian government such as Make in India, Smart Cities, Digital India,

V. R. Sankar Cheela (B) · B. Dubey
Environment Engineering Division, Department of Civil Engineering, Indian Institute of Technology Kharagpur, Kharagpur 721302, West Bengal, India
e-mail: vrsankarcheela@gmail.com

M. Rathinasamy et al. (eds.), *Water Resources and Environmental Engineering II*,
https://doi.org/10.1007/978-981-13-2038-5_16

and Swachh Bharat Abhiyan (Clean India Mission) focus on transforming India into a developed nation [2]. The smart city initiatives are aimed to provide sustainable solutions to e-governance and citizen services, waste management, water management, energy management, urban mobility, capacity building, and skill development centers. The waste management component focuses on waste to energy and fuel, waste to compost, wastewater to be treated, recycling and reduction of construction and demolition (C&D) waste [3].

In India, 62 million tonnes of waste is being generated annually. The collection efficiency of the waste is about 70% of the generated waste. About 22–28% of the waste collected is being treated, and rest is dumped on open land [4]. In the annual report compiled by Central Pollution Control Board (CPCB), it is reported that 553 compost and vermicompost units, 56 bio-methanation plants, 22 RDF plants, and 13 wastes to energy plants have been set up by municipal authorities. CPCB has developed a National Action Plan for solid waste management in compliance with National Green Tribunal (NGT). This is a time-targeted approach in transforming a city, to make it clean and green. The report constituted an approach for both state- and city-level waste management [5].

To enhance the existing waste management practices, Government of India conglomerated policies and structure for solid waste management. They are entitled Solid Waste Management (SWM) Rules 2016. The rules emphasize roles and responsibilities of stakeholders, criteria for setting up solid waste treatment and processing facilities, waste to energy, and time frame for implementation. In comparison with Municipal SWM rules 2000, new rules include segregation at source, community-based segregation, development of composting or bio-methanation at the source, integration of informal sector, recycle or recovery of resources, development of buffer zones for disposal, treatment, and processing of waste, process mechanism for periodical reviews. The main emphasis of these rules accounts on roles and responsibilities of stakeholders, and criteria for setting up of solid waste treatment and processing facilities. Standards and specification for disposal and treatment units, preparation of integrated solid waste management (ISWM) plan, formulation of bylaws, capacity building, and awareness programs are included as schedules.

Material and energy flows, pollution reduction, resource recovery, and utilization define the behavior of urban production and consumption. Sustainability of a system is critically affected by the urban metabolisms due to interactions of material inflow and waste outflows [6]. The behavior of urban waste streams can be characterized by the relationship between anthropogenic urban activity, man-made networks, and natural processes [7]. Waste management systems should be handled through engineered perspectives linking information intensive platform to enable policymakers and stakeholders to develop ecologically and economically sound urban planning systems [8]. Pollution prevention, energy recovery, material, and ecological conservation magnify the importance of the application of systems approach in integrated solid waste management (ISWM) [9]. Application of systems engineering approaches enables the process to identify, analyze, and predict the relationship between resource use, human activities, and environment [10]. They provide a wide scope for the effective decision-making process to shape urban ISWM in a more smart

and sustainable way [11]. In systems engineering approaches, spatial technologies, data handling, processing, and decision-making approaches are used for analyzing economic and environmental and social components. Spatial technologies facilitate capturing, processing, and communication of information to provide an innovative way of addressing the issue. Data acquisition, processing, transmission, and ability to handle large datasets using spatial technologies provide scope for the development of effective, efficient, automated, and intelligent solid waste management system [12].

This study aims to review the application of multi-criteria decision-making (MCDM), geographic information system (GIS), and life-cycle analysis (LCA) in solid waste management. This review provides an overview of the systems engineering approaches applications to develop a decision support tool in planning and designing an integrated solid waste management system for an urban local body.

2 Geographical Information Systems

GIS is a computer-based tool designed to store, organize, visualize, question, analyze, interpret, and display to understand the patterns and relationships of geographic and spatial data. Spatial and temporal analysis of real-world data can be modeled using GIS [13]. The definition of the GIS is more focused on technological approach and less toward decision-making process. For effective decision-making, non-spatial elements such as social, economic, cultural, and environmental datasets can be linked to spatial reference.

Spatial data acquired from different sources is entered into computer hardware system through digitization, entry of data by typing or scanning. Data available from the standard data sources and agencies can be used for developing the base files. The waste collection and bin location points, waste recycling, and treatment facilities of a given locality shall be updated through manual mode. The data collection is done based on the scope of the project for inclusion into the GIS interface. Administrative boundaries, demographics, road networks, land use patterns, facility locations, soil types, and hydrology layers are developed for creating the base map. The data developed is stored in the data management module as well as ensures the data integrity. The data retrieval, update and storage of the spatial data, and non-redundant data are organized and shared by different stakeholders. Spatial analysis, 3D analysis, spatial statistical analysis, and network analysis can be executed through retrieval, measurement, overlay, neighborhood, connective operations for analyzing the GIS data. Querying component enables the users to reach required geographic zones under the study. Data collection, digitization, and creation of base layers contribute to the development of the base map. Administrative boundaries, demographics, road networks, land use patterns, facility locations, soil types, and hydrology layers are used in creating the base map. Data inventory in the form of maps is developed for solid waste facilities including both spatial (location of bins, transfer station, recycling facilities, processing units, and landfill) and non-spatial elements (capacity, compacting abilities, volume, etc.). Map overlays and spatial allocation methods

Table 1 Applications of geographical information systems in solid waste management systems

Application	GIS	GPS	GPRS and GSM	RFID	Sensors and servers	RS	Location	Ref.
Collection systems	Yes	Yes	Yes	No	No	No	Vellore, India	[15]
	Yes	Yes	No	No	No	No	Pudong, China	[16]
SWM systems planning	Yes	Yes	No	No	No	No	Thailand	[17]
Route optimization	Yes	Yes	No	No	No	No	Pudong, China	[18]
	Yes	Yes	No	No	Yes	No	Trabzon, Turkey	[19]
Site selection	Yes	No	No	No	No	Yes	Mohammedia, Morocco	[20]
	Yes	No	No	No	No	Yes	Kolkata, India	[21]
	Yes	No	No	No	No	Yes	Nyahururu, Kenya	[22]
	Yes	No	No	No	No	Yes	Mysore, India	[23]
	Yes	No	No	No	No	Yes	Mafraq City, Jordan	[24]

GIS geographic information system; *GPS* global positioning system; *GPRS* general packet radio service; *GSM* global system for mobile communication; *RFID* radio frequency identification; *RS* remote sensing; *Ref.* reference

in GIS are applied for creating the suitability maps of the area under consideration [14]. Table 1 represents the applications of geographical information systems in solid waste management systems. Table 1 represents the applications of geographical information systems in solid waste management systems.

3 Multi-criteria Decision-Making

DSS is a computer-based information system designed to facilitate the better understanding of the components and process involved to improve the decision-making process. A model-based management system module in DSS consists of optimization, forecasting, and simulation models. This module equips the users to analyze and interpret the data. Site selection, regional planning, vehicle routing, and facility location are the major applications in SWM. In DSS process, an objective function is developed by using systems engineering models like linear programming (LP) and mixed integer programming (MIP) models. Then, the multi-criteria decision-making (MCDM) approaches are used for analyzing the data.

Multi-criteria decision-making is a branch of operations research that is capable of addressing complex problems featuring high uncertainty, multi-interests, and large data forms. The expectations of the decision-makers and other constraints are considered to identify and decide the alternatives. Alternatives are identified and evaluated against a set of attributes/constraints which are hard to quantify to develop the efficient solution. In MCDM, criteria are selected in a coherent, measurable, and independent manner. Based on the criteria, available, comparable, feasible, and practical alternatives are selected. Analytical hierarchy process (AHP), elimination and choice expressing reality (ELECTRE), preference ranking organization method for enrichment of evaluations (PROMETHEUS), fuzzy multi-criteria decision-making process (FMCDM), etc., are commonly used methods for performing MCDM. Pairwise comparison of the multiple criteria and multi-level hierarchical structure is applied to determine the relative weights for each alternative. The best alternative will be chosen using the method of aggregation.

MCDM methods provide a better scope for developing the criteria and alternatives by considering the experience and expert opinions for different stakeholders. Scenarios are assessed using both qualitative and quantitative criteria involving the participation of decision-makers of diverse thought processes in defining the indicators. The method is flexible for expanding the model from single to multiple decision-making models. Assigning the weights for each criterion includes the point of views of all the stakeholders. The results obtained by application of the different MCDM models may differ in prioritization, but the top alternatives remain constant with variation in the priorities. The scope for development of waste minimization, prevention, and management plans using MCDM analysis is limited. Evaluation analysis is subjected to variation with the addition and deletion of the criteria and the assignment of weights. Figure 1 represents the model of MCDM framework for selection of waste disposal facility in an urban local body.

4 Spatial Decision Support System

Spatial Decision Support System (SDSS) is an interactive, computer-based system designed to support stakeholders to achieve efficacy in decision-making. This combines conventional data, spatially referenced data, and decision logic for problem-solving and situational analysis. This support system provides a user-friendly interface to communicate, analyze, and process data among the stakeholders. GIS and MCDA are integrated to develop decision support system in a systematic approach to perform an extensive evaluation for making effective decisions. The applications of SDSS include natural resources management, health care, solid waste management, emergency management, water resources management, disaster management, tourism facility planning. In ISWM, applications of SDSS include solid waste systems planning, policy evaluation, collection route optimization, facility location and allocation problems, site selection for waste processing and disposal units, transfer stations, transportation problems, and waste systems planning.

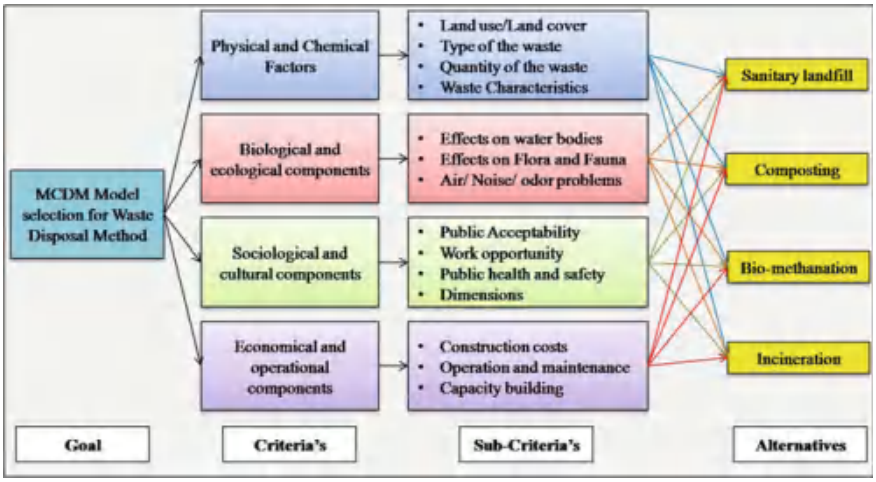

Fig. 1 Multi-criteria decision-making framework for selection of waste disposal facility in an urban local body

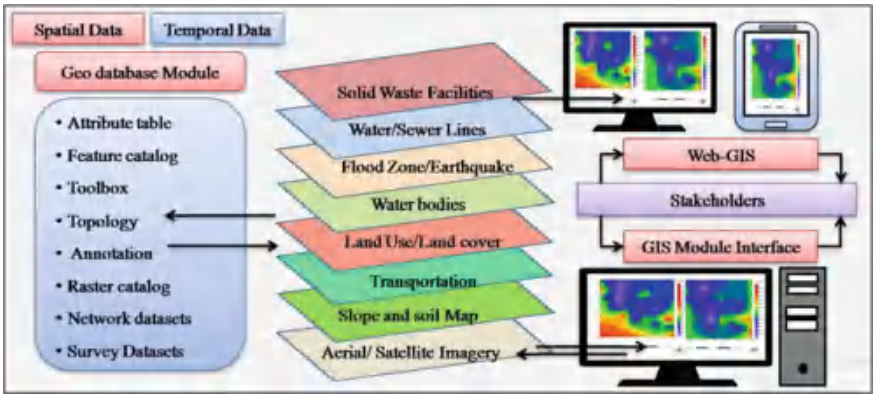

Fig. 2 Architecture of GIS and Web GIS-based spatial decision support systems

The GIS-based SDSSs have often been criticized for not providing tools for involving public participation factor. The GIS is successful in terms of the software and computing hardware. Due to the closed, synchronous, and place-based nature, public participation in community-based GIS-based projects was limited. This was addressed by introducing decision support tools that are accessible to stakeholders. Web-based SDSS, collaborative and participatory GIS technologies are designed for supporting decision-makers and other stakeholders. Figure 2 represents the architecture of GIS and Web GIS-based spatial decision support systems.

Application of GIS and MCDM approaches provides a better solution for site selection, location of collection and recycling points, and systems planning. Initial

screening was performed by researchers by developing land use maps for potentially suitable areas using GIS. The selection of the most suitable site was performed by developing priorities for evaluation and weighting of criteria using MCDM. Table 2 presents the application of spatial decision support systems in solid waste management systems.

5 Spatial Decision Support Systems Framework

The GIS operations in combination with MCDA methods and techniques resolved the problem of integrating stakeholders and computing techniques for better decision-making. This combination is capable of addressing, handling, and diminishing disagreements over facts, values among the stakeholders. The output is developed in the form of maps and other graphic displays by combining geographic data and the decision-maker's preferences, facilitating the end users for better interpretation and analysis of the data.

In Fig. 3, model framework for integration of GIS with MCDM is represented, in which the GIS application is integrated into the development of the criteria an evaluation of the alternatives. The decision-makers during the evaluation process can visualize the complete scenario through the maps developed. The module of a spatial query, buffer zone development provide the scope to understand the impact zones. The flood hazard plains, special economic zones, water bodies, disaster-prone zones, and national importance projects can be understood during a selection of final alternatives. The role of GIS in development of pair-wise matrix and weighting procedure is deficient. The best alternative selection is dependent on the effectiveness of the weights developed. To equip this component, the researchers have applied the results obtained from LCA for pair-wise comparison and development of weights.

6 Life-Cycle Analysis

The environmental interventions and potential impacts throughout a product's life study using environmental life-cycle analysis (LCA) as per International Organization for Standardization norms. The energy, materials used, and emissions released to the environment are used as inputs in LCA to assess the environmental burdens associated with a product or process. Human, health, ecological considerations, resource, and energy utilization factors are considered in determining the environmental impacts. The goal of LCA is to be decided initially based on the need and expected outcomes of the study. Development of the system boundary determines the scope of LCA. Based on the scope of the study, alternatives termed as scenarios are formulated. The functional unit is determined to for the LCA process so as to have a uniform platform to determine environmental impacts of the scenarios under consideration. Data inventory analysis is performed to determine the flow of energy,

Table 2 Application of spatial decision support systems in solid waste management systems

Application	Optimization method	GIS software	Location	Ref.
SWMP	MOMIP; MCDM	Yes	General	[25]
	MILP	Yes	Tehran, Iran	[26]
	MCA	No	Naples, Italy	[27]
	MINLP	No	Mexico	[28]
	MCDM	No	Bosnia and Herzegovina	[29]
	MILP	No	Hong Kong	[30]
	Funnel cost model	Yes	Parkland County, Canada	[31]
	NIL	Yes	Shenzhen City, China	[32]
	MILP	Yes	Coimbra City, Portugal	[33]
SWCT	MILP and ABM	Yes	Vietnam	[34]
	AHP	No	Da Nang City, Vietnam	[35]
	BILP and MILP	No	Campo Mourão, Brazil	[36]
	TSP and ABM	Yes	Kolkata, India	[37]
	GARP	Yes	Morelia, Mexico	[38]
	AHP	Yes	Davanagere, India	[39]
	HA and DA	Yes	Kampala, Uganda	[40]
	NIL	Yes	Ipoh City, Malaysia	[41]
RSW	MILP	Yes	Cogoleto, Italy	[42]
	IP	Yes	Taichung, Taiwan	[43]
	ANP	No	Area of Valencia, Spain	[44]
	NIL	Yes	Madrid, Spain	[45]
LSSA	Boolean technique	Yes	Victoria, Australia	[46]
	MCDA	Yes	Birjand, Iran	[47]
	AHP	Yes	Thrace region	[48]
	NIL	Yes	Bahir Dar Town, Ethiopia	[49]

(continued)

Table 2 (continued)

Application	Optimization method	GIS software	Location	Ref.
	MCDA	Yes	Bo, Sierra Leone	[50]
	MCDA	Yes	Polog, Macedonia	[51]
	MCDM	Yes	Province of Torino, Italy	[52]
	MCA	Yes	Konya, Turkey	[53]
	AHP	Yes	Karaj, Iran	[54]
	AHP	Yes	Beijing, China	[55]
	MCDA	Yes	Pondicherry, India	[56]
	Boolean technique	Yes	Cuitzeo Lake Basin, Mexico	[57]
	AHP	Yes	Jiroft City, Iran	[58]
HSSA	MCDA	Yes	Province of Avellino, Italy	[59]
	No	Yes	Qazvin Province, Iran	[60]
	MCDA	Yes	Kurdistan Province, Iran	[61]
	MCDM	Yes	Anatolian region, Turkey	[62]
	Nil	Yes	Turkey	[63]
TSSA	MCDA	Yes	Kilifi County, Kenya	[14]
	AHP	Yes	Santiago Island, Cape Verde	[64]
	AHP	Yes	Province of Avellino, Italy	[65]

ABM agent-based model; *AHP* analytical hierarchy process; *ANP* analytical network process; *BILP* binary integer linear programming; *CVM* contingent valuation method; *DA* deterministic approach; *FMCD* fuzzy multi-criteria decision-making; *GARP* genetic algorithm for rule-set production; *HA* heuristic approach; *HSSA* hazardous landfill site suitability analysis; *IP* integer programming; *LSSA* landfill site suitability analysis; *MCA* multi-criteria analysis; *MCDA* multi-criteria decision analysis; *MCDM* multi-criteria decision-making; *MILP* mixed integer linear programming; *MINLP* mixed integer nonlinear programming; *MOMIP* multi-objective mixed integer programming; *RSW* recycling of solid waste; *SWCT* solid waste collection and transportation; *SWMP* solid waste management planning; *TSP* traveling salesman problem; *TSSA* treatment plant site suitability analysis

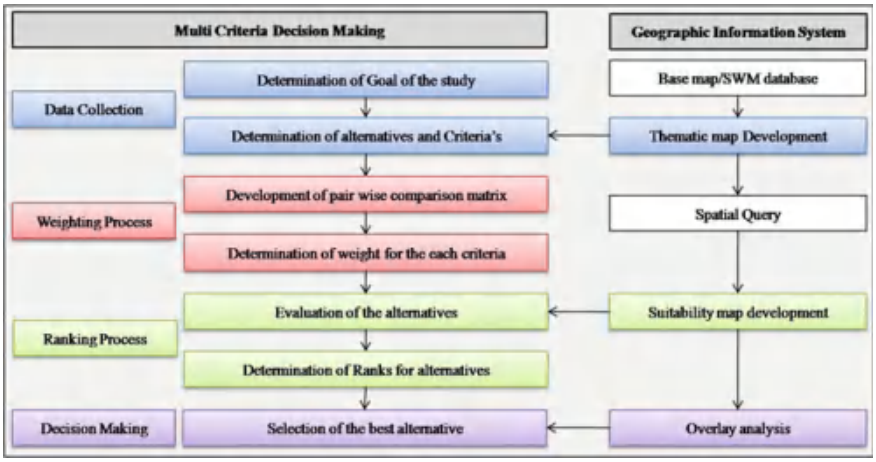

Fig. 3 Model frameworks for integration of GIS with MCDM

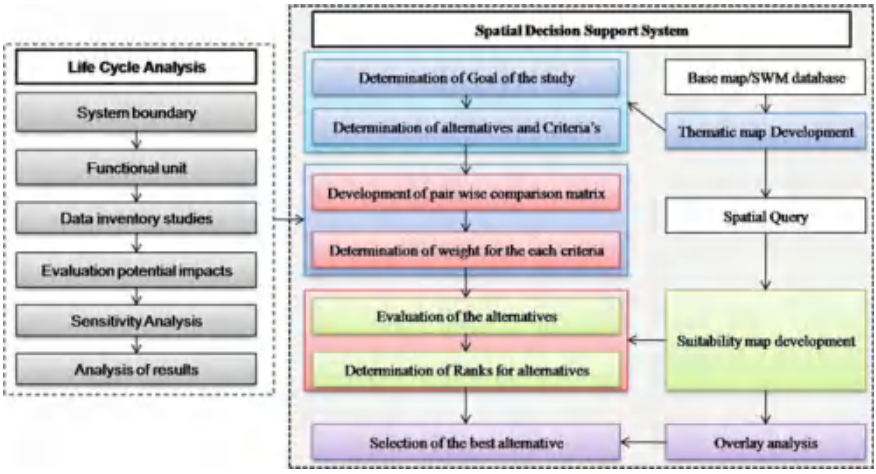

Fig. 4 Model frameworks for integration of LCA and SDSS

materials, and emissions across the system boundary. Material and energy mass balance are developed to understand the environmental interventions. The potential impacts and an environmental burden are determined and assessed using systematic analysis of the inventory data.

In Fig. 4, model framework for integration of LCA with SDSS is represented. The environmental burdens determined using LCA study are inputted in the SDSS for the development of the pair-wise matrices and weighting criteria. During the evaluation of alternatives in SDSS, alternatives with minimum environmental impact can be assessed using the weights developed from LCA study. The combination of different

scenarios can be performed, and the cumulative weight factor can be assessed. The sensitivity analysis component in LCA process enables us to assess the impacts of site-specific data.

LCA is being widely applied in decision-making and strategy planning of integrated solid waste management systems. Computer-aided tool following a hybrid approach by combining equations for inventory analysis and expert inputs in assessment and characterization of impacts is being applied by the authors in their studies. The components of the solid waste management design varied from location to location in characteristics of the waste, disposal options, treatment methods, and market for derived products. Potential management plans and improvements are identified by assessing the alternative options including economic, technical aspects. The LCA methodology provided a scope for an involvement of public and private actors in determining the best solution. Table 3 presents the applications of LCA in solid waste management systems. It presents the geographical location, functional unit, number of scenarios considered, impacts studied, and sensitivity analysis application. The impacts studies are classified into non-toxic, toxic, resources, and energy classes.

7 Summary and Conclusion

In a smart city, the waste management systems should be designed to reduce the stress on the environment. The systems should be planned, designed, optimized, and implemented to ensure the development of sustainable waste management systems. These include a holistic, comprehensive, and interdisciplinary framework synergizing technical, economic, and social components, stakeholders, and timescales. Collaborative planning, infrastructure development, capacity building, database management, and implementation play a vital role in building an integrated waste management system. A systems engineering framework combining SDSS and LCA provides a multidisciplinary approach for the urban planners. The development of the systems based on the site-specific process including spatial and temporal components will enhance sustainability. The integration of this framework and information and communication technologies (ICTs) provides a rationale for the policy- and decision-makers and urban local bodies to develop a smart waste management system. Figure 5 presents a framework for developing ISWM in a smart city by integrating SDSS, LCA, ICT and IoT components.

The evaluation of digital applications and application of a wide range of ICT tools provided a scope for advancements in database management and information transfer systems. The Internet of things (IoT) applications increased the managerial and behavioral potential in developing effective management systems in urban areas. Interactive communication and information exchange are an added advantage for effective planning. The applications of ICT in solid waste management can be enhanced by combining decision support systems, expert, and knowledge-based systems. The performance of the waste management systems can be evaluated by the

Table 3 Applications of life-cycle analysis in solid waste management systems

Geographical features	Functional unit	Scenarios studied	Sensitivity analysis	Studied impacts				Ref.
				Non-toxic	Toxic	Resources	Energy	
Hangzhou, China	Waste produced in a year	5	Yes	PC	PC	CC	NC	[66]
Naples, Italy		6	Yes	PC	PC	CC	NC	[67]
UK		4	No	PC	PC	NC	NC	[68]
London		10	Yes	PC	NC	CC	NC	[11]
Asturias, Spain		6	No	PC	PC	CC	NC	[69]
Tianjin City, Beijing		7	Yes	PC	PC	CC	CC	[70]
Sakarya, Turkey	1 t of MSW	5	No	CC	CC	CC	NC	[71]
Italy		4	Yes	Only GW	NC	CC	CC	[72]
Iran		5	Yes	PC	PC	CC		[73]
Thailand		5	No	CC	PC	CC	NC	[74]
Indonesia		5	Yes	PC	NC	NC	NC	[75]

(continued)

Table 3 (continued)

Geographical features	Functional unit	Scenarios studied	Sensitivity analysis	Studied impacts				Ref.
				Non-toxic	Toxic	Resources	Energy	
South Korea		4	No	CC	PC	CC	NC	[76]
China		4	Yes	CC	PC	CC	CC	[77]
Turkey		5	Yes	PC	PC	PC	NC	[78]
Denmark	1 t of wet household waste	7	No	CC	PC	NC	NC	[79]
Italy	1 t of OF	2	Yes	PC	PC	CC	NC	[80]
UK	101 kt of MSW	4	No	PC	NC	NC	CC	[81]

Non-toxic impact categories: global warming; ozone layer depletion; acidification; eutrophication
Toxic impact categories: ototoxicity; human toxicity; particulate matters; aquatic toxicity; terrestrial eco toxicity
Resources: Abiotic depletion potential
CC complete coverage; *PC* partial coverage; *NC* no coverage

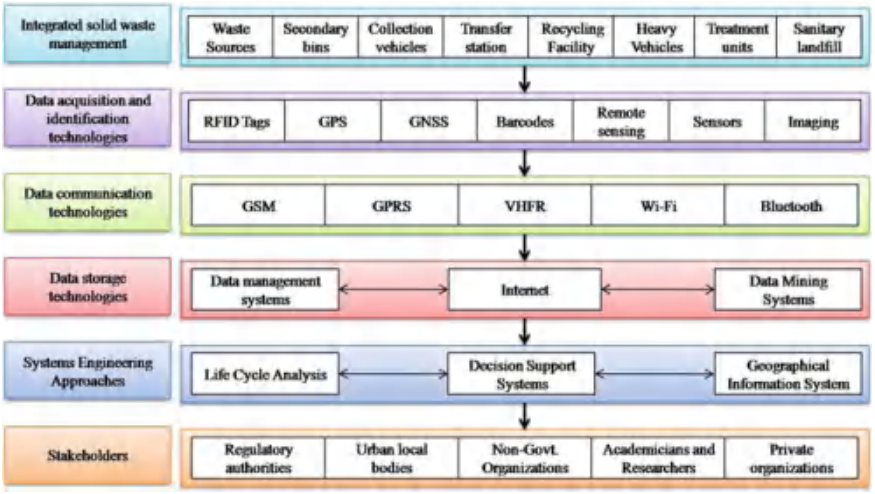

Fig. 5 Framework for developing ISWM in a smart city

local authorities through scientific analysis of the outcomes achieved by the application of these systems.

The mobility behavior of the vehicles plays a vital role in the design of the collection and transport systems. Dynamic interactive pattern modeling and prediction of the vehicle movements explore new dimensions for developing smart, sustainable, efficient, and effective waste collection and transport systems. Vehicle space–time interactions are developed from the trajectories of data acquisition and navigation instruments. The application of spatial and non-spatial technologies for data acquisition and identification generates digital information. Development of space–time database for the waste management enables the urban local bodies to design, optimize, and implement an effective waste management services.

Data communication systems development provided scope for quick transmission of data instantly to the remote areas. Rapid developments in the area of communication technologies developed opportunities to share and explore new dimensions in waste management. Communication protocols and wide area network (WAN) based on the leased line, switching logic, and cell relay are being handled by the Internet. The remote communications are being performed by the Internet using wireless, copper wire and fiber-optic access technologies. Short-range communication system is being applied for automatic data acquisition and interchange of instruction. Global system for mobile communication (GSM), general packet radio service (GPRS), and very high-frequency radio (VHFR) for long-range applications and wireless fidelity (Wi-Fi), Zigbee, and Bluetooth for short-range communication are being applied in SWM applications. The integration of SDSS and LCA with applications of ICT and Internet of things (IoT) for developing a smart city presents an overall structure for the decision-making, executing, and operation of the SWM systems.

Acknowledgements The authors acknowledge Ministry of Human Resources and Development, Government of India, and Sponsored Research and Industrial Consultancy (SRIC), IIT Kharagpur, for funding this study.

References

1. Yadav, V., Karmakar, S., Dikshit, A.K., Vanjari, S.: A feasibility study for the locations of waste transfer stations in urban centers: a case study on the city of Nashik, India. J. Clean. Prod. **126**, 191–205 (2016)
2. Potdar, A., Singh, A., Unnnikrishnan, S., Naik, N., Naik, M., Nimkar, I.: Innovation in solid waste management through Clean Development Mechanism in India and other countries. Process Saf. Environ. Prot. **101**, 160–169 (2016)
3. Ministry of Urban Development (MoUD): Report on "Smart Cities-Mission statement and Guidelines" http://smartcities.gov.in/upload/uploadfiles/files/SmartCityGuidelines(1).pdf. Accessed 7 Apr 2017
4. Press Information Bureau (PIB): Solid Waste Management Rules Revised After 16 Years; Rules Now Extend to Urban and Industrial Areas. Retrieved 6 Apr 2017 from http://pib.nic.in/newsite/PrintRelease.aspx?relid=138591
5. Central Pollution Control Board (CPCB): The National Action Plan for Municipal Solid Waste Management (suggestive/indicative). Retrieved 7 Apr 2017 from http://cpcb.nic.in/uploads/hwmd/Action_plan.pdf
6. Yan, Zhang, Yang, Z., Xiangyi, Y.: Urban metabolism: a review of current knowledge and directions for future study. Environ. Sci. Technol. **49**, 11247–11263 (2015)
7. Marrero, M., Puerto, M., Rivero-Camacho, C., Freire-Guerrero, A., Solís-Guzmán, J.: Assessing the economic impact and ecological footprint of construction and demolition waste during the urbanization of rural land. Resour. Conserv. Recycl. **117**, 160–174 (2017)
8. Simatele, D.M., Dlamini, S., Kubanza, N.S.: From informality to formality: perspectives on the challenges of integrating solid waste management into the urban development and planning policy in Johannesburg, South Africa. Habitat Int. **63**, 122–130 (2017)
9. Marshall, R.E., Farahbakhsh, K.: Systems approaches to integrated solid waste management in developing countries. Waste Manag. **33**, 988–1003 (2013)
10. Yang, Z., Zhou, X., Xu, L.: Eco-efficiency optimization for municipal solid waste management. J. Clean. Prod. **104**, 242–249 (2015)
11. Parkes, O., Lettieri, P., Bogle, I.D.L.: Life cycle assessment of integrated waste management systems for alternative legacy scenarios of the London Olympic Park. Waste Manag. **40**, 157–166 (2015)
12. Hannan, M.A., Abdulla Al Mamun, M., Hussain, A., Basri, H., Begum, R.A.: A review on technologies and their usage in solid waste monitoring and management systems: issues and challenges. Waste Manag. **43**, 509–523 (2015)
13. Lu, J.W., Chang, N.B., Liao, L.: Environmental informatics for solid and hazardous waste management: advances, challenges, and perspectives. Crit. Rev. Environ. Sci. Technol. **43**, 1557–1656 (2013)
14. Hariz, H.A., Dönmez, C.Ç., Sennaroglu, B.: Siting of a central healthcare waste incinerator using GIS-based multi-criteria decision analysis. J. Clean. Prod. **166**, 1031–1042 (2017)
15. Lella, J., Mandla, V.R., Zhu, X.: Solid waste collection/transport optimization and vegetation land cover estimation using geographic information system (GIS): a case study of a proposed smart-city. Sustain. Cities Soc. **35**, 336–349 (2017)
16. Rovetta, A., Xiumin, F., Vicentini, F., Minghua, Z., Giusti, A., Qichang, H.: Early detection and evaluation of waste through sensorized containers for a collection monitoring application. Waste Manag. **29**(12), 2939–2949 (2009)

17. Hiramatsu, A., Hara, Y., Sekiyama, M., Honda, R., Chiemchaisri, C.: Municipal solid waste flow and waste generation characteristics in an urban-rural fringe area in Thailand. Waste Manag. Res. **27**(10), 951–960 (2009)
18. Minghua, Z., Xiumin, F., Rovetta, A., Qichang, H., Vicentini, F., Bingkai, L., Giusti, A., Yi, L.: Municipal solid waste management in Pudong New Area, China. Waste Manag. **29**, 1227–1233 (2009)
19. Apaydin, O., Gonullu, M.: Route optimization for solid waste collection: Trabzon (Turkey) case study. Glob. NEST J. **9**, 6–11 (2007)
20. Maguiri, A.E., Kissi, B., Idrissi, L., Souabi, S.: Landfill site selection using GIS, remote sensing and multicriteria decision analysis: case of the city of Mohammedia, Morocco. Bull. Eng. Geol. Environ. **75**, 1301–1309 (2016)
21. Pradhan, J., Samanta, K.: Site suitability analysis using remote sensing and GIS for proper selection of solid waste disposal ground within Rajarhat Gopalpur Municipal Area, Kolkata, West Bengal. Int. J. Geomat. Geosci. **5**, 640–654 (2015)
22. Kimwatu, D.M., Ndiritu, M.G.: Application of GIS and remote sensing technologies in solid waste management: a case study of Nyahururu Municipality. Int. J. Sci. Res. **5**, 342–349 (2013)
23. Basavarajappa, H.T., Tazdari, P., Manjunatha, M.C., Balasubramanian, A.: Application of remote sensing and GIS on waste disposal site selection and environmental impact assessment around Mysore City, Karnataka, India. Int. J. Earth Sci. Eng. **6**, 1801–1808 (2013)
24. Hanbali Al, A., Alsaaideh, B., Kondoh, A.: Using GIS-based weighted linear combination analysis and remote sensing techniques to select optimum solid waste disposal sites within Mafraq City, Jordan. J. Geograph. Inf. Syst. **3**, 267–278 (2011)
25. Asefi, H., Lim, S.: A novel multi-dimensional modeling approach to integrated municipal solid waste management. J. Clean. Prod. **166**, 1131–1143 (2017)
26. Habibi, F., Ehsan, A., Seyed, J.S., Farnaz, B.: A multi-objective robust optimization model for site-selection & capacity allocation of municipal solid waste facilities: a case study in Tehran. J. Clean. Prod. **166**, 816–834 (2017)
27. Chifari, R., Renner, A., Lo Piano, S., Ripa, M., Bukkens, S.G.F., Giampietro, M.: Development of a municipal solid waste management decision support tool for Naples, Italy. J. Clean. Prod. **161**, 1032–1043 (2017)
28. Santibañez-Aguilar, J.E., Flores-Tlacuahuac, A., Rivera-Toledo, M., Ponce-Ortega, J.M.: Dynamic optimization for the planning of a waste management system involving multiple cities. J. Clean. Prod. **165**, 190–203 (2017)
29. Vučijak, B., Kurtagić, S.M., Silajdžić, I.: Multicriteria decision making in selecting best solid waste management scenario: a municipal case study from Bosnia and Herzegovina. J. Clean. Prod. **130**, 166–174 (2016)
30. Lee, C.K.M., Yeung, C.L., Xiong, Z.R., Chung, S.H.: A mathematical model for municipal solid waste management—a case study in Hong Kong. Waste Manag. **58**, 430–441 (2016)
31. Khan, M.M., Jain, S., Vaezi, M., Kumar, A.: Development of a decision model for the techno-economic assessment of municipal solid waste utilization pathways. Waste Manag. **48**, 548–564 (2016)
32. Wu, H., Wang, J., Duan, H., Ouyang, L., Huang, W., Zuo, J.: An innovative approach to managing demolition waste via GIS (geographic information system): a case study in Shenzhen City, China. J. Clean. Prod. **112**, 494–503 (2016)
33. Tralhão, L., Coutinho-Rodrigues, J., Alçada-Almeida, L.: A multiobjective modeling approach to locate multi-compartment containers for urban-sorted waste. Waste Manag. **30**, 418–2429 (2010)
34. Nguyen-Trong, K., Nguyen-Thi-Ngoc, A., Nguyen-Ngoc, D., Dinh-Thi-Hai, V.: Optimization of municipal solid waste transportation by integrating GIS analysis, equation-based, & agent-based model. Waste Manag. **59**, 14–22 (2017)
35. Son, L.H., Louati, A.: Modeling municipal solid waste collection: a generalized vehicle routing model with multiple transfer stations, gather sites & inhomogeneous vehicles in time windows. Waste Manag. **52**, 34–49 (2016)

36. Vecchi, T.P.B., Surco, D.F., Constantino, A.A., Steiner, M.T.A., Jorge, L.M.M., Ravagnani, M.A.S.S., Paraíso, P.R.: A sequential approach for the optimization of truck routes for solid waste collection. Process Saf. Environ. Prot. **102**, 38–250 (2016)
37. Das, S., Bhattacharyya, B.K.: Optimization of municipal solid waste collection & transportation routes. Waste Manag. **43**, 9–18 (2015)
38. Buenrostro-Delgado, O., Ortega-Rodriguez, J.M., Clemitshaw, K.C., Gonzlez-Razo, C., Hernndez-Paniagua, I.Y.: Use of genetic algorithms to improve the solid waste collection service in an urban area. Waste Manag. **4**, 20–27 (2015)
39. Hareesh, K.B., Manjunath, N.T., Nagarajappa, D.P.: Route optimization model for municipal solid waste management by decentralized system in Davangere City Hareesh. Int. J. Emerg. Technol. Adv. Eng. **5**, 102–105 (2015)
40. Kinobe, J.R., Bosona, T., Gebresenbet, G., Niwagaba, C.B., Vinneras, B.: Optimization of waste collection & disposal in Kampala city. Habitat Int. **49**, 126–137 (2015)
41. Malakahmad, A., Bakri, P.M., Mokhtar, M.R.M., Khalil, N.: Solid waste collection routes optimization via GIS techniques in Ipoh City, Malaysia. Procedia Eng. **77**, 20–27 (2014)
42. Anghinolfi, D., Paolucci, M., Robba, M., Taramasso, A.C.: A dynamic optimization model for solid waste recycling. Waste Manag. **33**, 87–296 (2013)
43. Lin, H.Y., Chen, G.H.: Regional optimization model for locating supplemental recycling depots. Waste Manag. **29**, 1473–1479 (2009)
44. Aragones-Beltran, P., Pastor-Ferrco, J.P., García-García, F., Pascual-Agulló, A.: An analytic network process approach for siting a municipal solid waste plant in the Metropolitan Area of Valencia (Spain). J. Environ. Manag. **91**, 1071–1086 (2010)
45. Lopez, A.J.V., Aguilar, L.M., Fernandez-Carrion Quero, S., del Jimenez, V.A.: Optimizing the collection of used paper from small businesses through GIS techniques: the Leganés case (Madrid, Spain). Waste Manag. **28**, 282–293 (2008)
46. Cheng, C., Thompson, R.G.: Application of Boolean logic & GIS for determining suitable locations for temporary disaster waste management sites. Int. J. Disaster Risk Reduct. **20**, 78–92 (2016)
47. Motlagh, Z.K., Sayadi, M.H.: Siting MSW landfills using MCE methodology in GIS environment (case study: Birjand plain, Iran). Waste Manag. **46**, 322–337 (2015)
48. Demesouka, O.E., Vavatsikos, A.P., Anagnostopoulos, K.P.: Suitability analysis for siting MSW landfills and its multicriteria spatial decision support system: method, implementation & case study. Waste Manag. **33**, 1190–1206 (2013)
49. Ebistu, T., Minale, A.: Solid waste dumping site suitability analysis using geographic information system (GIS) and remote sensing for Bahir Dar Town, North Western Ethiopia. Afr. J. Environ. Sci. Technol. **7**, 976–989 (2013)
50. Gbanie, S.P., Tengbe, P.B., Momoh, J.S., Medo, J., Kabba, V.T.S.: Modeling landfill location using geographic information systems (GIS) & multi-criteria decision analysis (MCDA): case study Bo, Southern Sierra Leone. Appl. Geogr. **36**, 3–12 (2013)
51. Gorsevski, P.P., Donevska, K., Mitrovski, C.D., Frizado, J.: Integrating multicriteria evaluation techniques with geographic information systems for landfill site selection: a case study using ordered weighted average. Waste Manag. **32**, 287–296 (2012)
52. Al-hanbali, A., Alsaaideh, B., Kiondoh, A.: Using GIS-based weighted linear combination analysis & remote sensing techniques to select optimum solid waste disposal sites within Mafraq City, Jordan. J. Geogr. Inf. Syst. **3**, 267–278 (2011)
53. Nas, B., Cay, T., Iscan, F., Berktay, A.: Selection of MSW landfill site for Konya, Turkey using GIS & multi-criteria evaluation. Environ. Monit. Assess. **160**, 491–500 (2010)
54. Moeinaddini, M., Khorasani, N., Danehkar, A., Darvishsefat, A.A., Zienalyan, M.: Siting MSW landfill using weighted linear combination and analytical hierarchy process (AHP) methodology in GIS environment: case study (Karaj). Waste Manag. **30**, 912–920 (2010)
55. Guiqin, W., Li, Q., Guoxue, L., Lijun, C.: Landfill site selection using spatial information technologies & AHP: a case study of Beijing, China. J. Environ. Manag. **90**, 414–2421 (2009)
56. Sumathi, V.R., Natesan, U., Sarkar, C.: GIS-based approach for optimized siting of municipal solid waste landfill. Waste Manag. **28**, 2146–2160 (2008)

57. Delgado, O.B., Mendoza, M., Granados, E.L., Geneletti, D.: Analysis of land suitability for the siting of inter-municipal landfills in the Cuitzeo Lake Basin, Mexico. Waste Manag. **28**, 1137–1146 (2008)
58. Javaheri, H., Nasrabadi, T., Jafarian, M.H., Rowshan, G.R., Khoshnam, H.: Site selection of municipal solid waste landfills using analytical hierarchy process method in a geographical information technology environment in Giroft. J. Environ. Health **3**, 177–184 (2006)
59. Feo, G.D., Gisi, S.D.: Using an innovative criteria weighting tool for stakeholders involvement to rank MSW facility sites with the AHP. Waste Manag. **30**, 370–382 (2014)
60. Abessi, O., Mohesn, S.: Site selection of a hazardous waste landfill using GIS technique & priority processing, a power plant waste in Qazvin Province case example. Environ. Sci. **6**, 121–134 (2009)
61. Sharifi, M., Hadidi, M., Vessali, E., Mosstafakhani, P., Taheri, K., Shahoie, S., Khodamoradpour, M.: Integrating multi-criteria decision analysis for a GIS-based hazardous waste landfill sitting in Kurdistan Province, western Iran. Waste Manag. **29**, 2740–2758 (2009)
62. Alumur, S., Bahar, Y.K.: A new model for the hazardous waste location-routing problem. Comput. Oper. Res. **34**, 1406–1423 (2007)
63. Yesilnacar, M.I., Cetin, H.: Site selection for hazardous wastes: a case study from the GAP area, Turkey. Eng. Geol. **81**, 371–388 (2005)
64. Tavares, G., Zsigraiová, Z., Semiao, V.: Multi-criteria GIS-based siting of an incineration plant for municipal solid waste. Waste Manag. **31**, 1960–1972 (2011)
65. Feo, G.D., Gisi, S.D.: Using MCDA & GIS for hazardous waste landfill siting considering land scarcity for waste disposal. Waste Manag. **34**, 2225–2238 (2010)
66. Havukainen, J., Zhan, M., Dong, J., Liikanen, M., Deviatkin, I., Li, X., Horttanainen, M.: Environmental impact assessment of municipal solid waste management incorporating mechanical treatment of waste and incineration in Hangzhou, China. J. Clean. Prod. **141**, 453–461 (2017)
67. Ripa, M., Fiorentino, G., Vacca, V., Ulgiati, S.: The relevance of site-specific data in life cycle assessment (LCA). The case of the municipal solid waste management in the metropolitan city of Naples (Italy). J. Clean. Prod. **142**, 445–460 (2017). Part 1
68. Turner, D.A., Williams, I.D., Kemp, S.: Combined material flow analysis and life cycle assessment as a support tool for solid waste management decision making. J. Clean. Prod. **129**, 234–248 (2016)
69. Fernandez-Nava, Y., Del Río, J., Rodríguez-Iglesias, J., Castrillón, L., Marañón, E.: Life cycle assessment of different municipal solid waste management options: a case study of Asturias (Spain). J. Clean. Prod. **81**, 178–189 (2014)
70. Zhao, W., der Voet, E.V., Zhang, Y., Huppes, G.: Life cycle assessment of municipal solid waste management with regard to greenhouse gas emissions: case study of Tianjin, China. Sci. Total Environ. **407**, 1517–1526 (2009)
71. Erses Yay, A.A.: Application of life cycle assessment (LCA) for municipal solid waste management: a case study of sakarya. J. Clean. Prod. **94**, 284–293 (2015)
72. Blengini, G.A., Fantoni, M., Busto, M., Genon, G., Zanetti, M.C.: Participatory approach, acceptability and transparency of waste management LCAs: case studies of Torino and Cuneo. Waste Manag. **32**, 1712–1721 (2012)
73. Rajaeifar, M.A., Tabatabaei, M., Ghanavati, H., Khoshnevisan, B., Rafiee, S.: Comparative life cycle assessment of different municipal solid waste management scenarios in Iran. Renew. Sustain. Energy Rev. **51**, 886–898 (2015)
74. Menikpura, S., Gheewala, S.H., Bonnet, S.: Framework for life cycle sustainability assessment of municipal solid waste management systems with an application to a case study in Thailand. Waste Manag. Resour. **32**, 509–518 (2012)
75. Gunamantha, M., Sarto, A.: Life cycle assessment of municipal solid waste treatment to energy options: case study of Kartamantul Region, Yogyakarta. Renew. Energy **41**, 277–284 (2012)
76. Yi, S., Kurisu, K.H., Hanaki, K.: Life cycle impact assessment and interpretation of municipal solid waste management scenarios based on the midpoint and endpoint approaches. Int. J. Life Cycle Assess. **16**, 652–668 (2011)

77. Hong, J., Li, X., Zhaojie, C.: Life cycle assessment of four municipal solid waste management scenarios in China. Waste Manag. **30**, 2362–2369 (2010)
78. Banar, M., Cokaygil, Z., Ozkan, A.: Life cycle assessment of solid waste management options for Eskisehir, Turkey. Waste Manag. **29**, 54–62 (2009)
79. Damgaard, A., Manfredi, S., Merrild, H., Stensoe, S., Christensen, T.H.: LCA and economic evaluation of landfill leachate and gas technologies. Waste Manag. **31**, 1532–1541 (2011)
80. Buratti, C., Barbanera, M., Testarmata, F., Fantozzi, F.: Life cycle assessment of organic waste management strategies: an Italian case study. J. Clean. Prod. **89**, 125–136 (2015)
81. Emery, A., Davies, A., Griffiths, A., Williams, K.: Environmental and economic modelling: a case study of municipal solid waste management scenarios in Wales. Resour. Conserv. Recycl. **49**, 244–263 (2007)

Unfolding Community Structure in Rainfall Network of Germany Using Complex Network-Based Approach

A. Agarwal, N. Marwan, U. Ozturk and R. Maheswaran

Abstract Many natural systems can be represented as networks of dynamical units with a modular structure in the form of communities of densely interconnected nodes. Unfolding structure of such densely interconnected nodes in hydro-climatology is essential for reliable parameter transfer, model inter-comparison, prediction in ungauged basins, and estimating missing information. This study presents the application of complex network-based approach for regionalization of rainfall patterns in Germany. As a test case study, daily rainfall records observed at 1,229 rain gauges were selected throughout Germany. The rainfall data, when represented as a complex network using event synchronization, exhibits small-world and scale-free network topology which are a class of stable and efficient networks common in nature. In total, eight communities were identified using Louvain community detection algorithm. Each of the identified communities has a sufficient number of rain gauges which show distinct statistical and physical rainfall characteristics. The method used has wide application in most of the real systems which can be represented by network enabling to understand modular patterns through time series analysis.

Keywords Complex network · Event synchronization · Rainfall network

1 Introduction

A complex network is a collection of nodes, interconnected with links in a non-trivial manner. In a functional network, links are set up between each pair of nodes based on how the nodes interact with each other. For example, in a family network, each person is considered as a node and the relationship between them is a link; in a computer network, each computer is a node and links are the connections between computers;

A. Agarwal (B) · U. Ozturk
Institute of Earth and Environmental Science, University of Potsdam, Potsdam, Germany
e-mail: aagarwal@uni-potsdam.de

A. Agarwal · N. Marwan · U. Ozturk · R. Maheswaran
Potsdam Institute for Climate Impact Research (PIK), 601203, 14412 Potsdam, Germany

M. Rathinasamy et al. (eds.), *Water Resources and Environmental Engineering II*,
https://doi.org/10.1007/978-981-13-2038-5_17

in brain networks, neurons are nodes and links represent the pairwise neurons' interaction. In the last decade, climatologists and hydrologists have successfully applied the same network concept to analyze different research questions of hydro-climatic science. Each node represents a geographical location of climatological data (rainfall, stream flow, temperature, air pressure, etc.) and links between nodes are set up based on their interaction or similar variability (correlation, synchronization).

Hydro-climatic systems often show the topology of interacting nodes embedded in space. Such spatial networks are usually organized in modules (communities) of densely interconnected nodes. The spatial embedding of the network can hide the underlying community structure, rendering the identification of communities a challenging task. The investigation of the community structure in such networks helps in better understanding the functional mechanism of the highly complex systems. For instance, the identification of communities in rainfall network is essential to obtain reliable information about rainfall in case of missing values or no observation. Reliable records of rainfall are vital for many hydraulic (flood studies, dam, dikes, diversion structures, power plants) and environmental studies (land use planning and management, stream habitat assessment, extreme events, and climate impact studies). The traditional approach for estimating missing values in hydrology is to pool the information from other hydrologically homogeneous watersheds; by performing clustering analysis, [1–3] which have been identified to lead to erroneous estimations.

In the past, there have been several attempts [4–10] to develop a general unified framework for identifying rainfall communities (rainfall coherent sub-systems) using different approaches. The methods, in general, range from similarities in the rainfall signature, [11–13], via geographical location and catchment characteristics [14, 15] to rainfall network complexity, model parameters, and uncertainty [16–19]. Razavi and Coulibaly provides a detailed review of several methods for clustering in hydro-climatology [19]. Even though there are a plethora of methods available for community detection, most of these methods are subjective and consider the spatial proximity of the region, which in turn is not always true [8]. Also, traditional clustering methods are not capable of unraveling the numerous connections of each rain gauge station within and outside the community. Information on node connections/interconnections is essential to understand the role of each station in the rainfall network. For instance, dead ends (stations having few connections) which might be influenced by sampling size whereas stations connecting two communities are hybrid nodes hence play an important role in the rainfall network. Also, stations having a high number of links within the community can be termed as a local center. This kind of analysis by community detection is essential to understand the relative roles of each of the member stations of the community and is critical information in uncertainty analysis for predictions in ungauged basins, regionalization, missing values, and hydro-monitoring [20].

To add such insights into community detection, we use a more data-centric approach based on the complex network which extracts a spatial pattern from the network. The fundamental advantage of using network approach is that it considers the entire network structure in contrast to the only node attributes used by traditional

approaches [21]. Also, complex network uses network distance for partition compared to pairwise distance used by various clustering algorithm which is suitable for portioning such a spatiotemporal dynamical system [22, 23]. This study aims to identify a homogeneous region in rainfall network as defined by similarity in the long-term rainfall variability. Such regions (communities) are of interest both to reveal inherent structure with the rainfall coherent sub-system and to use as potential climate indicators [24]. It is vital to note that spatial proximity is not taken into consideration while forming a network and identifying communities.

In this study, to construct a rainfall network, we use event synchronization (ES) similarity measure. ES has advantages over other time-delayed correlation techniques (e.g., Pearson lag correlation), as it allows us to use dynamics time delay (not fixed) which is suitable to study interrelations between series of non-Gaussian data, data with heavy tails [25, 26]. After calculating synchronization between all possible pair of stations, we apply a suitable threshold to construct rainfall network. Louvain community detection algorithm employed to identify homogeneous regions by maximizing modularity. As a test case study, we use 1,229 available observed rain gauges across Germany to form a rainfall network. Eight communities were identified, and each of the identified communities has a sufficient number of rain gauges which show distinct statistical and physical rainfall characteristics. In this paper, the only preliminary result has been shown on German rainfall network which has immense potential to be extended in the future for hydro-monitoring purposes.

The paper is organized in the following manner. Section 2 describes the methods used in this study such as event synchronization, community detection, and various network measures. Section 3 discusses the application of network on observed daily rainfall data of Germany, and subsequent results obtained are discussed in detail in Sect. 4. The summary of the study is briefed in Sect. 5.

2 Methods

2.1 Event Synchronization

Adapting the state-of-the-art method, event synchronization, we measure nonlinear synchronization between all possible pair of rain gauges [27]. The modified algorithm proposed works as follows: An event occurs in the signals $x(t)$ and $y(t)$ at time t_l^x and t_m^y, where $l = 1, 2, 3, 4 \ldots S_x$, $m = 1, 2, 3, 4 \ldots S_y$, and S_x, and S_y are the total number of events, respectively. In our study, we derive events from a more or less continuous time series by selecting all time steps with values above a threshold ($\alpha =$ 95th percentile). These events in $x(t)$ and $y(t)$ are considered as synchronized when they occur within a time lag $\pm\tau_{lm}^{xy}$ which is defined as follows:

$$\tau_{lm}^{xy} = \min\left\{t_{l+1}^x - t_l^x, t_l^x - t_{l-1}^x, t_{m+1}^y - t_m^y, t_m^y - t_{m-1}^y\right\}/2 \tag{1}$$

where S_x and S_y are the total number of such events (greater then threshold α) that occurred in the signal $x(t)$ and $y(t)$, respectively. The above definition of the time lag helps to separation of independent events which in turn allows to take into account the fact that different processes are responsible for the generation of events. We need to count the number of times an event occurs in the signal $x(t)$ after it appears in the signal $y(t)$ and vice versa, and this is achieved by defining quantities $C(x|y)$ and $C(y|x)$. Where

$$C(x/y) = \sum_{l=1}^{S_x} \sum_{m=1}^{S_y} J_{xy} \tag{2}$$

and

$$J_{xy} = \begin{cases} 1 \text{ if } 0 < t_l^x - t_m^y < \tau_{lm}^{xy} \\ \frac{1}{2} \text{ if } t_l^x = t_m^y \\ 0 \text{ else,} \end{cases} \tag{3}$$

Similarly, we can define $C(y|x)$, and from these quantities, we can obtain

$$Q_{xy} = \frac{C(x|y) + C(y|x)}{\sqrt{(S_x - 2)(S_y - 2)}} \tag{4}$$

Q_{xy} is a measure of the strength of event synchronization between signal $x(t)$ and $y(t)$. Also, it is normalized to $0 \leq Q_{xy} \leq 1$. This implies $Q_{xy} = 1$ for perfect synchronization between signal $x(t)$ and $y(t)$.

2.2 Community Detection

Complex networks often show subsets of nodes that are densely interconnected. These subsets are often known as communities [7]. The understanding and visualization of community structure provide insight into the network [28]. For instance, different communities within a network may have very different properties compared to the averaged properties of the complete network [29].

There exist several community detection approaches aiming at stratifying the nodes into communities in an optimal way (see [30] for an extensive review), but very few of those are applicable for a hugely complex network having more than thousand nodes [24]. In this study, we adopted the Louvain algorithm proposed by [31, 32]). The Louvain algorithm works to optimize modularity (Q), a network measure, an indicator of "community's partition correctness" in a way that the number of edges falling within the community should be maximum and minimum in between communities [33]. Modularity (Q) is calculated as:

$$Q = \frac{1}{2m} \sum_{i,j} \lfloor A_{ij} - P_{i,j} \rfloor \delta(C_i C_j) \tag{5}$$

where A_{ij} represents the number of edges between i and j and $P_{i,j} = \frac{k_i k_j}{2m}$ represent the expected number of edges between node i and j. k_i and k_j are the total number of links of nodes i and j, respectively. m is the total number of edges in a network calculated as $m = 1/2 \sum_{ij} A_{ij}$. C_i and C_j are the communities to which node i and j are assigned, and the $\delta -$ function $\delta(C_i C_j)$ is 1 if nodes i and j are in the same community and 0 otherwise.

2.3 Network Measures

Various network measures exist to characterize the network dynamics, but in this study, we use only three prime and widely used properties: the degree (k) and degree distribution, the clustering coefficient (CC), and the average path length (L).

The degree [26] of a node in the network emphasizes the number of connections linked to the node directly. It can explain the type of nodes to some extent such as hubs having the highest degree and non-hubs having a low degree. The degree distribution $p(k)$ of a network is then defined to be the fraction of nodes in the network with degree k. Thus, if there are N nodes in total in a network and N_k of them have degree k, we have $P(k) = N_K / N$.

In general, the clustering coefficient (CC) [7] is used to identify the modular organization of the network by quantifying the tendency of a node to share same neighbors of directly connected nodes (tendency to form a triangle). High values of CC represent well-interconnected nodes and suggest redundancy of information in the network. Also, high values of CC are interpreted to exhibit significant spatial coherence [7, 34, 35].

The average path length (L) is the average number of steps taken along the shortest paths between all possible pairs of network nodes [26]. It is a measure of the efficiency of information or mass transport in a network. Efficiency in the network is inversely related to path length. A network with small average path length is highly efficient because two nodes are likely to be separated by few links (Table 1).

2.4 Random and Scale-Free Network

We generate an equivalent random and scale-free network for the same number of nodes ($N = 1229$) and links (96,384) as rainfall network (RN). We have used MATLAB toolbox for network analysis provided by MIT [36].

A random network is constructed by starting with a set of N isolated nodes and adding successive edges between them at random. There exist several random

Table 1 Network measures

Degree	Clustering coefficient	Average path length
$D_i = \frac{\sum_{j=1}^{N} A_{i,j}}{N-1}$	$C = \frac{1}{N}\sum_{i \in N} C_i = \frac{1}{N}\sum_{i \in N} \frac{2E}{k_i(k_i-1)}$	$a = \sum_{v_i, v_j \in N} \frac{d(v_i, v_j)}{N(N-1)}$

N the total number of nodes in a network. D_i degree of node i.; the clustering coefficient for the ith node is represented as C_i where E is the number of links that are actually observed to exist between the k_i neighbors of node i. We use the average of all the local clustering coefficients over the network as a bulk measure of the clustering tendency or cliquishness of the network as a whole. a is average path length, V is the set of nodes in the network, and $d(v_i, v_j)$ is the shortest path from v_i to v_j

network models, and each of them produces different probability distributions on graphs. Most commonly studied is **Erdős–Rényi model** which is denoted as $G(N, p)$. In the $G(N, p)$ model, a network is formed by linking nodes randomly with probability p ($0 < p < 1$) independently from every other edge [37, 38].

$$\text{The expected number of edges } (L) \text{ in } G(n, p) \, is = C(N, 2)$$

For given L and N, we can estimate the probability (p) for the random network.

For the scale-free network, we use the **Barabási–Albert (BA) model** which uses a preferential attachment algorithm. Many existing natural and human-made systems such as the Web network, social network seem to be approximately scale-free and certainly contain few supernodes (called hubs) with an exceptionally high degree as compared to the other nodes of the network. The BA model tries to explain the existence of such nodes in real networks [39, 40].

The network begins with an initial connected $m_o = 2$ node, the links between which are chosen arbitrarily, as long as each node has at least one link. At each time step, we add a new node with m ($\leq m_0$) links that connect the new node to m nodes already in the network. Repeating the procedure, total number of edges (L) in the network will be mN, where N is the number of nodes. For a known total number of edges (L) and nodes (N), we can estimate the value of m.

3 Rainfall Network Construction

Precipitation data from Germany is studied to explore the utility of network theory in identifying the communities in rainfall network. Daily data from an extensive network of 1,440 rain gauge stations (Fig. 1a) in contiguous Germany is available. Out of which 1,229 rain gauge stations lie inside Germany (red dots in Fig. 1a). Two hundred and eleven stations outside Germany (green dots in Fig. 1a) are included in the analysis to minimize the spatial boundary effect in the network formation (these stations are finally excluded from the discussion). One hundred and ten years of daily data, from 1 January 1901 to 31 December 2010, are available from various stations

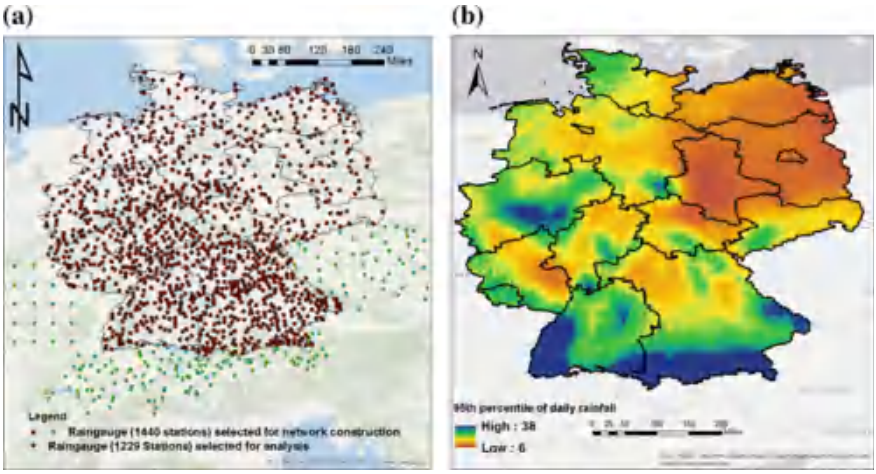

Fig. 1 (Left) Geographical location of gauging stations selected from Germany. (Right) 95th percentile of daily rainfall amounts for the observed data

operated by the German Weather Service. Data processing and quality control were performed according to Österle et al. [41].

We begin the network construction [29] by extracting event series from the 1,440 rain gauges representing extreme rainfall events, i.e., precipitation exceeding the 95th percentile at that station. By applying a threshold (95th percentile), we draw out extreme events from the given time series [24]. The 95th percentile is a good compromise between having a sufficient number of events at each location and a rather high threshold to study heavy precipitation. The strength of the connection between any two stations is established using the concept of event synchronization as discussed in [42]. If the value of ES is close to 1, it implies the two stations are highly synchronized, and if the value is close to 0, it indicates no synchronization [43].

In this study, we use an undirected network; i.e., we do not consider which of the two synchronized events happened first, to avoid the possibility of misleading directionalities of event occurrences in between rain gauges that are topographically close. Although the reconstructed network is based on all 1,440 nodes (to minimize the boundary effect), the subsequent topological analysis is performed only for the 1,229 stations lying inside Germany (red dots in Fig. 1a).

4 Result and Discussion

The *rainfall network* (*RN*) obtained using the 1,229 nodes contain total 96,384 pairwise links between them. The average degree for the entire RN is 95, the minimum is 0, and the maximum is 413. Several characteristics of the rainfall network are

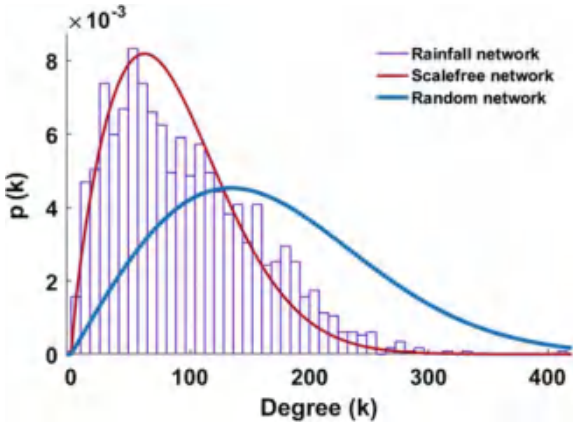

Fig. 2 Degree distribution of the German rainfall network (RN), random network, and scale-free network generated for an equal number of nodes and links

immediately clear. For instance, obtained RN is not a regular network since each node of the regular network exhibits equal degree. Also, the existence of supernodes (hubs) in the network, i.e., some nodes has a very high degree.

To understand the network topology, we compute the network properties: the degree distribution ($p(k)$), the clustering coefficients (CC),, and the average path length (L) [7] and then place the rainfall network (RN) into the context of known topologies. The degree distribution of the RN (Fig. 2) shows some resemblance with the degree distribution of a scale-free network [44] because scale-free networks have an asymmetric degree distribution which asymptotes to $P(k) \propto k^{-\gamma}$ at sufficiently large values of k, where γ ranges from 2.1 to 4 for a wide array of the observed network [7].

The small-world property of the RN is checked by clustering coefficient and average path length. A network has a small-world property if $C \gg C_{\text{random}}$ and $L \gtrsim L_{\text{random}}$ [7, 45]. For the *RN*, we find a global clustering coefficient of $C = 0.64$ and an average path length of $L = 3.92$, whereas the equivalent random graph has a clustering coefficient of $C_{\text{random}} = 0.12$, and an average path length of $L_{\text{random}} = 1.87$; thus, the rainfall network behaves as small-world network that exhibits scale-free behavior.

The scale-free network represents a network having supernodes (as already interpreted) also termed as "hubs" which have many more connections as compared to the rest of the nodes in the network as a whole following the power law/Pareto distribution. In general, a small-world network is characterized regarding stability and efficiency [7, 46]. Stability signifies that the network holds its integrity if some nodes of the network are randomly removed; i.e., the removal of the node will likely not fragment the network structure. In the context of rainfall network, this implies that if a randomly selected station is removed, then it is possible to recover most of the information. The efficiency of the network qualitatively characterizes the ease of information propagation in the network. A network with small average path length is highly efficient because two nodes are likely to be separated by few links.

The rainfall network constructed behaves as small-world network which, in turn, indicates the possible modular organization (communities) in the network. Hence, community mining has been performed in the study.

Identification of Modular Organization of the Network

While analyzing the network, it always remains a concern to explore the densely interconnected small subgroups, the communities. Here, it can be stated that with the enhanced knowledge of the community, their pattern of formation, the structure can give a deep insight into the network which is particularly true for small-world network. Also, the identification of the modular organization is helpful for coarse-graining the network [47, 48] which is very crucial while dealing with billions of nodes such as Web networks, brain networks, climate networks.

As already mentioned, a vast range of community detection algorithms exists (see [30] for an extensive review). However, considering the finding that the particular choice of the community detection algorithms has only a small impact [7], we only use one community detection algorithm, i.e., the Louvain algorithm which works for optimizing modularity on each step of the algorithm. In general, high modularity networks are densely linked within communities but sparsely linked between communities; i.e., the algorithm stops when the highest modularity is achieved.

The Louvain (maximizing modularity) community detection algorithm detects eight communities within the RN of Germany (Fig. 3).

Community structure, identified by modularity-based network analysis, shares specific elements which can be tied back to two general categories such as climate characteristics and physical characteristics. Therefore, the number of communities reflects the climatological diversity of Germany, and the number of stations per community sets the extent to which each distinct climatology "family" is sampled.

The spatial extent of the stations in the communities prominently shows the ability of the methods to capture the underlying driving forces. For instance, we do not impose any spatial constraints on the network, and there is no guarantee that community will be geographically cohesive, but as shown in Fig. 3 this is often the case. In fact, we observe a relationship between clustering coefficient and the number of stations in the community; namely, the higher the value of C, a large number of stations exist in the community and more geographically coherent they are. Although geographical proximity plays a vital role apart from that there is another governing mechanism, viz. physiographic features, climatic patterns, and statistical similarity of rainfall regimes which might influence the climate pattern. It is also important to emphasize, however, that such a modular structure is identified based on a cluster of actual connections, rather than based on our traditional way of geographic proximity, nearest neighbors, regional patterns, and linear correlations.

Table 2 shows the statistical and geographical interpretation of the resultant community which includes the mean, standard deviation, and coefficient of skewness of the precipitation distribution for each community. Higher mean precipitation shows a higher total amount of precipitation, larger standard deviation shows a stronger variation of data for the collecting period, and a larger coefficient of skewness indicates more extreme precipitation events [49].

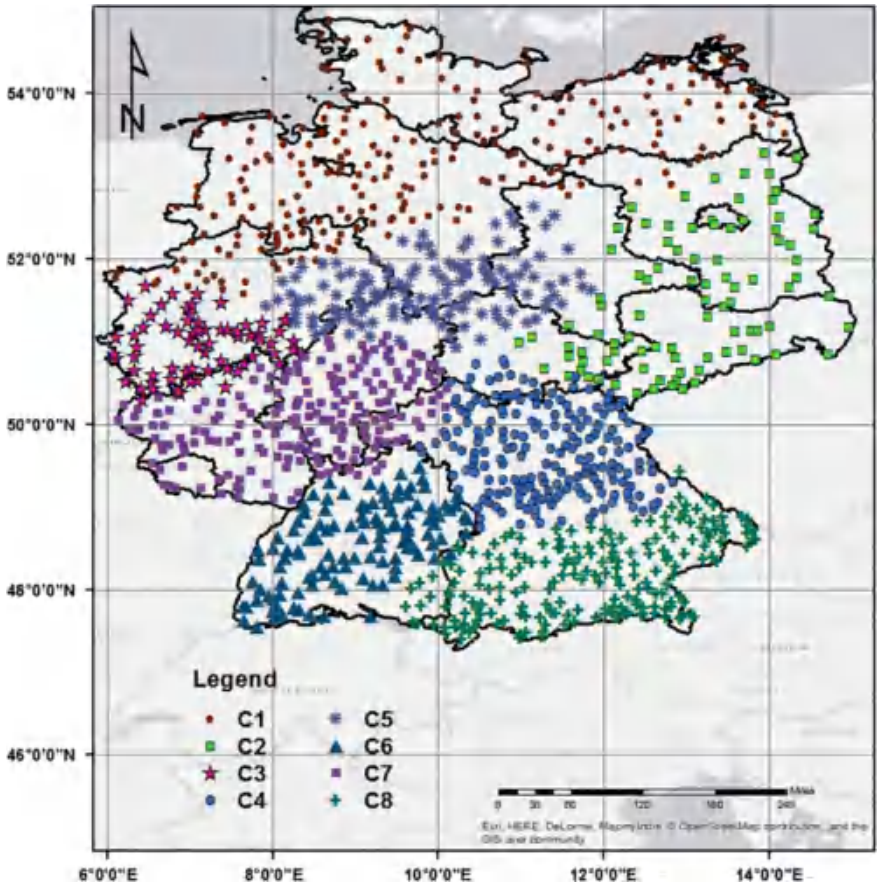

Fig. 3 Rain gauge stations map colored according to community membership. The communities were identified with maximizing modularity using Louvain algorithm

Intriguingly, resultant communities show numerous known relationships of precipitation along with new insights that are not obvious and hence may be of interest to a climate scientist. For example, community 8 (Fig. 3), which covers an almost mountainous region (Bavarian Alps), with daily mean of 3.0 mm and standard deviation of 6.34 mm (Table 2), represents the area with the highest daily mean and largest variation in the precipitation while community 2 (Fig. 3), which cover slow land areas (Mecklenburg lowlands), represents the region with the lowest mean and uniform precipitation. Community 2 (Mecklenburg lowlands) has a large coefficient of skewness, whereas communities 3 (Rhenish Massif region) and 6 (Black Forest region) show the smallest coefficient of skewness. All the communities show a positive coefficient of skewness, which indicates precipitation with a long tail toward high values.

Table 2 Summary of geographical and statistical analysis for each individual community. Communities formed by maximizing the modularity using Louvain algorithm. Elevation map for Germany is presented in the Fig. 1b

C. No.	Number of stations	Daily mean	Standard deviation	Skewness	Remarks
1	240 (20%)	1.92	4.02	4.46	Low elevation, wide geographic range
2	91 (7%)	1.69	4.01	6.04	Small community, mid elevation, Mecklenburg lowlands
3	68 (5%)	2.56	4.99	3.8	Smallest community, mid elevation, Rhenish Massif
4	193 (16%)	1.97	4.24	4.33	High elevation, Bavarian Forest
5	131 (11%)	2.03	4.31	4.65	Mid elevation, Rhenish Massif
6	118 (10%)	2.63	5.47	3.98	High elevation, Black Forest region
7	190 (15%)	2.06	4.38	4.23	Mid elevation, Rhineland-Palatinate
8	198 (16%)	3.0	6.34	4.13	Very high elevation, Bavarian Alps

Community 1 also shows low daily mean and uniform precipitation in a wide longitudinal geographic range consisting of low elevation stations. Communities 2 and 3 are the smallest communities which may have characteristics that are rare because they show either undersampled or uncommon hydro-climatological regimes, which make them vital if the aim of a rainfall network is to sample the inherent hydro-climatological diversity of that area [7]. In South Germany, both communities 4 and 6 (Fig. 3) represent the forest-dominated (Bavarian Forest and Black Forest region, respectively) high elevation regions having nearly same statistical and geographical properties (Table 2); then what makes them different? The answer must lie in the orographic barrier which lies along the 10°E longitude which causes an abrupt change of topography of the area resulting in different climate regimes for communities 4 and 6. These results also follow the study by Rheinwalt [50], which shows an abrupt change in the precipitation isochrones along the orographic barrier.

It is also interesting to understand how these network communities present different climate regime properties. For instance, both day-to-day precipitation dynamics and overall seasonal regimes exhibited by data from a particular rain gauge station are determined to a significant extent by the elevation whether the station receives daily precipitation as rain, snow, or some mixture of the two. Thus, it might be possible to understand the community structure, at least in part, by their stations' elevation. Comparing the communities with the corresponding stations' elevation reveals, to some degree, that they are stratified by elevation (Fig. 4). Overall, it can be stated that the singularities of sharp transition hidden in precipitation data are more significant

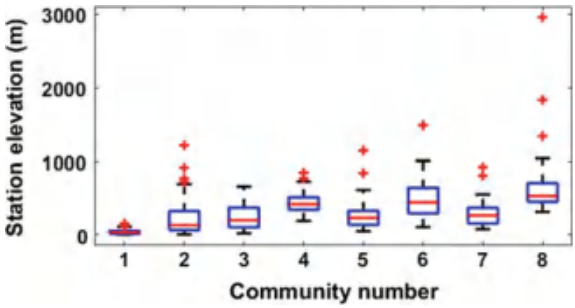

Fig. 4 Boxplots of mean basin elevation grouped by the communities. The number of stations in each community is mentioned in Table 2

than changes in the periodicity or data structure of the time series for community detection.

5 Summary

This study has shown the application of complex network-based method to unfold modular structure in complex natural systems using the dynamics of observed time series. We applied the method on observed rainfall time series and uncovered eight communities that are consistent with statistical and physical characteristics of rainfall. The results lead to the following concluding remarks:

- Preliminary investigation on the rainfall network of Germany shows that the network exhibits small world and scale-free behaviour which is a common class in many disciplines such as brain network, airport network. A small-world network implies stability, and the network is resilient to the loss of nodes whereas scale-free behaviour suggested that network consist of supernodes in the network which are vital to consider for many hydrologic applications such as missing information, prediction in ungauged basin etc. Hence, the advantage of using complex network-based approach is that network topology gives a beforehand idea of the behavior of communities and rain gauges in the network.
- The rainfall network based on event synchronization seems to be a formidable statistic in capturing the rainfall system dynamics. The 1,229 stations considered are categorized into eight communities each exhibiting distinct rainfall characteristics. We then show that these eight communities appear to be defined by their geographical proximity, which in turn corresponds to shared or different meteorological forcing. The number of communities reflects the diversity of such rainfall dynamical classes, and the number of stations per community sets the extent to which each regime is sampled.

In future, it would be interesting to extend the current work to understand the strength of connection among rain gauges within the community. In other words, microscopic investigation of the (intra-) intercommunity connection is essential to have better hydro-monitoring design of rain gauges. Also, it would be vital to extend the work to identify the universal role of each raingauge (node) such as hubs, non-hubs, dead-ends in communities and whole network.

Acknowledgements The author acknowledges Deutsche Forschungsgemeinschaft (DFG) (GRK 2043/1) for funding this research within the graduate research training group Natural Risk in a Changing World (NatRiskChange) at the University of Potsdam (http://www.uni-potsdam.de/natriskchange).

References

1. Agarwal, A., Maheswaran, R., Kurths, J., Khosa, R.: Wavelet spectrum and self-organizing maps-based approach for hydrologic regionalization—a case study in the Western United States. Water Resour. Manag. **30**(12), 4399–4413 (2016)
2. Blöschl, G., Sivapalan, M.: Scale issues in hydrological modelling: a review. Hydrol. Process. **9**(3–4), 251–290 (1995)
3. Saf, B.: Regional flood frequency analysis using L-moments for the West Mediterranean region of Turkey. Water Resour. Manag. **23**(3), 531–551 (2009)
4. Agarwal, A., Maheswaran, R., Sehgal, V., Khosa, R., Sivakumar, B., Bernhofer, C.: Hydrologic regionalization using wavelet-based multiscale entropy method. J. Hydrol. **538**, 22–32 (2016)
5. Carlón Allende, T., Mendoza, M.E., López Granados, E.M., Morales Manilla, L.M.: Hydro-geographical regionalisation: an approach for evaluating the effects of land cover change in watersheds. a case study in the Cuitzeo Lake Watershed, Central Mexico. Water Resour. Manag. **23**(12), 2587–2603 (2009)
6. Franchini, M., Suppo, M.: Regional analysis of flow duration curves for a limestone region. Water Resour. Manag. **10**(3), 199–218 (1996)
7. Halverson, M.J., Fleming, S.W.: Complex network theory, streamflow, and hydrometric monitoring system design. Hydrol. Earth Syst. Sci. **19**(7), 3301–3318 (2015). https://www.doi.org/10.5194/hess-19-3301-2015
8. Jha, S.K., Zhao, H., Woldemeskel, F.M., Sivakumar, B.: Network theory and spatial rainfall connections: an interpretation. J. Hydrol. **527**, 13–19 (2015)
9. Lakhanpal, A., Sehgal, V., Maheswaran, R., Khosa, R., Sridhar, V.: A non-linear and non-stationary perspective for downscaling mean monthly temperature: a wavelet coupled second order Volterra model. Stoch. Environ. Res. Risk Assess. **31**, 2159–2181 (2017)
10. Sehgal, V., Lakhanpal, A., Maheswaran, R., Khosa, R., Sridhar, V.: Application of multi-scale wavelet entropy and multi-resolution Volterra models for climatic downscaling. J. Hydrol. (2016)
11. Atiem, I.A., Harmanciolu, N.B.: Assessment of regional floods using L-moments approach: the case of the River Nile. Water Resour. Manag. **20**(5), 723–747 (2006)
12. de Vos, N.J., Rientjes, T.H.M., Gupta, H.V.: Diagnostic evaluation of conceptual rainfall-runoff models using temporal clustering. Hydrol. Process. **24**(20), 2840–2850 (2010)
13. Yang, L., Tian, F., Smith, J.A., Hu, H.: Urban signatures in the spatial clustering of summer heavy rainfall events over the Beijing metropolitan region: urban modification of heavy rainfall. J. Geophys. Res. Atmos. **119**(3), 1203–1217 (2014)
14. Ramachandra Rao, A., Srinivas, V.V.: Regionalization of watersheds, vol. 58. Springer, Netherlands, Dordrecht (2008)

15. Burn, D.H., Boorman, D.B.: Estimation of hydrological parameters at ungauged catchments. J. Hydrol. **143**(3–4), 429–454 (1993)
16. Agarwal, A., Rathinasamy, M., Kurths, J., Khosa, R.: SOM technique. Unpublished (2016)
17. Bock, A.R., Hay, L.E., McCabe, G.J., Markstrom, S.L., Atkinson, R.D.: Parameter regionalization of a monthly water balance model for the conterminous United States. Hydrol. Earth Syst. Sci. **20**(7), 2861–2876 (2016)
18. Oudin, L. Andréassian, V. Perrin, C. Michel, C., Le Moine, N.: Spatial proximity, physical similarity, regression and ungaged catchments: a comparison of regionalization approaches based on 913 French catchments. Water Resour. Res. **44**(3) (2008)
19. Razavi, T., Coulibaly, P.: Streamflow prediction in ungauged basins: review of regionalization methods. J. Hydrol. Eng. **18**(8), 958–975 (2013)
20. Agarwal, A. Marwan, N., Rathinasamy, M., Ozturk, U., Merz, B., Kurths, J.: Optimal design of hydrometric station networks based on complex network analysis. Hydrol. Earth Syst. Sci. Discuss. 1–21 (2018)
21. Jia, C. Li, Y., Carson, M.B., Wang, X., Yu, J.: Node attribute-enhanced community detection in complex networks. Sci. Rep. **7**(1) (2017)
22. Steinhaeuser, K., Chawla, N.V., Ganguly, A.R.: An exploration of climate data using complex networks. ACM SIGKDD Explor. Newsl. **12**(1), 25 (2010)
23. Steinhaeuser, K., Chawla, N.V., Ganguly, A.R.: Complex networks as a unified framework for descriptive analysis and predictive modeling in climate science. Stat. Anal. Data Min. **4**(5), 497–511 (2011)
24. Sun, A.Y., Xia, Y., Caldwell, T.G., Hao, Z.: Patterns of precipitation and soil moisture extremes in Texas, US: a complex network analysis. Adv. Water Resour. **112**, 203–213 (2018)
25. Tass, P., et al.: Detection of n: m phase locking from noisy data: application to magnetoencephalography. Phys. Rev. Lett. **81**(15), 3291–3294 (1998)
26. Stolbova, V., Martin, P., Bookhagen, B., Marwan, N., Kurths, J.: Topology and seasonal evolution of the network of extreme precipitation over the Indian subcontinent and Sri Lanka. Nonlinear Process. Geophys. **21**(4), 901–917 (2014)
27. Quian Quiroga, R., Kraskov, A., Kreuz, T. Grassberger, P.: Performance of different synchronization measures in real data: a case study on electroencephalographic signals. Phys. Rev. E. **65**(4) (2002)
28. Girvan, M., Newman, M.E.J.: Community structure in social and biological networks. Proc. Nat. Acad. Sci. **99**(12), 7821–7826 (2002) https://www.doi.org/10.1073/pnas.122653799
29. Agarwal, A., Marwan, N., Maheswaran, R., Merz, B., Kurths, J.: Quantifying the roles of single stations within homogeneous regions using complex network analysis. Hydrology (2018)
30. Fortunato, S.: Community detection in graphs. Phys. Rep. **486**(3–5), 75–174 (2010)
31. Blondel, V.D., Guillaume, J.-L., Lambiotte, R., Lefebvre, E.: Fast unfolding of communities in large networks. J. Stat. Mech Theory Exp. **2008**(10), P10008 (2008)
32. Rubinov, M., Sporns, O.: Weight-conserving characterization of complex functional brain networks. NeuroImage **56**(4), 2068–2079 (2011)
33. Conticello, F., Cioffi, F., Merz, B., Lall, U.: An event synchronization method to link heavy rainfall events and large-scale atmospheric circulation features. Int. J. Climatol. (2017)
34. Boers, N., Bookhagen, B., Barbosa, H.M.J., Marwan, N., Kurths, J., Marengo, J.A.: Prediction of extreme floods in the eastern Central Andes based on a complex networks approach. Nat. Commun. **5**, 5199 (2014)
35. Sivakumar, B., Woldemeskel, F.M.: Complex networks for streamflow dynamics. Hydrol. Earth Syst. Sci. **18**(11), 4565–4578 (2014)
36. Bounova, G., de Weck, O.: Overview of metrics and their correlation patterns for multiple-metric topology analysis on heterogeneous graph ensembles. Phys. Rev. E **85**(1) (2012)
37. Gilbert, E.N.: Random Graphs. Ann. Math. Stat. **30**(4), 1141–1144 (1959)
38. Newman, M.E.J., Strogatz, S.H., Watts, D.J.: Random graphs with arbitrary degree distributions and their applications. Phys. Rev. E **64**(2) (2001)
39. Albert, R., Barabási, A.-L.: Statistical mechanics of complex networks. Rev. Mod. Phys. **74**(1), 47–97 (2002)

40. Cohen, R., Havlin, S.: Scale-free networks are ultrasmall. Phys. Rev. Lett. **90**(5) (2003)
41. Österle, H., Werner, P., and Gerstengarbe, F.: Qualitätsprüfung, Ergänzung und Homogenisierung der täglichen Datenreihen in Deutschland, 1951–2003: ein neuer Datensatz, 7. Deutsche Klimatagung, Klimatrends: Vergangenheit und Zukunft, 9–11. Oktober 2006, München, (2006)
42. Agarwal, A., Marwan, N., Rathinasamy, M., Merz, B., Kurths, J.: Multi-scale event synchronization analysis for unravelling climate processes: a wavelet-based approach. Nonlinear Process. Geophys. **24**(4), 599–611 (2017)
43. Ozturk, U., Wendi, D., Crisologo, I., Riemer, A., Agarwal, A., Vogel, K., López-Tarazón, J. A. and Korup, O.: Rare flash floods and debris flows in southern Germany. Sci. Total Environ. **626**, 941–952 (2018) https://doi.org/10.1016/j.scitotenv.2018.01.172
44. Barabási, A.-L. and Albert, R.: Emergence of scaling in random networks. Science **286**(5439), 509–512 (1999) https://doi.org/10.1126/science.286.5439.509
45. Watts, D.J., Strogatz, S.H.: Collective dynamics of 'small-world' networks. Nature **393**(6684), 440–442 (1998)
46. Newman, M.E.J.: Detecting community structure in networks. Eur. Phys. J. B Condens. Matter **38**(2), 321–330 (2004) https://www.doi.org/10.1140/epjb/e2004-00124-y
47. Chen, J., Lu, J., Lu, X., Wu, X., Chen, G.: Spectral coarse graining of complex clustered networks. Commun. Nonlinear Sci. Numer. Simul. **18**(11), 3036–3045 (2013)
48. Gfeller, D., De Los Rios, P.: Spectral coarse graining of complex networks. Phys. Rev. Lett. **99**(3) (2007)
49. Hsu, K.-C., Li, S.-T.: Clustering spatial–temporal precipitation data using wavelet transform and self-organizing map neural network. Adv. Water Resour. **33**(2), 190–200 (2010)
50. Rheinwalt, A., Boers, N., Marwan, N., Kurths, J., Hoffmann, P., Gerstengarbe, F.-W. and Werner, P.: Non-linear time series analysis of precipitation events using regional climate networks for Germany. Climate Dynamics **46**(3–4), 1065–1074 (2016) https://www.doi.org/10.1007/s00382-015-2632-z

Comparative Analysis of the Performance of Wavelet-Based and Stand-alone Models in Capturing Non-stationarity in Climate Downscaling

Vinit Sehgal, Venkataramana Sridhar and Maheswaran Rathinasamy

Abstract Non-stationarity is an intrinsic property of all natural processes, and addressing the same is crucial for climatic downscaling models. Wavelet-based models have been used to address the non-stationarity in the individual predictor (explanatory) time series where each predictor is "decomposed" into its discrete wavelet components at multiple time–frequency resolutions. However, in the warming climate, the predictor–predictand relationships (PPRs) are getting unpredictable. Hence, it is important to understand if the wavelet-based approach can capture the non-stationary PPR better than the stand-alone models. This paper provides an experimental approach to compare the strength of wavelet-based and stand-alone regression models when applied to downscale mean monthly temperature, from general circulation models (GCMs). For this study, we use Can CM4 GCM model to downscale temperature at multiple locations in the Krishna River Basin. Regression coefficients of the recursively updated models are compared for the wavelet-based and the stand-alone models for the length of the validation period. The comparison shows that the regression coefficients from the wavelet-based models capture higher variance compared to the stand-alone models and hence were able to capture the changing PPRs in the downscaling models with greater accuracy. The statistical performance indices reinforce the finding that wavelet-based models consistently outperformed the stand-alone models.

Keywords Climatic downscaling · Wavelet analysis · Non-stationarity · GCM Krishna Basin

V. Sehgal
Water Management and Hydrological Science, Texas A & M University, College Station 77840, USA

V. Sridhar (B)
Department of Biological Systems Engineering, Virginia Polytechnic Institute and State University, Blacksburg, VA 24061, USA
e-mail: vsri@vt.edu

M. Rathinasamy
MVGR College of Engineering, Vizianagaram, India

M. Rathinasamy et al. (eds.), *Water Resources and Environmental Engineering II*,
https://doi.org/10.1007/978-981-13-2038-5_18

1 Introduction

Climatic downscaling is very important from the perspective of inferring information about physical processes at a finer resolution than the observational scale of the available dataset. Several factors, for example, (i) increased concerns about global-scale climatic variability, especially with regard to the climate change, (ii) simultaneous advancements in the development and application of the general circulation models (GCMs) and the land surface models (LSMs), and (iii) availability of coarse-scale remote sensing products, have led to increased demand of reliable downscaling models. In the cases where observations at the finer scale are not readily available for understanding the process at the subregional and local scales, downscaling of climate model data helps to bridge the gap between the information at a coarse scale (to the magnitude of several hundred km) and subregional/local scale [1–5].

Due to the relative ease of computation, elaborate research has been carried out in developing suitable statistical models for obtaining predictor–predictand relationships (PPRs) for climatic downscaling. Artificial intelligence (AI) and machine learning techniques such as automated regression [6, 7], artificial neural networks (ANNs) [8, 9], support vector machines (SVM) [10–12], relevance vector machine (RVM) [13] have been particularly popular among researchers for developing the relationship between the predictors and predictand variables at multiple resolutions for several hydrological variables like precipitation [3, 14], streamflow [15], soil moisture [16, 17], groundwater storage [18, 19], evapotranspiration [20, 21], etc.

However, the predictor–predictand is influenced by the inherent non-stationarity of the climatic processes [22–25]. Despite the importance of the subject, the effect and mitigation of the non-stationarity in the predictor–predictand relationship is inadequately studied [26, 27]. Recently, Sehgal et al. [3] proposed a wavelet-based multiresolution model based on second-order Volterra for precipitation downscaling. The models used wavelet analysis to capture the non-stationarity of the input–output time series at multiple time–frequency resolutions. The objective of this investigation is to extend the study carried out by Sehgal et al. [3] to downscale mean monthly temperature from CanCM4 GCM and compare the relative strengths of wavelet-based and stand-alone regression models in capturing the non-stationarity in the PPR in the downscaling application.

The case study is applied to five locations in Krishna Basin, India. The downscaling models are recursively updated for each month for the validation period, and the regression coefficients for the wavelet-based models and the stand-alone regression models are compared in order to evaluate the relative change in the coefficients with time in the validation period. Performance evaluation for the two classes of models is also carried out using various statistical indices for the validation period in order to establish the efficacy of wavelet-based multiresolution approach over the stand-alone methodology.

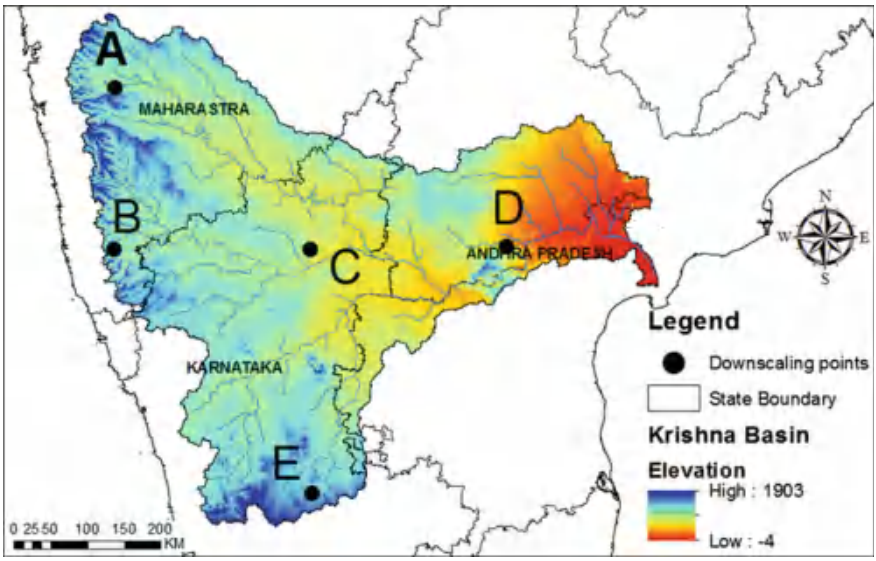

Fig. 1 Basin map of the study region showing the elevation of the basin, downscaling points, and the adjoining areas

2 Case Study and Dataset

2.1 Study Basin

The focus area of this study is Krishna River Basin of the Indian peninsula (73° 17′–81°9′E and 13° 10′–19° 22′N). Majority landmass of the basin is agricultural land (~75%), while water bodies cover around 4% of the total area of about 259,000 km^2. The basin receives precipitation primarily through the southwestern monsoon (~80% of the total precipitation received by the basin), which remains active normally from June to October. Figure 1 provides the map of the Krishna River Basin with adjoining areas, topography, and points selected for the application of the downscaling models.

2.2 Data Description

Reanalysis data of the monthly mean atmospheric variables prepared by National Centres for Environmental Prediction–National Centre for Atmospheric Research (NCEP-NCAR) is extracted for the selected downscaling points with the resolution of 2.5° × 2.5° for January 1969 to December 1994. CanCM4 (grid size 2.8° × 2.8°, later interpolated to the NCEP resolution) GCM model developed by Canadian

Centre for Climate Modelling and Analysis is chosen based on the skill score as described by Cai et al. [28]. The study uses seventy variables at each grid point, common to both CanCM4 and NCEP. The predictors at seventeen different pressure levels, i.e., 1000, 925, 850, 700, 600, 500, 400, 300, 250, 200, 150, 100, 70, 50, 30, 20, 10 (in mb), are considered which include air temperature (TA), eastward wind (UA), northward wind (VA), and geo-potential height (ZG), and others at surface levels include surface temperature (TS), sea level pressure (PSL).

For this study, downscaling is carried out at five locations as shown in Fig. 1, named A, B, C, D, and E. The training dataset is obtained from the NCEP models for a period of January 1969–December 1993, while GCM data from January 1994 to December 2004 is used for model validation. Observed temperature data from the India Meteorological Data (IMD) for the period 1969–2004 served as the target for training and validating the models at finer spatial resolution ($1° \times 1°$).

3 Modeling Development

A wavelet is a small oscillatory function with zero mean, localized in both time and frequency domains. Convolution of a time series can be achieved using wavelet transform corresponding to multiple time and frequency domains by using scaled (stretched or compressed) instance of a mother wavelet. Continuous wavelet transform (CWT) is used to perform these convolutions at every position and scale of the data, which may not be feasible in several applications due to computationally expense. On the contrary, the discrete wavelet transform (DWT) follows a dyadic scheme where the wavelet coefficients are calculated at multiple scales (frequency) and position (time), thus providing the time–frequency realization of the dataset in a computationally prudent manner. Wavelet transform does not include potentially erroneous assumptions of the processes or parameters, yet providing information of the variability in the data at multiple time scales independently, making it suitable for application in studying complex processes, as in climatic downscaling.

The input variables are classified into several clusters based on their multiscale wavelet entropy (MWE) [29, 30] using the *k*-means technique [31–33]. The appropriate number of clusters are selected to be 12, 10, 11, 9, and 10, respectively, for stations A, B, C, D, and E based on two validity indices, namely Davies-Bouldin (DB) index and Dunn's index [34–38]. Principal components of each cluster are obtained with a cumulative explained variance of 90–95% of the original cluster. These principal components are used as the inputs to the P-MLR models. Discrete wavelet components (DWCs) are obtained for each of the representative variables from all clusters post-PCA and the observed temperature dataset up to three dyadic levels to obtain multiple time–frequency realizations. These DWCs are used to model the DWC of the downscaled temperature data. Outputs from the models for each resolution are later added to obtain the downscaled temperature in the original time domain. These models are called W-P-MLR models. Figure 2 shows the flowchart for the models developed for this study. To evaluate the sensitivity of the models under study to a

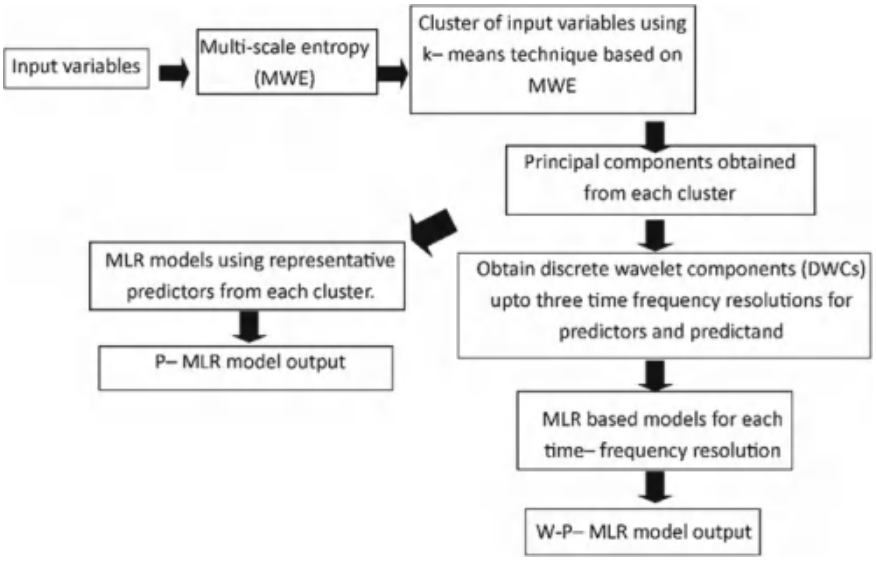

Fig. 2 Flowchart for the proposed W-P-MLR and P-MLR models

non-stationary PPR, a recursive updating approach [39] is employed where the models are updated every month for the validation period, and the regression coefficients from MLR are evaluated.

4 Results and Discussion

Table 1 provides the statistical performance evaluation of P-MLR and W-P-MLR models for five stations under study using normalized root-mean-square error (NRMSE), coefficient of determination (R^2), and accuracy for the validation period. Description of these statistical indices can be found in Sehgal et al. [3]. It can be observed that the wavelet-based models consistently outperform the stand-alone P-MLR models for all five stations.

The suitability of the W-P-MLR and stand-alone MLR models in application to the non-stationary dataset is based on analyzing the regression coefficients of the recursively updated models and comparing the variability in the coefficients of the two types of models over the validation period (120 months). The constituent models of W-P-MLR, i.e., models based on the A3, D3, D2, and D1 wavelet sub-time series, and the P-MLR models are updated each month recursively for the length of the validation dataset. The regression coefficients obtained from the models of each class are analyzed for the five downscaling locations. As per the expectation, it is observed that the regression coefficients pertaining to the wavelet sub-time series (A3, D3, D2, and D1) show a greater degree of variability of the regression coefficients compared

Table 1 Statistical performance evaluation of the P-MLR and W-P-MLR models

	R^2	NRMSE	NMAE	Accuracy
Station A				
W-P-MLR	0.871	0.084	0.070	87.88
P-MLR	0.80	0.106	0.086	73.48
Station B				
W-P-MLR	0.86	0.087	0.068	87.88
P-MLR	0.807	0.099	0.080	84.85
Station C				
W-P-MLR	0.92	0.072	0.059	86.36
P-MLR	0.808	0.107	0.084	71.21
Station D				
W-P-MLR	0.92	0.071	0.057	86.36
P-MLR	0.82	0.099	0.076	76.52
Station E				
W-P-MLR	0.87	0.095	0.075	85.61
P-MLR	0.81	0.102	0.078	79.55

to the P-MLR models. The variance of the coefficients pertaining to each regressor is normalized (divided by the range of regression coefficients) for easy comparison across models. Upon comparing the normalized variance for each model (Figs. 3 and 4), it is observed that the regression coefficients for models pertaining to the wavelet-based scheme display higher degree of variability over time. This indicates an adaptation of the wavelet-based models to the changing PPR.

The adaptability of the W-P-MLR models to the changing PPR over time can be attributed to the fact that the inputs for the W-P-MLR models were decomposed to multiple time–frequency resolutions, thus representing the underlying process between the predictors and the predictand with greater detail. While the high fre-

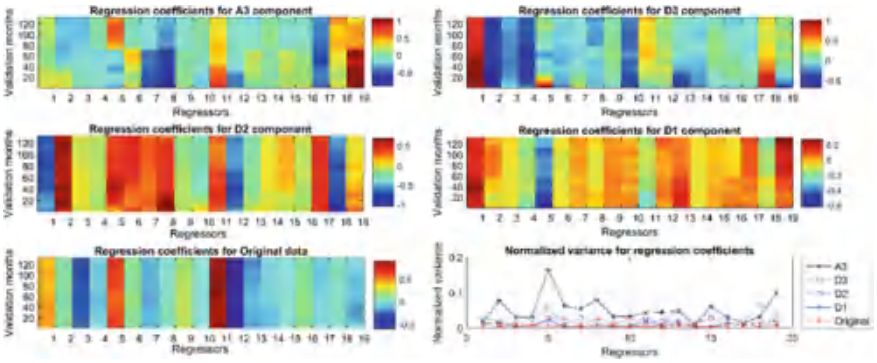

Fig. 3 Regression coefficients and normalized variance for the regression coefficients (bottom right) for the constituting models of the W-P-MLR models and P-MLR models for Station C

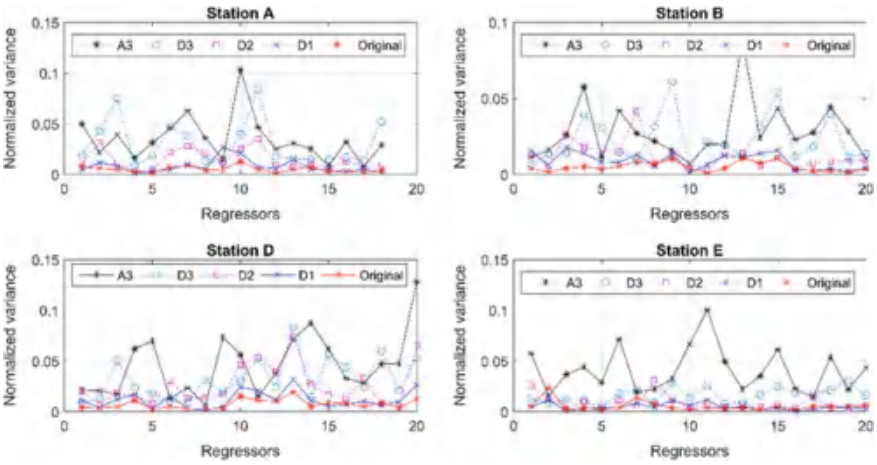

Fig. 4 Regression coefficients for the constituting models of the W-P-MLR models and P-MLR models for Station A, B, D, and E

quency (transient) features of the process were captured at the D1 and D2 components, D3 and A3 sub-time series captured the long-term, seasonal variations on the process. This segregation of information at multiple scales allowed the models to capture the changing PPR with greater accuracy as evident from the performance evaluation in this study.

5 Conclusion

This study compares the performance of two set of models, i.e., wavelet-based and stand-alone MLR, in downscaling mean monthly temperature for five locations at Krishna Basin, India. The recursively updated regression coefficients from the models under study are used to evaluate if utilization of wavelet analysis is helpful in adapting to changing predictor–predictand relationship (PPR) in an inherently non-stationary climate system. It can be observed that the wavelet-based models outperform the stand-alone P-MLR models in all statistical performance indices. Also, the regression coefficients for the W-P-MLR models adapted to the changing PPR more aggressively compared to the P-MLR models, thus indicating the suitability of wavelet-based models in climatic downscaling studies. The comparison shows that the coefficients from the wavelet-based models show higher variance compared to the stand-alone models. While the coefficients from recursive stand-alone models did not exceed the 95% confidence interval (CI) obtained from the training dataset, wavelet-based models, adapted to the changing PPR and hence the coefficients' range exceeded

the 95% CI obtained from the training dataset using the respective class of models. Hence, not only the wavelet-based models outperformed the stand-alone models in terms of statistical performance indicators, but also responded and adapted to the changing PPR owning to the non-stationary climatic processes.

References

1. Carter, T.R., Kenkyū, K.K.K.C.K.: IPCC Technical Guidelines for Assessing Climate Change Impacts and Adaptations: Part of the IPCC Special Report to the First Session of the Conference of the Parties to the UN Framework Convention on Climate Change. London (1994)
2. Lakhanpal, A., Sehgal, V., Maheswaran, R., Khosa, R., Sridhar, V.: A non-linear and non-stationary perspective for downscaling mean monthly temperature: a wavelet coupled second order Volterra model. Stoch. Environ. Res. Risk Assess., 1–23
3. Sehgal, V., Lakhanpal, A., Maheswaran, R., Khosa, R., Sridhar, V.: Application of multi-scale wavelet entropy and multi-resolution Volterra models for climatic downscaling. J. Hydrol. **556**, 1078–1095 (2016)
4. Wigley, T., Jones, P., Briffa, K., Smith, G.: Obtaining sub-grid-scale information from coarse-resolution general circulation model output. J. Geophys. Res. Atmos. **95**, 1943–1953 (1990)
5. Wood, A.W., Leung, L.R., Sridhar, V., Lettenmaier, D.: Hydrologic implications of dynamical and statistical approaches to downscaling climate model outputs. Clim. Change **62**, 189–216 (2004)
6. Ghosh, S., Mujumdar, P.: Future rainfall scenario over Orissa with GCM projections by statistical downscaling. Curr. Sci. **90**, 396–404 (2006)
7. Goyal, M.K., Ojha, C.: Downscaling of surface temperature for lake catchment in an arid region in India using linear multiple regression and neural networks. Int. J. Climatol. **32**, 552–566 (2012)
8. Cawley, G.C., Haylock, M.R., Dorling, S.R., Goodess, C., Jones, P.D.: Statistical downscaling with artificial neural networks. In: ESANN, pp. 167–172 (2003)
9. Jeong, D., St-Hilaire, A., Ouarda, T., Gachon, P.: Comparison of transfer functions in statistical downscaling models for daily temperature and precipitation over Canada. Stoch. Env. Res. Risk Assess. **26**, 633–653 (2012)
10. Aksornsingchai, P., Srinilta, C.: Statistical downscaling for rainfall and temperature prediction in Thailand. In: Proceedings of the International Multiconference of Engineers and Computer Scientists, Citeseer (2011)
11. Anandhi, A., Srinivas, V., Nanjundiah, R.S., Nagesh Kumar, D.: Downscaling precipitation to river basin in India for IPCC SRES scenarios using support vector machine. Int. J. Climatol. **28**, 401–420 (2008)
12. Sachindra, D., Huang, F., Barton, A., Perera, B.: Statistical Downscaling of General Circulation Model Outputs to Catchment Streamflows (2011)
13. Ghosh, S., Mujumdar, P.: Statistical downscaling of GCM simulations to streamflow using relevance vector machine. Adv. Water Resour. **31**, 132–146 (2008)
14. Zhan, C., Han, J., Hu, S., Liu, L., Dong, Y.: Spatial downscaling of GPM annual and monthly precipitation using regression-based algorithms in a mountainous area. Adv. Meteorol. (2018)
15. Wang, C., Xu, J., Chen, Y., Bai, L., Chen, Z.: A hybrid model to assess the impact of climate variability on streamflow for an ungauged mountainous basin. Clim. Dyn. **50**, 2829–2844 (2018)
16. Alemohammad, S.H., Kolassa, J., Prigent, C., Aires, F., Gentine, P.: Global Downscaling of Remotely-Sensed Soil Moisture using Neural Networks
17. Moller, J., Jovanovic, N., Garcia, C.L., Bugan, R.D., Mazvimavi, D.: Validation and downscaling of Advanced Scatterometer (ASCAT) soil moisture using ground measurements in the Western Cape, South Africa. South Afr. J. Plant Soil **35**, 9–22 (2018)

18. Goodarzi, M., Abedi-Koupai, J., Heidarpour, M.: Investigating impacts of climate change on irrigation water demands and its resulting consequences on groundwater using CMIP5 models. Groundwater (2018)
19. Miro, M.E., Famiglietti, J.S.: Downscaling GRACE remote sensing datasets to high-resolution groundwater storage change maps of California's Central Valley. Remote Sens. **10**, 143 (2018)
20. Guo, B., Zhang, J., Xu, T.: Comparison of two statistical climate downscaling models: a case study in the Beijing region, China. Int. J. Water **12**, 22–38 (2018)
21. Sachindra, D., Perera, B.: Annual statistical downscaling of precipitation and evaporation and monthly disaggregation. Theoret. Appl. Climatol. **131**, 181–200 (2018)
22. Salvi, K., Ghosh, S., Ganguly, A.R.: Credibility of statistical downscaling under nonstationary climate. Clim. Dyn. **46**, 1991–2023 (2016)
23. Wang, Y., Sivandran, G., Bielicki, J.M.: The stationarity of two statistical downscaling methods for precipitation under different choices of cross-validation periods. Int. J. Climatol. **38**, e330–e348 (2018)
24. Sridhar, V., Nayak, A.: Implications of climate-driven variability and trends for the hydrologic assessment of the Reynolds Creek Experimental Watershed, Idaho. J. Hydrol. **385**, 183–202 (2010). https://doi.org/10.1016/j.jhydrol.2010.02.020
25. Jin, X., Sridhar, V.: Impacts of climate change on hydrology and water resources in the Boise and Spokane River Basins. J. Am. Water Resour. Assoc. **48**(2), 197–220 (2012). https://doi.org/10.1111/j.1752-1688.2011.00605.x
26. Hertig, E., Jacobeit, J.: A novel approach to statistical downscaling considering nonstationarities: application to daily precipitation in the Mediterranean area. J. Geophys. Res. Atmos. **118**, 520–533 (2013)
27. Sachindra, D., Perera, B.: Statistical downscaling of general circulation model outputs to precipitation accounting for non-stationarities in predictor-predictand relationships. PLoS ONE **11**, e0168701 (2016)
28. Cai, X., Wang, D., Zhu, T., Ringler, C.: Assessing the regional variability of GCM simulations. Geophys. Res. Lett. **36** (2009)
29. Agarwal, A., Maheswaran, R., Sehgal, V., Khosa, R., Sivakumar, B., Bernhofer, C.: Hydrologic regionalization using wavelet-based multiscale entropy method. J. Hydrol. **538**, 22–32 (2016)
30. Agarwal, A., Maheswaran, R., Khosa, R.: (2015). Hydrologic Regionalization Using Wavelet Based Multiscale Entropy Technique. Department of Civil Engineering, IIT Delhi
31. Ball, G.H., Hall, D.J.: A clustering technique for summarizing multivariate data. Behav. Sci. **12**, 153–155 (1967)
32. Kanungo, T., Mount, D.M., Netanyahu, N.S., Piatko, C.D., Silverman, R., Wu, A.Y.: An efficient k-means clustering algorithm: analysis and implementation. IEEE Trans. Pattern Anal. Mach. Intell. **24**, 881–892 (2002)
33. MacQueen, J.: Some methods for classification and analysis of multivariate observations. In: Proceedings of the Fifth Berkeley Symposium on Mathematical Statistics and Probability, Oakland, CA, USA, pp. 281–297 (1967)
34. Bolshakova, N., Azuaje, F.: Machaon CVE: cluster validation for gene expression data. Bioinformatics **19**, 2494–2495 (2003)
35. Davies, D.L., Bouldin, D.W.: (1979). A cluster separation measure. IEEE Trans. Pattern Anal. Mach. Intell., 224–227
36. Dunn, J.C.: A Fuzzy Relative of the ISODATA Process and Its Use in Detecting Compact Well-Separated Clusters (1973)
37. Halkidi, M., Batistakis, Y., Vazirgiannis, M.: On clustering validation techniques. J. Intell. Inf. Syst. **17**, 107–145 (2001)
38. Kasturi, J., Acharya, R., Ramanathan, M.: An information theoretic approach for analyzing temporal patterns of gene expression. Bioinformatics **19**, 449–458 (2003)
39. Sehgal, V., Chatterjee, C.: Auto updating wavelet based MLR models for monsoonal river discharge forecasting. Int. J. Civ. Eng. Res. **5**, 401–406 (2014)

Author Index

M. Rathinasamy et al. (eds.), Water Resources and Environmental Engineering II,
https://doi.org/10.1007/978-981-13-2038-5